PB 265 892

REPORT NO.
EERC 76-32
DECEMBER 1976

EARTHQUAKE ENGINEERING RESEARCH CENTER

INFILLED FRAMES IN EARTHQUAKE-RESISTANT CONSTRUCTION

by

R. E. KLINGNER
V. V. BERTERO

Report to Sponsor:
National Science Foundation

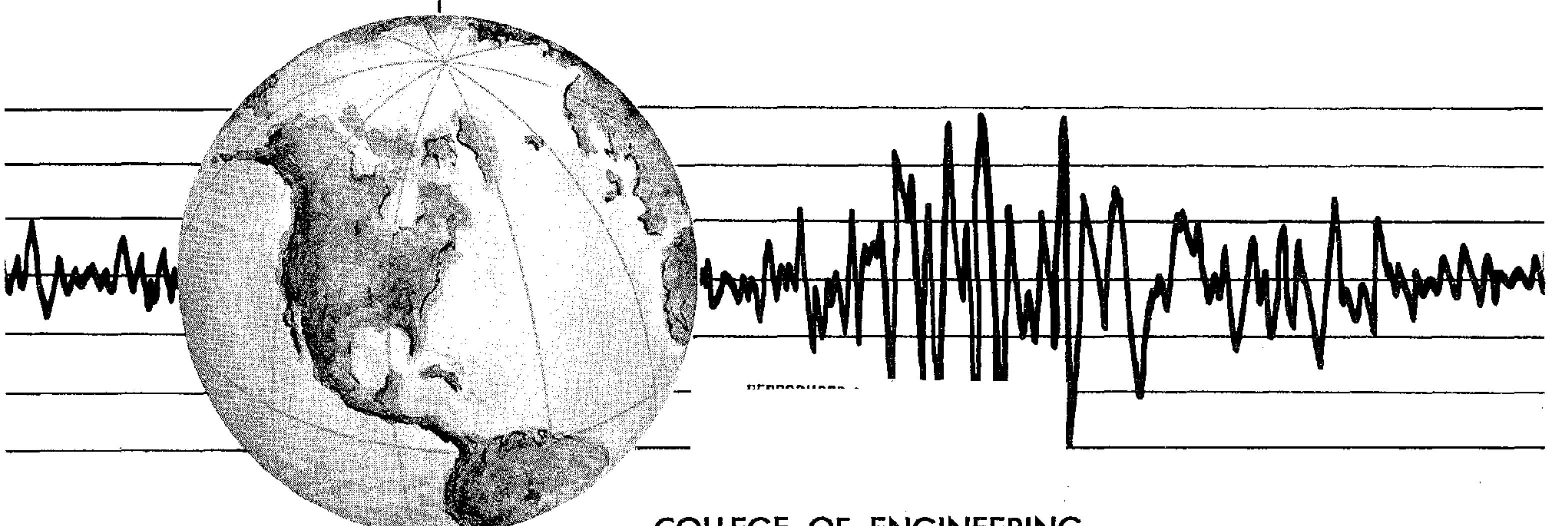

COLLEGE OF ENGINEERING

UNIVERSITY OF CALIFORNIA · Berkeley, California

See back of report for up to date listing of
EERC reports

i

BIBLIOGRAPHIC DATA SHEET	1. Report No. EERC 76-32	2.	3. Recipient's Accession No.
4. Title and Subtitle "Infilled Frames in Earthquake-Resistant Construction"			5. Report Date December 1976
			6.
7. Author(s) R.E. Klingner and V. V. Bertero			8. Performing Organization Rept. No. 76-32
9. Performing Organization Name and Address Earthquake Engineering Research Center University of California, Berkeley 47th Street and Hoffman Boulevard Richmond, California 94804			10. Project/Task/Work Unit No. (a)0-21997 (b)0-21198
			11. Contract/Grant No. (a) AEN 7307734 A02 (b) ENV 76-04263
12. Sponsoring Organization Name and Address National Science Foundation 1800 G Street, N.W. Washington, D. C. 20550			13. Type of Report & Period Covered
			14.

15. Supplementary Notes

16. Abstracts

The effects of engineered masonry infill panels on the seismic hysteretic behavior of reinforced concrete frames are investigated experimentally and analytically. The experimental phase consists of quasi-static cyclic load tests on a series of one-third-scale model subassemblages of the lower three stories of an eleven-story, three-bay frame with infills in the two outer bays. Emphasis is placed on simulating the proper force and displacement boundary conditions. The engineered infilled frames are designed and constructed in accordance with the following guidelines: 1) Frame members (particularly the columns) are designed for high rotational ductility and resistance to degradation under reversed cyclic shear loads; 2) Gradual panel degradation is achieved by using closely-spaced infill reinforcement; and 3) Panel thickness is limited so that the infill cracking load is less than the available column shear resistance.

The infilled frames are found to offer many advantages over comparable bare frames, particularly, with respect to their performance under strong ground motions. The analytical phase consists of developing relatively simple, macroscopic mathematical models for predicting the experimentally observed bare and infilled frame behavior. In particular, the infilled frame model is found to give excellent predictions of the observed response. It is concluded that the procedure used can be applied to the analysis of large, engineered infilled frame structures. The aseismic design implications of these results are discussed, and areas for further investigation are recommended.

17b. Identifiers/Open-Ended Terms

17c. COSATI Field/Group

18. Availability Statement	19. Security Class (This Report) UNCLASSIFIED	21. No. of Pages 291
Release Unlimited	20. Security Class (This Page UNCLASSIFIED	22. Price MF A01 PC A13

FORM NTIS-35 (REV. 10-73) ENDORSED BY ANSI AND UNESCO. THIS FORM MAY BE REPRODUCED USCOMM-DC 8265-P74

INFILLED FRAMES IN EARTHQUAKE-RESISTANT CONSTRUCTION

by

R. E. KLINGNER

Assistant Professor of Civil Engineering
University of Texas, Austin, formerly

Research Assistant
University of California, Berkeley

and

V. V. BERTERO

Professor of Civil Engineering
University of California, Berkeley

A report on research sponsored by
the National Science Foundation

Report No. EERC 76-32
Earthquake Engineering Research Center
College of Engineering
University of California
Berkeley, California

December 1976

ABSTRACT

The effects of engineered masonry infill panels on the seismic hysteretic behavior of reinforced concrete frames are investigated experimentally and analytically. The experimental phase consists of quasi-static cyclic load tests on a series of one-third-scale model subassemblages of the lower three stories of an eleven-story, three-bay frame with infills in the two outer bays. Emphasis is placed on simulating the proper force and displacement boundary conditions. The engineered infilled frames are designed and constructed in accordance with the following guidelines:

1) Frame members (particularly the columns) are designed for high rotational ductility and resistance to degradation under reversed cyclic shear loads;
2) Gradual panel degradation is achieved by using closely-spaced infill reinforcement; and
3) Panel thickness is limited so that the infill cracking load is less than the available column shear resistance.

These infilled frames are found to offer many advantages over comparable bare frames, particularly, with respect to their performance under strong ground motions. The analytical phase consists of developing relatively simple, macroscopic mathematical models for predicting the experimentally observed bare and infilled frame behavior. In particular, the infilled frame model is found to give excellent predictions of the observed response. It is concluded that the procedure used can be applied to the analysis of large, engineered infilled frame structures. The aseismic design implications of these results are discussed, and areas for further investigation are recommended.

ACKNOWLEDGEMENTS

This report is based on the dissertation written for the degree of Doctor of Philosophy in Engineering by R. E. Klingner under the direct supervision of Professor Vitelmo V. Bertero. The valuable insights and advice provided by Professor Anil K. Chopra are gratefully acknowledged.

The research reported herein was sponsored by the National Science Foundation under Grant No. AEN 7307734A02, subproject no. 0-21997, and Grant No. ENV76-04263, subproject no. 0-21198. The tests were conducted in the Structural Engineering Laboratory of the Department of Civil Engineering, University of California, Berkeley.

The authors would like to acknowledge the assistance of Barry Lotz and Don Clyde who did more than was expected in every phase of the experimental investigation, which probably would not have been possible without them. Earl Cleave and Ralph Payne fabricated the structural steel, and Tony Costa helped greatly with the instrumentation. Walter Dickey offered valuable advice on masonry practice, and David Vasquez infilled the models. Leonard Hashizume drafted the figures and Lucy Tsai polished and assembled the manuscript.

TABLE OF CONTENTS

1. INTRODUCTION

1.1 Statement of Problem

Earthquake damage reports from many different regions document the generally poor performance of infilled frame structures subjected to strong ground motions [1,2,3]. Typical reports describe the hazard to life and property represented by the often explosive failure of exterior masonry infills. In addition, many instances have been noted in which the presence of the infill decreased the earthquake resistance of a structure's framing system. Two examples of this were the Mene Grande and Amalfi buildings, both of which were severely damaged in the 1967 Caracas earthquake [1].

In spite of this, infills are commonly used all over the world in regions of high seismicity, particularly where resources and skilled labor are scarce and masonry continues to be the most economical construction material. Knowledge regarding the seismic response of infilled frames is a vital step in reducing the tragic loss of life and property often associated with the failure of masonry infills, and in deciding whether or not such infills should be used in structures designed to resist strong earthquakes.

1.2 Objectives and Scope

The main objective of the research described herein was to investigate the effects of infills on the hysteretic behavior of ductile, reinforced concrete frames under quasi-static loads simulating the principal effects of strong earthquake ground motions. The investigation was concerned exclusively with ductile, reinforced concrete frames, infilled with panels of reinforced unit masonry laid in place. However, it is believed that some of the results are applicable to other panel materials as well. The investigation comprised four phases: 1) literature survey and initial planning; 2) design; 3) construction and testing; and 4) analytical evaluation of results. These phases are briefly discussed below and subsequently covered in greater detail.

1) Literature Survey and Initial Planning. - To gain familiarity with previous work in this field and to aid in planning the investigation, an extensive literature review was carried out prior to commencing the research described herein. This review was continued and updated throughout the investigation. The principal results of this literature review are discussed in Chapter 2, and the entire survey is presented in Appendix A.

From information acquired during this literature survey, hypotheses were advanced concerning the principal stages of infilled frame structural response, and the general design principles which might result in desirable behavior under severe cycles of load and deformation reversals, such as those expected from severe seismic excitations. It was decided to test these hypotheses experimentally and analytically. The available laboratory facility and research budget prohibited epxerimental study of the behavior of the entire building. Thus, it was necessary to select the most basic subassemblage structural unit of a prototype building, to study experimentally the behavior of this subassemblage, and to use the results to predict the behavior of the entire structure. The purpose of this investigation required that this basic subassemblage be valid for the study of bare as well as infilled frames. The hypothesized behavior inferred from the literature survey was used in selecting the most basic structural unit from a chosen prototype.

2) Design. - Following the selection of a suitable prototype building and subassemblage, design of the bare frame prototype was carried out in two steps:

a) Service load design for gravity loads and equivalent static seismic lateral forces consistent with those prescribed by the 1970 UBC, and using the design provisions of the 1971 ACI Code.

b) Modification of the service load design to resist strong earthquakes, using Newmark's standard inelastic response spectra and accepted principles of inelastic analysis and limit state design for high displacement ductility.

The designed prototype frame was scaled down geometrically by a factor of three, and designs were completed for the loading attachments, restraints, and construction accessories necessary to test this model.

Based on hypotheses of general infilled frame design principles, this bare frame model was revised to permit the placement of infills, and to resist the forces due to infills. A final design was produced for an infilled frame model. In designing the model, emphasis was placed on simulating the proper force and displacement boundary conditions.

3) Construction and Testing. - The models were constructed in the testing laboratory. Tensile tests were carried out on each type

of reinforcing steel used. Tests were performed to determine the compressive strength and modulus of rupture of the concrete used for each specimen. The infilling was carried out by a mason under the direct supervision of the investigator and extensive tests were carried out to determine the mechanical characteristics of representative masonry prisms, as well as those of the mortar, grout, and block units comprising them.

A bare frame was first tested to obtain its mechanical behavior; all other tests were carried out on infilled frames. The results reported herein pertain to the first test series, involving 1) a bare frame (test #1); 2) this same frame, infilled with clay blocks after test #1; 3) a virgin (previously untested) frame, infilled with clay blocks; and 4) a virgin frame, infilled with concrete blocks.

To simulate the principal effects of strong earthquake ground motions, axial loads, lateral loads, and associated overturning moments were applied using hydraulic actuators controlled through a closed-loop feedback system. The models were extensively instrumented; while all the transducer output was read at discrete intervals using a low-speed scanner, some data were monitored continuously. Test results are presented in the body of the report, and detailed accounts of each test are included in Appendix D.

4) <u>Analytical Evaluation of Results</u>. - Simplified mathematical models were developed to describe the experimentally observed behavior of the bare and infilled frames. The response predicted by these models was compared with that observed experimentally.

2. LITERATURE SURVEY AND INITIAL PLANNING

2.1 Literature Survey

As initially stated, one purpose of this study was to investigate the suitability and effectiveness of infilled frames in resisting strong earthquakes. Two questions arose at the start of this investigation:

1) How is the response--elastic and inelastic--of a frame structure affected by the presence of infill panels?
2) Can the earthquake resistance of frame structures be improved using infilled panels? If so, how should the frames and panels be designed in order to enhance desirable performance and minimize damage costs?

With these questions in mind, it was decided to carry out a comprehensive review of existing literature related to the performance of infilled frames. The purposes of this review were: 1) to learn the then-current level of knowledge regarding infilled frames and other related structural components, and 2) to clarify the purpose and scope of the planned investigation.

This literature survey, continued to date, covers experimental and analytical research related to the mechanical behavior of infilled frames. The entire review and accompanying bibliography are presented in Appendix A. The principal results of the review are given below.

2.1.1 Experimental Investigations

Until very recently, experimental research on infilled frames was concerned with the effects of infilling on the response of frame structures in the elastic range only, i.e. prior to the onset of significant panel cracking. Investigators were primarily interested in the development of empirical formulas for predicting the increase in lateral in-plane stiffness and strength provided by infilling. A frame and infill were found to behave initially as an integral unit whose stiffness could be predicted from deep beam theory [4,5]. Under higher lateral loads, it was observed that the panel separated from the bounding frame, except at diagonally opposite compression corners. Polyakov [6] and others suggested that the infill panel could be modeled as an equivalent diagonal compression strut.

This "equivalent strut" concept has been refined considerably since its introduction. Holmes [7,8] originally found that the strength and stiffness of the infilled frame were best calculated using an equivalent strut with modulus and thickness equal to that of the actual panel material, and a width equal to one-third of the diagonal length of the panel. Stafford Smith [9-13] later proposed that the width of the equivalent strut depended on the relationship between the frame and panel stiffness, and offered a series of empirical relationships giving equivalent widths which were typically between one-fourth and one-tenth the length of the panel diagonal. This work has recently been extended by Mainstone [14-16].

Benjamin and Williams [5] observed that after the formation of this equivalent strut, the strength of an infilled frame depended on the resistance of the frame columns--particularly the compression column--to moment, axial force, and the shear produced by the action of the compression strut against the frame. In his investigations of the behavior of infilled frames subjected to cyclic lateral loads, Esteva [17] found that distributed infill cracking resulted in large amounts of energy being dissipated through the friction developed across cracks. This was also observed by Alexander, et al. [18].

Recent investigations have corroborated the findings of Benjamin and Williams with respect to the strength of infilled frames. Kahn [19] observed that the action of the infill on the bounding frame increased the tendency for the frame members to fail in shear. Fiorato, et al. [20] found that after panel cracking, the presence of infilling caused a five-story, single-bay infilled frame model to behave as a knee-braced frame. This idealization was also used in a study by Leuchars and Scrivener [21].

2.1.2 Analytical Investigations

Analytical investigations of infilled frames may be placed in two categories: those which attempt to model the elastic stiffness and ultimate strength of infilled frames using simplifying concepts such as that of the equivalent strut; and those which utilize stress functions, finite difference procedures, or, more commonly, finite element representations of the infill and bounding frame, in order to compute the stiffness and strength of the overall assemblage.

Because some nonlinearity due to the infill and frame separating usually occurs well prior to the formation of significant cracks in the panels themselves, the latter approach involves considerable complexity even if it is assumed to apply only to response under moderate load levels. This approach is further complicated when the investigation is extended to load levels consistent with severe panel cracking, since it becomes necessary to follow analytically the complicated process of crack propagation and bond deterioration between grout and reinforcing steel which characterize infilled frame behavior in this range. These and other aspects of this microscopic approach are explored in papers by Moss and Carr [22] and Cervenka [23].

Generally speaking, this last type of approach has been disappointing in view of the large amounts of computational effort required to obtain meaningful results. It is probable its accuracy is limited by the present lack of knowledge regarding such topics as infill material characteristics, bond deterioration between grout and reinforcing steel, and shear transfer across cracks. In any event, such programs are presently unsuitable for analyzing structures large or complex enough to be of practical interest.

2.2 Initial Planning

The literature review revealed that some experimental investigators had found that infilled frames were stiffer and stronger than otherwise identical bare frames [5,14,20,21], and could also dissipate considerable amounts of energy after infill cracking [17,18]. However, review of results of recent tests of infilled frames subjected to load and deflection reversals [19,21] does not, in the author's opinion, indicate improvement in response over bare frames. Behavior was characterized by brittle frame failure and low energy dissipation.

Two principal reasons were hypothesized for this apparent discrepancy. Firstly, previous investigations involved only single panels or incomplete subassemblages. Realistic force and displacement boundary conditions were not imposed. Secondly, infilled frame specimens used in previous investigations were not designed specifically to develop high energy dissipation and to suppress undesirable behavior such as brittle frame failure.

It was decided to study infilled frame behavior experimentally using several series of models of a multipanel subassemblage, permitting increased accuracy in the duplication of the boundary conditions in panels located away from points of load application. Furthermore, each model series was to be constructed with different amounts and types of panel and frame reinforcement to investigate the effects of changes in these parameters on overall model response. The investigation described herein concerns the first series of models, which was designed to achieve high energy dissipation, and to prevent or delay brittle frame failure which could result from panel failure. Relatively large amounts of panel and frame reinforcing were used. Subsequent studies will investigate the comparative performance of series of models with significantly less reinforcement.

With respect to the analytical investigation, the literature review indicated that macroscopic mathematical models--those involving simplifying concepts such as the equivalent diagonal compression strut--would be more appropriate than microscopic ones for the analysis of large or complex systems. Because such analysis was one of the original objectives of this investigation, it was decided to develop a macroscopic mathematical model based on the equivalent strut concept. The investigation would be primarily experimental. The purpose of the analytical phase would be to develop a physically reasonable macroscopic model capable of predicting the essential aspects of experimentally observed infilled frame behavior, yet simple enough to permit its use in predicting the overall behavior of large infilled frame structures, or in subsequent parametric studies involving infilled frame subassemblages.

3. DESIGN AND FABRICATION OF TEST SPECIMENS

The experimental investigation was carried out in several steps. First, the decisions noted in Section 2.2 were expressed in the form of guidelines for planning the experiment. Specifically:

1) To use a multipanel test assemblage, and to simulte as correctly as possible the force and displacement boundary conditions.

2) To design the infilled frame specifically for high energy dissipation. Previous work by Esteva and Alexander, et al., suggested that energy dissipation would be increased if the infill cracking were distributed over the panel instead of being concentrated in one large diagonal crack. It was decided to try to obtain distributed panel cracking through closely-spaced horizontal and vertical reinforcement.

3) To design to prevent or delay brittle frame failure which could result from panel failure. This was achieved by designing the frame members for high rotational ductility and shear resistance under cyclic loading reversals, and by examining closely the relationship between column shear resistance and infill panel strength. This is further discussed below. As will be noted later, these guidelines are emphasized because of their effect on the final behavior of the model infilled frame subassemblage.

The next step was the selection of a reasonably simple prototype building. Because many typical infilled frame buildings are in the ten- to fifteen-story range in height, it was decided to use an eleven-story reinforced concrete frame studied previously by Biggs and Grace [24]. The plan and elevation views of the prototype building are shown in Figs. 1 and 2. A prototype subassemblage from the transverse end frame was selected for this study. This frame was considered open in all bays for the bare frame prototype, and infilled in the two outer bays for the infilled frame prototype. Because the dynamic response of typical building structures to ground motions is due primarily to the first-mode response, overall maximum force levels are generally reached at or near the base of a structure. Therefore it was decided to locate the prototype subassemblage in the lower three and one-half stories of this end frame, as shown in Fig. 3. Geometric and structural symmetry about the frame centerline suggested the choice of a prototype subassemblage comprising one and one-half bays by three and one-half stories. Assuming the action of seismically induced horizontal inertial forces to be that of antisymmetric loads on a symmetric structure, the proper centerline force and displacement boundary conditions were imposed by requiring zero vertical displacement and zero moment at the ends of the cantilever beams. The lack of symmetry in the inelastic range due to the effect of axial forces in the infilled frame and the effect of gravity forces in the coupling girders are believed to be of secondary importance.

3.1 Preliminary UBC Bare Frame Design

In order to check the service condition design of Biggs and Grace and identify any possible modifications to the prototype, a preliminary bare frame design was first carried out. Dead loads were computed based on the data given in Reference 24, and live loads were taken to be 50 psf. It was decided to base the design on the provisions of the 1970

UBC [25], the latest available at the start of this investigation. Using Sections 2615 and 2630 of the UBC, critical design load combinations were given by:

$$1.5\ D + 1.8\ L$$

$$1.40\ (D + L \pm E)$$

$$0.9\ D \pm 1.25\ E$$

Equivalent static lateral loads representing the effects of seismically induced inertial forces, were computed according to two procedures.

1) The building was modeled using TABS, a computer program specially developed for static and dynamic structural analysis [26]. The model used the original member sizes, and considered the effects of finite column widths and beam depths. Young's modulus for concrete was calculated in accordance with Section 8.3.1 of the 1971 ACI Code [27] using f'_c equal to 27.58 MPa (4000 psi). The contribution of the floor slabs to beam stiffness was included in accordance with Section 8.7.2 of the 1971 ACI Code. Reduction in beam flexural stiffness due to cracking was considered by using an effective moment of inertia equal to 40% of that of the uncracked section. This ratio was subsequently checked and found to be valid for the final beam designs. The fundamental period of vibration of the eleven-story frame structure was calculated to be 1.30 seconds. Based on this value, equivalent static lateral forces were calculated by Section 2314 of the 1970 UBC, using a value of Z equal to 1.0 (Zone III), and a value of K equal to 0.67, corresponding to a ductile moment-resisting space frame. This nomenclature is defined in Reference 25.

2) Although Section 2314 of the 1970 UBC does not explicitly specify a design response spectrum for calculating equivalent lateral forces, its base shear calculation formula implies the spectrum shown in Fig. 4. In accordance with Section 2630(a) of the 1970 UBC, this equivalent spectrum was scaled up by a factor of 1.40, resulting in peak spectral response accelerations of 0.0933 g, as shown in Fig. 4. Newmark's maximum spectral values for a standard basis earthquake were scaled to produce the equivalent Zone 3 ground spectrum which, when modified in accordance with Reference 28, would also produce maximum spectral response accelerations of 0.0933 g in buildings with 3% critical damping, founded on firm soil. This amount of damping was used because it is a realistic value for a clean, reinforced concrete frame responding in the elastic range. Assuming 3% damping in all modes, the root-mean-square (RMS) combination of the first five modes, as computed by TABS, was used to calculate an envelope of equivalent story shears. The base shear obtained by this second method was within a few percent of the UBC base shear. In the upper floors, however, the second method gave story shears which were larger and considered more accurate. Therefore, these were used in combination with gravity loads to compute the forces required for member design. For consistency, the story shears computed by the second method were factored to give a base shear equal to that of the UBC method. Load combinations were computed using the TABS program. The members were designed to meet the 1971 ACI Code and its Appendix A ("Special Provisions for Seismic Design"), using Grade 60 steel and f'_c = 27.58 MPa (4000 psi).

3.2 Revised UBC Design, New Column Sizes

The original columns of Reference 24 measured 305 mm by 762 mm (12" by 30"). The results of the preliminary design indicated that owing to their low shear-span ratio, such columns might have low resistance to cyclic shear reversals. Therefore, the preliminary design was revised for columns measuring 457 mm (18 in.) square. This revised service load design was carried out by the 1971 ACI Code and its Appendix A, with the following exceptions:

1) Beams were designed for the shear consistent with the development of their maximum moments ($\phi = 1.0$) at sections located at a distance of two-thirds the clear span apart. Such a hinge placement could be developed under combined lateral and gravity loads. The total shear was assumed to be carried by the transverse steel alone.

2) Columns were designed for the shears consistent with the development of maximum balance point moments ($\phi = 1.0$) acting in opposite senses at a distance d/2 from adjacent beam faces (double curvature, with the inflection point at column midheight). Again, shear was assumed to be carried by steel only. This is a very conservative assumption for columns, where the axial force is assumed to be the compressive force corresponding to the balance point of the moment-axial force interaction diagram.

3) Beam-column connections (joints) were designed with transverse reinforcing sufficient to resist the shear produced by the development of maximum moments (acting in the same sense) in the framing beams at the column faces.

The final service condition design was similar to that of

Reference 24.

3.3 Bare Frame Design for Strong Earthquakes

Because the revised bare frame design indicated that the selected prototype was basically satisfactory, it was decided to continue with this prototype. The previous design was now modified to resist strong earthquake ground motions.

Lateral forces were calculated using the ground spectrum suggested by Newmark: $\ddot{u}_{g\ max} = 0.50$ g, $\dot{u}_{g\ max} = 610$ mm/sec (24 in./sec), and $u_{g\ max} = 457$ mm (18 in.). The building was assumed to be founded on rock or firm soil, with 5% critical damping in all modes, and an available displacement ductility of 5.0. Then-current procedures [29] were used to compute the reduced elasto-plastic design response spectra (Fig. 5), which were much more severe than the service condition spectra of Fig. 4. The critical load combination was taken as the sum of:

1) story shears from the RMS combination of the first five modal responses to the reduced elasto-plastic design response spectra shown in Fig. 5; plus

2) factored gravity loads (1.5 D + 1.8 L), with the live load reduced for tributary area by Section 2306 of the 1970 UBC. These factors were used instead of (0.9 D + 1.2 E) because the latter are less critical for columns, such as those used here, whose moment resistance does not decrease significantly for axial loads less than the balance point axial load. It is recognized that the maximum gravity loads calculated using (1.5 D + 1.8 L) are conservative. The factors were used to account in an approximate manner for the potential effects

of concurrent vertical accelerations.

This load combination and the building geometry were used as input to BADAS-2, an elasto-plastic design program [30]. This program found the required member resistances by storywise optimization. The necessary beam and column resistances at each floor level were very close to those obtained by hand calculation using a sidesway collapse mechanism consisting of a one-story subassemblage. Member design was carried out using actual realistic material properties. Park and Kent's stress-strain curves for confined concrete [31] were used with f'_c = 27.58 MPa (4000 psi). Spalling was assumed to take place at a concrete strain of 0.0035. Because the actual average yield stress for Grade 60 deformed reinforcing bars is about 469 MPa (68 ksi), that value was used instead of the nominal 414 MPa (60 ksi). Strain hardening was assumed to begin at a steel strain of 0.007 with a strain-hardening modulus of 10343 MPa (1500 ksi). A maximum (and ultimate) stress of 655 MPa (95 ksi) was assumed to be reached at a steel strain of 0.15.

Beam designs were checked using the computer program RCCOL5 [32], which calculated moment-curvature relationships using the section geometry and material properties discussed above. No ϕ factors were used. Sufficient closely-spaced transverse steel was provided to:

1) resist all the shear consistent with the development of ultimate moments at hinge regions located a distance of one-half the clear span apart (Figure 6). It was found that this hinge location pattern might result from extreme combinations of vertical and lateral

loads. The hinge separation was reduced from that used in Section 3.2 because it was considered desirable to design more conservatively against loss of ductility due to shear failure produced by cycles of extreme reversal.

2) provide the rotational ductility (as calculated by the formulas of Mattock and Corley) consistent with the assumed available overall displacement ductility of 5.0; and

3) reduce the unsupported length of the longitudinal steel so that longitudinal steel buckling would be prevented or delayed even after the onset of strain hardening.

To simplify design detailing and to improve hysteretic behavior under full deformation reversals, the beams were designed with equal top and bottom longitudinal reinforcement. To allow for the formation of hinge regions away from the column faces due to combinations of lateral and vertical loads, all beams were designed with equal reinforcement carried along their entire length.

Using the RCCOL5 program, moment-axial force interaction curves were calculated for several trial column sections and compared with the critical moment-axial force combinations calculated by the BADAS-2 computer program. To obtain increased resistance to cyclic shear reversals, it was decided to use spiral reinforcing instead of the rectangular hoops used in the revised bare frame service load design. Columns at each joint were designed to resist the combined action of 1.2 times the joint forces (moments and shears acting at the interfaces of the beams and the joint) consistent with the development at these interfaces of the ultimate moment capacities of the framing beams, acting in the same sense (Fig. 7). Spiral reinforcement was designed to:

1) resist all the shears consistent with the development of maximum column moments in opposite senses at a distance d/2 from the beam faces limiting each clear story height, i.e. column double curvature over a height equal to the clear story height less two lengths of d/2 each, with the inflection point located at the column midheight (Fig. 8).

2) protect the longitudinal steel against buckling, even in the strain-hardening range; and

3) provide the necessary confinement as prescribed by A.6 of Appendix A of the 1971 Code.

Figure 9 shows the moment-axial force interaction diagram calculated (using the RCCOL5 program) for the final model column design. Because of the relatively high percentage of longitudinal steel, the moment capacity is not sensitive to variations in axial force at or below the balance point axial force. This figure also shows two moment-axial force interaction curves which apply when shear capacity controls. The first of these, calculated considering the shear resistance of the concrete only, represents the internal force combinations expected to produce shear cracking under monotonically increasing loads. The second curve, calculated considering the shear resistance of spirals only, represents the flexural capacity (governed by shear) under full cycles of reversed loading.

Because it was anticipated that the model would be constructed to one-third scale, the design of all members was carried out using bar sizes which when divided by three would result in available deformed bar sizes. A "strong column, weak girder" design philosophy was used. The columns were assumed to remain elastic except at the base of the building. They were designed for rotational capacities corresponding to story drifts of at least 0.02, even under maximum factored gravity loads. The critical regions of all members were designed for rotational ductilities of at least 5.0, consistent with the assumed available overall displacement ductility of 5.0 used in constructing the reduced elasto-plastic design response spectrum.

3.4 Infilled Frame Design

The infilled frame was designed for strong earthquakes according to the basic guidelines mentioned at the start of this chapter:

1) to obtain distributed panel cracking through closely-spaced horizontal and vertical reinforcing; and

2) to prevent or delay shear failure of the frame members, by designing them for high resistance to cycles of shear reversal, and by examining closely the relationship between column shear resistance and infill panel strength.

The first guideline was satisfied by specifying prototype panel reonforcement consisting of #6 bars at 305 mm (12 in.). This resulted in steel percentages of about 0.6% in each direction, significantly higher than that required by Section 2418(j)3 of the 1970 UBC [25], which specifies a minimum of 0.2% total (both directions), and at least #3 bars at 1.22 m (4 feet). This panel steel was spliced to dowels passing through the confined core of the frame members, thus connecting the panel integrally to the frame.

The first part of the second guideline--high resistance to cycles of shear reversal--was already satisfied by the high percentages of transverse steel used in the beams and columns of the final bare frame design for strong earthquakes. Achieving the second part of this guideline was more difficult: as mentioned in Section 2.1.1, it was reasoned that under low levels of loading, the infill panels would act monolithically with the bounding frame. Following the partial separation of the panel from the frame, the assemblage would behave as a braced frame. Upon reaching the maximum load, the shear resistance of the panels would suddenly decrease, and part of the shear formerly carried by the panels would be transferred impulsively to the columns. If the shear resistance of the columns were insufficient to carry this impulsive load, the columns would either fail immediately in shear or be very susceptible to rapid degradation in the critical region of the column subjected to flexure, axial force, and the shear induced by the equivalent compression strut. To prevent or delay this kind of failure, it was necessary to design the columns and panels so that the total shear resistance of all the columns in a given story would be greater than the maximum shear that that story could resist working as a braced frame due to the panel action. Because of the relatively high elastic lateral stiffness of the panels compared to the columns, prior to panel cracking most of the lateral load would be carried by the panels. Therefore, it was necessary to design the columns and panels so that the total shear resistance of all columns in a given story would be greater than the maximum shear resistance of the panels in that story. In this case, the total shear resistance of each pair of columns would have to be greater than the shear resistance of a single panel.

Using the resistance of the spirals plus the resistance of the total concrete section ($v_c = 0.166 \sqrt{f'_c}$ MPa, or $v_c = 2 \sqrt{f'_c}$ psi), the maximum available shear resistance of a single prototype column was calculated to be about 983 kN (221 k). Using $f_t = 0.62 \sqrt{f'_c}$ MPa ($f_t = 7.5 \sqrt{f'_c}$ psi), an approximate finite element analysis showed that a panel 305 mm (12 in.) in thickness, loaded diagonally in compression, would fail under a shear of 1156 kN (260 k) for f'_c = 10.34 MPa (1500 psi) and 2046 kN (460 k) for f'_c = 17.93 MPa (2600 psi). Analyses based on the A.I.J. standards for shear walls [33] gave values as high as 4163 kN (930 k). However, it was believed that a value of about 2224 kN (500 k) was most realistic for a masonry panel twelve inches thick. In order for the maximum available shear resistance of two columns to exceed the shear resistance of a single panel, the maximum prototype panel thickness would therefore be:

$$304.8 \text{ mm} \times 2 \frac{(983 \text{ kN})}{(2224 \text{ kN})} = 269.4 \text{ mm, or } 10.61 \text{ in.}$$

A prototype panel thinner than this would not cause immediate column shear failure after panel cracking. As is noted in the next section, the available testing facilities favored the use of a one-third scale for the model subassemblage, consistent with a maximum panel thickness of:

$$\frac{269.4}{3} \text{ mm} = 89.81 \text{ mm, or } 3.54 \text{ in.}$$

Therefore, it was decided to look for model brick units less than this thickness. Because they were readily available, it was decided to use model units with a thickness of 51 mm (2 in.) placed to form single-wythe panels having this same thickness.

3.5 Scaling and Final Model Design

Because of the dimensions of the available testing facilities, it was decided to model the prototype subassemblages to one-third scale. Designs for the base and infilled frames were revised to permit direct geometric scaling of reinforcement by a factor of 1/3, maintaining the same mechanical characteristics in the model as in the prototype. The final bare frame design is shown in Figs. 10a, 10b, and 10c, and the infilled frame design is shown in Fig. 10d.

The model subassemblage was post-tensioned to reaction blocks through a base block, which was designed as follows: The ultimate lateral resistance of the infilled model subassemblage was calculated by several conservative methods and found not to exceed 667 kN (150k). Elastic analyses were performed using TABS to calculate the relation between shear and the overturning moent, which was applied by an equivalent couple using axial jacks, as shown in Fig. 10d. The resulting envelope of maximum lateral and axial loads was used to identify critical load combinations for the base, which was then designed in accordance with the 1971 ACI Code. In a similar manner, each of the loading attachments was designed against its critical load combination.

The necessary construction sequence for the bare and infilled models was planned in detail. Loading conditions were calculated corresponding to each phase of construction, e.g., lifting in a horizontal position, transferring to a vertical position for infilling, lifting in a vertical position, and placing in the test apparatus. The final model design was checked and found to be adequate against each of these loading conditions.

3.6 Bare Frame Construction

After bending, placing, and tying the steel, the steel cages of the frames were laid horizontally in specially-designed formwork. After the installation of weldable steel strain gages, the models were cast horizontally in a single pour, using concrete mixed at the site. The mix, with a 28-day compressive strength of about 27.5 MPa (4000 psi), was designed to have a slump of about 127 mm (5 in.) to facilitate placement around the closely-spaced transverse steel. Aggregates were scaled to preserve the prototype relationship between aggregate size and reinforcing steel separation. At each pour, 16 to 20 6 in. x 12 in. (152 mm x 305 mm) control cylinders were taken. Also, four 5 in. x 6 in. x 20 in. (127 mm x 152 mm x 508 mm) beams were cast for modulus of rupture tests. All cylinders and beams were damp-cured next to the freshly-cast model frame, and were stripped at the same time as the model, usually seven to ten days after casting. After stripping, the control specimens and the model were air-cured under identical conditions. Cylinders were tested at intervals up to and including the date of testing of their respective model subassemblage. Details of the mix design, cylinder and beam tests, and test results corresponding to each model subassemblage, are given in Appendices C and D.

All necessary steel was obtained at once, in order to ensure that each bar size came from a single heat. Tensile tests were performed on all types of deformed bars and plain wire, using machined specimens whenever possible. Details of the procedures used in these tests, and the results obtained, can be found in Appendix B.

3.7 Infilled Frame Construction

As mentioned previously, the test series described herein consisted of four tests. A bare frame was first tested, then infilled for retesting. Two other frames were then cast and infilled, making a total of one bare frame test and three infilled frame tests. As shown in Fig. 11, two types of scale models of hollow-core block units frequently used in practice were selected for constructing the infill panels of the specimens. These were clay units, measuring approximately 51 mm x 25 mm x 102 mm (2 in. x 1 in. 2 4 in.), obtained from Canadian Refractories, Ltd., and concrete units, measuring approximately 51 mm x 51 mm x 102 mm (2 in. x 2 in. x 4 in.), obtained from the National Bureau of Standards.

It was necessary to develop a construction technique for infilling the frames that would leave the panel firmly attached to the bounding frame, and at the same time permit placement of horizontal and vertical steel in single-wythe panels. The first objective was achieved by splicing the panel steel to dowels anchored in the confined regions of the bounding frame members. The second was achieved by cutting bond beam units for use in those courses requiring horizontal steel, and by passing vertical steel through the cores in the blocks.

In the bare frame which was tested before infilling, dowels were hooked into the model's base and the confined cores of beams and columns at the four-inch spacing used in the panels. After test #1, the bare frame was rotated to the vertical position and infilled by cutting the vertical panel steel to the clear panel height and lap splicing it to the dowels anchored in the base. The blocks were laid in running bond by slipping them over the vertical bars until the midheight of the panel was reached. Courses of bond beam units were laid at four-inch intervals, and horizontal steel was placed there and lap spliced to the column dowels. After the midheight of the panel had been reached, the vertical steel was lap spliced to the dowels projecting down from the underside of the first floor (the first level above the base) and the remaining courses were laid using sawed units which were slipped sideways onto the vertical steel. All courses were grouted in four-inch lifts as the work proceeded, and the gap between the top course and the bottom of the first floor beam was filled with stiff mortar.

The other two models were cast using dowels in the columns and base, as in the first specimen. However, instead of using integral beam dowels, the beams were cast with one-inch diameter holes, aligned with the vertical dowels in the base (Fig. 12). After rotating the bare frames to the vertical position, the panels were laid without grouting, using courses of sawed bond beam units at four-inch intervals, and lap splicing the horizontal steel to the columns there. Particular care was taken throughout to keep the vertical cores clean and free of debris. When the entire panel had been laid in this manner, the vertical cores were rodded clean and washed out using cleanouts cut in the units at the bottom course. Vertical steel was cut long enough to extend the clear panel height up through the beam above the panel, and far enough above this beam to serve as vertical dowels for the next panel. Then the gaps at the top and bottom of the panel were blocked off, and the entire panel was grouted in all cores, using the "high lift" method [34]. Grout was poured into the cores through the holes left in the beams. Then the vertical reinforcing bars were inserted into these holes and pushed down through the grout until they touched the base, forming an untied lap splice with the base dowels. This procedure was then repeated for the other two panels. The last specimen, infilled with concrete block units, used welded instead of lapped splices between the horizontal panel steel and the column dowels.

In all cases, the mortar used corresponded to UBC type "S", composed of approximately one part Type II Portland cement, to one-half part of lime, to three parts of #30 Monterey sand. Grout consisted of one part Type II Portland cement to three parts Olympia top sand. Extensive compression tests were conducted on masonry units, mortar samples, grout samples, and grouted masonry prisms. Descriptions of the specimens, test procedures, and principal results, are given in Chapter 4 and in Appendix B.

The additional shear resistance produced in the bare frame by infilling made it necessary to strengthen the specimen at the level of lateral load application. This was done as shown in Fig. 13, using two light structural channels to transfer the shear through a row of 5/8-inch threaded rods to a concrete infill 51 mm (2 in.) thick, reinforced vertically with #4 bars at 102 mm (4 in.), and horizontally with #2 deformed bars at 102 mm (4 in.).

4. MECHANICAL CHARACTERISTICS OF MATERIALS

Six different structural materials were used in constructing the model subassemblages: concrete; reinforcing steel; clay block units; concrete block units; mortar; and grout. To predict and interpret the behavior of the models, it was necessary to determine the mechanical characteristics of each of these materials. Appendix B describes the experiments which were carried out to obtain these characteristics. This chapter summarizes the results which were obtained.

4.1 Reinforcing Steel

The complete results obtained from tesile tests are presented in Appendix B. The principal results with regard to strengths are given below:

Type	f_y lower		f_{max}	
	S.I.	English	S.I.	English
#7	501. MPa	72.6 ksi	692. MPa	100.3 ksi
#4	512.	74.2	741.	107.5
#3	470.	68.2	652.	94.5
#2 deformed	506.	73.4	729.	105.8
USS #5 Wire	670.	97.	678.	98.4
USS #11 Wire	703.	102.	759.	110.1

4.2 Concrete

Mix proportions are given in Appendix B. The following results were obtained from compressive tests of standard 6 in. x 12 in. cylinders

(152 mm x 305 mm) and from modulus of rupture tests on beams measuring 5 in. x 6 in. x 20 in. (127 mm x 152 mm x 508 mm):

Specimen	Age at Testing	Concrete Compression Strength		Modulus of Rupture	
		S.I.	English	S.I.	English
	(days)	(MPa)	(psi)	(MPa)	(psi)
1) Bare Frame	98	25.9	3750	$0.83 \sqrt{f_c}$	$9.9 \sqrt{f_c}$
2) Bare Frame, Infilled with Clay Units	248	26.1	3780	$0.86 \sqrt{f_c}$	$10.3 \sqrt{f_c}$
3) Virgin Frame, Infilled with Clay Units	189	22.0	3190	$0.98 \sqrt{f_c}$	$11.8 \sqrt{f_c}$
4) Virgin Frame, Infilled with Concrete Units	182	27.6	4000	$0.94 \sqrt{f_c}$	$11.3 \sqrt{f_c}$

4.3 Block Units

Compressive tests were carried out on several samples of clay and concrete block units:

Type of Block	Average Compressive Strength	
	S.I.	English
	(MPa)	(ksi)
Clay	42.1	6.11
Concrete	14.5 26.9	2.1 3.9

While very consistent values were obtained for the clay blocks, considerable scatter was noted for the concrete units. Some of these had sand pockets which crumbled easily; others, without such pockets, were much stronger. The two average figures given correspond to these two cases respectively. As will be discussed later, similar scatter was observed in the compressive strengths of grouted masonry prisms constructed using these concrete blocks.

4.4 Mortar and Grout

Compressive tests were carried out on two-inch diameter (51 mm) cylinder specimens of the mortar used to infill each panel of each infilled frame model. Compressive tests were carried out on 2 in. x 2 in. x 4 in. prism specimens (51 mm x 51 mm x 102 mm) of the grout used for each panel:

	Mortar			Grout		
Specimen	Proportions	Strength		Proportions	Strength	
		S.I.	English		S.I.	English
		MPa	Ksi		MPa	Ksi
Bare Frame, Infilled with Clay Blocks						
panel 1	1:1/2:2	30.8	4.47	1:3	13.2	1.91
panel 2	1:1/2:2	28.9	4.18	1:3	28.6	4.15
panel 3	1:1/2:2	29.2	4.23	1:3	21.9	3.18
Virgin Frame, Infilled with Clay Blocks						
panel 1	1:1/2:3	19.0	2.76	1:3.25	24.9	3.61
panel 2	1:1/2:3	27.5	3.99	1:3	24.3	3.53
panel 3	1:1/2:3	33.0	4.79	1:3	24.5	3.55
Virgin Frame, Infilled with Concrete Blocks						
panel 1	1:1/2:3	37.6	5.45	1:3	22.2	3.22
panel 2	1:1/2:3	31.9	4.63	1:3	13.8	2.00
panel 3	1:1/2:3	35.0	5.08	1:3	24.7	3.58

4.5 Masonry Prisms

Numerous masonry prisms were constructed with mortar and grout mixed to the different proportions used in the various model sub-assemblages. Compressive strength and modulus were measured:

Specimen	Prism Compressive Strength		Modulus of Elasticity	
	S.I.	English	S.I.	English
Bare Frame, Infilled with Clay Blocks,				
all panels	26.4 MPa	3.83 ksi	8826.	1280
Virgin Frame, Infilled with Clay Blocks				
panel 1	23.5	3.41	8343.	1210
panels 2 & 3	22.5	3.26	7722.	1210
Virgin Frame, Infilled with Concrete Blocks	18.96	2.75	9653.	1400

These strength values have been corrected for the effects of prism slenderness according to Section 2404 of the 1970 UBC. Uncorrected values were used for modulus computation.

4.6 Concluding Remarks

The data in Appendix B permit a detailed study of the reliability of the values obtained for the mechanical characteristics of each of the materials tested. A brief commentary on some of the more significant findings follows. Very little scatter was observed in the mechanical characteristics of steel and concrete, the materials used to construct the bare frame. With the exception of the clay block units, however, considerable scatter was observed for the mechanical characteristics of all elements used to construct the infill panels. In particular, the mortar and grout characteristics were very sensitive to the amount of water used, as well as the time which elapsed between mixing the material and taking the specimen. The workmanship and construction supervision were believed to be excellent. It is therefore probable that similar mortar and grout specimens, obtained under field conditions associated with normal workmanship, would exhibit even greater variations in mechanical characteristics. This indicates that microscopic analytical idealizations, which usually require precise values for local mechanical characteristics, may be difficult if not impossible to use in realistic mathematical modeling of unit masonry.

However, it is interesting to note that in spite of the large scatter in values obtained for the mechanical characteristics of the constituent materials of the infill panels, considerably less scatter was obtained for the characteristics of the masonry prisms themselves. It is believed that this is due to two principal factors:

1) The grout in all cores of the infill acts to increase the homogeneity and isotropy of the panel; and

2) The presence of the grout causes a change in the fundamental failure mechanism of the prism under compressive load: ungrouted masonry usually fails by splitting of the units caused by the spreading of the relatively flexible mortar in the bed joints. Grouted masonry, however, generally fails by splitting off of the face shells of the units due to expansion of the relatively flexible grout in the cores. The failure of ungrouted masonry, then, depends on

material characteristics in very small regions--each bed joint. The failure of grouted masonry depends more on the overall characteristics of the grout throughout the panel.

Because of this, it is believed that macroscopic mathematical idealizations (see Chapter 6) are much more suited to the analysis of grouted masonry panels (or homogeneous concrete panels) than to the analysis of ungrouted panels. It is suspected that incomplete grouting, which often occurs in practice due to the presence of air or debris in the grout cores, may result in panels which are not nearly as amenable to macroscopic idealizations as those considered herein.

5. TESTING PROCEDURE AND EXPERIMENTAL RESULTS

5.1 Test Setup

As mentioned previously, the geometric and structural symmetry of the prototype transverse end frame suggested the use of the three-and-one-half story, one-and-one-half bay subassemblage shown in Fig. 3. Available laboratory facilities permitted the testing of one-third scale models of this subassemblage, as shown in Fig. 10. Boundary conditions were satisfied by the vertical displacement constraints imposed by the struts connecting the cantilever beam ends. The specimens were tested horizontally as shown in Fig. 14a. The base of each model was tied to heavy reinforced concrete reaction blocks using twelve post-tensioning rods, loaded to 222 kN (50 k) each. The reaction blocks were themselves post-tensioned to the tie-down slab of the test bay.

Both columns of each model were supported vertically (out-of-plane) by rollers placed at the level of lateral load application, allowing free lateral movement. In addition, an out-of-plane restraint system prevented vertical movements greater than $\pm$ 3 mm at nine points: the six beam-column joints, and the ends of the cantilever beams. The purpose of this restraint system was to prevent out-of-plane instability.

During all three infilled frame tests, the panels were supported by air mattresses whose pressure was regulated to balance the dead weight of the panels alone. It was reasoned that without such support, tests carried out with the model in a horizontal position would unrealistically apply a constant 1.0 g acceleration perpendicular to the plane of the panels. While the mattresses may be retarded slightly the deterioration of the panels, it is believed that their influence was insignificant compared to that of the closely-spaced panel reinforcement.

5.2 Loading System

The models were loaded as shown in Figs. 14b and 14c. Lateral loads simulating the effects of in-plane shear due to lateral inertial forces, were applied at the three-and-one-half story level using a hydraulic actuator with a capacity of 1560 kN (350 k). Column loads simulating the effects of gravity loads and the overturning moment associated with the lateral load, were applied through two actuators with a capacity of 1560 kN (350 k) each. All actuators were connected to the built-in high pressure hydraulic system available at the testing facility, and were controlled using the closed loop loading system shown schematically in Fig. 14d. This system, which was specially developed for cyclic load tests of large frame-wall subassemblages, permitted either load or displacement feedback control of the lateral actuator through an MTS servocontroller [35]. Additional servo-controllers connected to the axial load actuators enabled predetermined column loads to be applied, followed by proportions of the incremental load applied by the lateral actuator. Thus, the system permitted load or displacement control and the simultaneous application of any desired combination of initial column load, lateral shear, and associated oveturning moment applied as an equivalent couple through the column actuators.

The loading sequence for each test consisted of the following steps:

1) The cantilever beam struts were left free and the column loads were applied to simulate unfactored dead plus live loads;

2) The struts were tightened;

3) The desired program of lateral loads or displacements was applied. The correct overturning moment as calculated from elastic analyses was simultaneously applied using column jacks;

4) When the desired load program was completed, the cantilever beam struts were disconnected; and

5) The axial loads were removed.

The ratio between lateral force and corresponding overturning moment, was calculated by elastic analysis of the entire end frame. Elastic analysis of the bare frame gave a ratio of shear to overturning moment which was duplicated using the proportion of axial to lateral load shown in Fig. 14b. Elastic analysis of the infilled end frame gave the ratio shown in Fig. 14c, which was used initially in the infilled frame tests. During the course of these tests panel degradation caused the infilled frame to behave as a weakly-braced frame; such behavior was expected to alter the lateral force-overturning moment ratio. To account for any changes, the proportion of axial to lateral loads was changed during each infilled frame test, based on the amount of panel damage observed (i.e. extent of transition from monolithic deep beam to bare frame behavior). In infilled frame test #1, the ratio was changed twice, once from the infilled frame ratio to an intermediate ratio, and again from the intermediate ratio to that corresponding to the bare frame. Comparison of successive cycles to equal displacements showed that these changes did not have a significant effect on the overall force-displacement characteristics of the model. However, it was believed that their effect on column hinge formation was significant, and therefore the same procedure was used to vary the ratio between lateral and axial forces in all the infilled frame tests.

5.3 Instrumentation

In this initial test series, it was decided to use the minimum amount of instrumentation to monitor 1) all loads applied to the specimen; 2) lateral displacements at each floor level; 3) internal forces necessary for checks of static equilibrium; and 4) key response quantities which provided information about changes in overall structural response.

The bare frame was instrumented as shown in Fig. 15. Applied loads were monitored through force transducers connected to the actuator shafts. Displacements were monitored using linear potentiometers (LP's) connected to fixed reference points. Forces in the struts connecting the cantilever beams, and the strut connecting the two stub columns, were monitored using force transducers consisting of four-arm bondable strain gage bridges. Column rotations at the base and relative rotations at the first floor interior beam-column connection, were monitored using linear variable differential transformers (LVDT's) attached to rigid yokes set perpendicular to member axes. Clip gages (see Appendix C) at the column bases permitted detailed analysis of longitudinal steel pullout there.

Similar instrumentation was used for the infilled frame specimens, as shown in Fig. 16. However, neither the force in the strut connecting the two column stubs, nor rotations at the column bases, were monitored. In addition to clip gages at the base of the columns, weldable strain gages were placed on the column longitudinal reinforcement to indicate yielding of the column steel. Clip gages placed along the first story height of each column permitted study of overall bending deformations at that level.

Bare frame instrumentation comprised 21 different channels; infilled frame specimens had from 28 to 32 channels, depending on the tests. Output from all of these was read at discrete intervals using a low-speed scanner connected to a magnetic tape unit, and some channels were monitored continuously using XY recorders.

5.4 Testing of Specimens

As discussed briefly in Section 3.7, tests were conducted on the following four models:

1) a bare frame (test #1);
2) this same frame, infilled with clay blocks after test #1;
3) a virgin frame, infilled with clay blocks; and
4) a virgin frame, infilled with concrete blocks.

The general procedures and overall results of the bare and infilled frame tests are discussed below. Details of each of the four tests are given in Appendix D.

5.5 Bare Frame Test

After the application of simulated gravity loads using axial jacks, this frame was subjected to the first few cycles of the lateral loading program shown in Fig. 17. This program was designed to meet the following two main objectives:

1) to subject the frame to cycles of full load reversal at the level of base shear consistent with that of the UBC service load design of Section 3.2; and

2) to subject the frame to cycles of full deflection reversal at deflections sufficiently high to permit observation of the frame's inelastic response, yet small enough so that the resulting damage level would be low enough to permit subsequent infilling and retesting.

The pattern of the loading program--cycling with full load reversals to monotonically increasing maximum loads--was selected not only because it represents in an approximate manner the effects of the first few cycles of base shear response to strong far-field ground motions, but also because it is one of the most efficient loading programs for acquiring valuable data regarding hysteretic behavior when the number of test specimens is limited.

Figure 18 shows the resulting tip displacement as a function of lateral load. Failure occurred through the formation of a sidesway mechanism at a maximum lateral load of about 50 kN (11.3 k). As shown in Fig. 18, this experimentally-observed lateral load agreed very well with that predicted by a second-order collapse analysis using individual member resistances and a failure mechanism corresponding to the observed damage. Judging by its performance under quasi-static cyclic load, the seismic resistance of the bare frame was significantly affected by its lateral flexibility and consequent susceptibility to P-Δ effects. As discussed in detail in Appendix D, the bare frame's inelastic resistance was limited in particular by deterioration of strength and stiffness in the interior beam-column connections.

5.6 Infilled Frame Tests

The loading programs and lateral load-deflection curves for the three infilled frame tests are shown in Figs. 17 and 19 through 22.

The loading program used for tests #2 and #2 was an extension of that used for the bare frame test--complete load reversals at monotonically increasing peak amplitudes. However, a different type of loading program was used for test #3. Following the 1971 San Fernando earthquake, it was suggested that a dominant feature of near-field ground acceleration records is the presence of large acceleration pulses associated with the propagation of horizontal shear waves from the focal region [36]. The presence of these pulses may result in rapid near-monotonic loading of the structure into the inelastic range. This type of loading may be critical for structures with a high tendency toward brittle failure [36]. The loading program for test #3 was based on this type of near-field record: after a few cycles at service-level loads, the shear was monotonically increased until the start of serious panel damage. The structure was then cycled as before, under full load reversals, resulting in displacement reversals with gradually increasing peak amplitudes.

In Section 2.1, it was hypothesized from the results of the literature investigation, that the response of infilled frames to cyclic shear would follow this sequence:

1) Initially, the frame and panel would behave as a monolithic deep beam.

2) Boundary separation would occur at the interface between the frame and the infills, and the structural action of the subassemblage would be similar to that of a frame braced by equivalent diagonal compression struts.

3) Assuming that brittle frame failure were avoided, the inelastic response of the infilled frame would be similar to that of a braced frame with degrading equivalent diagonal compression struts.

These hypotheses were verified. Additional observations of response under large story drifts provided further information regarding the overall behavior mechanism of infilled frames constructed in accordance with the guidelines given at the beginning of this section. Specific information on the results of each test is given in Appendix D, and some of these results are related to material characteristics in Section 5.7. The following description is intended to summarize those aspects of infilled frame response which were observed in all three tests, and to aid in correlating the detailed information of Appendix D. The results will first be described in general, and then specific examples will be used to illustrate each response stage.

The general failure sequence was the same for all three infilled frame specimens:

1) Initially, cracks formed in each panel in directions consistent with the principal tensile stress orientations predicted by deep beam

theory.

2) After the separation of the infills from the bounding frame, the assemblage behaved essentially as a frame braced by equivalent diagonal compression struts. When the panel resistance began to decrease due to crushing and shear in these equivalent struts, the entire subassemblage exhibited a gradual decrease in shear strength under load reversal.

3) Spalling occurred at frame regions subjected to critical combinations of axial forces, moment, and infill-induced shear. Typically, this spalling occurred in the beams or columns near the connections. Reduced frame member stiffness at these critical regions resulted in increasing local inelastic deformations. Eventually, the number of such regions increased sufficiently to produce a sidesway mechanism, whose lateral resistance was controlled by the strength of these inelastic regions as well as by the residual infill resistance.

4) Repeated cycles of loading reversal produced an increased amount of "pinching" in the load-deflection curve, characteristic of shear-degrading structures, and the strength of the subassemblage asymptotically approached that of the corresponding bare frame mechanism.

Figures 23 through 35 illustrate specifically the physical appearance and load-deflection behavior associated with each of the four response stages discussed above. The photos and load-deflection curves were obtained from test #3. However, similar behavior was observed in the other two infilled frame tests as well.

Point "1" of Fig. 23 coresponds to the stage of monolithic behavior. Figure 24 shows the deep beam cracking pattern characteristic of that stage. The start of separation between the infill and frame is illustrated in Fig. 25. Point "2" of Fig. 23 corresponds to Fig. 26, which illustrates the development of the equivalent diagonal compression strut, in this case, in the first story panel (panel #1). Figure 27 shows the physical appearance of this panel as the strut began to degrade near the base of the exterior (left-hand) column. This stage corresponds to Point "3" on the load-deflection curve (Fig. 23). However, the start of degradation of this equivalent strut did not cause failure of the subassemblage. Points "4" and "5" of Fig. 28 represent reversals of deflection between +7 cm and -2 cm. These points were associated with the damage levels shown in Figs. 29 and 30, respectively. As discussed in detail in the next section, this damage was characterized by increased panel deterioration due to crushing and shear along the compression diagonal.

Continued cycles of deformation reversal at increased maximum tip deflections (approximately $\pm$ 10 cm, or $\pm$ 4 in.) gave load-deflection characteristics as indicated by Points "6", "7", and "8" of Fig. 31. The damage resulting from these deflection reversals is shown in Figs. 32 through 36. Examination of the figures will show that continued cycling led to: 1) formation of inelastic regions in the frame members near the beam-column connections; 2) spalling of the frame members near these critical regions; 3) development of the sidesway mechanism shown schematically in Fig. 31; and 4) strength asymptotically approaching the second-order collapse load of the corresponding bare frame mechanism, as shown in Fig. 31.

As may be seen from Figs. 20 through 22, although all three infilled frame models exhibited a decrease in strength following the initial drop in panel resistance, this decrease was gradual. All infilled models exhibited excellent energy dissipation characteristics, even at tip deflections greater than $\pm$ 10 cm, corresponding to story drifts in excess of 0.03. Figure 36 shows the largest hysteretic loop obtained for the bare frame test (test #1), superimposed on the hysteretic loops obtained for the virgin frame infilled with concrete blocks (test #4). The hysteretic behavior of the infilled frame is clearly far superior with respect to energy dissipation. This superiority can be expressed quantitatively by comparing the amount of energy dissipated by the infilled frame versus the bare frame. To be able to compare energy dissipation at any given level of displacement reversal, it is convenient to compute for each model the energy dissipated in a given cycle (the area bounded by the hysteretic curve for that cycle), normalized by the total peak-to-peak displacement variation for that cycle. These calculations were carried out for the four specimens, and the results are presented in Fig. 37. As explained in Appendix D, variations in the loading programs and failure modes produce some differences among the three curves of Fig. 37 corresponding to the infilled frames. However, when the results presented in Fig. 37 as well as those in Figs. 18 and 20 through 22 are examined, it is clear, with respect both to stiffness at service levels and to maximum energy absorption and dissipation capacity at all levels of displacement reversal, that tremendous gains resulted from infilling the frames. In all cases, it was possible to achieve distributed infill cracking and high energy dissipation, and to minimize brittle shear failure in the bounding frame.

It should be noted that the ductile behavior of this type of infilled frame is considerably different from ductile shear wall behavior. A ductile shear wall is designed to fail in flexure. Under complete load reversals, this type of failure often results in the opening of cracks which run completely across the whole cross-section of the wall. Rotational ductility is then generally limited by resistance to sliding shear failure, or to a type of failure characterized by crushing and spalling along a horizontal band extending across the wall. These types of failure are particularly likely to occur at the base of the wall, or at horizontal construction joints.

However, the type of infilled frame considered herein is designed to respond inelastically as a braced frame. Its failure is governed by crushing of the equivalent diagonal compression strut. To ensure that an infilled frame subassemblage will fail as a braced frame rather than as a ductile shear wall, it must be designed so that the lateral shear necessary to cause flexural failure considerably exceeds that required to produce infill crushing. For example, the model infilled frame subassemblage studied herein was idealized as a beam-column using the computer program RCCOL5. Under the expected range of axial loads, the subassemblage was found to have a yield moment corresponding to a shear of about 756 kN (170 k) applied at the level of the lateral actuator. It was decided that a reasonable upper bound to the shear required to cause panel crushing, could be computed by assuming such crushing to occur at a nominal panel shear stress of 0.83 $\sqrt{f'_c}$ MPa or 10 $\sqrt{f'_c}$ psi. The prism tests described in Chapter 4 showed the compressive strength of the panels to be at most 24.1 MPa, or 3500 psi. Therefore an upper bound on the shear resistance of a single panel was computed by multiplying this nominal maximum stress by the area of a horizontal section through the panel:

$$V_{max} = 51 \text{ mm} \times 1880 \text{ mm} \times 4.075 \text{ MPa} = 391 \text{ kN, or } 88 \text{ k}$$

It is clear that in this case the resistance of the panel to diagonal crushing was much less than the load required to produce flexural yielding. As anticipated, braced frame behavior was observed rather than shear wall behavior in all infilled frame tests: maximum resistances ranged from about 270 kN to 320 kN (60 to 72 k), well below the calculated upper bound of 391 kN (88 k).

Whether a subassemblage behaves as a braced frame or as a shear wall, depends principally on the aspect ratio and thickness (strength) of the panel. Infilled frames with large aspect ratios (ratio of height to width) will generally fail in flexure because of their comparatively low flexural strength. Infilled frames with low aspect ratios will generally have failure modes governed by panel thickness: A given frame, infilled with weak panels, will behave as a lightly braced frame. As the strength of the panels is increased, the frame members themselves may fail in shear as a result of panel cracking. If this is prevented by suitable design guidelines, as in our case, the subassemblage will behave as a heavily braced frame. The use of even stronger infills will result in monolithic shear wall behavior, with failure occurring in flexure, shear-flexure, or sliding shear. The type of design studied herein behaves inelastically as a braced frame; there is little tendency toward sliding shear failure, and the cracked panels dissipate considerable energy without significantly affecting the integrity of the frame.

5.7 Remarks Regarding Hysteretic Behavior

The responses of the bare and infilled frame specimens tc cycles of load and deflection reversals, are described generally in ths chpater and specifically in Appendix D. It is worthwile to discuss further some specific aspects of the observed infilled frame behavior:

The tests indicate that initial panel deterioration (crushing of the equivalent strut) may occur in any panel. At first, the lowest panel is subjected to higher stresses because the overturning moment is greatest there. However, after the model begins to behave as a braced frame, the three compression diagonals are subjected to almost identical forces. As noted in Chapter 6, analyses show that small differences in force do exist, owing to slight differences in panel as aspect ratios and to the stiffness distribution of the frame itself. Because approximately equal forces act along the compression diagonals of all three panels, the question of which panel crushes first, depends chiefly on local mechanical characteristics of each panel and of the frame joints. These in turn depend heavily on the quality control of materials and workmanship. Apart from these considerations, the following specific characteristics were found to contribute to the initiation of crushing in a particular panel:

1) Lap splices in horizontal panel steel.- As noted in the text, the infilled frame models used in tests #2 and #3 were constructed with simple lap splices in the horizontal panel steel. In both of these tests, cracks formed along the vertical lines marking the cutoff point for the horizontal dowels anchored in the frame column. Because no such cracks formed along the vertical line of welded splices in the horizontal panel steel, it is probable that the crucial weakness of the lap splice is the local concentration of tensile stress which it creates, rather than the reduction in steel area at the end of the splice.

2) Lap splices in vertical steel.- These are an unavoidable consequence of the construction technique used. They did not seem to influence the cracking pattern of the first two infilled frames. However, it is believed that they contributed to the horizontal shear crack which formed across the center of panel #2 in the last model tested. This crack may also have formed because of a relatively poor horizontal mortar joint at that level, or because the welded horizontal splices prevented cracking in the vertical direction. An infill panel which is lightly cracked along its compression diagonal will be able to resist essentially the same shear as an uncracked panel, because the compression stress paths run parallel to the crack. However, even small horizontal shear cracks across a panel will significantly reduce its shear resistance, because shears must be carried by friction across the crack, instead of in compression. Therefore, the panels should probably be designed against horizontal

panel cracking. This could be achieved by:

a) using lap splices instead of welded ones in the horizontal steel, to encourage vertical rather than horizontal panel cracks;

b) cutting the vertical dowels to varying heights, to avoid the creation of a single plane of weakness in the panel; and

c) using high-lift grouting in preference to low-lift, in order to minimize the weakening effect of poor horizontal grout joints.

Following the start of crushing in any given panel, the following factors were found to determine whether or not deterioration would subsequently occur in other panels:

1) The shear stiffness at beam-column connections (joints) adjacent to a given panel. - When a particular panel started to degrade, shear deformations increased there, resulting in the formation of hinge regions in the frame members bordering the panel. Because these hinge regions formed near the member ends, they were associated with a deterioration of the beam-column connections. The exterior connections deteriorated slowly, principally through the formation of shear cracks through the beams at the column faces due to reactions of the diagonal struts against the beams. However, the interior beam-column joints usually began to deteriorate rapidly due to pull-through of the longitudinal beam steel. As a result, severe cracking in a panel was usually followed by deterioration of one or both of the interior beam-column connections bounding that panel. This caused a reduction of local shear stiffness at these connections, and a consequent local increase in stress at the corners of undamaged panels located next to the degraded joints. This local increase in stress usually resulted

in a local crushing failure there, which triggered overall degradation of the entire panel. In other words, the deterioration process spread from one infill panel to another primarily through the interior beam-column connections.

2) The amount of damage in each of the other panels when the strength of the first panel starts to degrade. - The maximum resistance of each specimen coincided with the start of degradation in one of the panels. Because the resistance of this first panel then began to deteriorate in a relatively rapid manner, the forces acting in the other panels were decreased to levels significantly less than those required to initiate crushing. Therefore, regardless of local frame damage, some panels remained relatively undamaged throughout the entire test. The location of these relatively undamaged panels was found to determine the location of hinge regions in the frame, and hence the final collapse mechanism of the infilled frame. In some cases, the hinge positions and resulting mechanism changed during the test, as a consequence of changes in relative damage in each panel as the test progressed.

At the start of this investigation, there was considerable uncertainty over the most effective placement and quantity of panel steel. Experimental observations regarding this were complicated by the fact that at least three distinct modes of infill panel reinforcement behavior were noted during the tests:

1) Monolithic deep beam. - In this range, it is believed that both the percentage and spacing of panel steel are important. Vertical steel acts as longitudinal reinforcement, and both vertical and horizontal

steel resist shear and aid in the development of distributed cracking. It is believed that in this range the spacing of panel steel may be more important than the percentage: closer panel steel spacing will result in closer spacing of panel cracks, and smaller width of each crack.

2) Braced frame behavior with slight panel damage. - In this range, the deformation pattern of the model changes from flexural to that of a braced frame, and begins to be controlled by shear deformations in each panel. Since small shear deformations produce only second-order strains in horizontal and vertical panel steel, it is believed that in this stage of response as well, steel percentage is of less importance than close steel spacing, which as before will continue to encourage distributed panel cracking.

3) Braced frame behavior with severe panel damage. - In this range, the panel steel may again carry loads, due to the complex stress paths in the degrading panels. Close spacing aids in holding the broken pieces of masonry and in retarding the degradation of the panels. Therefore, the amount and spacing of horizontal and vertical panel steel, are both important.

It is recognized that the use of single-wythe masonry panels imposes severe restrictions on the orientation, spacing, and percentage of panel steel. Tests with precast concrete panels might suggest more effective panel reinforcing patterns. However, the results obtained to date indicate that the spacing of reinforcement (in both directions) is at least as important as the percentage of reinforcement. Further tests may provide more information regarding this point.

The validity of the equivalent strut concept depends, among other things, on verification of the physical mechanisms by which shear resistance is maintained in a deteriorating masonry panel. Understanding these mechanisms is of value in interpreting experimental data, and also in formulating valid analytical models:

1) Initially the panel resists diagonal compression elastically. Cracks form in the mortar joints in a direction roughly perpendicular to the principal tensile stresses, and may propagate into the units themselves. As long as the cracks are narrow, however, they do not significantly decrease the strength or stiffness of the panel upon reloading in the opposite direction.

2) When the load increases so that the combination of horizontal and vertical compressive stresses reaches the failure envelope [37,38], crushing occurs along the compression diagonal. The consequent shortening of this diagonal allows one half of the panel to move sideways with respect to the other, as shown in Fig. 38. Resistance in this range is due to friction in horizontal cracks, steel tension across vertical cracks, and dowel action across horizontal cracks. As the load is increased, panel shear deformation increases by a combination of new crushing and further slippage along horizontal crack surfaces.

3) As soon as part of the panel has moved sideways with respect to the other following crushing of the diagonal strut, load reversal causes closure of the vertical cracks opened in (2) above. This closure does not occur immediately and the load-deflection curve exhibits some pinching as a result. Potential resistance is provided

by friction along the horizontal cracks and compression at the closed vertical cracks. However, stress concentrations cause the formation of diagonal cracks in the opposite direction long before significant compressive stress can be developed at closed vertical cracks. As a result, the only significant resistance mechanism is that of friction due to interlock along the cracks in the horizontal (bed) joints. This friction is already limited to less than the original value by previous crushing, and decreases steadily due to degradation along the horizontal cracks. Consequently, the available resistance of the panel also decreases.

4) Gross deterioration of the panel involves decreased interlock due to degradation, accompanied by a widening of the two intersecting zones of diagonal crushing. This diagonal crushing increases the shear deformation necessary to mobilize strut resistance, and results in an accentuation of the pinching in the load-deflection curves. The rate of strength and stiffness degradation in this range depends primarily on the effectiveness of the panel reinforcement in holding the pieces of the panels together.

6. ANALYTICAL INVESTIGATION

As was pointed out in Section 1.2, the available laboratory facilities and research budget made it necessary to carry out the experimental investigation of infilled frame behavior using a scale model subassemblage. To gain better understanding of the fundamental mechanisms behind the experimentally observed response, to permit generalization of the results to other infilled frames of the same type, and to develop procedures suitable for the analysis of large infilled frame structures, it was decided to conduct an analytical investigation. The main objective of this analytical investigation was to develop a physically reasonable mathematical model capable of predicting the essential aspects of observed model infilled frame behavior. This was carried out in several steps. Details of the required calculations are given in Appendix E.

Because of the large amount of time and effort required to write a general nonlinear structural analysis program, it was decided to carry out the analytical investigation using an existing computer program as a basis. After a study of the available programs, it was decided to use ANSR-I, a general purpose program for analysis of nonlinear structural response, recently written at U.C. Berkeley by D. P. Mondkar and G. H. Powell [39].

6.1 Prediction of Bare Frame Behavior

For this phase, the ANSR-I program was used with the two-component model beam-column element recently written for it by a graduate student, D. Row, at Berkeley [40]. The one-third scale subassemblage was modeled as a plane frame consisting of rigid finite-width joints connected by one-dimensional beam-column elements. An initial attempt was made to model the reinforced concrete members with elements having bilinear moment-rotation characteristics only. However, this approach was not sufficiently accurate. It was finally decided to model the beams labeled "B1" in Fig. 10a using elements having five-segment moment-rotation characteristics. Beam type "B2" was idealized as having a quadrilinear moment-rotation relationship, and the columns were modeled using bilinear elements only. Details of the procedures used are given immediately below and in Appendix E, and the final bare frame idealization is shown in Fig. 39.

As noted above, the beams were modeled using either three or four parallel beam elements, each having essentially a linear elasto-perfectly plastic moment-rotation characteristic. The strengths and stiffnesses of these constituent elements were calculated so that their combined moment-rotation relationship would be consistent with the moment-curvature relation calculated for each of the two beam types used in the specimen (B1 or B2, Fig. 10a). These actual moment-curvature relationships were calculated using the computer program RCCOL5 [32]. This procedure is illustrated in Figs. 40 and 41. Steel and concrete mechanical characteristics were obtained from the tests conducted as described in Appendix B. To avoid conceptual errors from the use of multiple yield surfaces associated with multi-member columns, the columns were modeled using single bilinear elements only. As shown in Fig. 42, the stiffness and strain-hardening characteristics for these elements were calculated to correspond as closely as possible to the actual characteristics of the specimen's columns, as determined from theoretical moment-curvature diagrams calculated using RCCOL5. The points labeled "A", "B", and "C" in Fig. 42 may be considered to indicate yielding of the idealized bilinear column under different values of axial force. Together with an assumed balance point axial force of 222 kN (50k), these points can be used to construct a moment-axial force interaction diagram for the idealized bilinear column (Fig. 43). Within the range of axial forces of interest in this study, the idealized diagram closely approximates the moment-axial force interaction diagram previously calculated for the actual column.

The analytical model was subjected to the same type of loading program used in Test #1: axial loads were first applied, and the analytical model was then subjected to cycles of lateral load and associated overturning moment. Figure 44 shows the analytical results, compared with the previously obtained experimental curves for top lateral deflection as a function of lateral load.

It can be seen that agreement was excellent at all stages except at the reloading portion. Physically, this was due to the fact that flexural cracks at hinge regions did not close immediately upon load reversal. Hence the actual strength did not pick up as rapidly as predicted by the analytical idealization. However, because the behavior of the infilled frame idealization is dominated by the behavior of the infills themselves, the bare frame model was considered sufficiently accurate for the objectives of this analytical investigation.

6.2 Prediction of Infilled Frame Behavior

The principal objective of this study has been to develop a physically reasonable mathematical model capable of predicting the essential aspects of experimentally observed infilled frame behavior. Previous analytical investigations [22,23,41] have developed microscopic models in which finite elements were used to model the panel materials, reinforcing steel, and the bond-slip relation between them. The results obtained from such complex models have been generally disappointing in view of the tremendous computational effort required to produce them. It is believed that this is due principally to the present lack of knowledge regarding the mechanical behavior of masonry materials under combined states of stress or strain. Even if such microscopic models were accurate, however, they would probably not be practical for analyses of large infilled frame structures.

Therefore, it was decided to try to develop a macroscopic model. Experimental results had indicated that infilled frames designed and constructed in accordance with the guidelines of Section 3.4, behaved essentially as a combination of two types of structural components: 1) the frame members themselves; and 2) the infills, which strengthened the frames, stiffened them, and dissipated large amounts of energy through distributed cracking. The presence of the engineered infills changed the basic behavior from that of a bare frame, to that of a braced frame. The process of infill panel degradation greatly influenced the location of critical regions in the frame members, and, consequently, the final mechanism of the infilled frame subassemblage. However, the forces induced by the infills did not significantly reduce the available rotational ductility of the developed critical regions under cycles of reversed loading.

Based on these observations, it was decided to develop a simplified macroscopic mathematical model based on the equivalent strut concept, which had proved useful in interpreting observed experimental results [15,16]. Because the behavior of the engineered infills studied herein was so carefully controlled, it was hypothesized that a simple model would be sufficiently accurate, as well as offering obvious advantages in computational efficiency.

It was decided that the analytical model of the subassemblage should predict the following aspects of infilled frame behavior:

1) initial stiffness;
2) initial strength; and
3) degrading stiffness and strength behavior, particularly the pinching effect associated with the deterioration of infill stiffness.

To accomplish this, it was considered convenient to model the infilled frame subassemblage using two separate types of elements:

1) As was done for the bare frame analysis, multiple two-component elements would be used to model the beams. Each individual element would have linear-elastic perfectly plastic moment-rotation characteristics. Single two-component elements only would be used to model the columns.

2) As shown in Fig. 45, a pair of equivalent diagonal strut elements would be used to model each infill panel. These elements would be designed to exhibit strength, stiffness, and deterioration characteristics similar to those observed in the experiments.

Three different equivalent strut models were developed during the investigation. Each successive model involved a slight increase in complexity, and produced results more closely approximating those obtained experimentally.

6.2.1 Strut Model #1

It was hypothesized that the strut model should duplicate the following main aspects of the experimentally observed infill behavior:

1) initial stiffness and strength;

2) decreased strength with increased deformation; and

3) decreased stiffness on reloading.

A macroscopic equivalent strut element was written for the nonlinear general analysis program ANSR-I, with the mechanical characteristics indicated in Fig. 46. Note that the complete infilled frame response combines the behavior of the frame members and two equivalent diagonal struts per panel, one in each direction. The following behavior description refers to a single strut only:

1) Elastic Loading (path OA)

This is defined by

$$S = \frac{EA}{L} v$$

where S is the axial force in the strut; E is Young's modulus for the infill material, obtained as in Chapter 4; v is the axial deformation in the strut, positive values corresponding to extension; L is the length of the strut, taken here as the distance between diagonally-opposite nodes; and A is the product of the panel thickness and the effective width of the strut. This width can be calculated as shown in Appendix E.

2) Strength Envelope Curve (path AB)

This curve is defined by

$$S = Af_c(e^{\gamma v})$$

where A, S, and v are defined as above, and f_c is the compression strength as determined from prism tests. The strength degradation parameter, γ, is selected on the basis of experience. A value of 1.0 was used in all analyses described here. The envelope curve was defined by a decaying exponential because this was the simplest class of mathematical expressions reflecting the desired characteristics of decreasing strength with increased deformation. As will be noted subsequently, it is probable that some increase in accuracy could be achieved by defining the strength envelope curve in terms of more complicated classes of functions.

3) Elastic Unloading (path BC)

In this range, the strut unloads elastically, with a stiffness equal to the elastic loading stiffness of path OA.

4) Tension Curve (path CC'D)

Initially, an actual equivalent diagonal strut has some tensile resistance, due to the tensile strength of the panel material (usually very low) and the action of the panel steel (also low). Tensile cracking of the strut causes this tensile resistance to drop immediately. The tensile resistance which is available from then on is that due to the action of the panel steel alone. In developing Strut Model #1, it was decided that the complexity necessary to model this drop in tensile resistance was not justified in view of the generally minor effects of infill tensile strength. The idealized tension curve was defined by

$$S = Af_t$$

where S and A are defined as above, and f_t is a constant nominal resistance whose value is based on the observed tensile resistance of the panel reinforcement. All the strut models described here permit specification of arbitrary values of f_t. However, panel tensile resistance was not observed to have any significant effect on the behavior of the experimental models, and f_t was therefore assigned a zero value in all the analyses described herein.

5) <u>Reloading Curve</u> (path DE)

The experimental models were observed to exhibit decreased stiffness upon reloading. Therefore, this reloading curve was defined by a straight line connecting the point on the tension curve corresponding to maximum positive deformation (point D), with the point on the strength envelope curve corresponding to maximum negative deformation (point B).

6) <u>Further Elastic Cycles</u> (path EFGG'E)

Strut Model #1 was defined to exhibit elastic loading and unloading during further cycles within the area defined by the strength envelope curve, the tension curve, and the reloading curve. For example, the strut unloads elastically from point E until reaching the tension curve at point F. Decreasing deformation causes movement along the tension curve from point F to point G. Reloading in compression causes the strut to reload elastically until reaching the previously defined reloading curve at point G'. The strut then continues to reload along this curve until reaching point E again. Strut extensions beyond the deformation corresponding to point D (for instance, to point D'), cause the reloading curve to be redefined in terms of the coordinates of points B and D'. A similar redefinition takes place following compressive deformations in excess of the value corresponding to point B.

Using this Strut Model #1, the entire infilled frame subassemblage was modeled as shown in Fig. 47. This model comprised 46 elements, 18 nodes, and 40 degrees of freedom. The following material parameters were used for the equivalent strut elements:

E = 8290 MPa (1200 ksi), as determined from prism tests on clay blocks.

f_c = 2.41 MPa (3500 psi), as determined from prism tests on clay blocks.

f_t = 0.0, as explained previously.

A = 12900 mm^2 (20 in^2). This figure was obtained by multiplying the nominal thickness of the panel (51 mm, or 2 in.) times the equivalent strut width calculated in Appendix E (254 mm or 10 in.).

γ = 1.0, as explained previously.

The entire model was tested by subjecting it to the first part of the short loading program shown in Fig. 48. The results are shown in Fig. 49. The ANSR-I computer program did not allow the model to be loaded by a program of specified tip displacements. Because the analytical idealization was designed to exhibit decreasing strength for increasing deformations (beyond those required for panel cracking), a program of applied loads would clearly result in overall instability of the model after panel cracking. In order to ensure stability of the degrading structure, it was therefore necessary to restrain it laterally by means of a horizontal support spring connected to the point of lateral load application. Figure 49 (and all other similar figures in this section) shows the results with the effects of the spring removed.

Figure 49 also shows the corresponding experimentally-obtained curve from Test #4 (Fig. 22). Comparison of these two curves shows that use of Strut Model #1 produced an excellent representation of the experimentally-observed initial stiffness and strength. However, the degrading behavior was not modeled correctly. Panel damage from post-cracking excursions in one direction did not reduce the maximum panel resistance available in the opposite direction.

6.2.2 Strut Model #2

To correct the above-noted deficiency of Strut Model #1, this model was refined to exhibit the mechanical behavior shown in Fig. 50 and described below:

1) through 4) same as Strut Model #1 (path OABCC'D)

5) Reloading Curve (path DB or D'B')

As before, the strut reloads, possibly with reduced stiffness. Strut Model #2, however, defines the reloading curve in a manner slightly different from that of Strut Model #1, to reflect more accurately the effect of previous damage history on panel strength and stiffness. Experimentally, it was observed that after reaching a given resistance level in one direction, an infilled frame model was not able to develop more than this resistance in the other direction, when the load was reversed. Physically, this can be explained by the fact that the two equivalent diagonal compression struts share the portion of material at the center of the panel, and therefore are not physically independent. Suppose that a single-panel infilled frame, whose panel is idealized by two equivalent struts, is loaded laterally in the positive direction. One strut will be placed in compression, and the other one will be placed in tension. The compression strut will load elastically, reach the strength envelope curve, and suffer increasing damage as it moves along the path AB of Fig. 50. The tension strut will offer some nominal tensile resistance, and will intersect and move along the tension curve on a path such as OG'D. Now suppose the direction of the lateral load is reversed. The strut which was originally in compression will unload and go into tension along a path such as BCC'FGD. The strut which was originally in tension will now reload. How should this reloading curve be defined? For Strut Model #1, the strut which was originally in tension would reload along a reloading curve defined by a straight line connecting points D and A and would therefore eventually develop its virgin compressive resistance. Since this strut compressive resistance is initially the most significant contribution to total infilled frame lateral resistance, this would imply that the infilled frame could develop, upon loading reversal, a lateral resistance equal to the original resistance. This in fact is the type of overall analytical behavior illustrated in Fig. 49. But as noted above, this behavior is incorrect. Experimental tests showed that the infilled frame developed, upon reversal of loading, a lateral resistance equal at most to the degraded resistance in the original direction. In terms of the strut model, this implies that the strut which was originally in tension (at point D, say), will not reload along a line DA (Fig. 50), but rather along a line DB. The reloading curve for a given strut should be defined to connect the point on the tension curve corresponding to that strut's maximum positive deformation (point D), with the point on the strength envelope curve corresponding to the maximum negative deformation of the opposite strut in the same panel. However, because of the way in which element data are stored during execution of the ANSR-I program, this type of behavior was very difficult to prescribe, and an alternative procedure was therefore devised: in the range of panel deformations associated with significant panel cracking, experiments showed that the most significant panel deformation was in shear. When a panel idealized by two equivalent compression struts deforms in shear, the axial deformations of the struts are equal in magnitude but opposite in sign, and the maximum negative (compressive) deformation of a given strut is equal in magnitude to the maximum positive (tensile) deformation of the other strut. Therefore it was possible to define the reloading curve in the following manner: for the single cycle of reversed loading considered in this example, the reloading curve for a given strut should be defined to connect the point on the tension curve corresponding to that strut's maximum positive deformation (point D), with the point on the strength envelope curve corresponding to the maximum positive deformation of the same strut. This definition of the reloading curve was much easier to incorporate into the analytical model. Finally, consider extending this definition to loading programs other than the single cycle of reversal considered above: suppose an equivalent strut has been loaded onto the strength envelope curve (along path OAB, say), and then unloaded to the tension curve but without significant reversal. When that strut is reloaded, its strength will clearly not be governed by the negligible amount of damage (compressive deformation) suffered by the opposite strut. The strength of the reloaded strut will depend on the damage that it itself has suffered, i.e., on its <u>own</u> maximum <u>negative</u> (compressive) deformation. For the case of a general lateral load program, the reloading curve for a given strut was therefore defined to be the straight line connecting the point on the tension curve corresponding to that strut's maximum positive (tensile) deformation, with the point on the strength envelope curve corresponding to the maximum (absolute value) deformation--positive <u>or</u> negative--previously experienced by that <u>same</u> strut. Referring to Fig. 50, consider the following two examples: First, suppose that a strut has been loaded following the path OABCC'FGD. Because the maximum compressive deformation (point B) is greater in magnitude than the maximum tensile deformation (point D), the former will govern, and the strut will have a reloading curve defined by the straight line DB. Physically, this would represent a case in which the panel had been subjected to some load reversal, but not enough to damage the opposite strut more than the strut under consideration. Therefore, the damage in the reloading strut (a function of the maximum compressive deformation of that strut) would control. Second, suppose that a strut has been loaded following the path OABCC'FGDD'. Because the maximum compressive deformation (point B) is now less in magnitude than the maximum tensile deformation (point D'), the latter will now govern, and the strut will have a reloading curve defined by the straight line D'B', where B' and D' are located at equal distances but opposite directions from the vertical axis of Fig. 50. Physically, this would represent a case in which the panel had been subjected to severe load reversal, resulting consequently in damage to the opposite strut.

Therefore, damage to that opposite strut would control. Such damage would be a function of the maximum compressive deformation of that opposite strut, which in turn would be essentially equal - as explained above - to the maximum tensile deformation of the strut under consideration.

6) Further Elastic Cycles (path EFGG"E)

Strut Model #2 was defined identically to Strut Model #1 in this range. Because of the change in definition of the reloading curve between Strut Models #1 and #2, however, redefinitions of the reloading curve could occur following increases in maximum strut deformation in either sense. For example, referring to Fig. 50, the reloading curve DB would be redefined after strut deformations along the path DBB', or after strut deformations along the path GDD'.

With the same element properties and loading program as before, the use of Strut Model #2 produced the results shown in Fig. 51. That same figure also shows the experimental behavior observed in Test #3 (Fig. 21) for cycles of load reversal in the same deflection range. Because only the reloading curve had been changed from Strut Model #1 to Strut Model #2, the analytically predicted initial strength and stiffness continued to agree well with the experimental results. Strength degradation under monotonic load was also reproduced well. However, it may be seen that upon reversal of loading, Strut Model #2 did not produce the observed pinching effect associated with the opening of cracks in the panels.

6.2.3 Strut Model #3

To correct this deficiency, it was decided to introduce some additional refinements into the reloading behavior of Strut Model #2. As discussed in the previous subsection, this strut model exhibited linear reloading behavior. Actually, the experimental observations discussed in Section 5.7 showed that reloading behavior consisted of two distinct phases. In the first phase, the previously formed vertical panel cracks close. Until this closure is complete, the panel's lateral strength and stiffness are essentially zero. Closure occurs when the panel is returned to its undeformed configuration (or, in terms of the equivalent strut idealization, when deformations in the equivalent struts are zero). In the second phase, following panel crack closure, the panel reloads, but with reduced stiffness and strength compared to the virgin elastic behavior. In terms of the equivalent strut idealization, the compression strut reloads with reduced stiffness and strength.

In accordance with the above experimental observations, the reloading behavior of Strut Model #2 was slightly modified to produce a new model, Strut Model #3. This model exhibited the mechanical behavior which is shown in Fig. 52 and described below:

1) through 4) same as for Strut Models #1 and #2 (path OABCC'D)

5) Elastic Unloading (path DE or D'E')

As noted in Subsection 6.2.1, equivalent strut tensile resistance is due primarily to the action of the panel steel. As an equivalent strut with open tension cracks begins to reload, the steel crossing those cracks will unload. This effect is not believed to significantly affect the panel's mechanical behavior, which is dominated at this stage by the opposite strut. This elastic unloading stiffness was defined to be identical to the initial elastic stiffness (path OA). It is believed that this definition, though arbitrary, is not unreasonable.

6) Reloading Curve #1 (path EO or E'O)

This curve corresponds to the first phase of reloading discussed above. Reloading is characterized by zero stiffness and strength until the equivalent strut deformation returns to zero.

7) Reloading Curve #2 (path OB or OB')

This curve corresponds to the second phase of reloading discussed above. Reloading is characterized by reduced stiffness and strength compared to the virgin elastic behavior of path OA. Reloading curve #2 of this strut model is defined almost exactly as for Strut Model #2: for a given strut, reloading curve #2 is the straight line connecting point O with the point on the strength envelope curve corresponding to the maximum (absolute value) deformation - positive or negative - previously experienced by that same strut. The examples given in Subsection 6.2.2 may be applied almost verbatim to this case: if damage in the reloading strut controls, then reloading curve #2 will be defined from point O to point B; if damage to the opposite strut controls, the curve will be defined from point O to point B', where B' and D' are located at equal distances but opposite directions from the vertical axis of Fig. 52.

8) Further Elastic Cycles (path FGHH'F)

Strut Model #3 is identical to Strut Model #2 in this range.

As with Strut Model #2, redefinition of reloading curve #2 would occur following increases in maximum strut deformation in either sense. For example, referring to Fig. 52, reloading curve #2 (path OB) would be redefined after strut deformations along the path OBB', or after strut deformations along the path HDD'.

With the same properties as before, the complete idealized subassemblage (using Strut Model #3) was subjected to the extended loading program shown in Fig. 53. Limitations of time precluded an attempt to subject this analytical model to the exact loading programs used for the experimental tests. However, the extended analytical loading program was designed to duplicate the essential features of the experimental loading programs. Figure 54 shows the analytical results, together with the experimental behavior observed in Test #2 (Fig. 20). Comparison of these two curves shows that the use of Strut Model #3 produces an excellent representation of the experimentally observed stiffness, strength, and degradation characteristics of the entire infilled frame subassemblage, throughout a wide range of load and displacement reversals.

It should be noted that Strut Model #3 produces an analytical subassemblage model which will not in general exhibit the experimentally observed phenomenon of decreasing lateral resistance with cycles of full displacement reversal to constant maximum amplitude. Also, the analytically predicted decrease in load following initial panel crushing is in some cases slightly less than that observed experimentally. As noted in Subsection 6.2.1, Strut Model #3 could be modified to reflect this by introducing slight refinements in the envelope curve. However, it is believed that this strut model can efficiently achieve the overall objectives of the analytical portion of this investigation, and that the procedure developed here can be used in analyzing the response of large infilled frame structures which meet the guidelines of Section 7.1.

6.3 Remarks

The original objective of developing a physically reasonable mathematical model of infilled frame behavior was achieved. Unlike those studied previously, the infilled frames investigated herein were designed specifically for high energy dissipation and resistance to brittle failure under cycles of complete load and displacement reversal. The resulting controlled behavior made it possible to idealize such infilled frames using a relatively simple macroscopic idealization. A comparison of the results shown in Fig. 54 indicates that this mathematical idealization, based on the equivalent strut concept, closely approximates the stiffness, strength, and degradation characteristics of the experimental model subassemblages. The idealization applies only to infilled frames designed according to the guidelines of Section 3.4, and only to frames infilled with complete panels. Without further study, it should not be applied to partial infills, nor to infills with openings.

It is recognized that the successful use of this mathematical idealization depends on having good estimates of equivalent strut widths. As noted in Subsection 2.1.1, many formulas are available for calculating these widths. The accuracy of such formulas depends on the procedures used to derive them. The equivalent strut widths used herein were calculated in Appendix E by empirical formulas developed by Mainstone

[16]. Increasingly accurate formulas can be expected to increase the accuracy of results obtained with the analytical techniques developed herein. However, the validity of these techniques for predicting overall lateral force-deformation behavior does not depend on the correctness of any particular strut width formula.

This mathematical idealization is efficient for use in nonlinear analyses of large infilled frame structures. For example, the whole model subassemblage was analyzed using a model comprising 18 nodes, 40 degrees of freedom, and 46 members. The response throughout more than three cycles of full displacement reversal, well into the stage of extensive panel degradation, was carried out using about 100 load steps. All operations were performed in core, and required 7.0 minutes of central processor time and a total storage of 39000 decimal on the CDC-6400. It is believed that significant cost reductions could be achieved by increasing the size of the load steps used, and by judicious reduction of the amount of output data requested at each load step.

7. SUMMARY, CONCLUSIONS, AND RECOMMENDATIONS

7.1 Summary

One-third scale model structural subassemblages of a bare frame and three infilled frames were subjected to axial loads plus quasi-static cycles of reversed shear and overturning moment, simulating the principal effects of gravity loads plus earthquake-like excitations on the prototype structure. The infilled frames were designed and constructed according to the following specific guidelines:

1) The frame members (particularly the columns) should possess high rotational ductility and resistance to degradation under cycles of reversed shear loads;
2) Gradual panel degradation should be achieved by using closely-spaced infill reinforcement; and
3) The panel thickness should be limited so that the infill cracking resistance in any story will be less than the combined available shear resistance of the columns in that story.

The bare frame was subjected to several cycles of full load reversal at service load levels, followed by one-and-one-half cycles of full deflection reversal to a maximum average story drift of 0.017. The frame developed a maximum lateral resistance of about 50 kN (11.3 k), very close to the theoretical second-order rigid-plastic collapse load corresponding to a collapse mechanism with the observed pattern of critical regions. Bare frame behavior was characterized by a low initial lateral stiffness of about 50 kN/cm (27 k/in.). This was further decreased by loss of stiffness in the interior beam-column connections due to pull-through of the beam longitudinal steel. As a result, the cyclic resistance of the bare frame was limited by P-Δ effects. At its maximum deflection of 5 cm (2 in.), the normalized energy dissipation of the bare frame was about 80 kN-cm per centimeter of displacement (18 k-in. per inch).

The three infilled frames were also subjected to several cycles of full load reversals at service loads, followed by repeated cycles of full load and/or deflection reversal designed to simulate the principal effects of extreme ground motions. Under service load levels, the infilled frames behaved as monolithic deep beams, with an initial lateral stiffness of at least 250 kN/cm (143 k/in.). Increased load levels resulted in the separation of the infill panels from the frame, except at the two diagonally-opposite compression corners. This led to the development of equivalent diagonal compression struts in the panels, and therefore to a braced frame behavior by the subassemblage. Further load increases caused crushing of some of these equivalent struts, at loads in the range of 280 kN (63 k) to 320 kN (72 k). The secant stiffness of the subassemblages at these load levels was about 110 kN/cm (63 k/in.). Crushing of an equivalent strut (usually the one located in the weakest panel of the subassemblage) marked the start of serious panel degradation. The subassemblages behaved from then on as frames braced by gradually degrading struts in one or more panels.

The relative amounts of damage in each panel determined the locations of the hinge regions which then developed in the frame members near the beam-column connections. The number of hinge regions increased sufficiently to form a collapse mechanism, and the strength of the infilled frame subassemblages gradually decreased to the second-order rigid-plastic collapse load corresponding to that of the bare frame mechanism. The presence, behavior, and failure of the infill panels did not significantly reduce the rotational ductility of the frame members. In all cases, testing was continued up to average story drifts in excess of 0.03. Following the start of significant panel cracking, the normalized energy dissipation of the infilled frames was at least 150 kN/cm per centimeter of displacement (34 k/in. per inch). Throughout all deflection ranges, the infilled frames dissipated at least twice as much energy per centimeter of displacement as the bare frames. The infilled frames dissipated an average total cumulative energy in excess of 2000 kN/cm (177 k/in.), far more than the bare frame total of about 270 kN (24 k/in.).

Relatively simple macroscopic mathematical models, based on the equivalent strut concept, were developed to represent the essential aspects of the elastic and inelastic mechanical behavior of infilled frames meeting the above guidelines. These mathematical models were incorporated into ANSR-I, a recently developed general purpose computer program for nonlinear structural analysis, and this was used to study the analytically-predicted response of the tested subassemblages.

7.2 Conclusions

Infilled frames designed and constructed in accordance with the guidelines stated in Section 7.1 have several advantages over comparable bare frames, particularly if they may be subjected to strong ground motions.

Owing to the increased stiffness (500%) and maximum lateral strength [from 50 kN (11.3 k) to 300 kN (67 k)] provided by infills, behavior is greatly improved under service loads, moderate ground shaking, and even under the largest expected excedance of standard live loads. The increase in strength and energy absorption and dissipation capacities achieved by the addition of engineered infills is so large that it far exceeds the detrimental effects of possible increases in inertial forces due to increased stiffness and consequent decrease in period.

For severe ground motions demanding elastic base shears in excess of that corresponding to the bare frame rigid-plastic collapse load, the stiffness provided by infills significantly reduces the influence of P-Δ effects on seismic response. Significant panel cracks occurred at tip deflections of at least 13 mm (0.5 in.), corresponding to average story drifts of 0.004. Prior to this, infilled frame damage was limited to cracks less than 2 mm (1/16 in.) in width.

Even under extreme ground motions demanding average story drifts in excess of 0.02, the engineered infilled frame is superior to the bare frame with respect to energy dissipation and resistance to incremental collapse. A bare frame dissipates energy primarily through large inelastic rotations at hinge regions near beam-column connections. Strain-hardening at these regions often results in anchorage deterioration at beam-column connections. The consequent loss of connection stiffness increases the danger of incremental collapse of the bare frame. However, in the engineered infilled frame, the panels dissipate very large amounts of energy through hysteretic behavior (friction across panel cracks, accompanied by gradual degradation of the panel's initially high stiffness and strength). Because of this, the danger of incremental collapse is reduced.

Procedures have been described for developing macroscopic mathematical models predicting the essential aspects of experimentally observed behavior. When used with a modern, general purpose nonlinear analysis program, these models predict theoretical behavior agreeing very well with observed experimental results, in all response stages. It is believed that these procedures can be applied to other infilled frames meeting the guidelines of Section 7.1.

7.3 Aseismic Design Implications

Designers should be aware of the fundamental differences between the inelastic seismic responses of conventional ductile frames, ductile shear walls, and engineered infilled frames. These differences are discussed in Sections 5.2, 7.1, and 7.2.

Because infilled frames engineered according to the basic guidelines of Section 7.1 are clearly superior to comparable bare frames in all response stages, designers should be encouraged to use them instead of bare frames filled only by conventional brittle infills or architectural panels. Efficient design against strong earthquakes demands the elimination, whenever possible, of relatively heavy elements (such as partitions) which do not contribute directly to overall structural resistance. Purely architectural elements should be replaced by efficient structural components such as engineered infills, which can also serve architectural functions. The design of the building should be carried out considering the distinct stiffness and strength contributions of all available resistance mechanisms (e.g. ductile shear walls, ductile frames, engineered infilled frames) to overall structural response under all seismic excitation limit states. It is believed that the additional design and construction expense involved in such a procedure will be justified by increased safety due to structural redundancy, and by decreases in some costs due to the more efficient use of infill or partition materials.

If the results of this study are corroborated by subsequent investigations, efforts should be made to incorporate the engineered infilled frame concept into applicable building codes. In particular, it is believed that results similar to those obtained herein, can be achieved using prefabricated reinforced concrete panels. These would be considerably cheaper than unit masonry, and also more consistent with current construction practices in this country. Concrete panels would also be less susceptible to the face-shell spalling which characterized the degradation of the unit masonry infills studied herein. This spalling was observed to occur at average story drifts in excess of about 0.015. Although the spalled pieces measured at most 10 cm (4 in.) across, it is realized that such debris could represent a hazard, particularly with respect to exterior panels. Damage from falling debris would have to be prevented in such cases by providing appropriate external reinforcement to hold in any spalled debris.

This study was concerned with complete infill panels only. It is believed that such infills are desirable because of their greater strength and energy dissipation capacity compared to panels with door or window openings, or with a gap between the panel and the frame. However, as long as the infilled frames are designed in accordance with the guidelines of Section 7.1, the use of complete infills is probably not essential to the avoidance of brittle frame failure. Similarly, while the workmanship of the frames themselves is vital, inferior panel workmanship will probably lead to decreased performance but not to brittle failure of the frame.

7.4 Recommendations

The results of this study suggest further investigation in the following areas:

To investigate the performance of engineered infills made of other materials besides unit masonry, e.g. cast-in-place concrete, precast concrete (single and multiple panels), or gunite. Emphasis should be placed on the use of panels made of lightweight aggregate concrete.

To investigate the relatively importance of panel steel spacing as opposed to panel steel percentage by testing infills with less reinforcement than those considered herein.

To refine the design procedures necessary to meet the basic guidelines of Section 7.1, and to extend those procedures to the case of partial infills or infills with openings.

To refine the macroscopic analytical model and confirm its practicality for the analysis of large infilled frame structures.

To investigate the predicted dynamic response of engineered infilled frame subassemblages to base excitation, using the macroscopic mathematical models developed in Chapter 6.

To compare this predicted response with that obtained experimentally using infilled frame subassemblages mounted on a shaking table.

To study ways in which the engineered infilled frame concept developed herein could be adapted to meet the need for economical earthquake-resistant structures in developing countries.

REFERENCES

1. Hanson, Robert D. and Degenkolb, Henry J., The Venezuelan Earthquake, July 29, 1967, AISI, 1969.

2. Glogau, O. A., "Masonry Performance in Earthquakes", Bulletin of the New Zealand National Society for Earthquake Engineering, Vol. 7, no. 4, December, 1974.

3. Uzsoy, S. Z. and Citipitioglu, E., "Influence of Infill Walls on Building Frames: An Example from the May 12, 1971 Earthquake in Turkey", Bulletin of the Seismological Society of America, 62, 5, October 1972.

4. Benjamin, Jack R. and Williams, Harry A., "The Behavior of One-Story Reinforced Concrete Shear Walls", Journal of the Structural Division, ASCE, May 1957.

5. Benjamin, Jack R. and Williams, Harry A., "The Behavior of One-Story Brick Shear Walls", Journal of the Structural Division, ASCE, July 1958.

6. Polyakov, S. V., "Masonry in Framed Buildings: An Investigation into the Strength and Stiffness of Masonry Infilling", (English translation), Moscow, 1957.

7. Holmes, Malcolm, "Steel Frames with Brickwork and Concrete Infilling", Institution of Civil Engineers (ICE), vol. 19, 1961

8. Holmes, Malcolm, "Combined Loading on Infilled Frames", Institution of Civil Engineers (ICE), vol. 25, 1963.

9. Stafford Smith, Bryan, "Lateral Stiffness of Infilled Frames", Journal of the Structural Division, ASCE, December 1962.

10. Stafford Smith, Bryan, "Behavior of Square Infilled Frames", Journal of the Structural Division, ASCE, February 1966.

11. Stafford Smith, Bryan, "The Composite Behavior of Infilled Frames", Proceedings of the Symposium on Tall Buildings, University of Southampton, April 1966, Pergamon Press, 1967

12. Stafford Smith, Bryan, "Model Test Results of Vertical and Horizontal Loading of Infilled Frames", ACI Journal, August 1968.

13. Stafford Smith, Bryan and Carter, C., "A Method of Analysis for Infilled Frames", Institution of Civil Engineers (ICE), vol. 44, September/December 1969.

14. Mainstone, R. J., "On the Stiffnesses and Strengths of Infilled Frames", Current Paper CP 2/72, Building Research Station, February 1972. Reprinted from Proceedings, Institution of Civil Engineers, 1971 Supplement (iv), Paper 7360 S.

15. Mainstone, R. J. and Weeks, G. A., "The Influence of a Bounding Frame on the Racking Stiffness and Strengths of Brick Walls", Current Paper CP 3/72, Building Research Station, February 1972. Also published in Proceedings, Second International Brick Masonry Conference (SIBMAC), 1971.

16. Mainstone, R. J., "Supplementary Note on the Stiffnesses and Strengths of Infilled Frames", Current Paper CP 13/74, Building Research Station, February 1974.

17. Esteva, Luis, "Behavior Under Alternating Loads of Masonry Diaphragms Framed by Reinforced Concrete Members", Proceedings of the International Symposium on the Effects of Repeated Loading of Materials and Structures (RILEM), Vol. V, Mexico City, 1966.

18. Alexander, C. M. et al., "Cyclic Load Tests on Shear Wall Panels", Proceedings of the Fifth World Conference on Earthquake Engineering, Rome, 1972.

19. Kahn, L. F., "Reinforced Concrete Infilled Shear Walls for Aseismic Strengthening", Report Nos. UMEE 76R1 and UMEE 76R2, Dept. of Civil Engineering, University of Michigan, Ann Arbor, 1976.

20. Fiorato, A. E., Sozen, M. A. and Gamble, W. L., "An Investigation of the Interaction of Reinforced Concrete Frames with Masonry Filler Walls", University of Illinois, Nov. 1970.

21. Leuchars, J. M. and Scrivener, J. C., "Masonry Infill Panels Subjected to Cyclic In-Plane Loading", Proceedings of the South Pacific Regional Conference of the New Zealand National Society for Earthquake Engineering, Wellington, N.Z., May 1975.

22. Moss, P. J. and Carr, A. J., "Aspects of the Analysis of Frame-Panel Interaction", Bulletin of the New Zealand Society for Earthquake Engineering, Vol. 4, no. 1, March 1971.

23. Cervenka, V., "Inelastic Finite Element Analysis of Reinforced Concrete Panels Under In-Plane Loads", Ph.D. Dissertation, Dept. of Civil Engineering, University of Colorado, Boulder, 1970.

24. Biggs, J. M. and Grace, Peter H., "Seismic Response of Buildings Designed by Code for Different Earthquake Intensities, MIT Structural Publication No. 358, Massachusetts Institute of Technology, January 1973.

25. Uniform Building Code, 1970 Edition, Volume I, International Conference of Building Officials, 1970.

26. Wilson, E. L. and Dovey, H. H., "Static and Earthquake Analysis of Three Dimensional Frame and Shear Wall Buildings", Report No. EERC 72-1, Earthquake Engineering Research Center, University of California, Berkeley, May 1972.

27. Building Code Requirements for Reinforced Concrete (ACI 318-71), American Concrete Institute, 1971.

28. Newmark, N. M. and Hall, W. I., "Procedures and Criteria for Earthquake Resistant Design", Building Standards for Disaster Mitigation, National Bureau of Standards, Building Science Series 46, February 1973.

29. Newmark, N. M., "Current Trends in the Seismic Analysis and Design of High Rise Structures", Earthquake Engineering, Prentice-Hall, Inc., Englewood Cliffs, N.J., 1970.

30. El-Hafez, M. B. and Powell, G. H., "Computer Aided Ultimate Load Design of Unbraced Multistory Steel Frames", Report No. EERC 73-3, Earthquake Engineering Research Center, University of California, Berkeley, 1973.

31. Kent, D. C. and Park, R., "Flexural Members with Confined Concrete", Journal of the Structural Division, ASCE, Vol. 97, no. ST 7, July 1971.

32. Mahin, S. A. and Bertero, V. V., "An Evaluation of Some Methods for Predicting Seismic Response of Reinforced Concrete Buildings, Report No. EERC 75-5, Earthquake Engineering Research Center, University of California, Berkeley 1975.

33. A.I.J. Building Code Requirements for Reinforced Concrete and their Commentaries, Architectural Institute of Japan, April, 1971 (in Japanese).

34. Schoolhouse Section Circular Nos. 9 and 10 (High Lift Grouting Method), State of California Office of Architecture and Construction, 1968. Reprinted in 1974 Masonry Codes and Specifications, Masonry Industry Advancement Committee, 1974.

35. Bertero, V. V., et. al., "Pseudo-Dynamic Testing of Wall Structure Systems", Proceedings of the ASCE-EMD Specialty Conference, University of California, Los Angeles, March 1976.

36. Bertero, V. V., "Identification of Research Needs for Improving Aseismic Design of Building Structures", Report No. EERC 75-27, Earthquake Engineering Research Center, University of California, Berkeley, 1975.

37. Kupfer, Helmut, Hilsdorf, Hubert K. and Rusch, Hubert, "Behavior of Concrete Under Biaxial Stress", ACI Journal, August 1969.

38. Yokel, Felix and Fattal, S. George, "A Failure Hypothesis for Masonry Shear Walls", NBSIR 75-703, Center for Building Technology, National Bureau of Standards, May 1975.

39. Mondkar, D. P. and Powell, G. H., "ANSR-I: General Purpose Program for Analysis of Nonlinear Structural Response", Report No. EERC 75-37, Earthquake Engineering Research Center, University of California, Berkeley, 1975.

40. Row, D., Ph.D. thesis in preparation, University of California, Berkeley.

41. Franklin, H. A., "Nonlinear Analysis of Reinforced Concrete Frames and Panels", UC - SESM Report No. 70-5, Dept. of Civil Engineering, University of California, Berkeley, March 1970.

42. Wang, T. Y., Bertero, V. V., and Popov, E. P., "Hysteretic Behavior of Reinforced Concrete Framed Walls", Report No. EERC 75-23, Earthquake Engineering Research Center, University of California, Berkeley, 1975.

43. Uniform Building Code Standards, 1973 Edition, International Conference of Building Officials, 1973.

44. Mayes, R. L. and Clough, R. W., "State-of-the-Art in Seismic Shear Strength of Masonry - An Evaluation and Review", Report No. EERC 75-21, Earthquake Engineering Research Center, University of California, Berkeley, 1975.

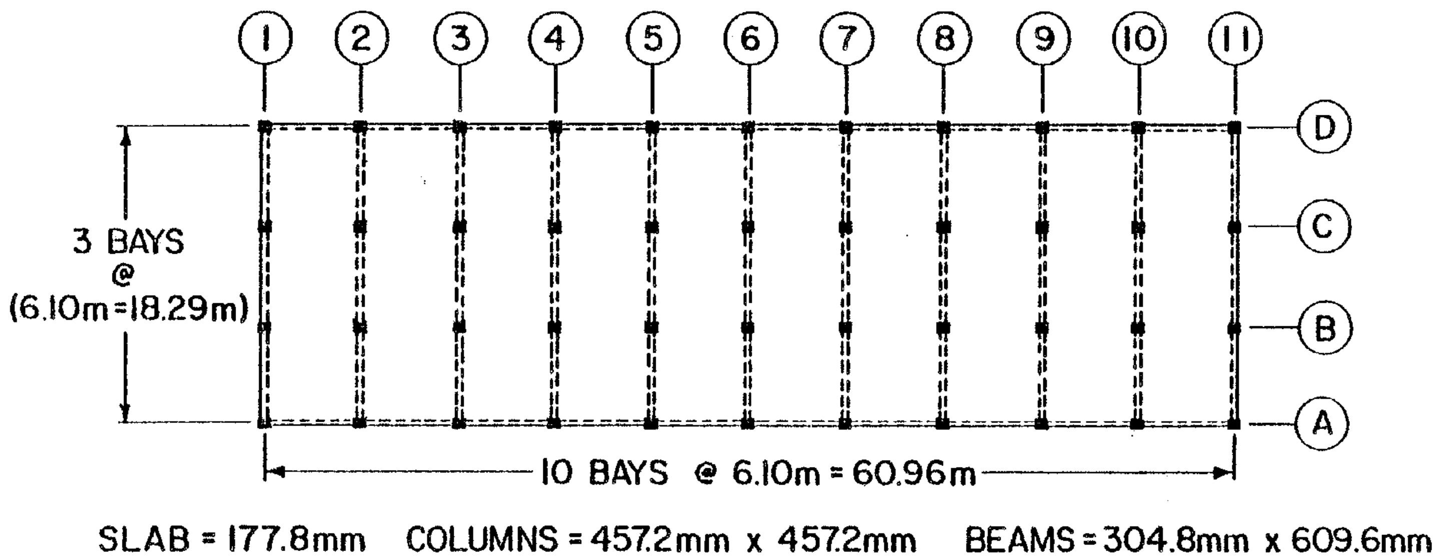

FIG. 1 PLAN VIEW OF PROTOTYPE BUILDING

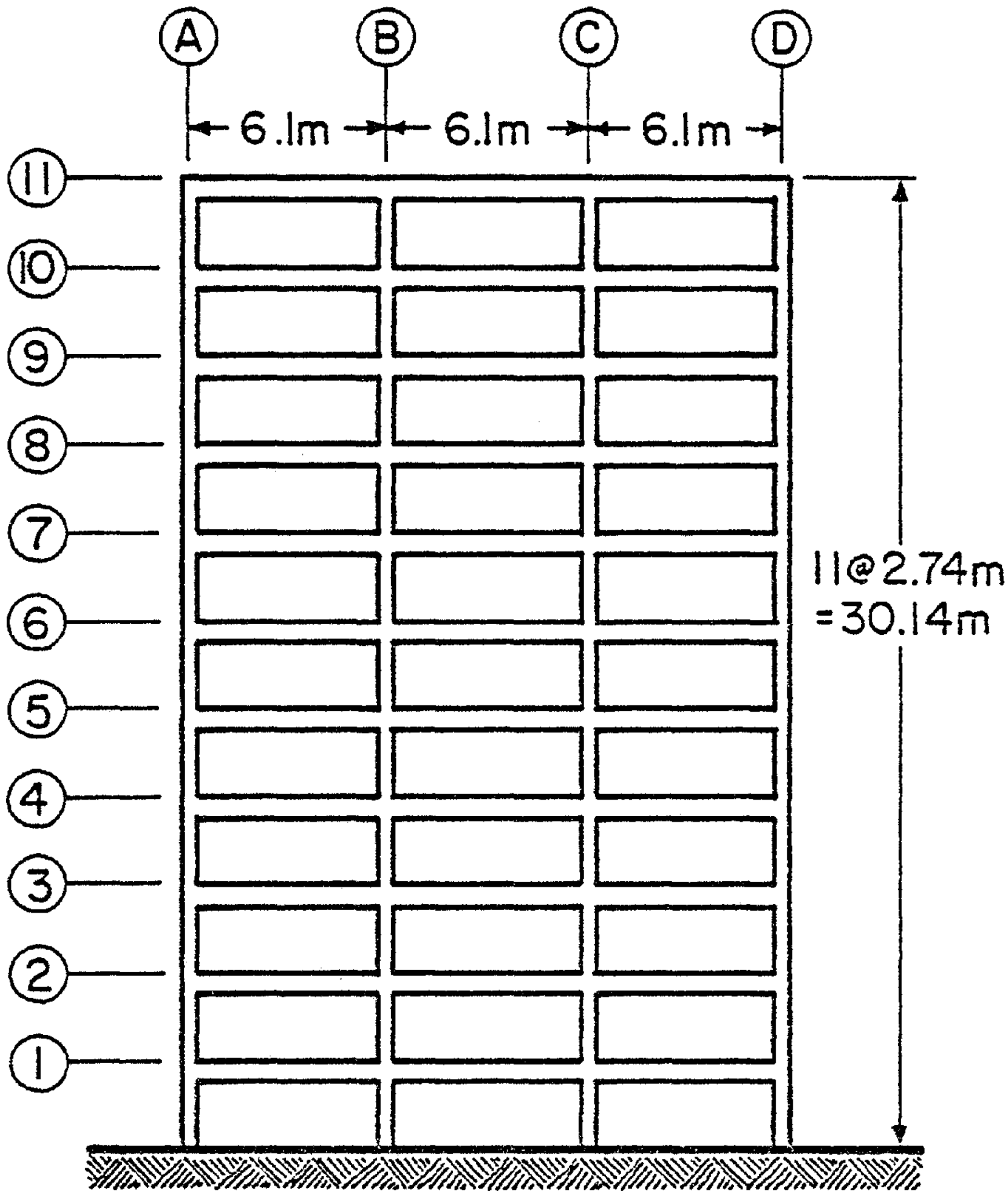

FIG. 2 ELEVATION OF PROTOTYPE END FRAME

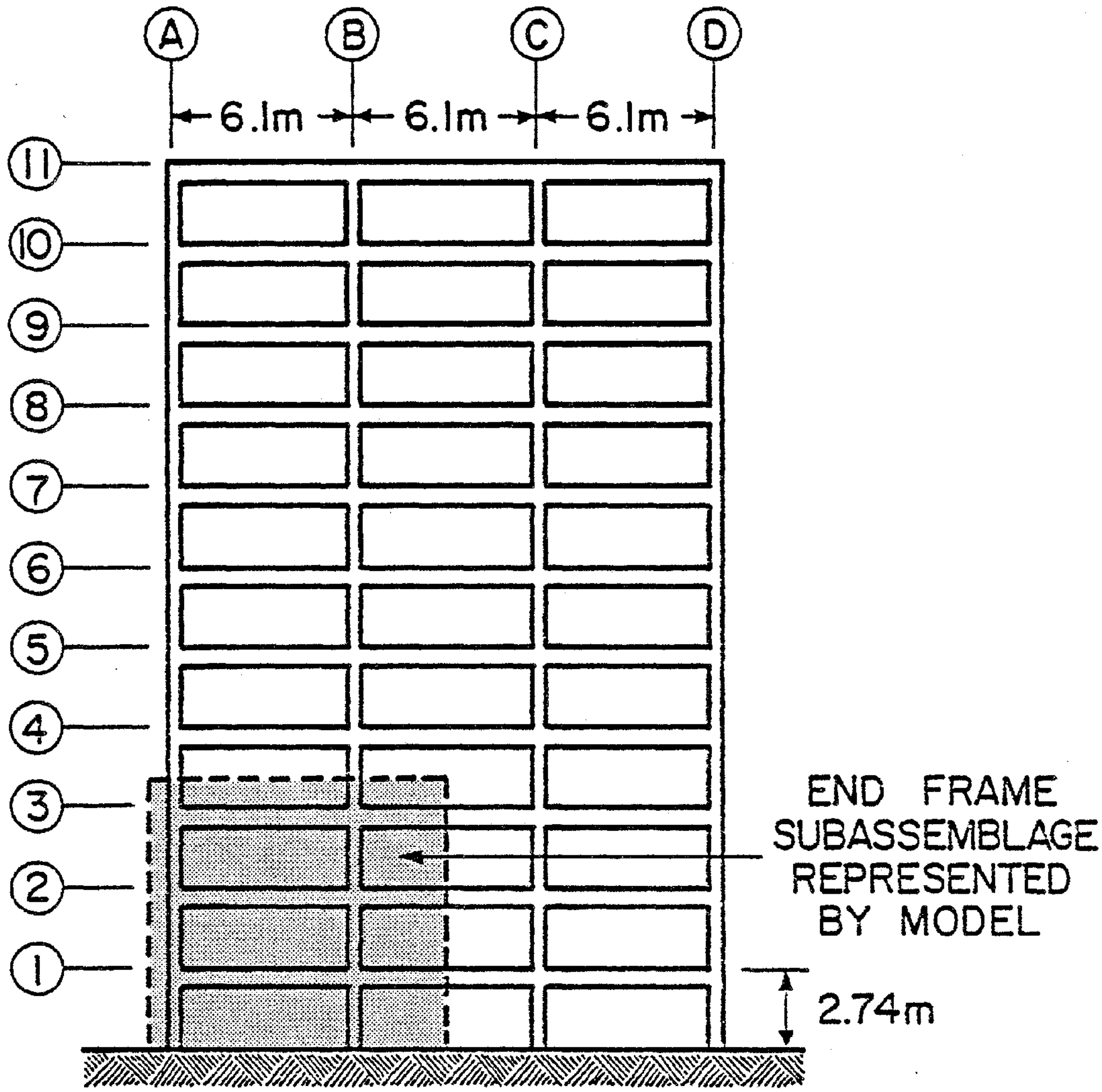

FIG. 3 END FRAME ELEVATION SHOWING LOCATION OF SUBASSEMBLAGE

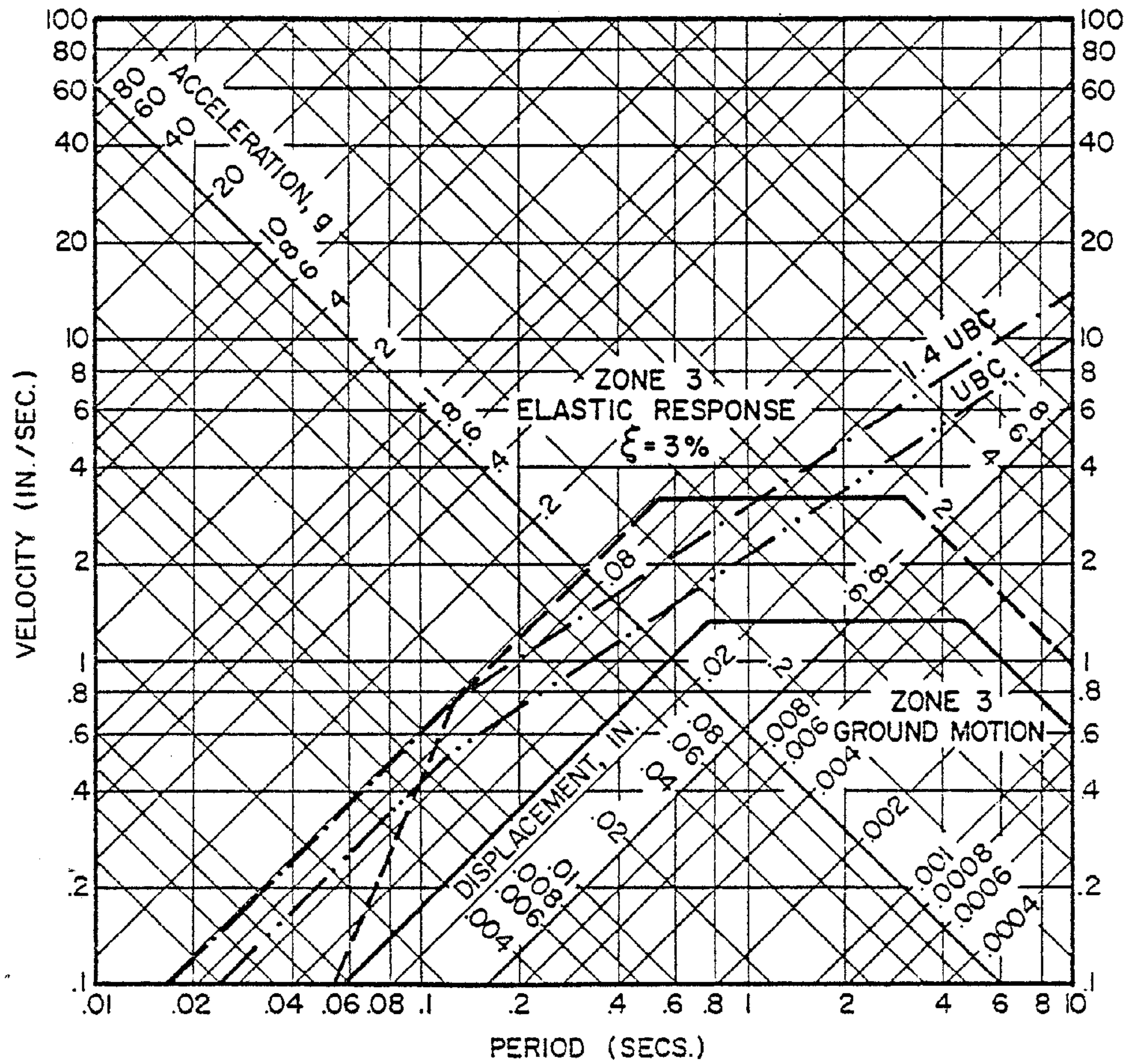

FIG. 4 ELASTIC DESIGN SPECTRA

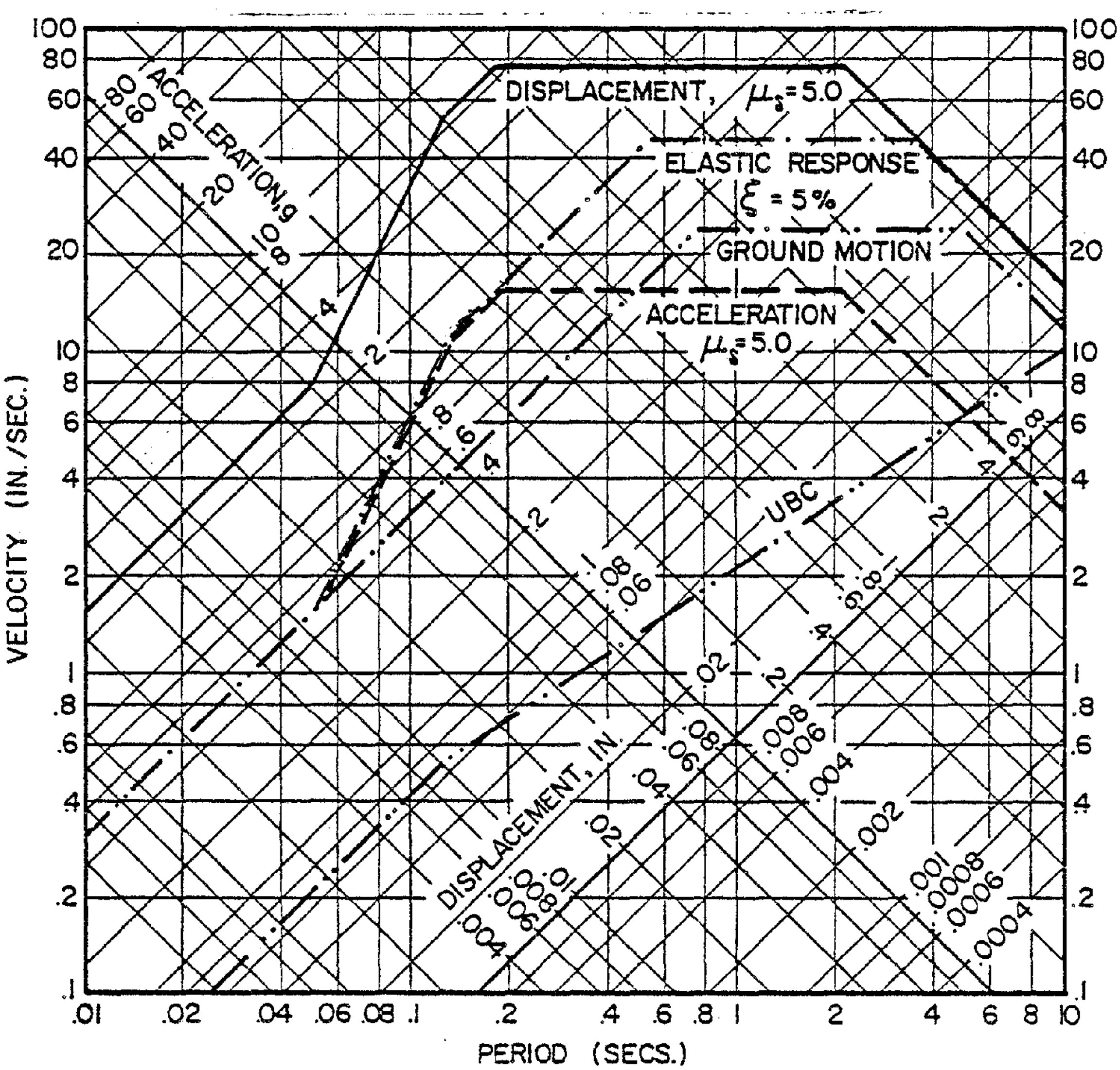

FIG. 5 ELASTO-PLASTIC DESIGN SPECTRA

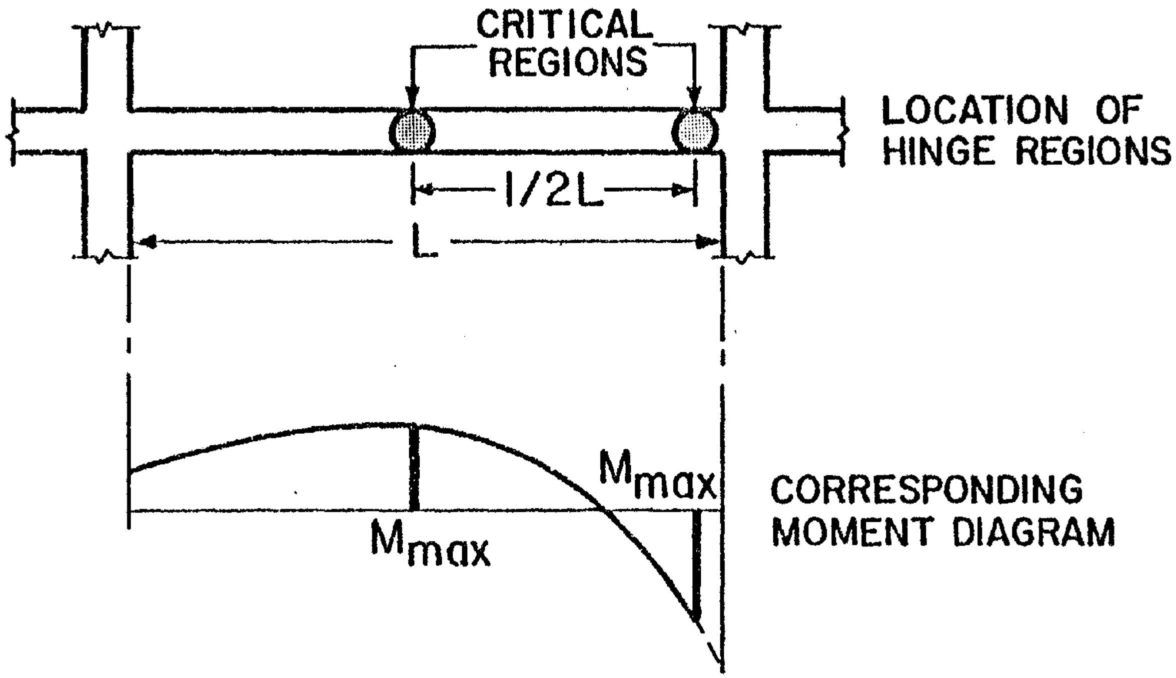

FIG. 6 LOCATION OF CRITICAL REGIONS FOR DESIGN OF BEAMS AGAINST SHEAR

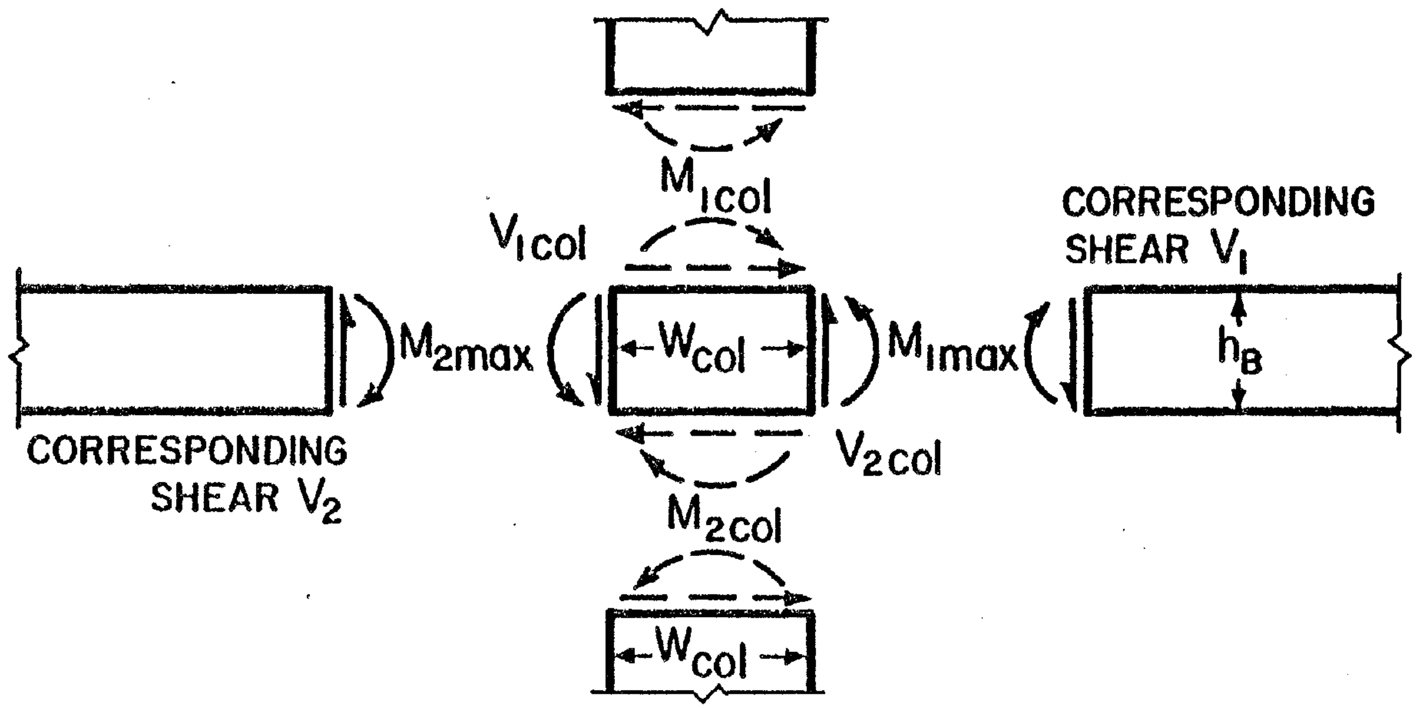

$$M_{1col} + M_{2col} = \left[M_{1max} + M_{2max} + \frac{W_{col}}{2}(V_1 + V_2) - \frac{h_B}{2}(V_{1col} + V_{2col})\right]$$

FIG. 7 CRITERION USED FOR STRONG-COLUMN, WEAK-BEAM DESIGN

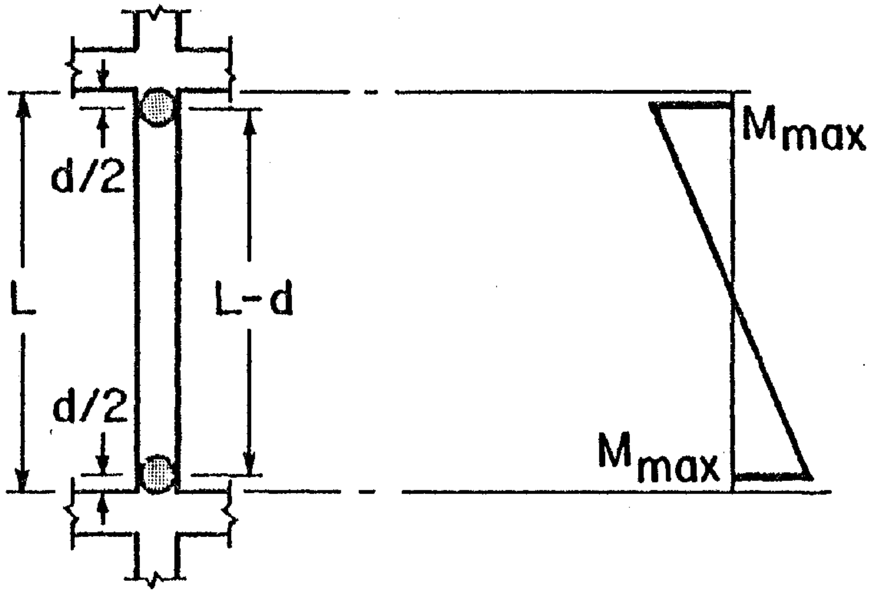

LOCATION OF CRITICAL REGIONS

CORRESPONDING MOMENT DIAGRAM

FIG. 8 LOCATION OF CRITICAL REGIONS FOR DESIGN OF COLUMNS AGAINST SHEAR

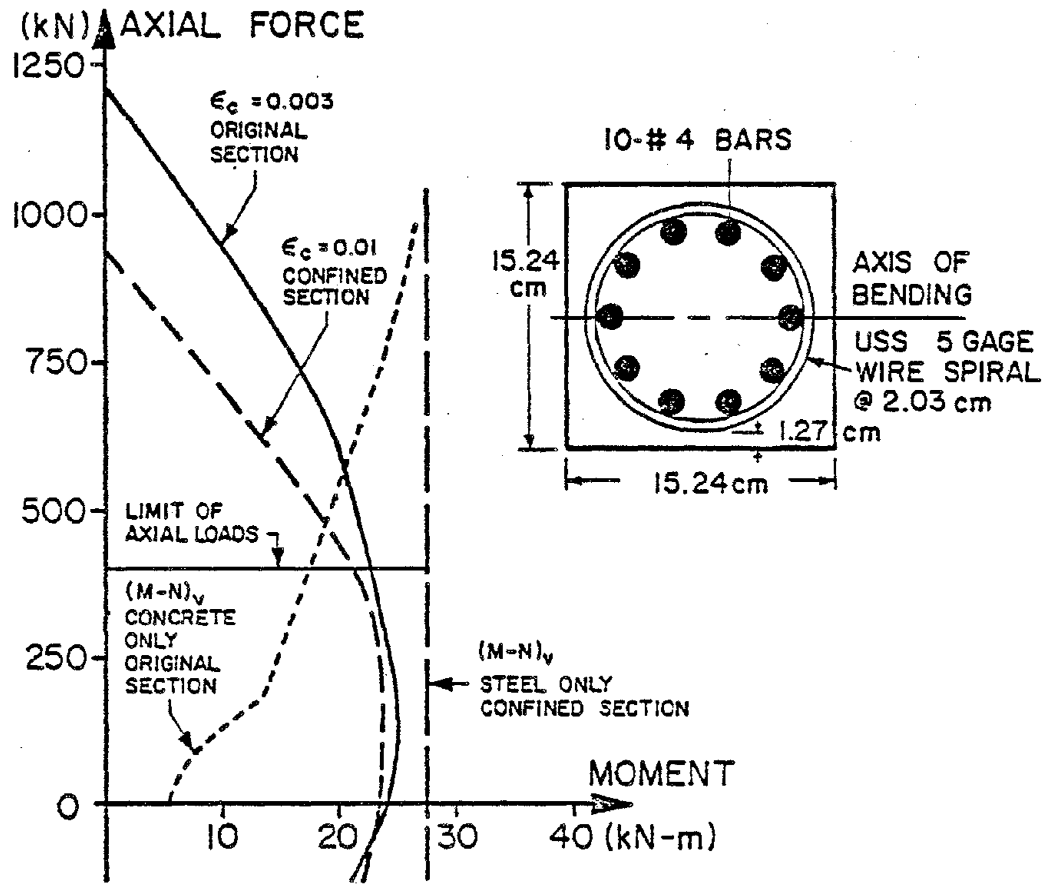

FIG. 9 MOMENT-AXIAL FORCE INTERACTION DIAGRAM FOR MODEL COLUMN

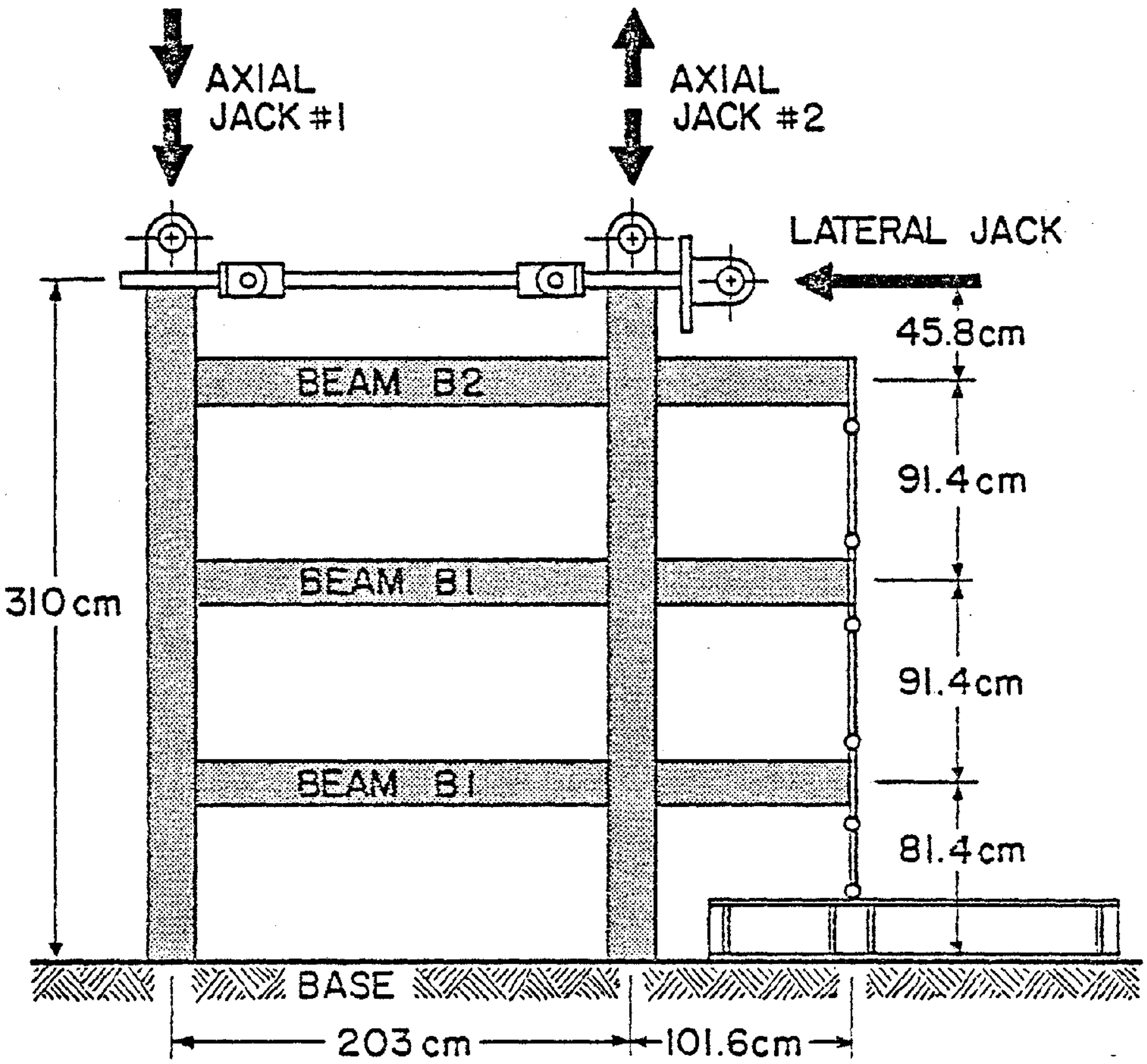

FIG. 10a BARE FRAME SPECIMEN

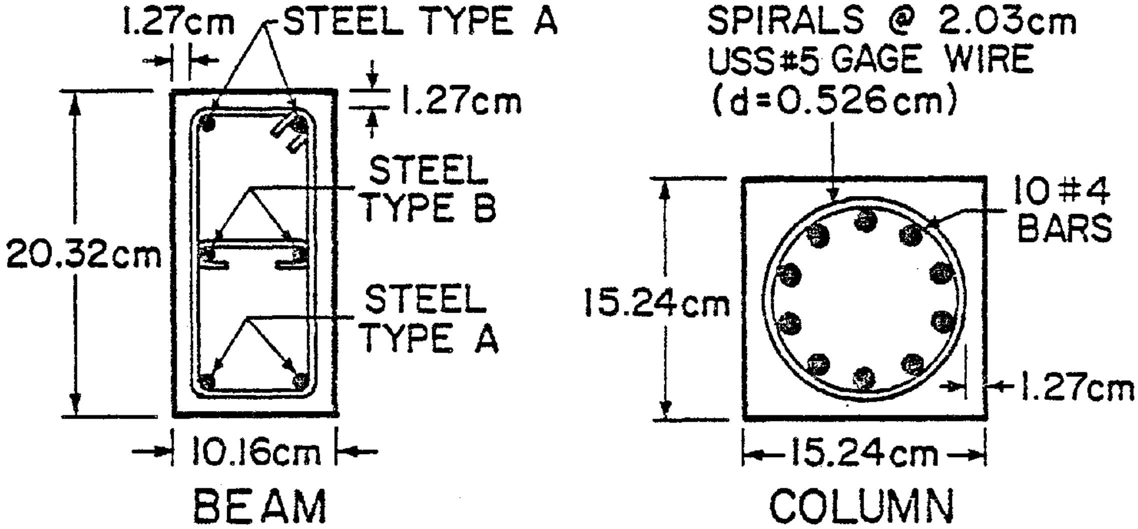

	STEEL TYPE		
BEAM TYPE*	A	B	TRANSVERSE REINFORCEMENT
B 1	#3	#2 DEFORMED	HOOPS AND CROSSTIES @ 2.54 cm
B 2	#3	USS #11 GAGE WIRE	USS #11 GAGE WIRE (d = 0.306 cm)

GRADE 60 STEEL

*REFER TO FIG. 10a

NOMINAL f_y= 414 MPa

FIG. 10b DESIGN DETAILS OF FRAME MEMBERS

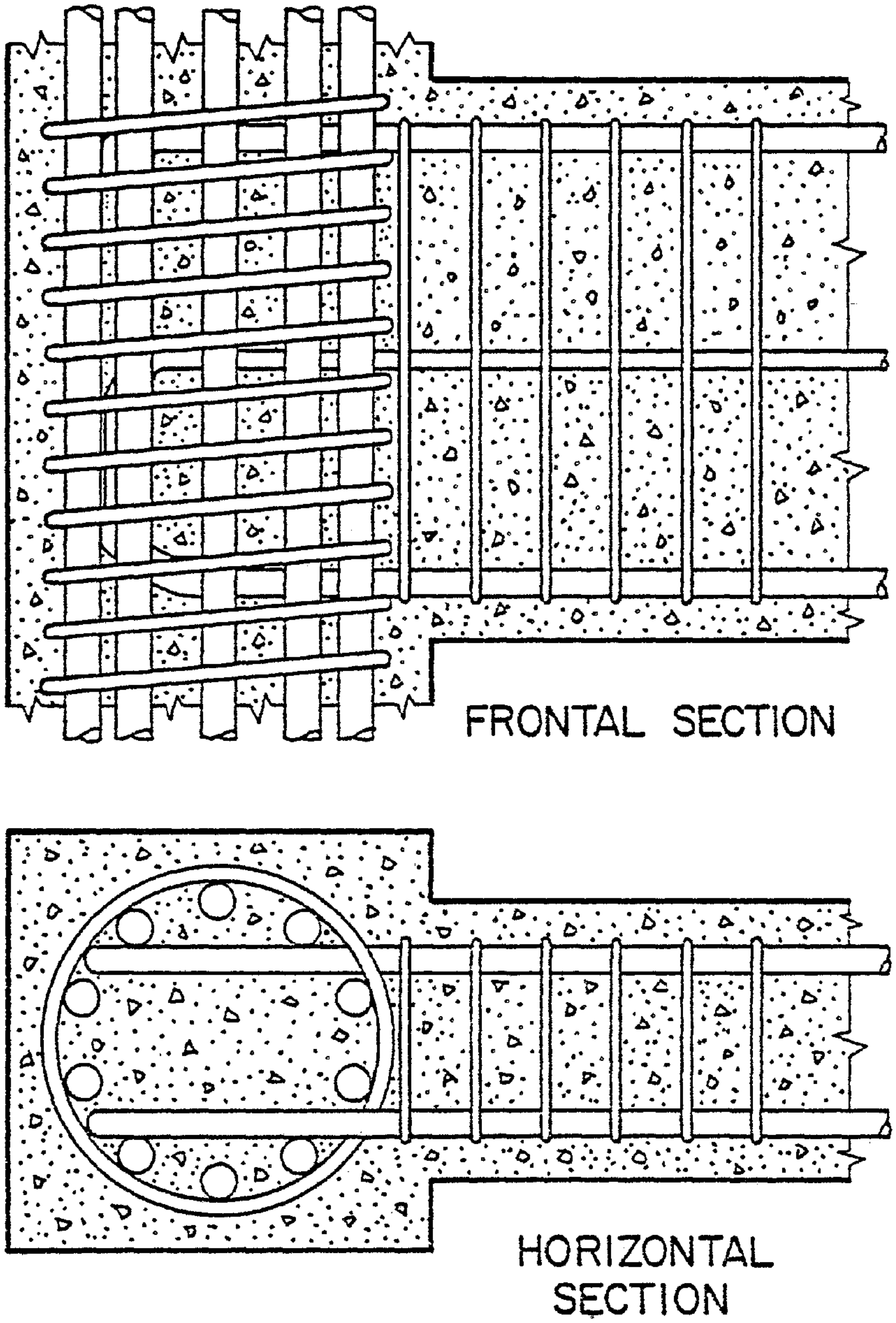

FIG. 10c DETAIL OF FIRST-FLOOR EXTERIOR BEAM-COLUMN CONNECTION

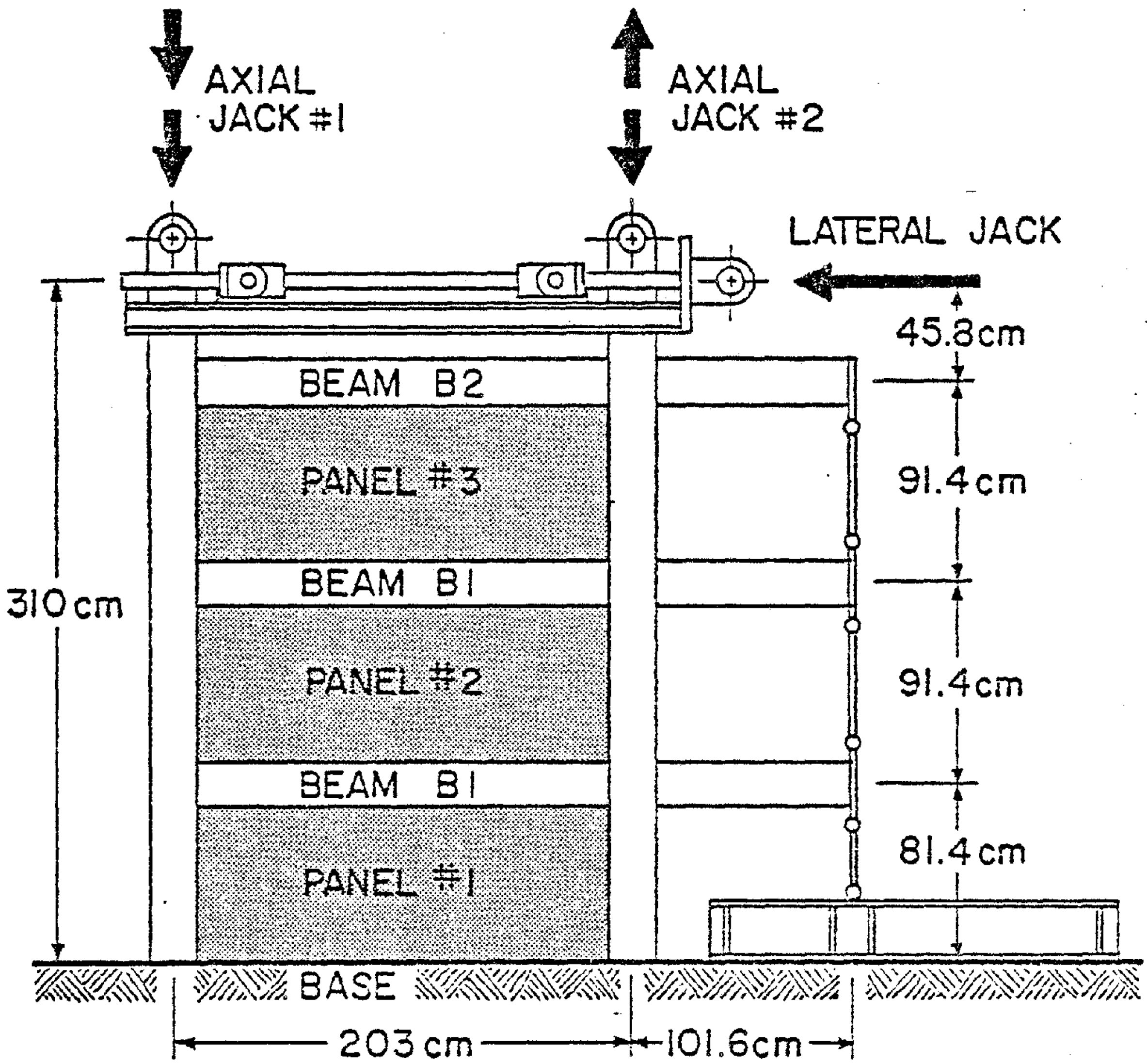

FIG. 10d INFILLED FRAME SPECIMEN

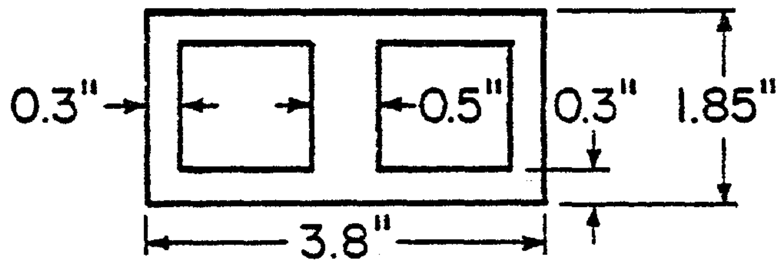

CLAY UNIT 1 in. HIGH (NOMINAL)

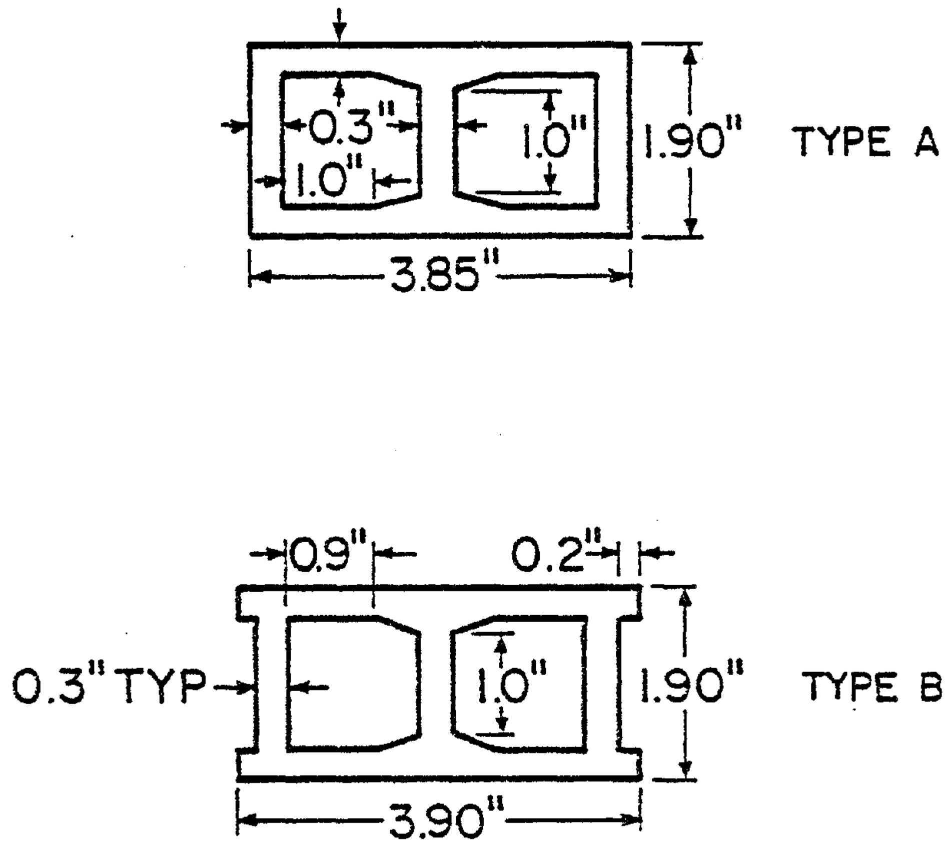

CONCRETE UNITS 2 in. HIGH (NOMINAL)

FIG. 11 MODEL BLOCK UNITS

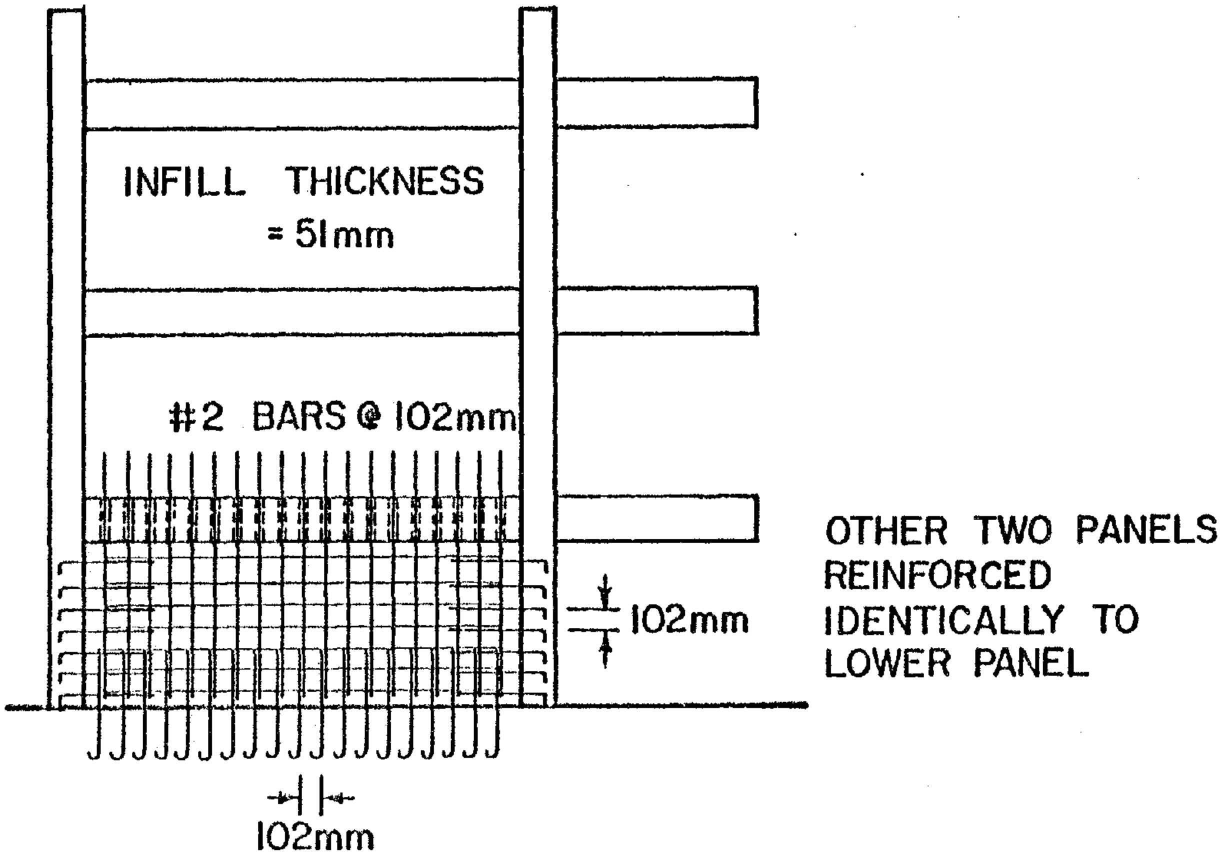

FIG. 12 INFILL PANEL REINFORCEMENT DETAIL

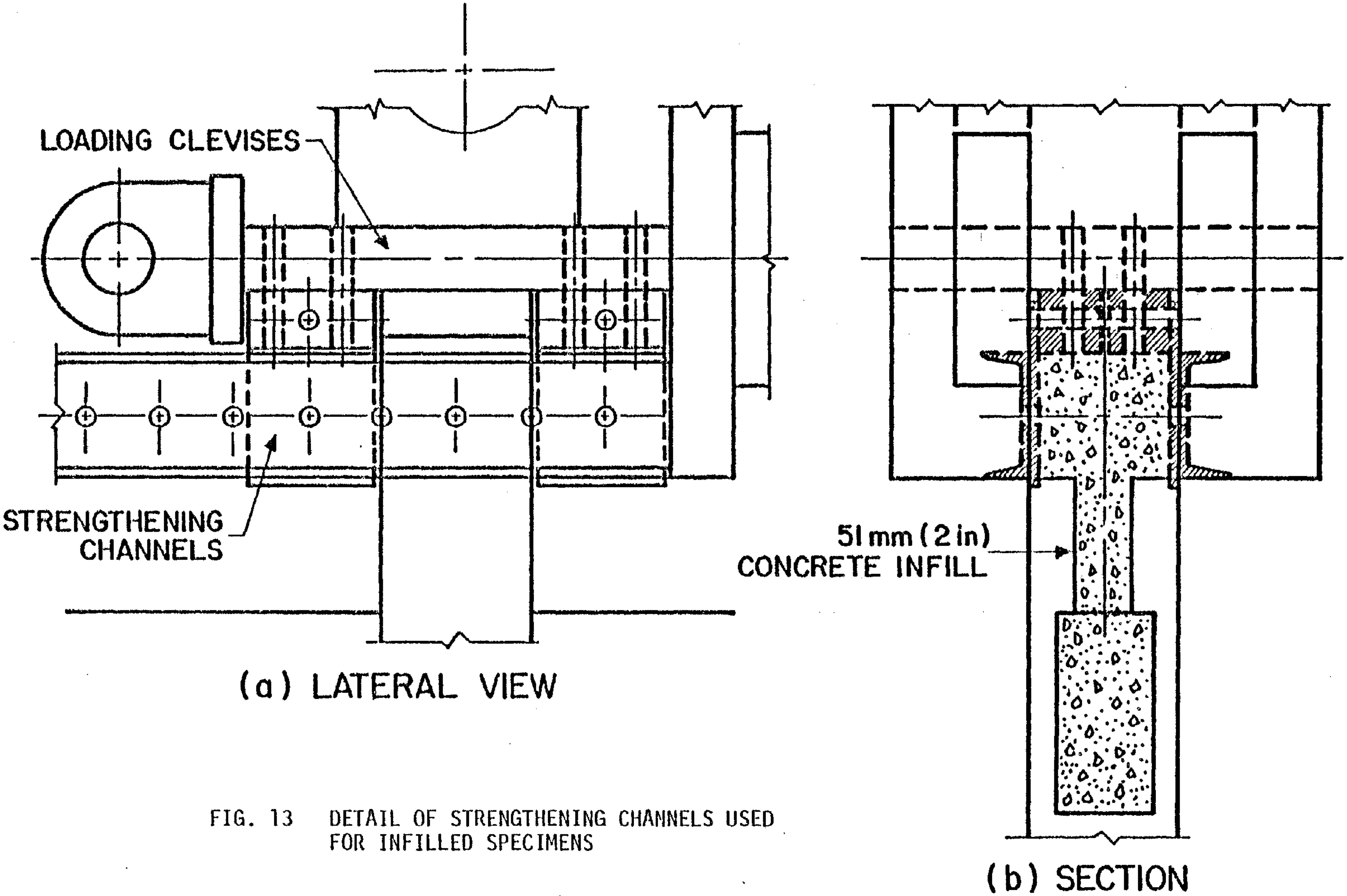

FIG. 13 DETAIL OF STRENGTHENING CHANNELS USED FOR INFILLED SPECIMENS

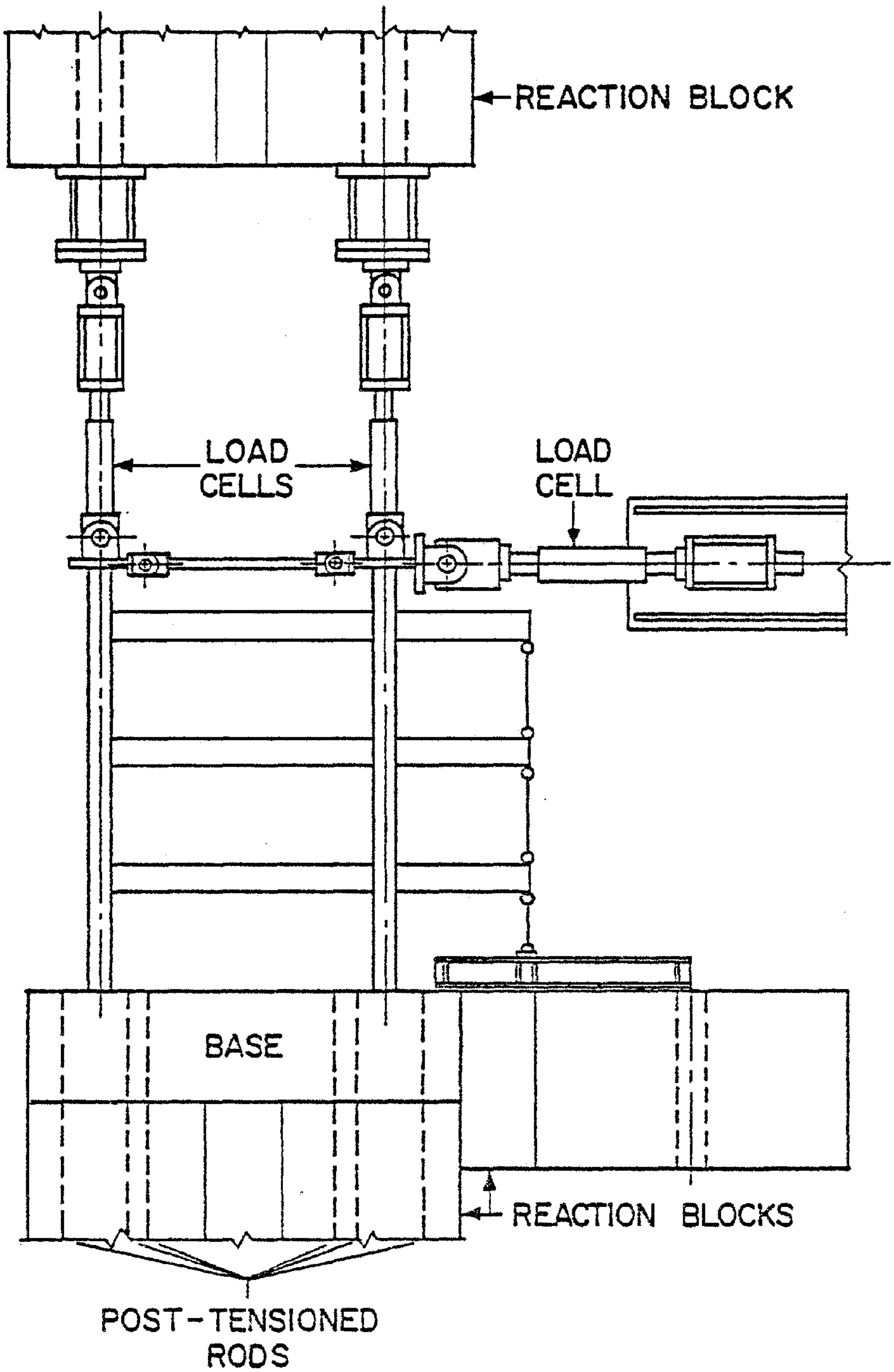

FIG. 14a TEST SETUP

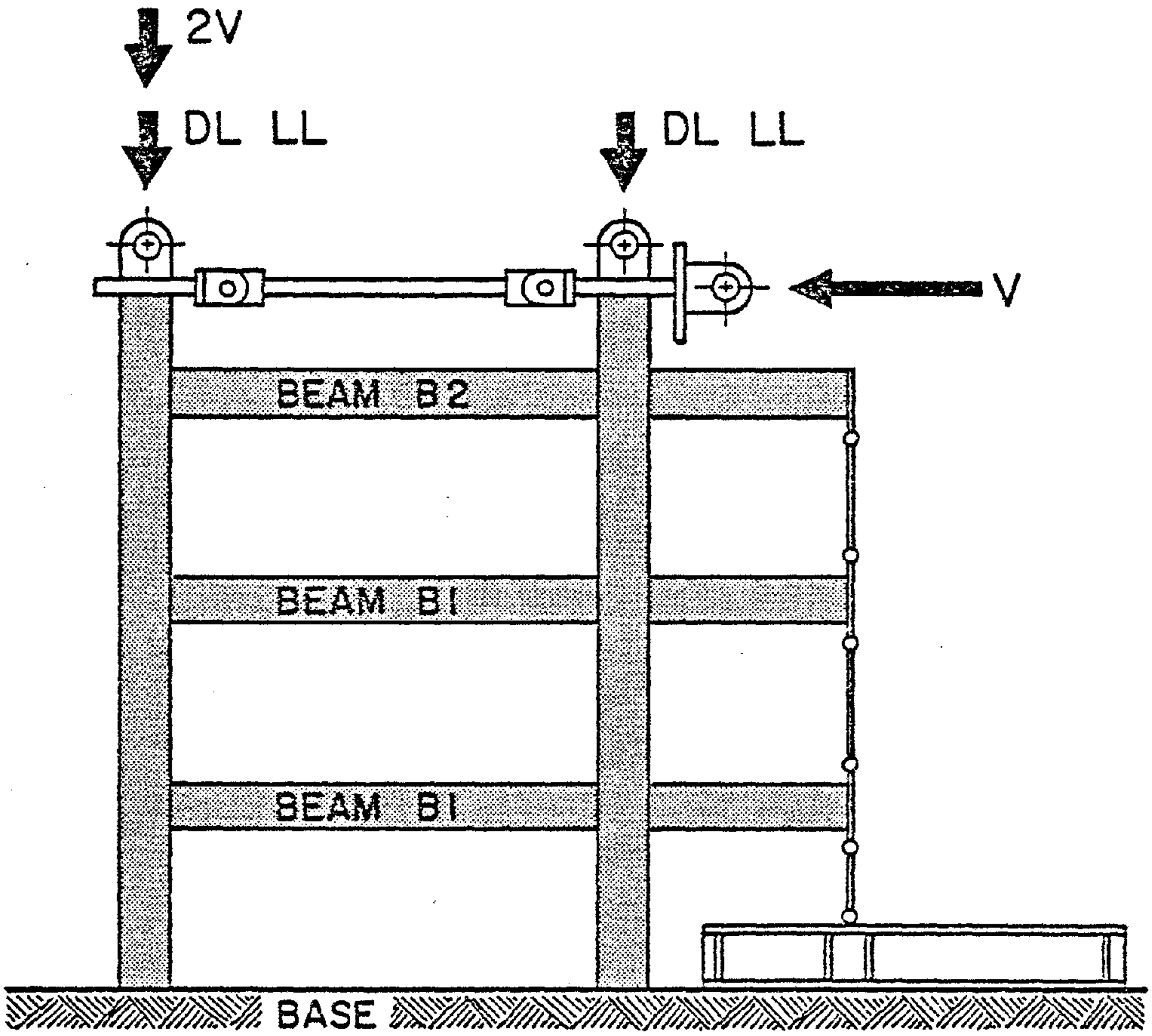

FIG. 14b LOADING PATTERN USED FOR BARE FRAME

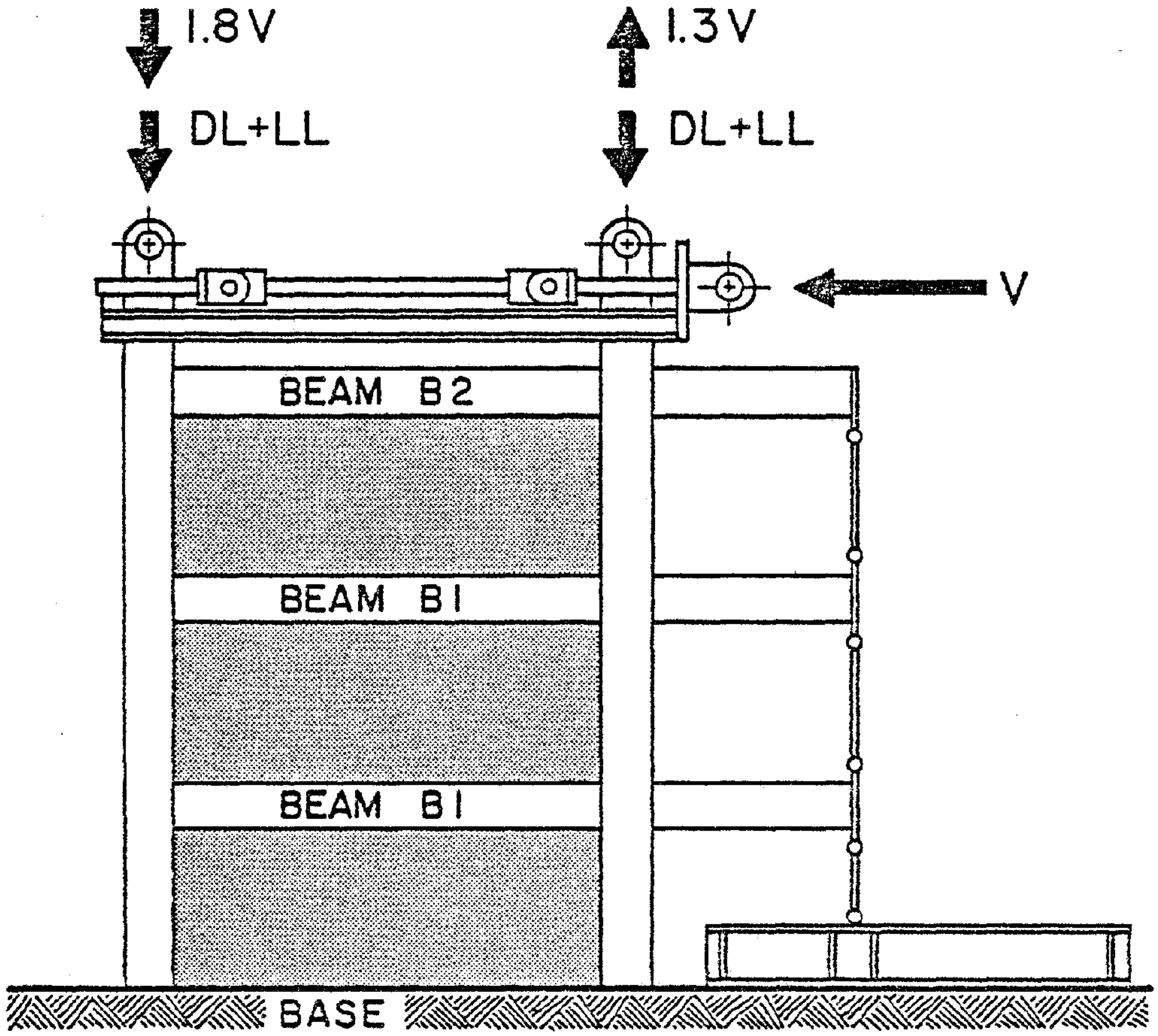

FIG. 14c LOADING PATTERN USED FOR INFILLED FRAMES

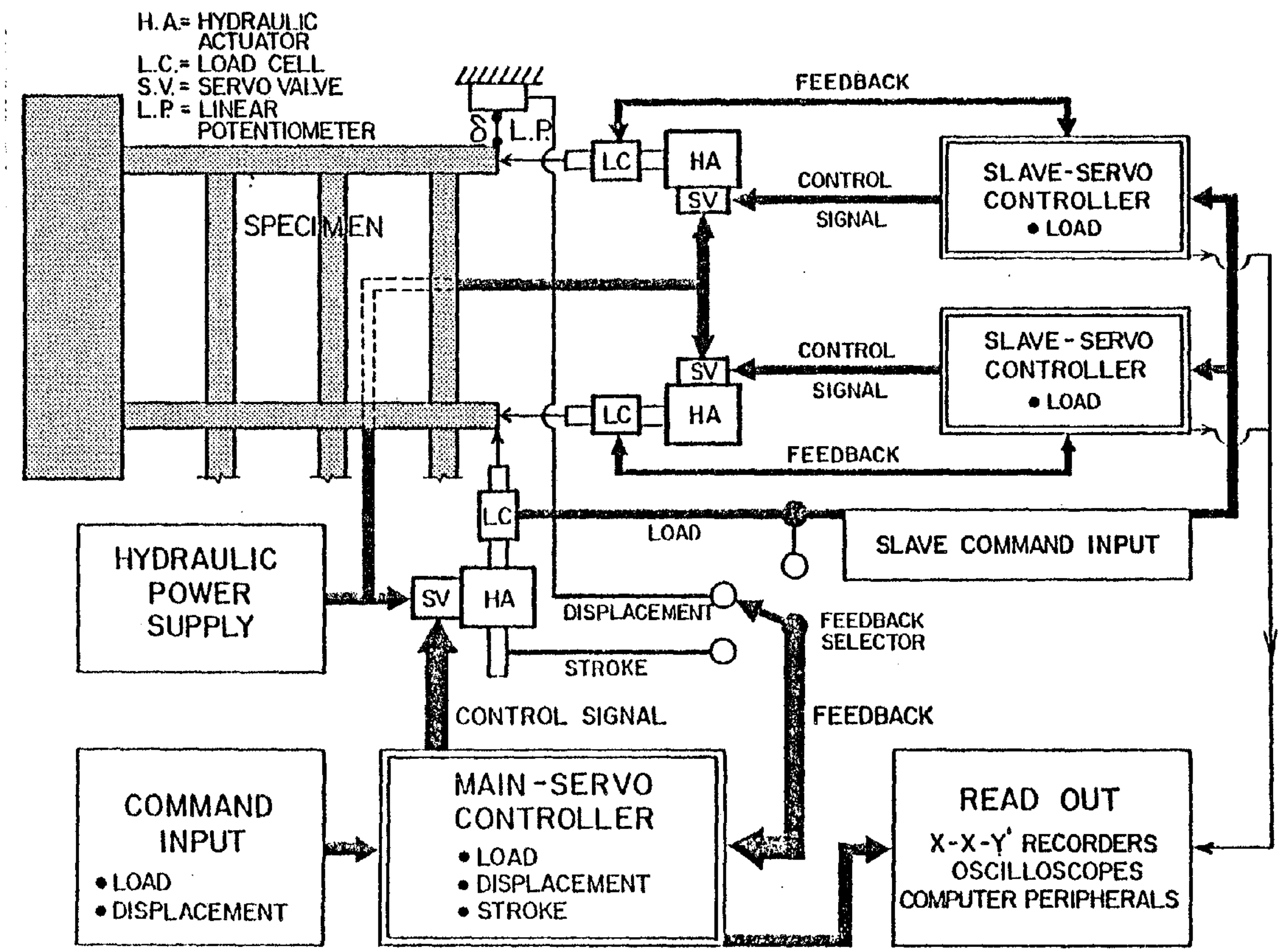

FIG. 14d SERVO-HYDRAULIC SYSTEM

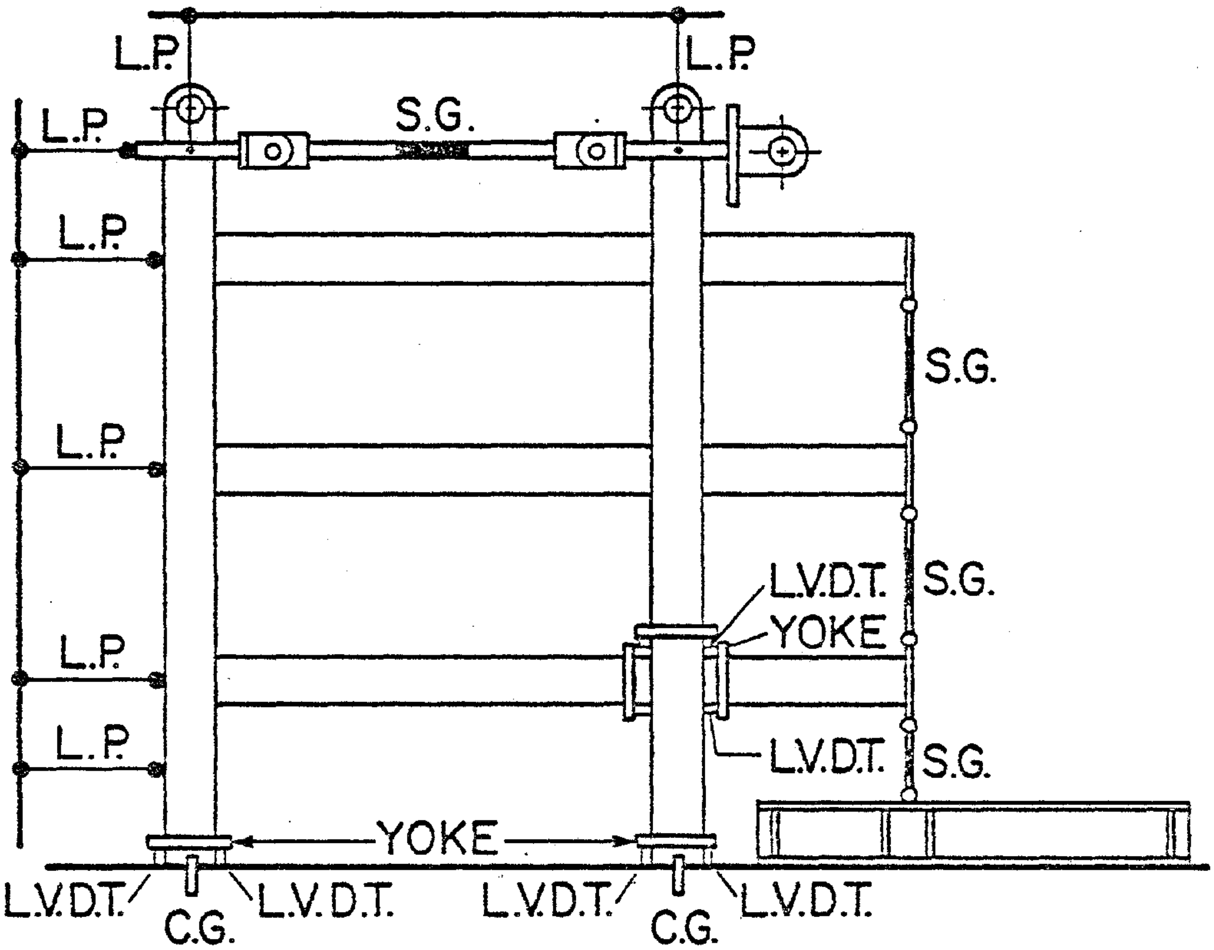

L.P. = LINEAR POTENTIOMETER
C.G. = CLIP GAGE
S.G. = STRAIN GAGE
L. V. D. T. = LINEAR VARIABLE DIFFERENTIAL TRANSFORMER

FIG. 15 BARE FRAME INSTRUMENTATION

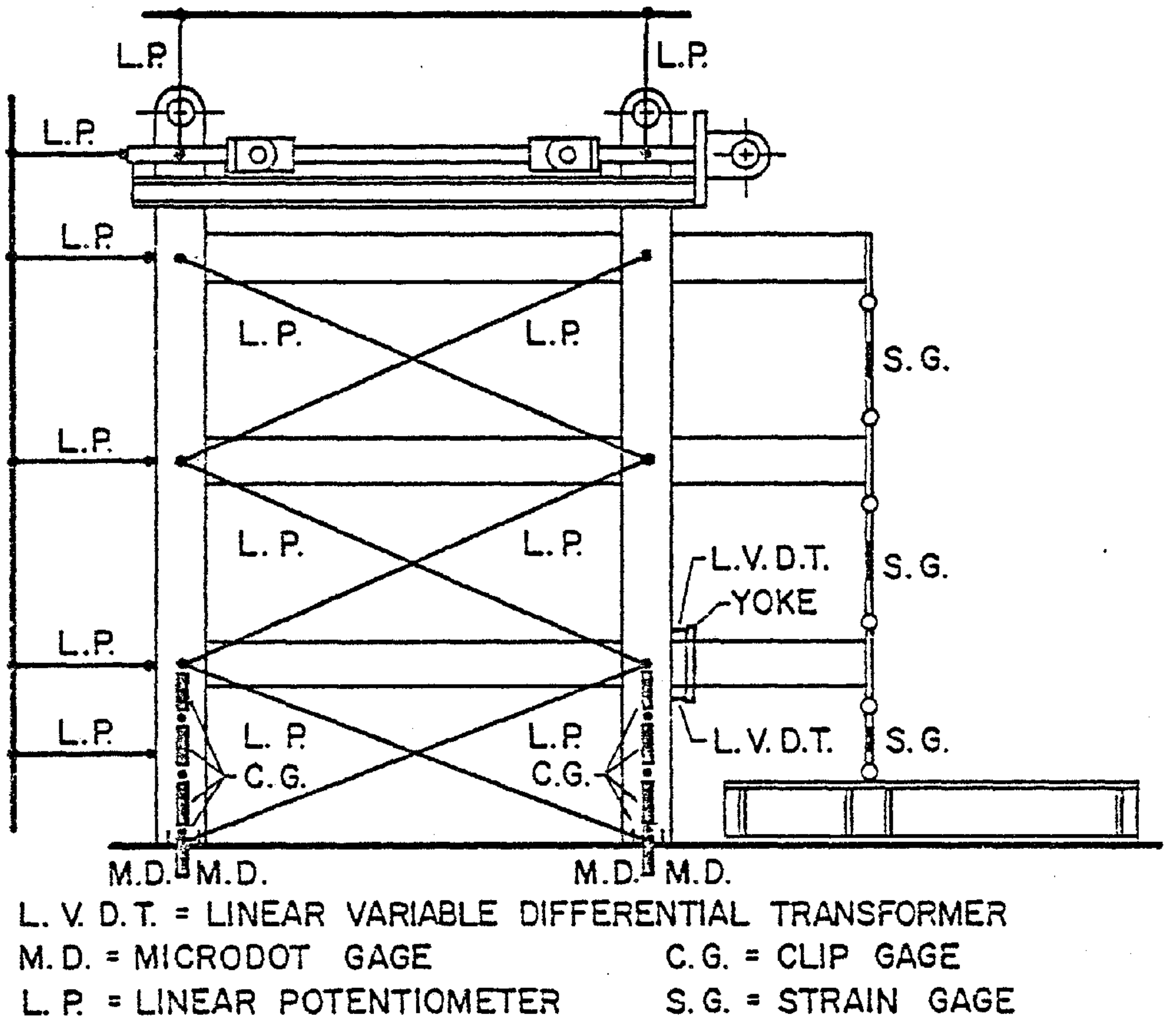

FIG. 16 INFILLED FRAME INSTRUMENTATION

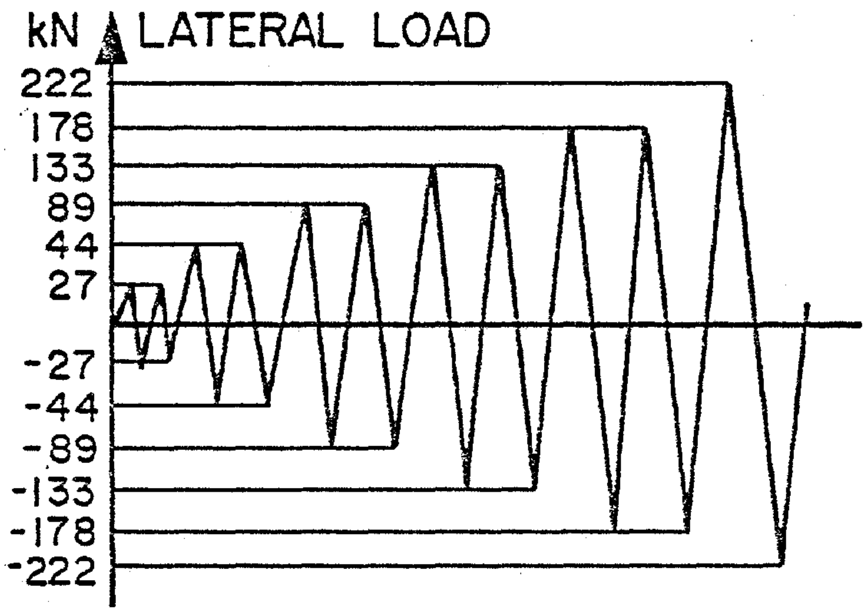

FIG. 17 LOADING PROGRAM FOR TESTS #1, #2, AND #4

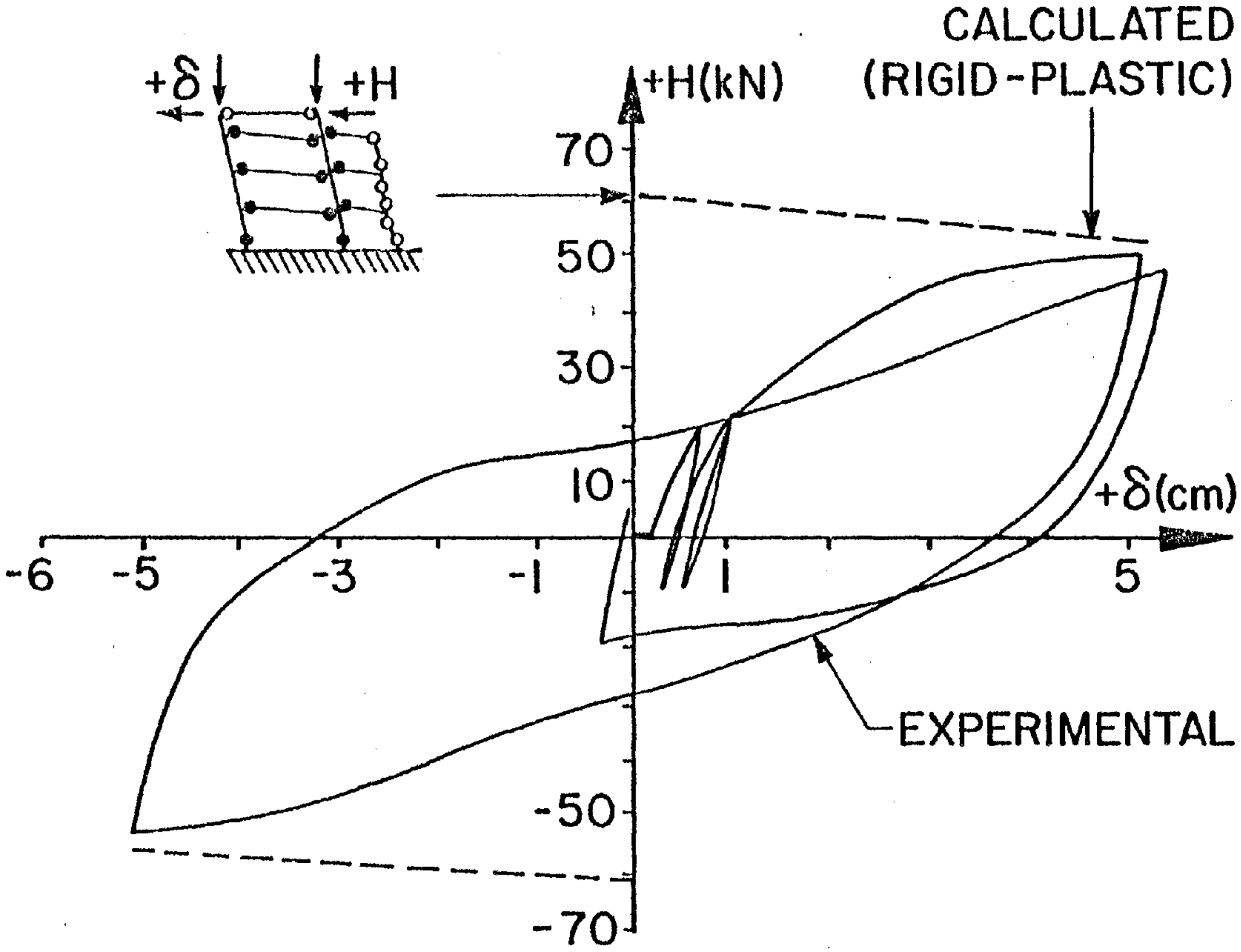

FIG. 18 LATERAL LOAD-DEFLECTION RELATIONSHIP - BARE FRAME (TEST #1)

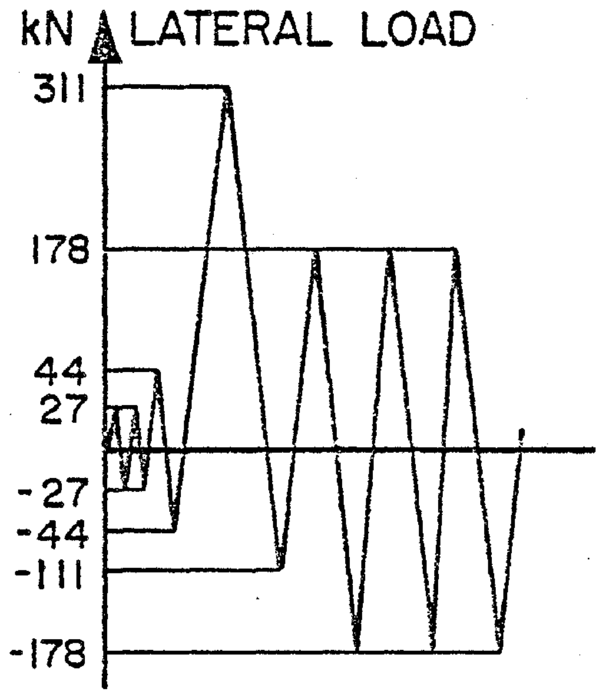

FIG. 19 LOADING PROGRAM FOR TEST #3

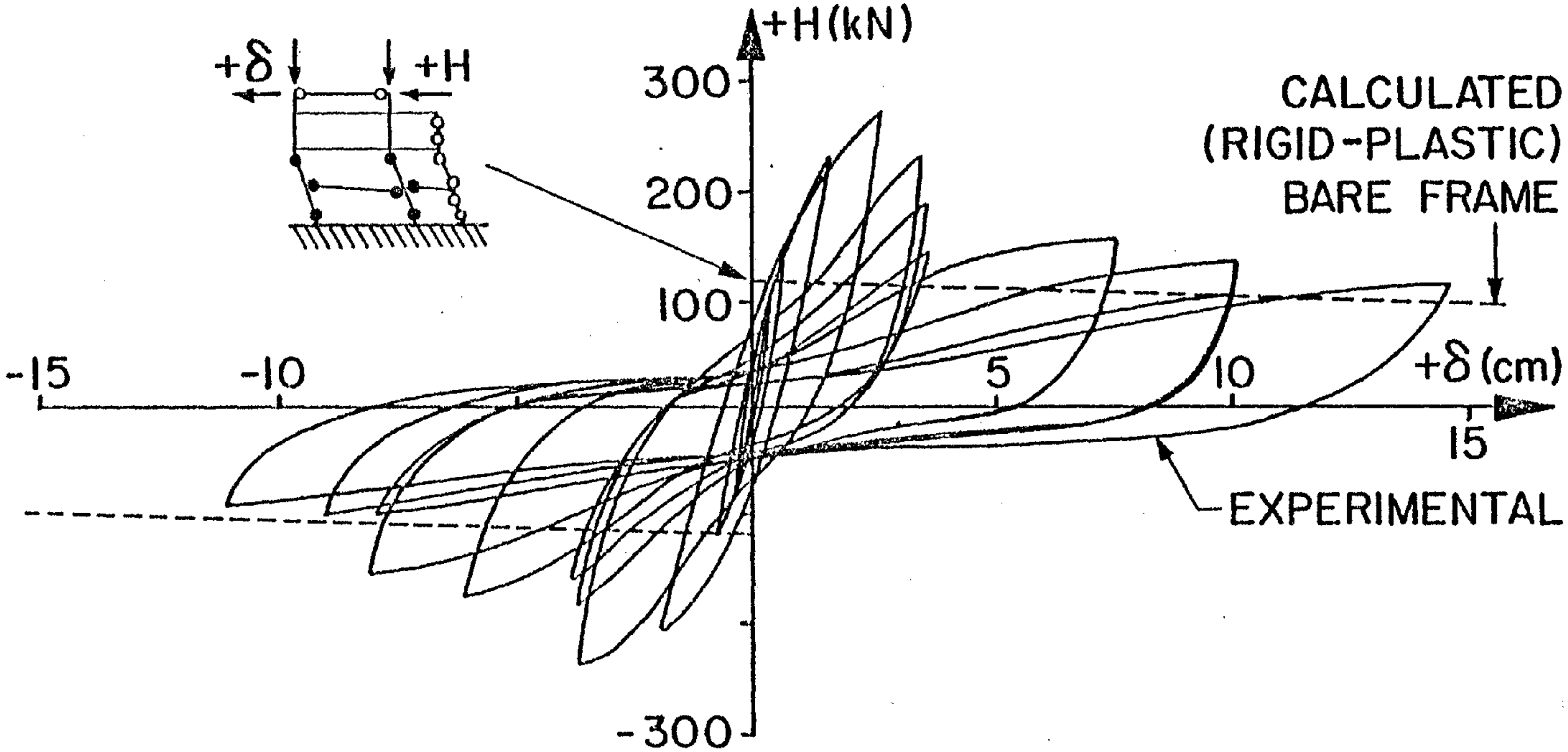

FIG. 20 LATERAL LOAD-DEFLECTION RELATIONSHIP - INFILLED BARE FRAME (TEST #2)

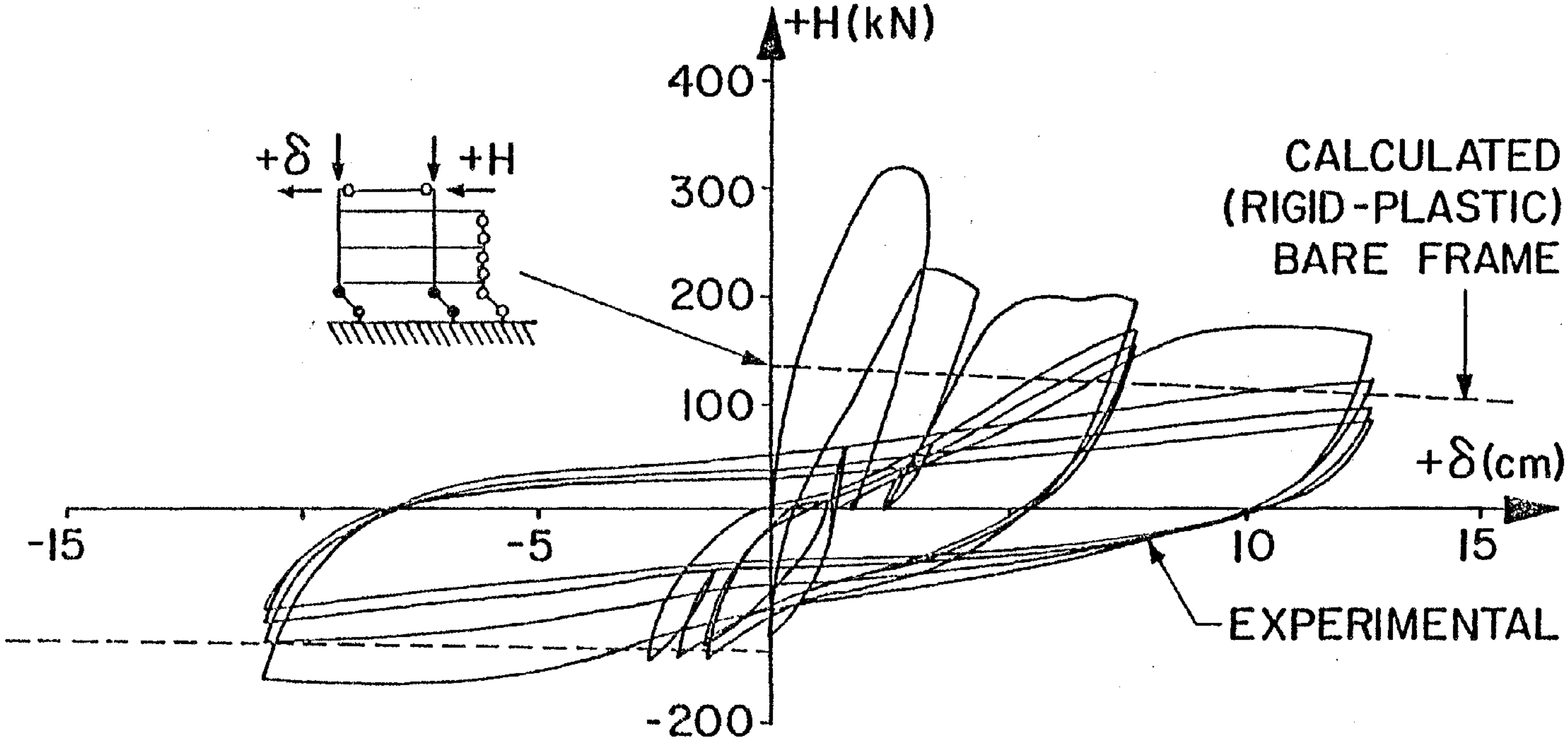

FIG. 21 LATERAL LOAD-DEFLECTION RELATIONSHIP - VIRGIN FRAME, CLAY INFILL (TEST #3)

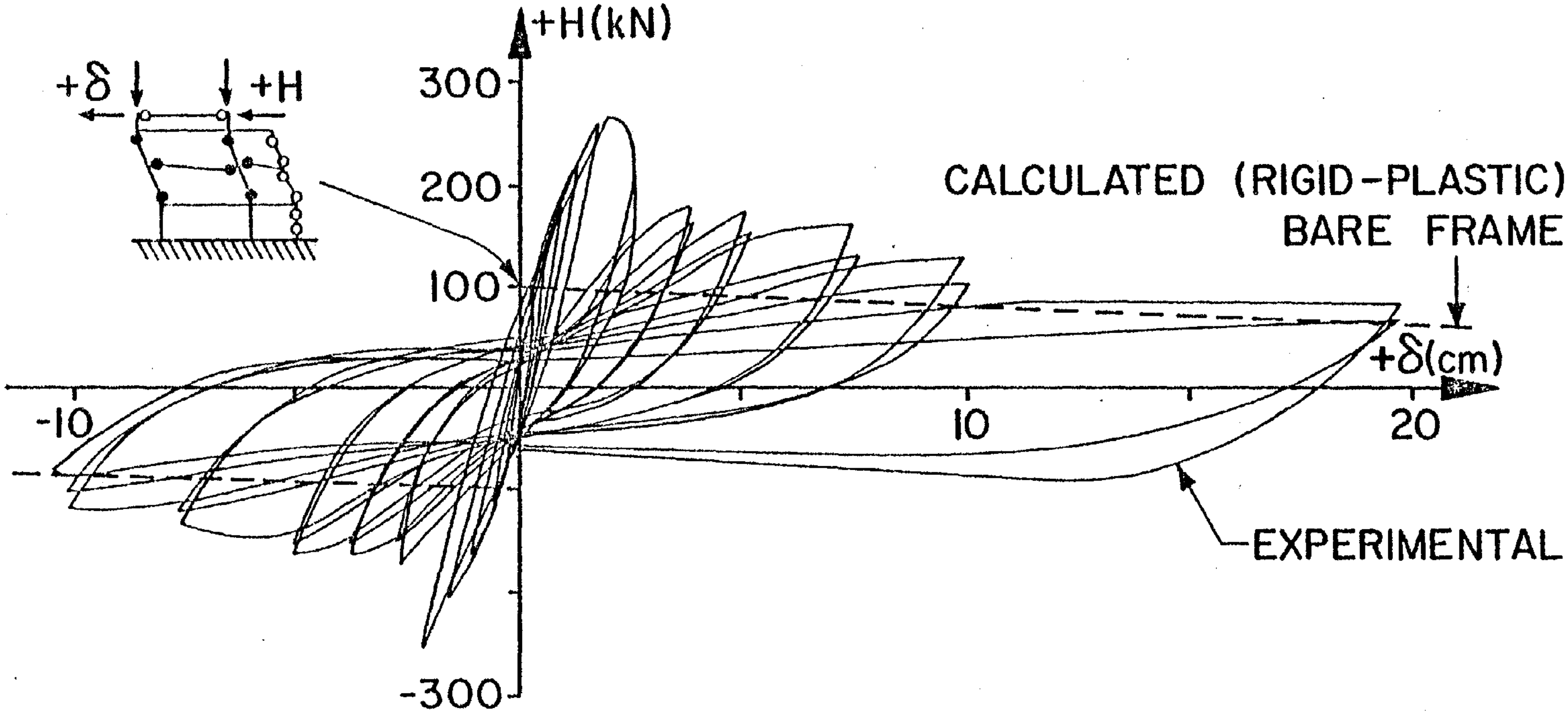

FIG. 22 LATERAL LOAD-DEFLECTION RELATIONSHIP - VIRGIN FRAME, CONCRETE BLOCK INFILL (TEST #4)

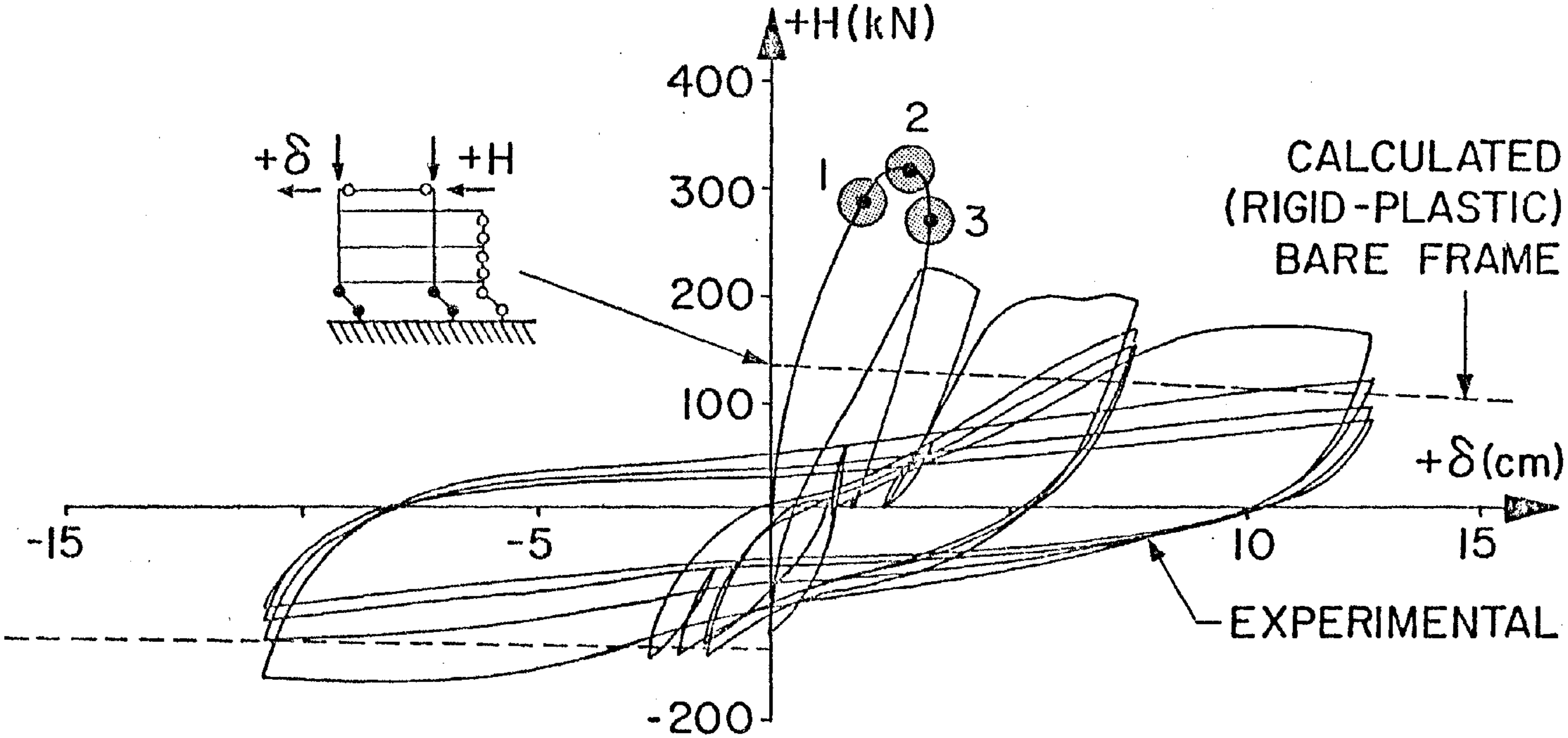

FIG. 23 LATERAL LOAD-DEFLECTION RELATIONSHIP - VIRGIN FRAME, CLAY INFILL (TEST #3)

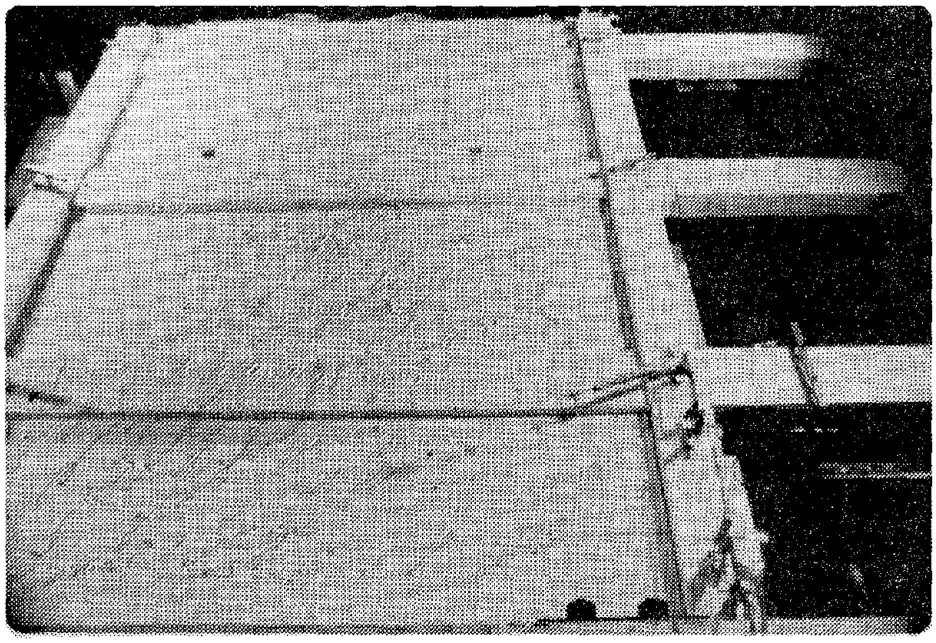

FIG. 24 CRACKING PATTERN CHARACTERISTIC OF MONOLITHIC BEHAVIOR

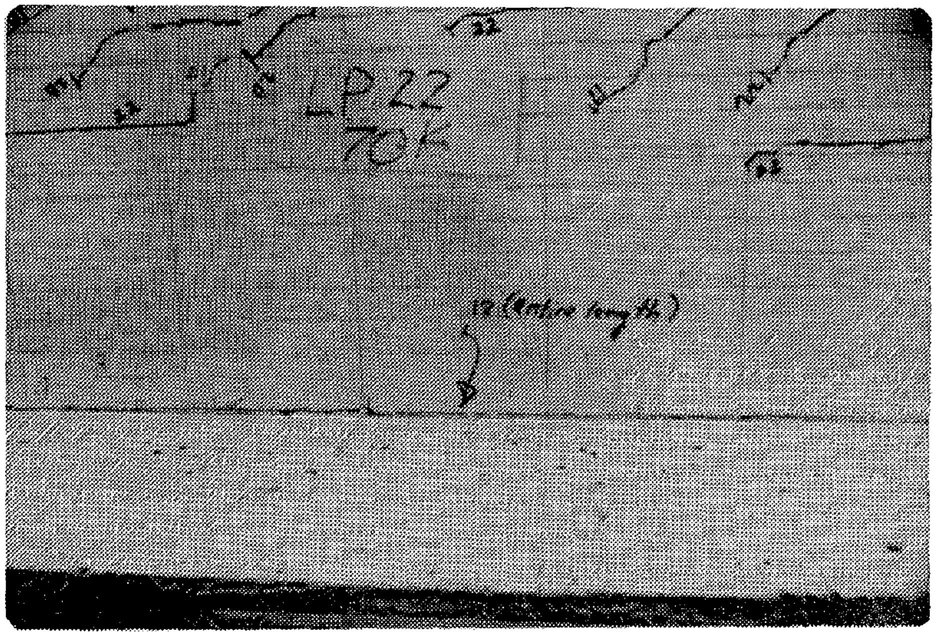

FIG. 25 SEPARATION BETWEEN FRAME AND INFILL

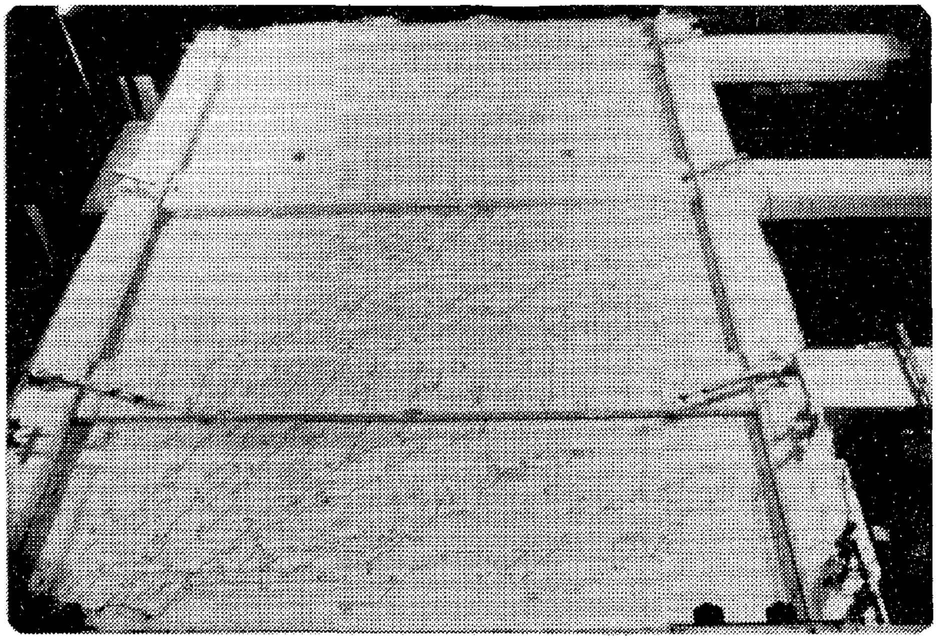

FIG. 26 DEVELOPMENT OF EQUIVALENT DIAGONAL COMPRESSION STRUT

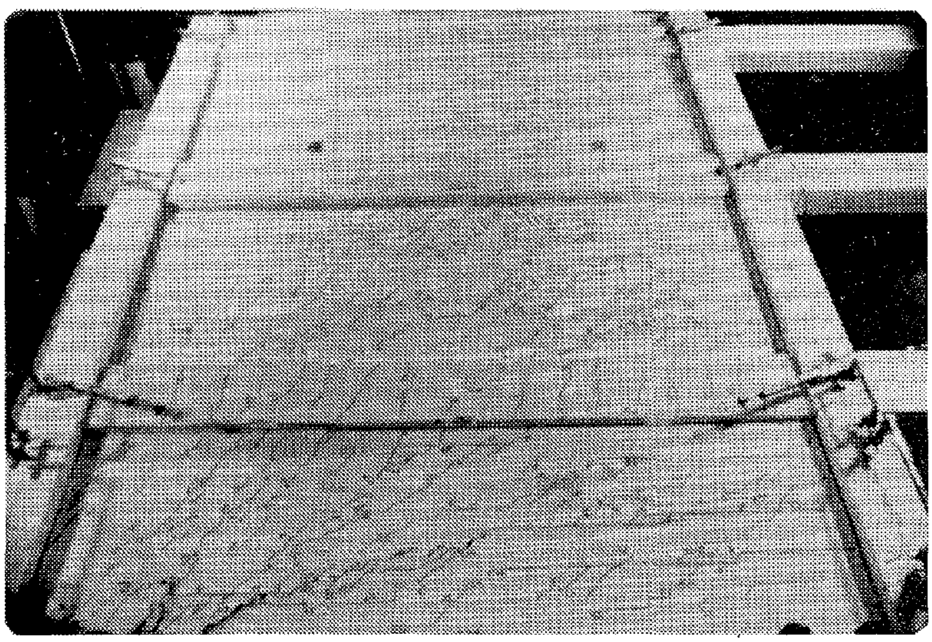

FIG. 27 DEGRADATION OF EQUIVALENT DIAGONAL COMPRESSION STRUT

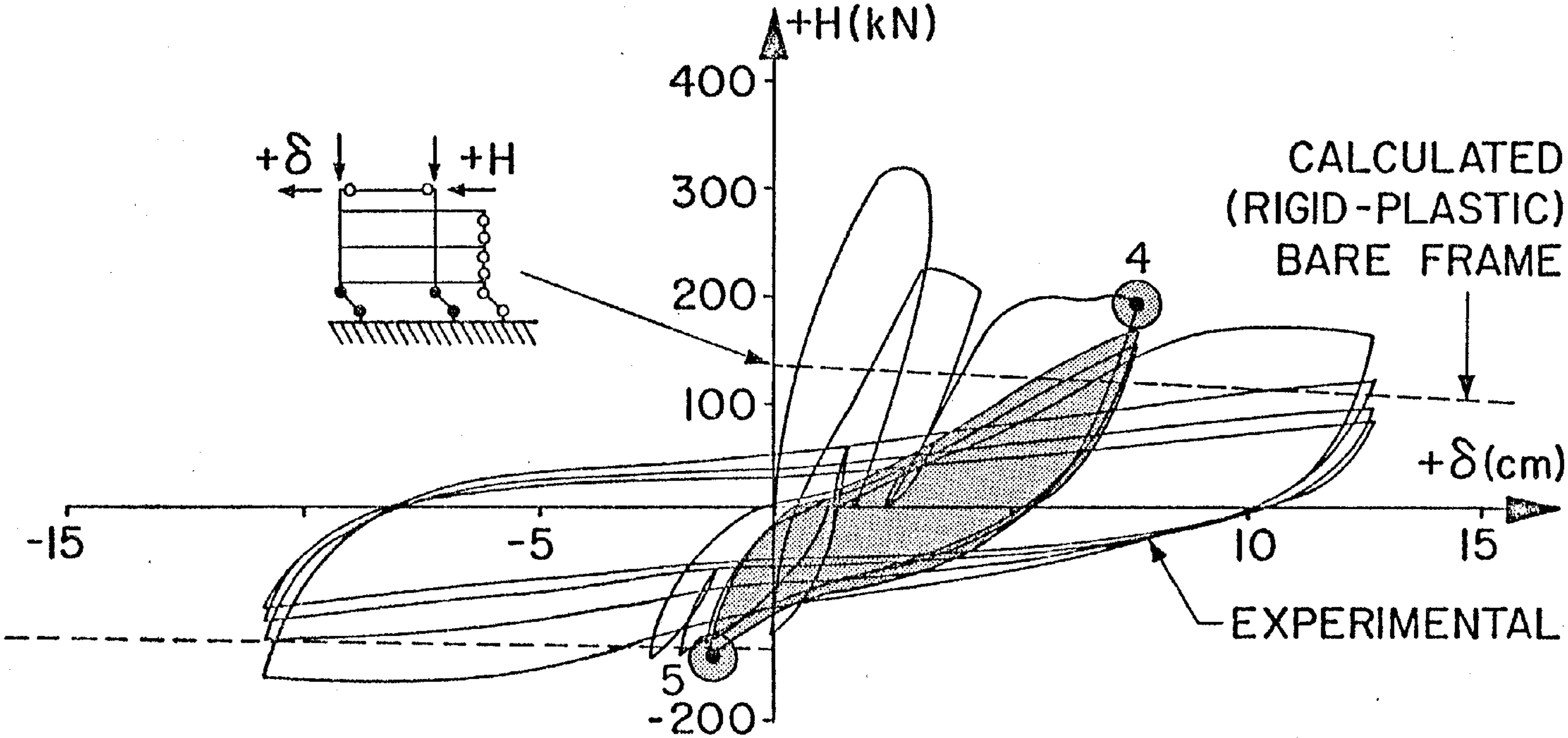

FIG. 28 LATERAL LOAD-DEFLECTION RELATIONSHIP - VIRGIN FRAME, CLAY INFILL (TEST #3)

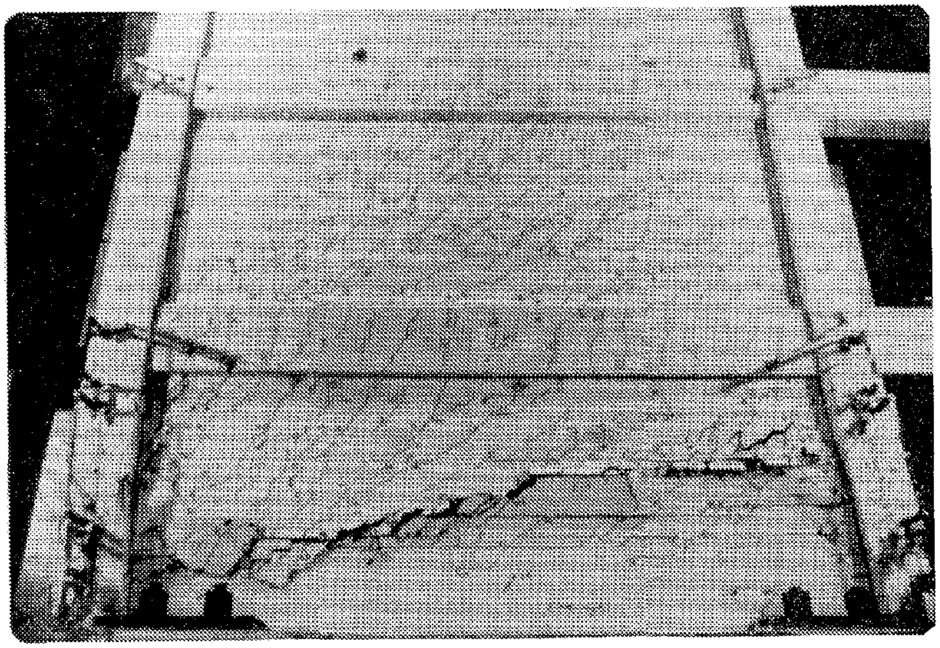

FIG. 29 INCREASED DAMAGE TO EQUIVALENT DIAGONAL COMPRESSION STRUT

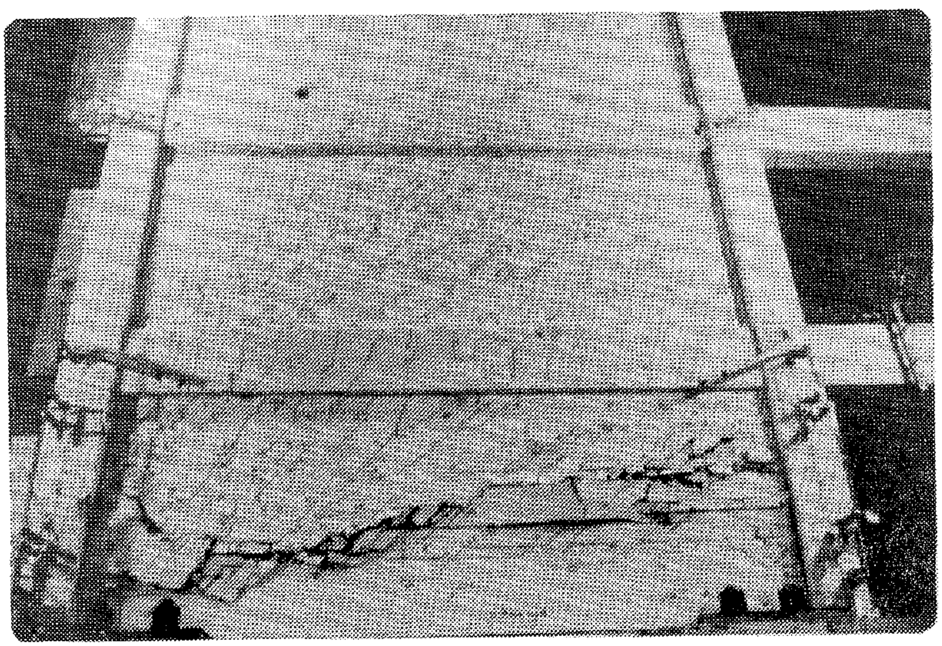

FIG. 30 DAMAGE CAUSED BY LOAD REVERSAL

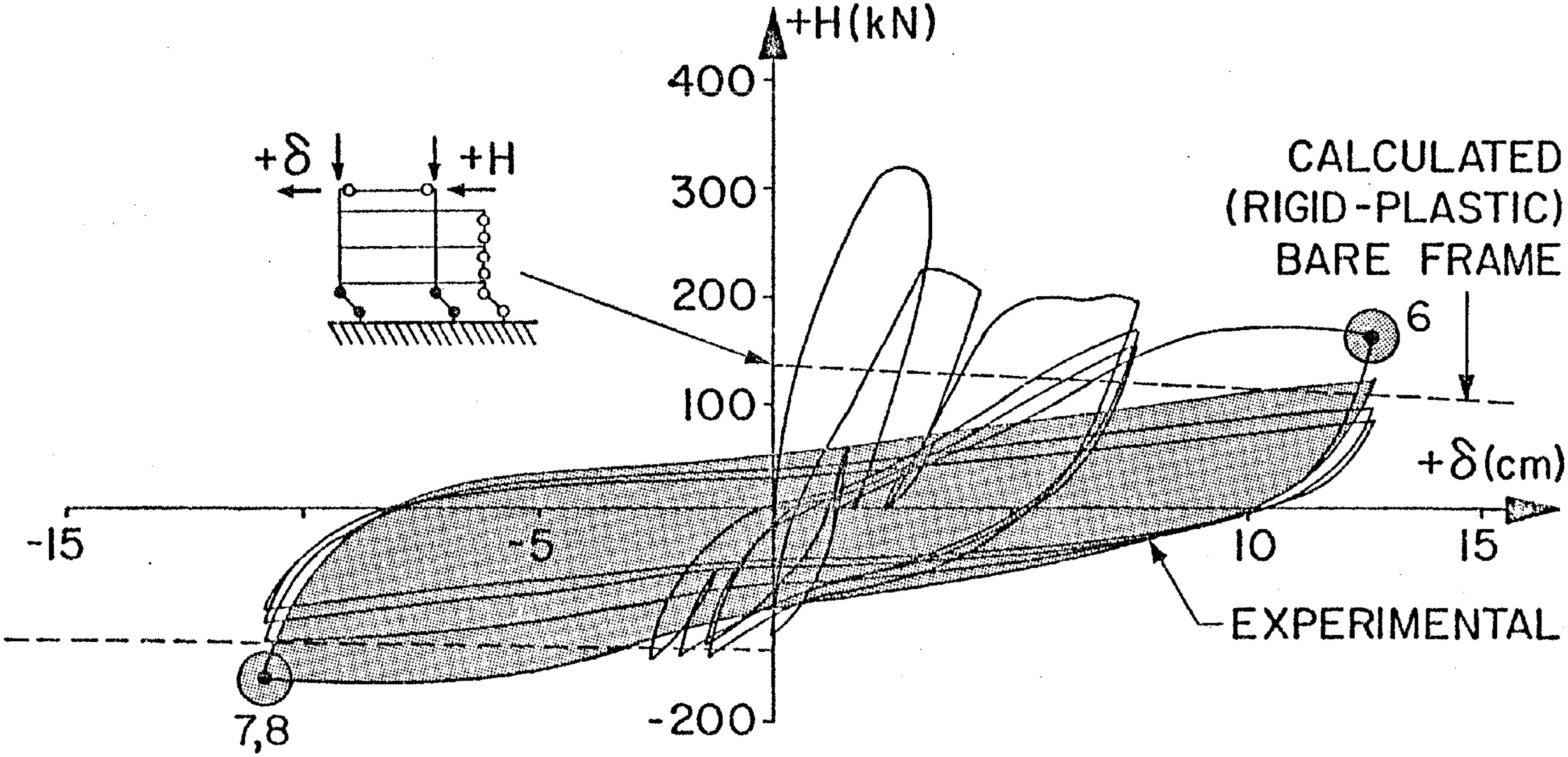

FIG. 31 LATERAL LOAD-DEFLECTION RELATIONSHIP - VIRGIN FRAME, CLAY INFILL (TEST #3)

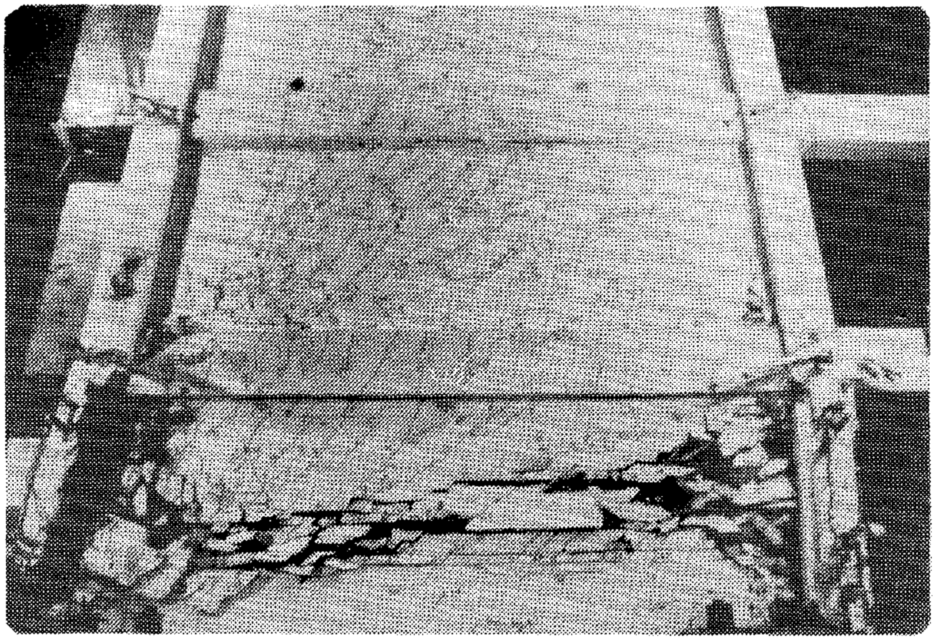

FIG. 32 DAMAGE FROM FURTHER REVERSAL

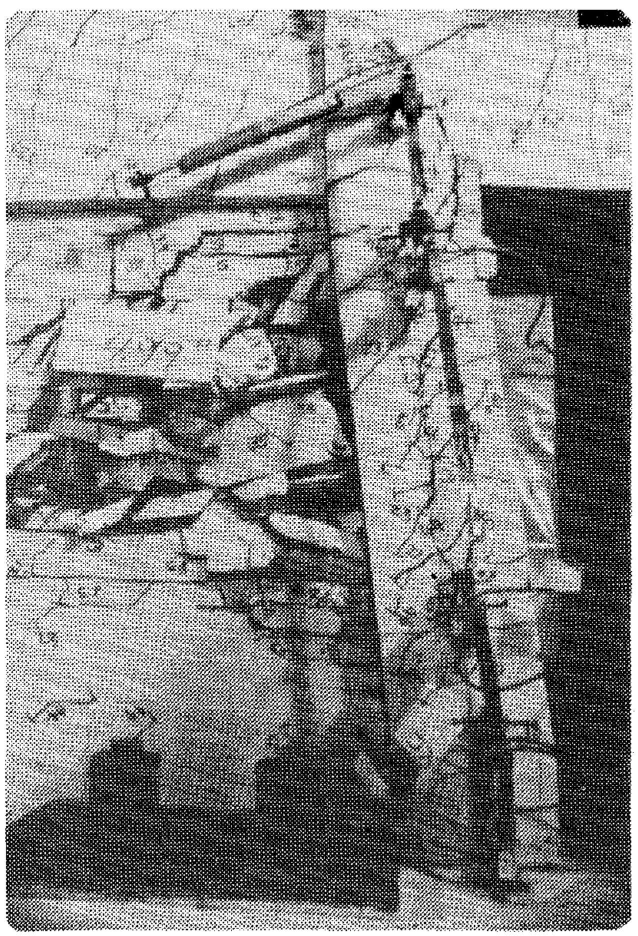

FIG. 33 DEFORMATION OF INTERIOR COLUMN AT FIRST STORY

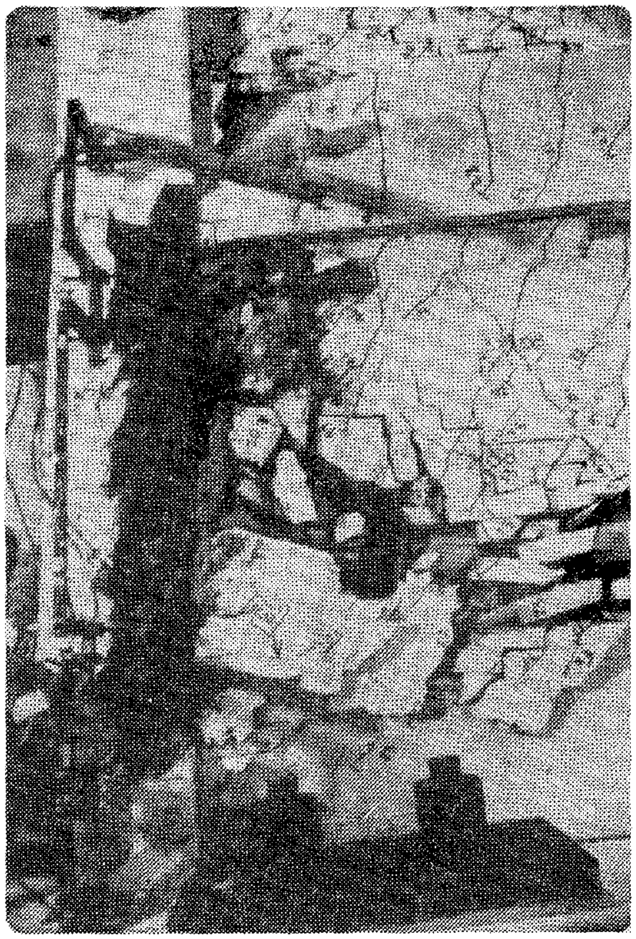

FIG. 34 SPALLING OF CONCRETE FROM EXTERIOR COLUMN AT FIRST STORY

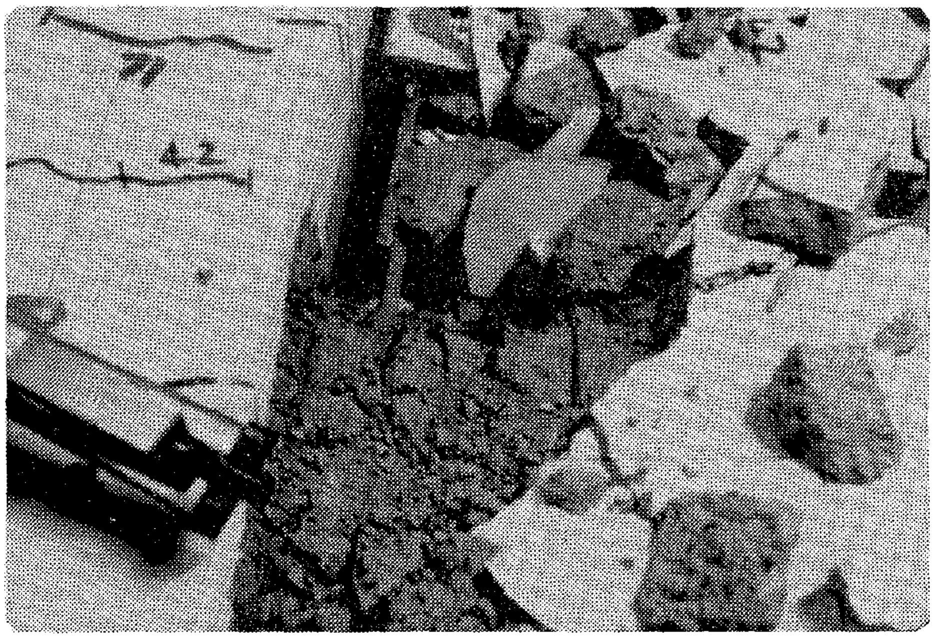

FIG. 35 DETERIORATION NEAR FIRST-FLOOR EXTERIOR BEAM-COLUMN JOINT

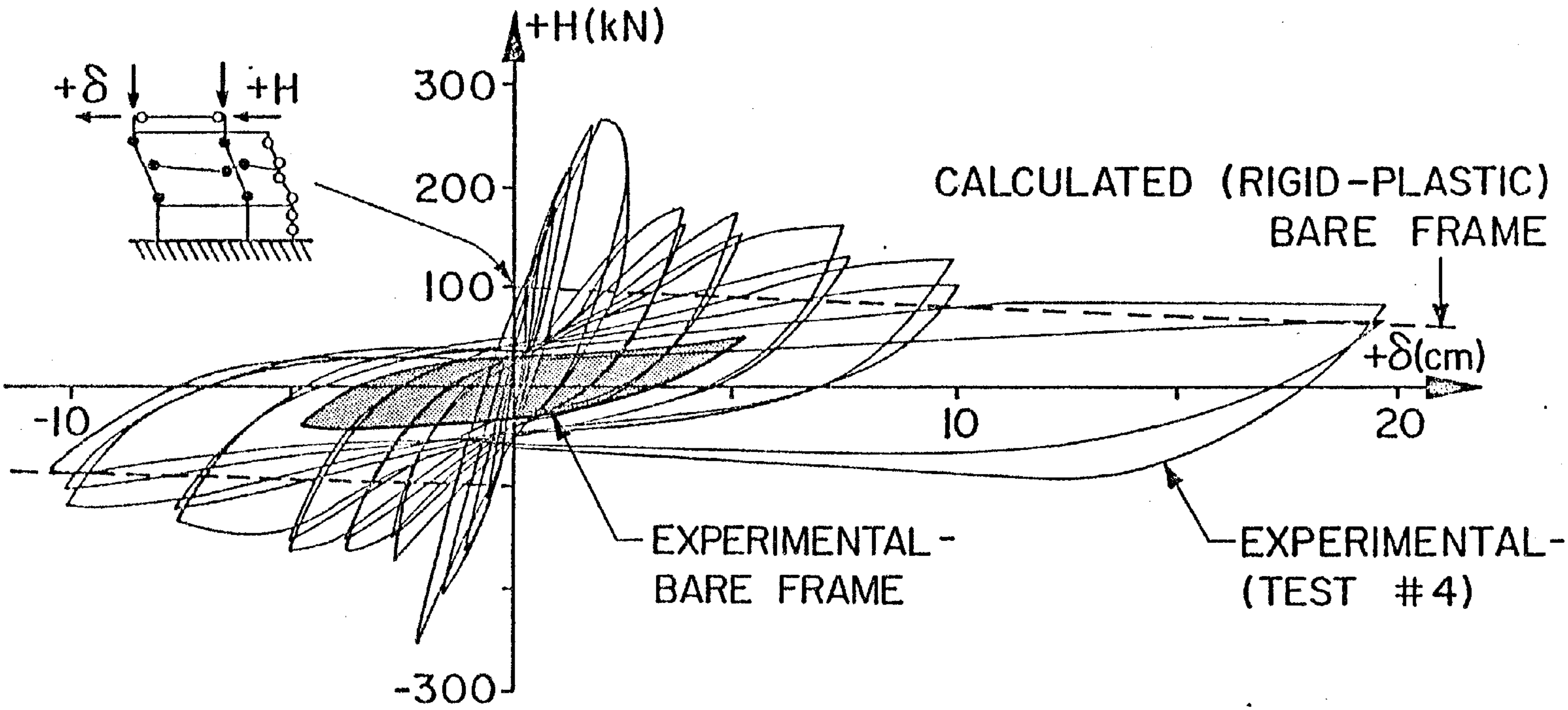

FIG. 36 COMPARISON OF HYSTERETIC BEHAVIOR BETWEEN BARE FRAME (TEST #1) AND INFILLED FRAME (TEST #4)

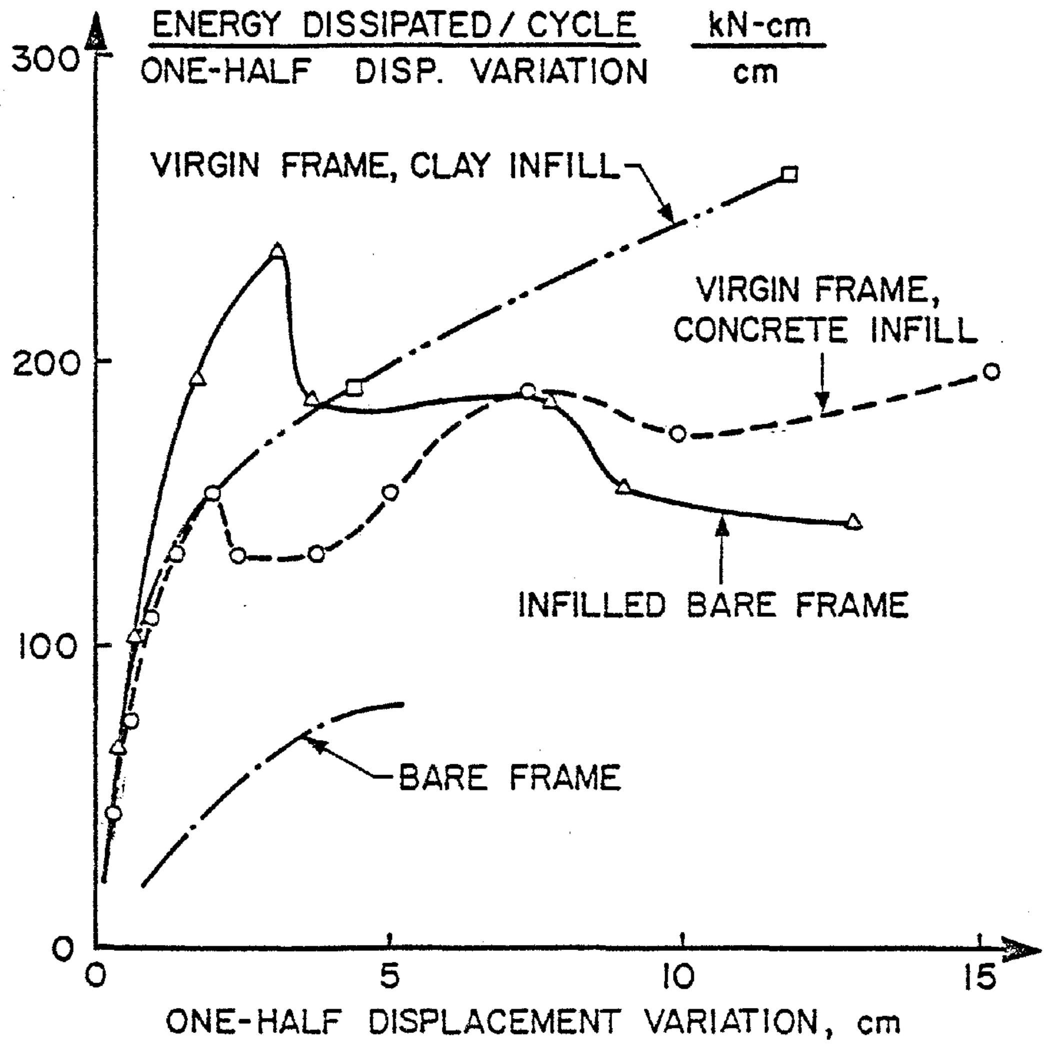

FIG. 37 ENERGY DISSIPATION

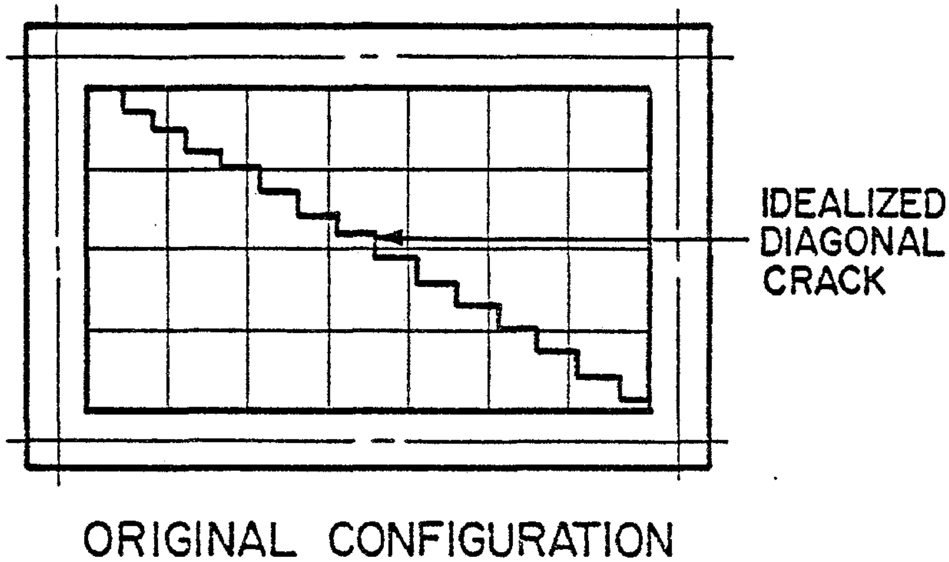

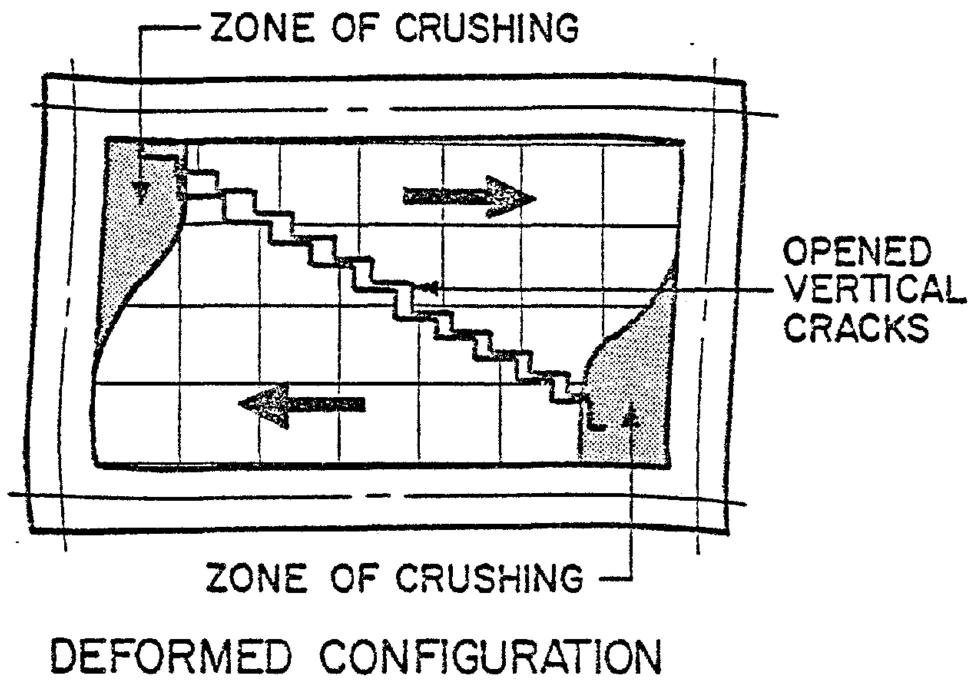

FIG. 38 PRINCIPAL MECHANISM OF PANEL DEGRADATION

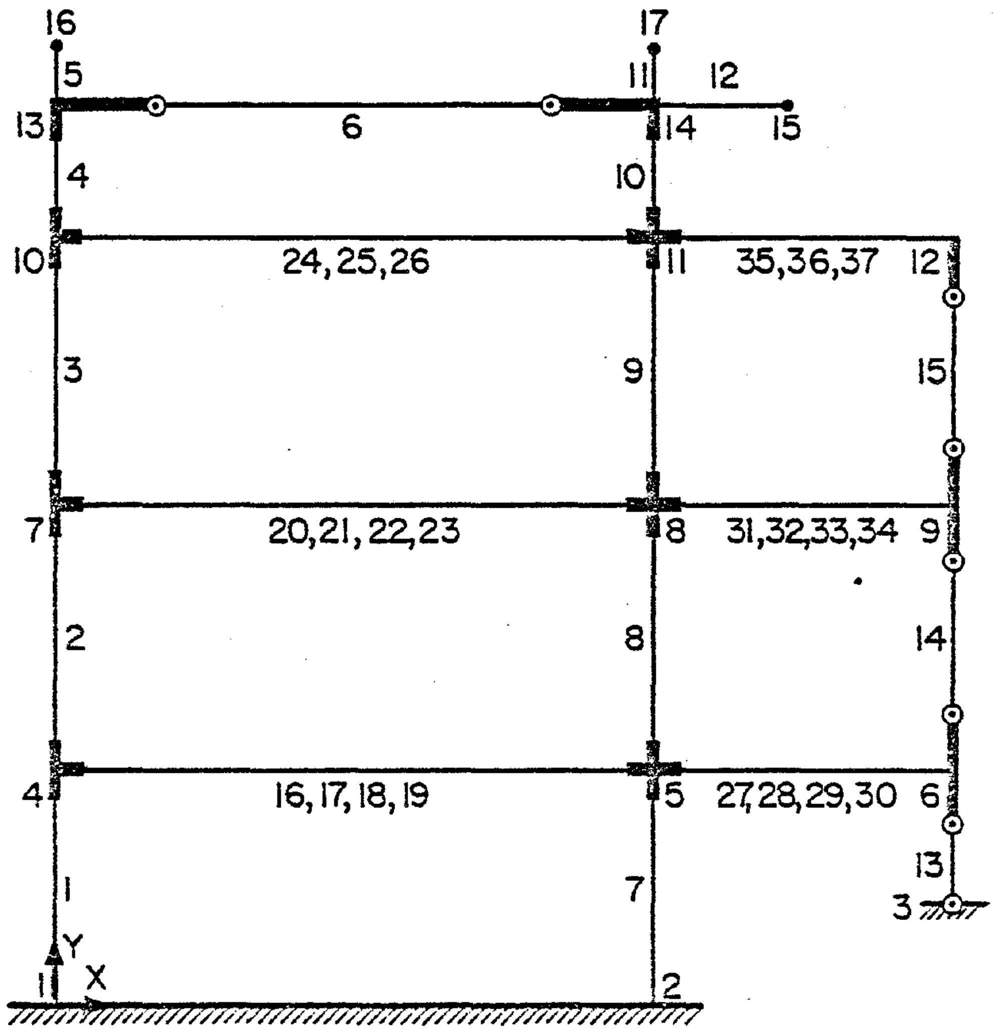

FIG. 39 ANALYTICAL IDEALIZATION OF BARE FRAME SUBASSEMBLAGE

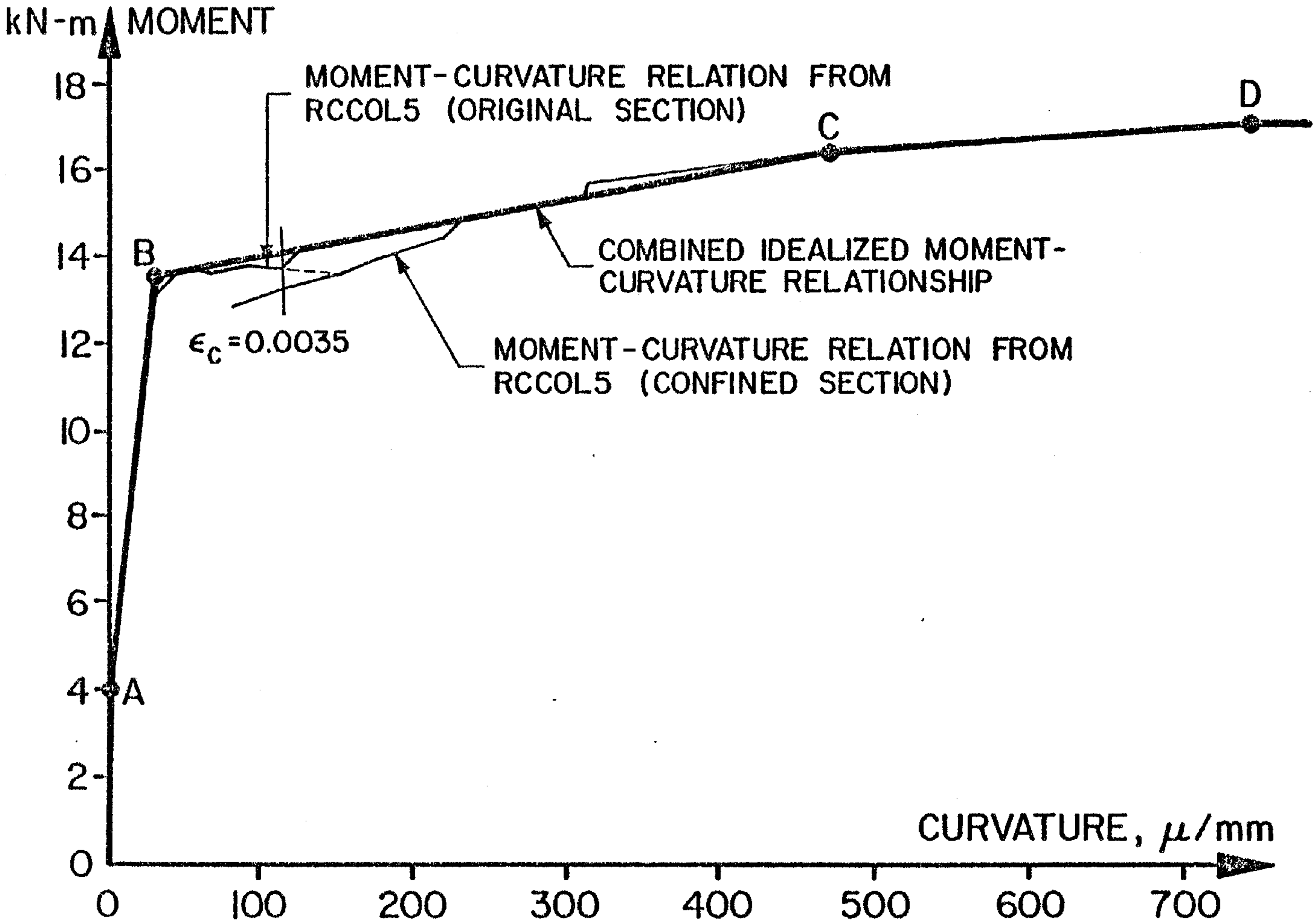

FIG. 40 IDEALIZED MOMENT-CURVATURE RELATIONSHIP FOR BEAM B1

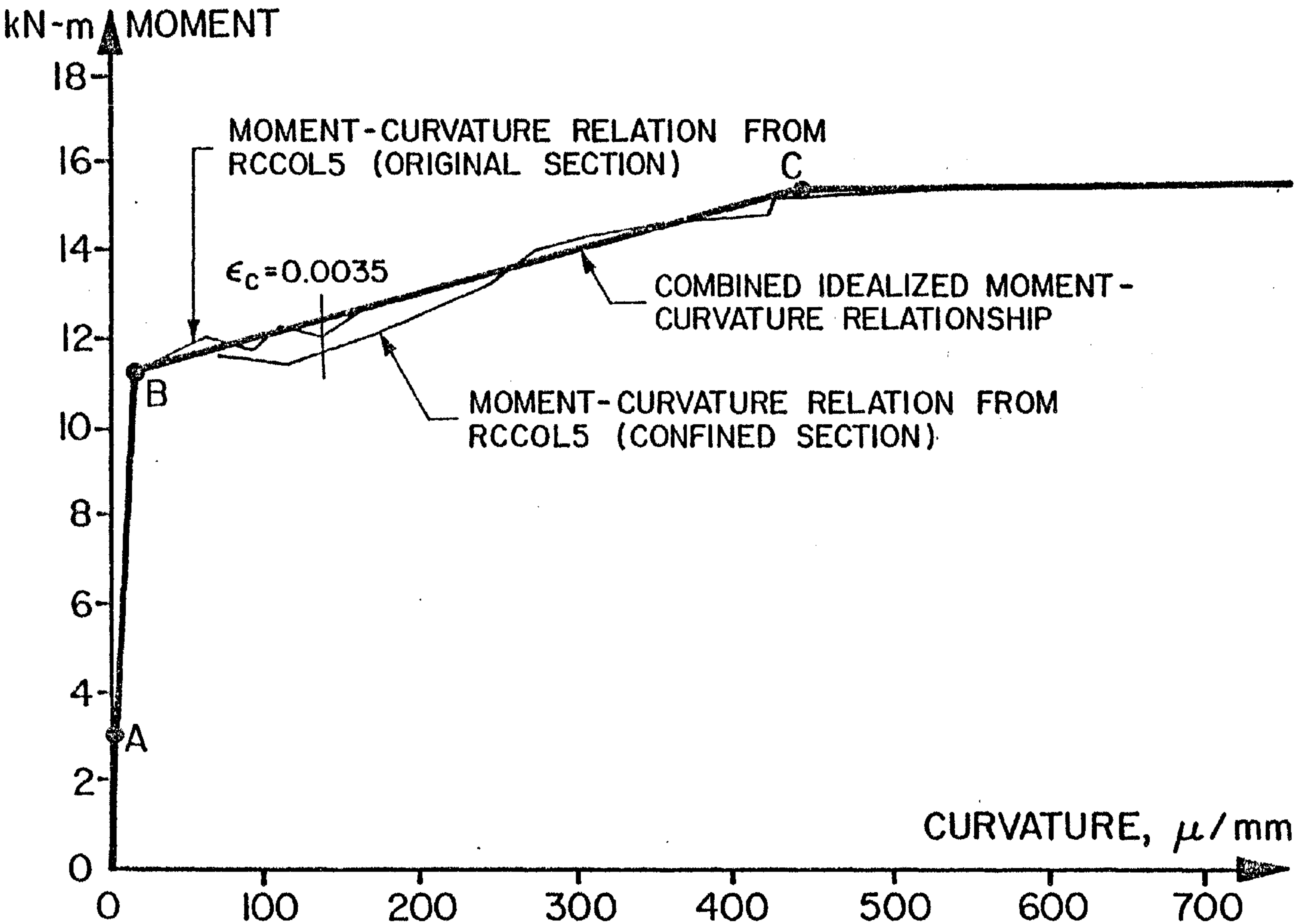

FIG. 41 IDEALIZED MOMENT-CURVATURE RELATIONSHIP FOR BEAM B2

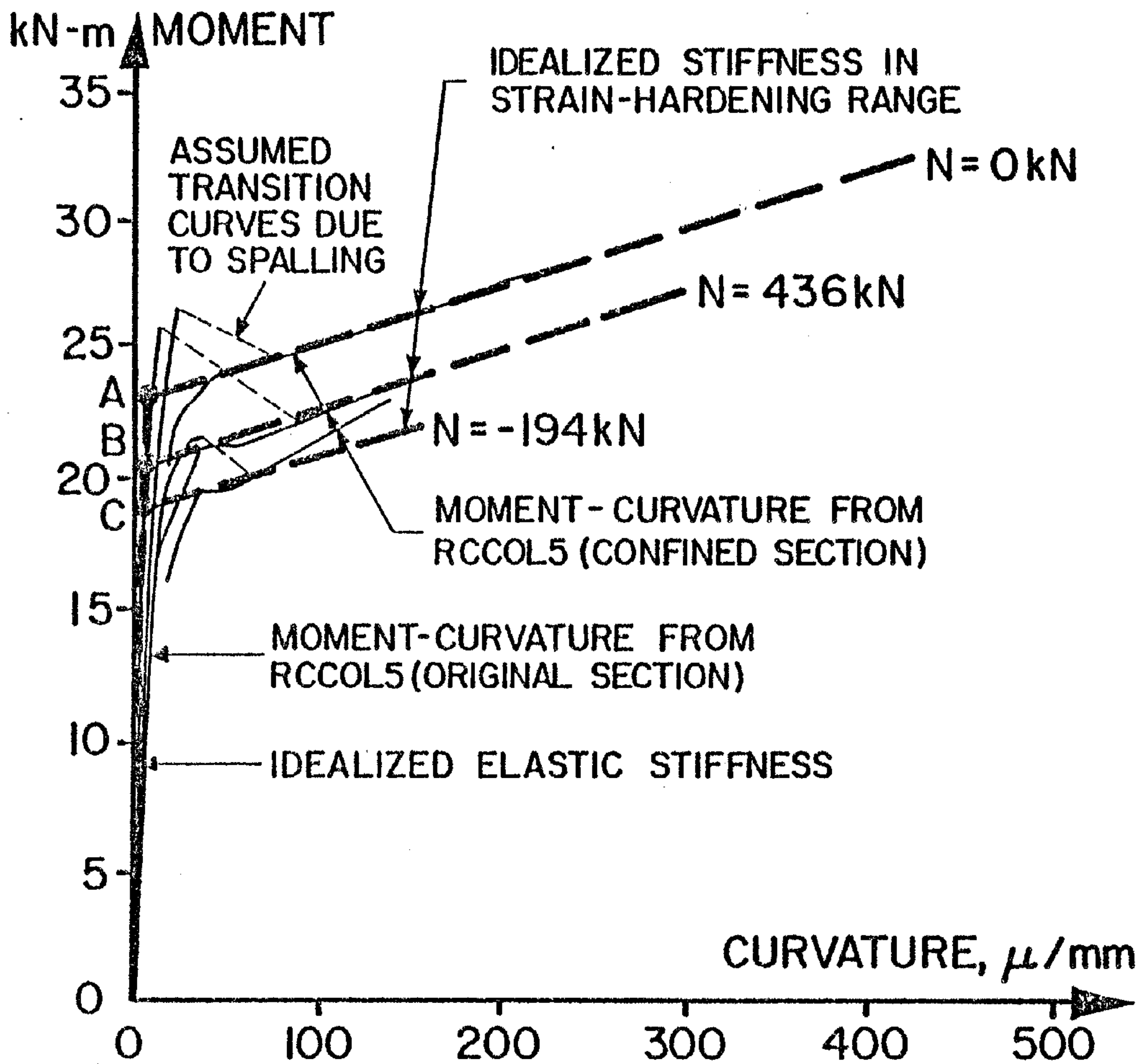

FIG. 42 IDEALIZED BILINEAR MOMENT-CURVATURE RELATIONSHIP FOR COLUMNS

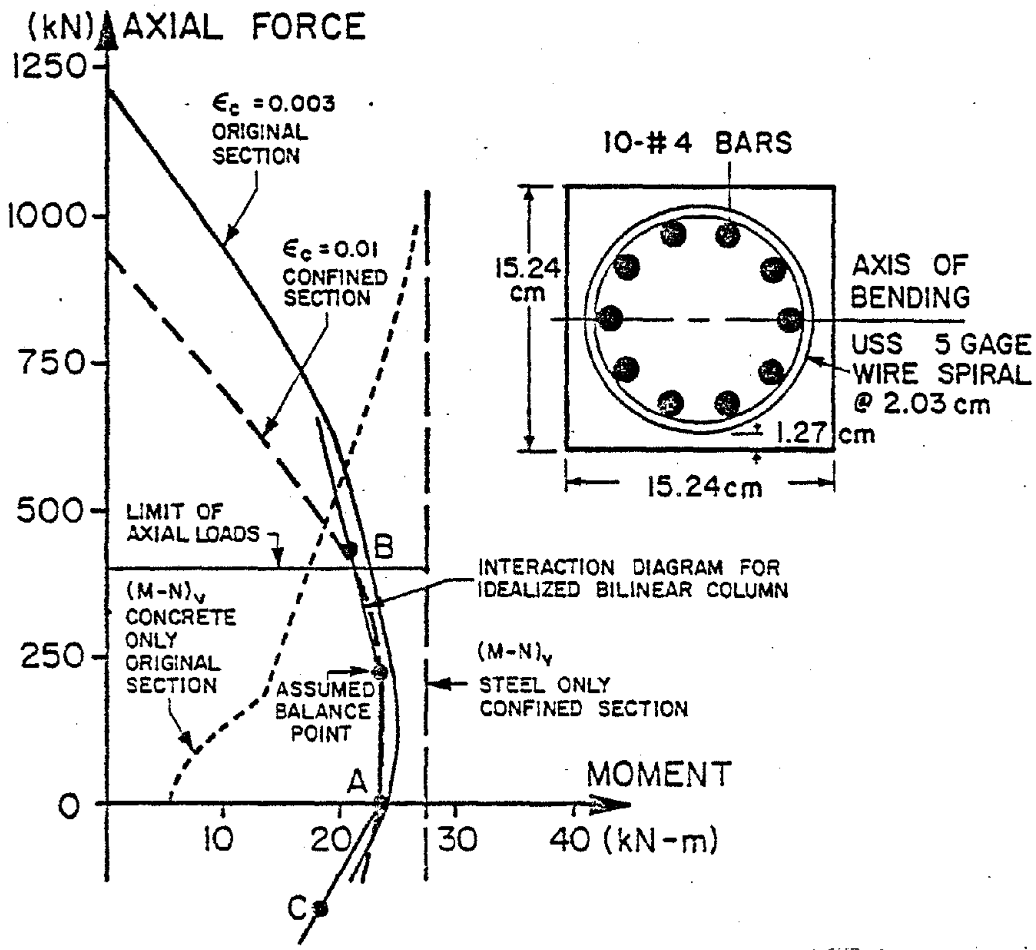

FIG. 43 COMPARISON OF MOMENT-AXIAL FORCE INTERACTION DIAGRAMS FOR IDEALIZED AND ACTUAL MODEL COLUMNS

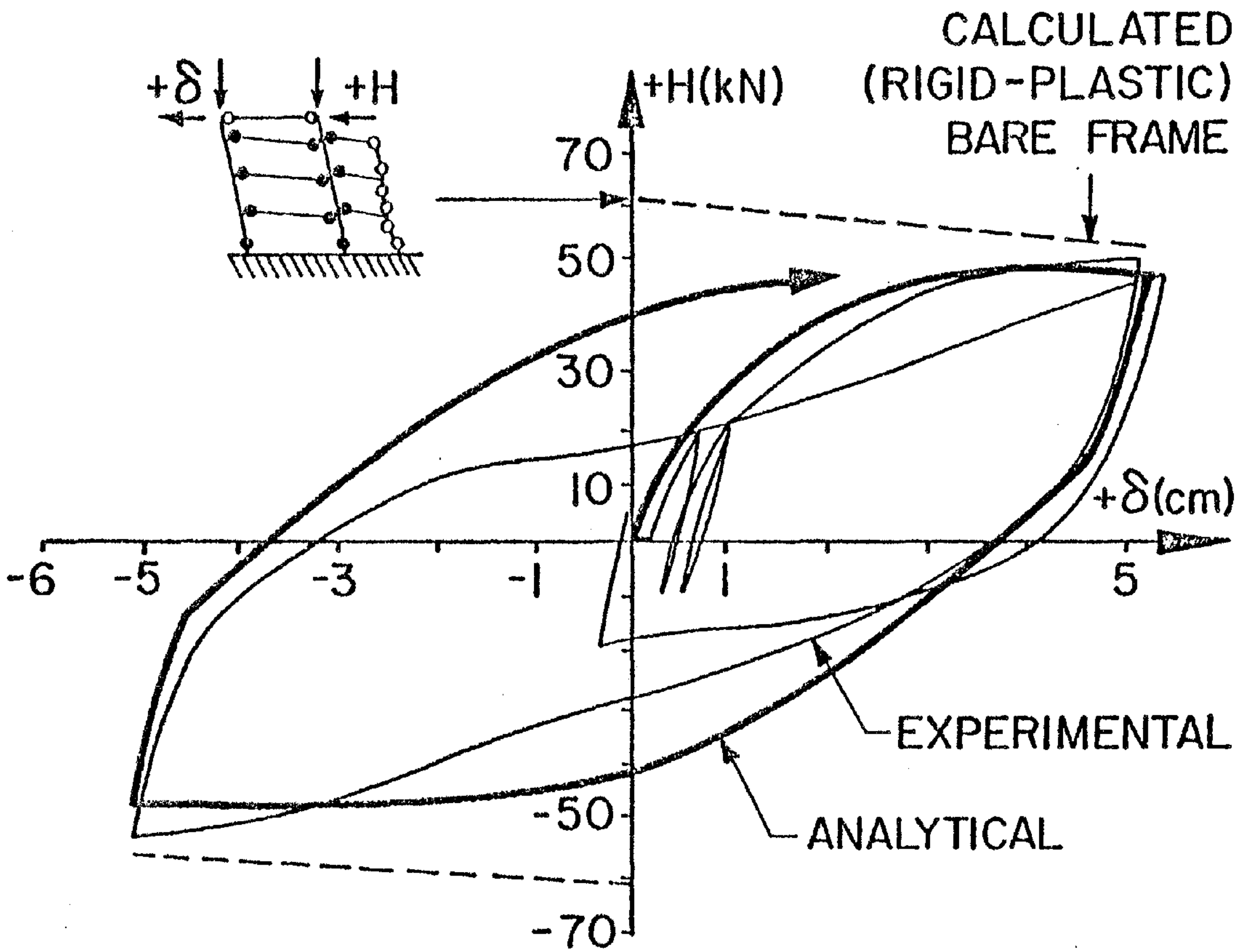

FIG. 44 COMPARISON OF BARE FRAME EXPERIMENTAL RESPONSE (TEST #1) WITH THAT PREDICTED ANALYTICALLY

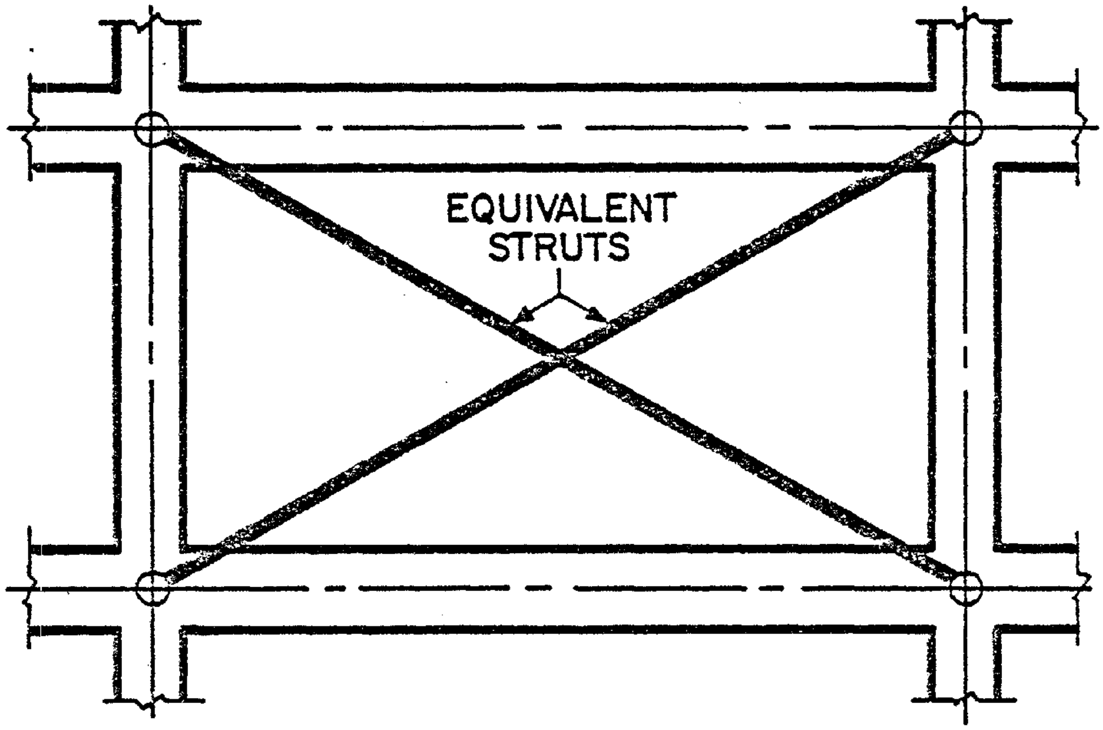

FIG. 45 ANALYTICAL IDEALIZATION OF INFILL PANEL AS TWO EQUIVALENT STRUTS

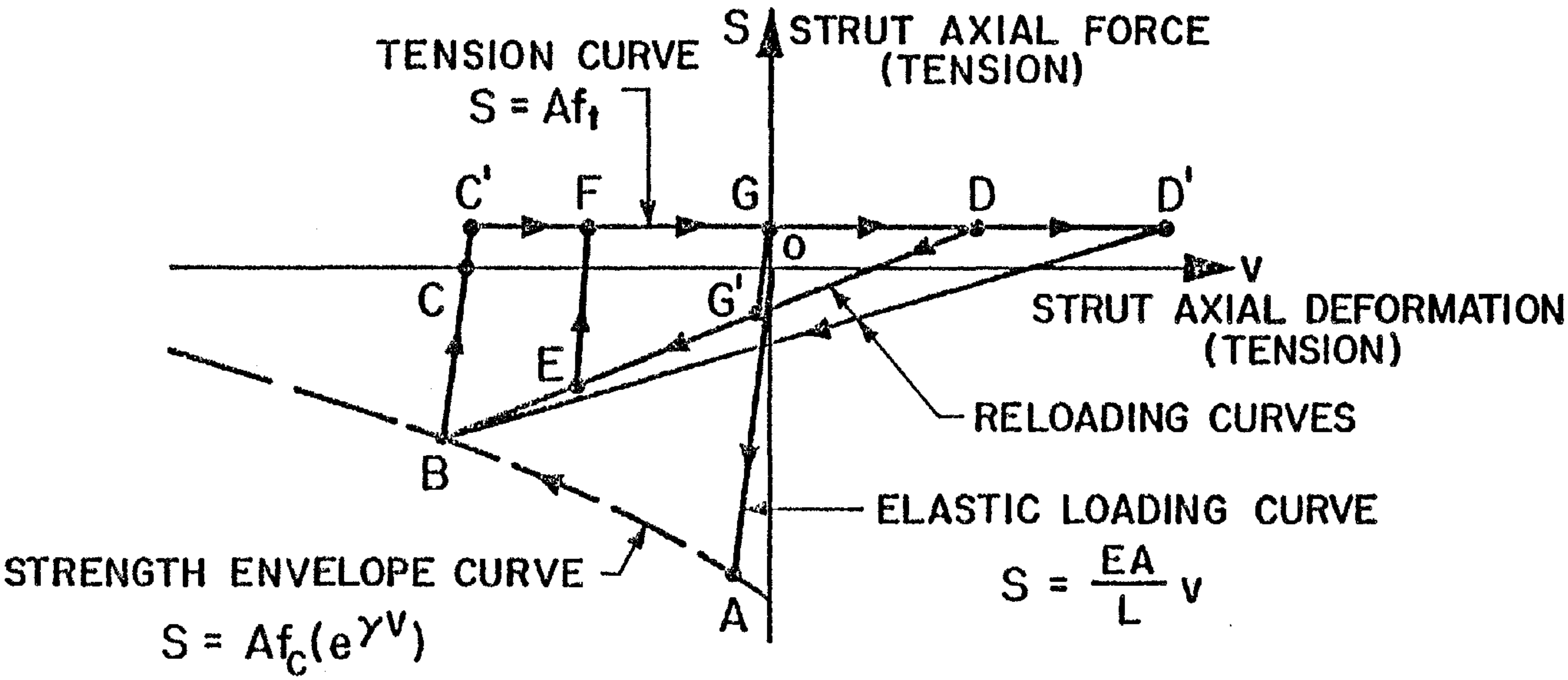

FIG. 46 MECHANICAL BEHAVIOR OF STRUT MODEL #1

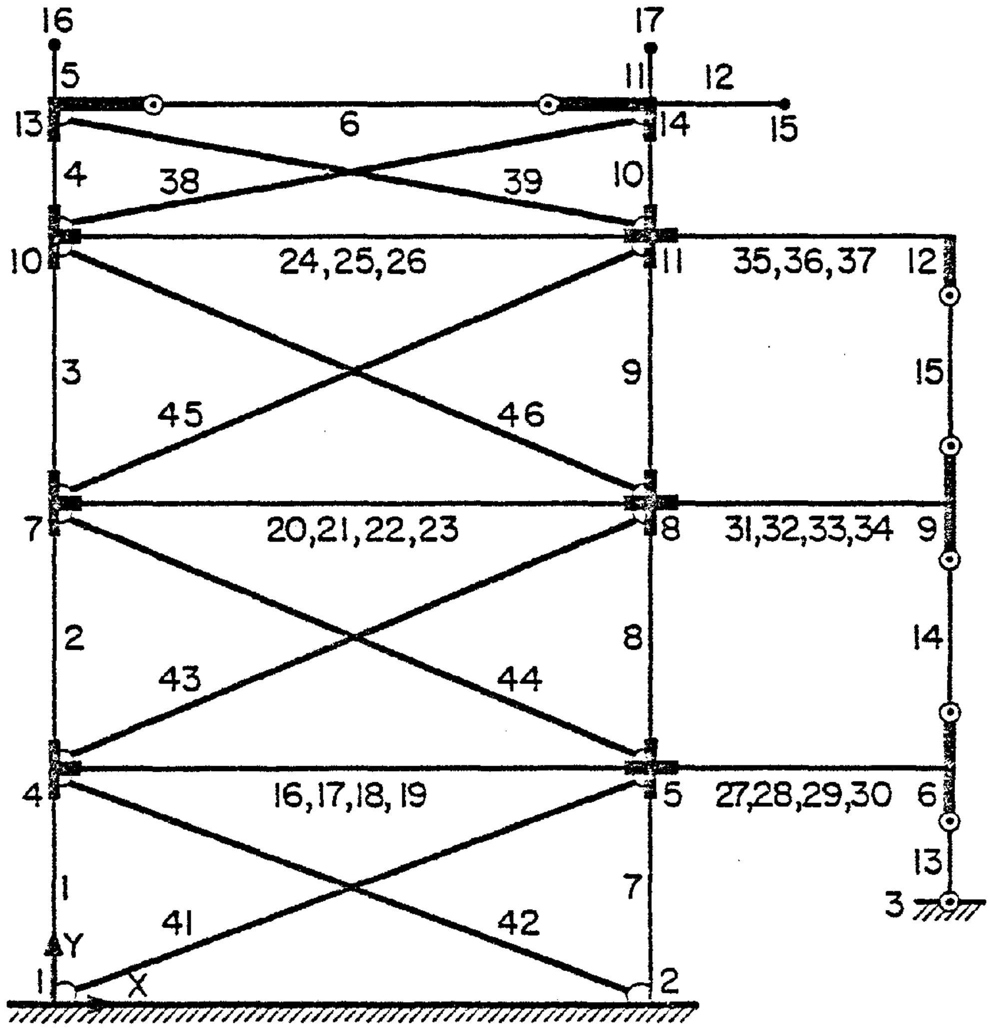

FIG. 47 ANALYTICAL IDEALIZATION OF INFILLED FRAME SUBASSEMBLAGE

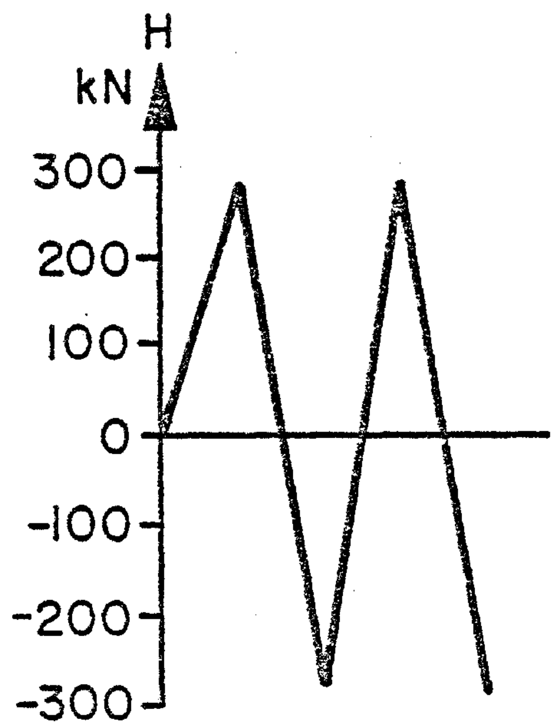

FIG. 48 LOADING PROGRAM USED FOR ANALYTICAL PREDICTION OF RESPONSE

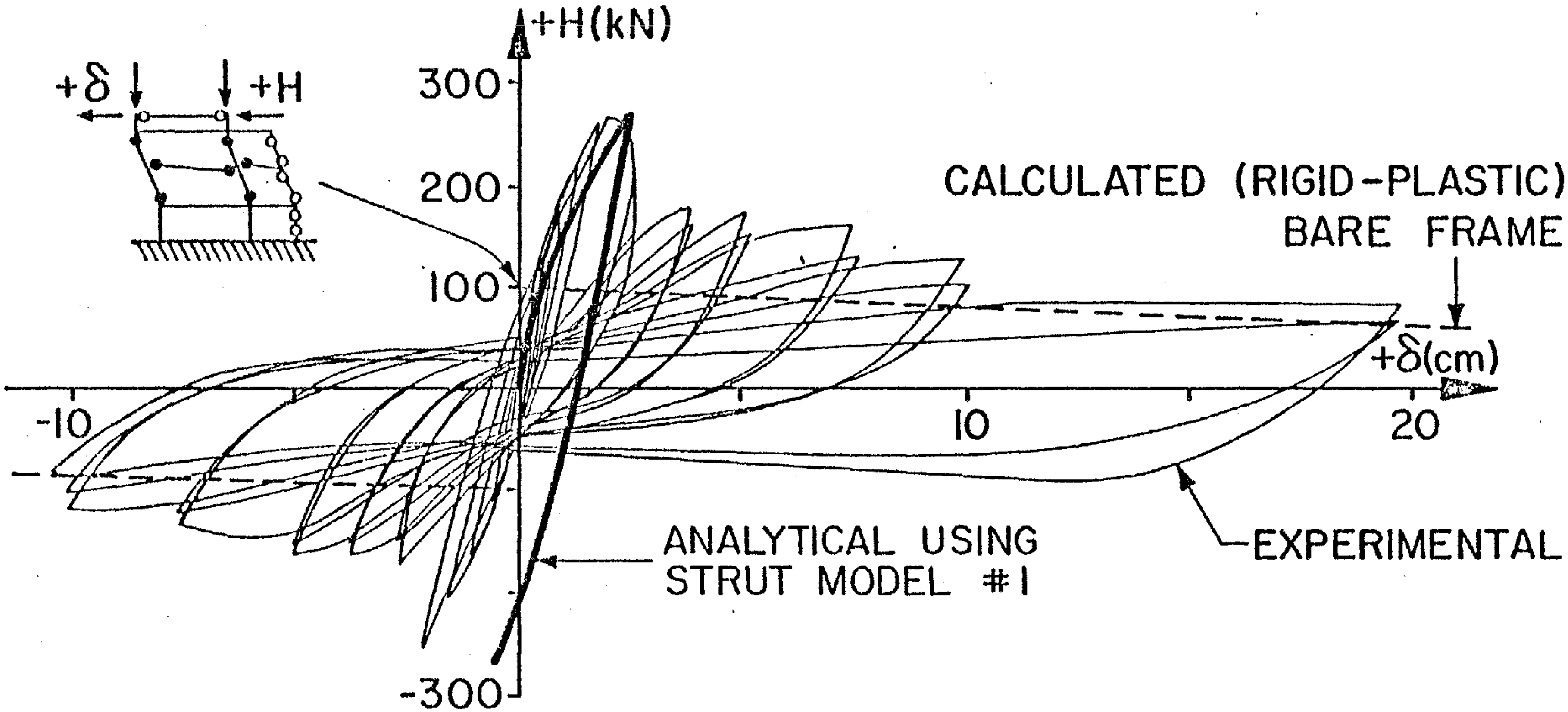

FIG. 49 COMPARISON OF EXPERIMENTAL RESPONSE (TEST #4) WITH THAT PREDICTED USING STRUT MODEL #1

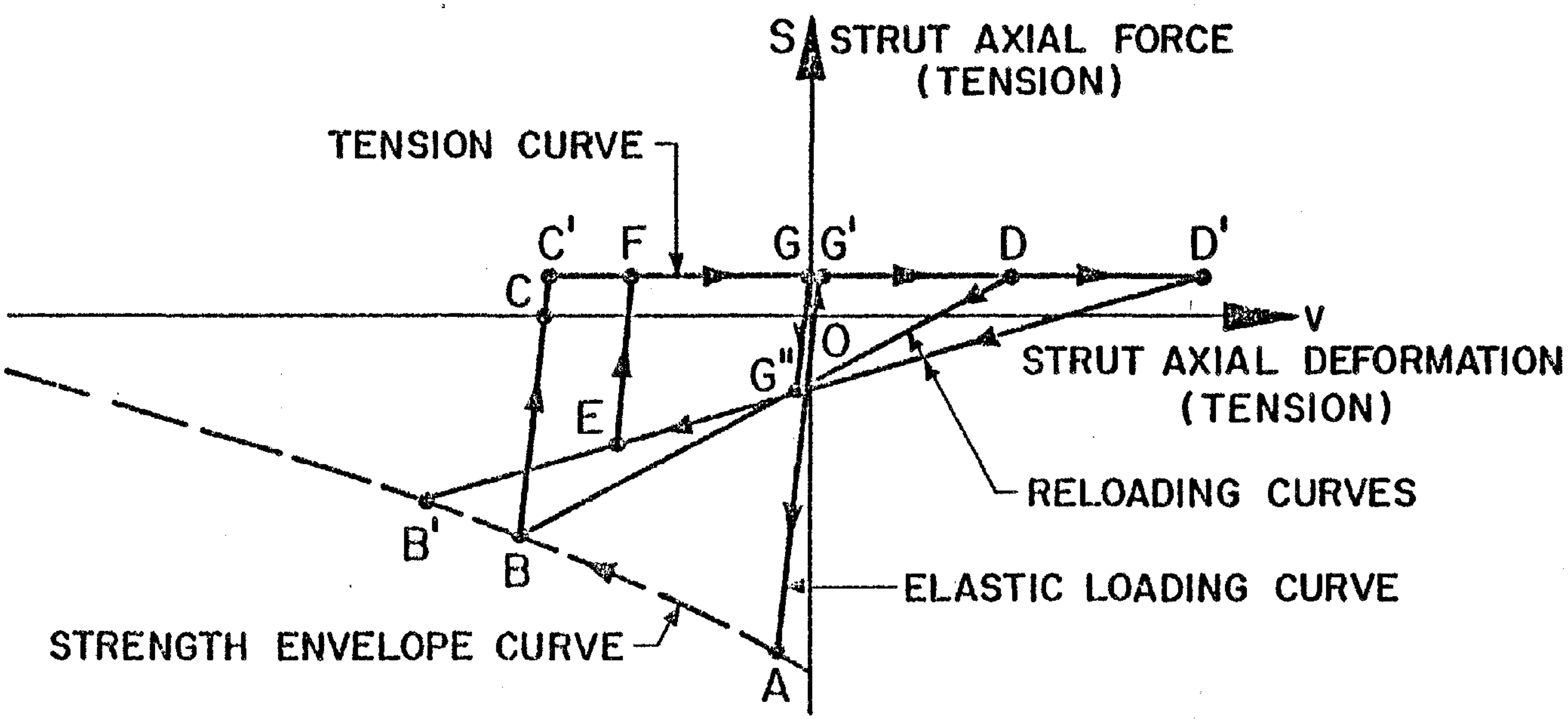

FIG. 50 MECHANICAL BEHAVIOR OF STRUT MODEL #2

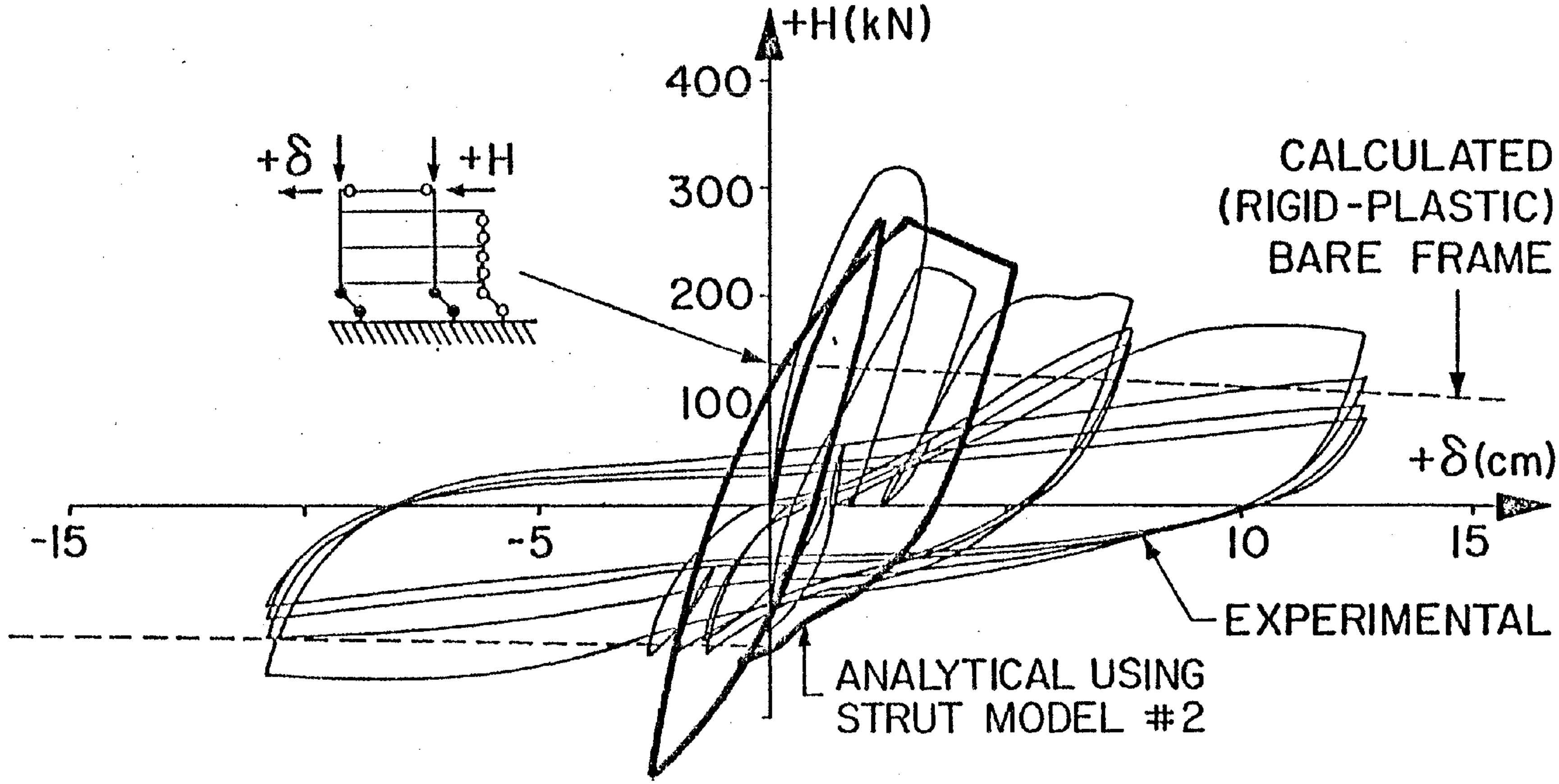

FIG 51 COMPARISON OF EXPERIMENTAL RESPONSE (TEST #3) WITH THAT PREDICTED USING STRUT MODEL #2

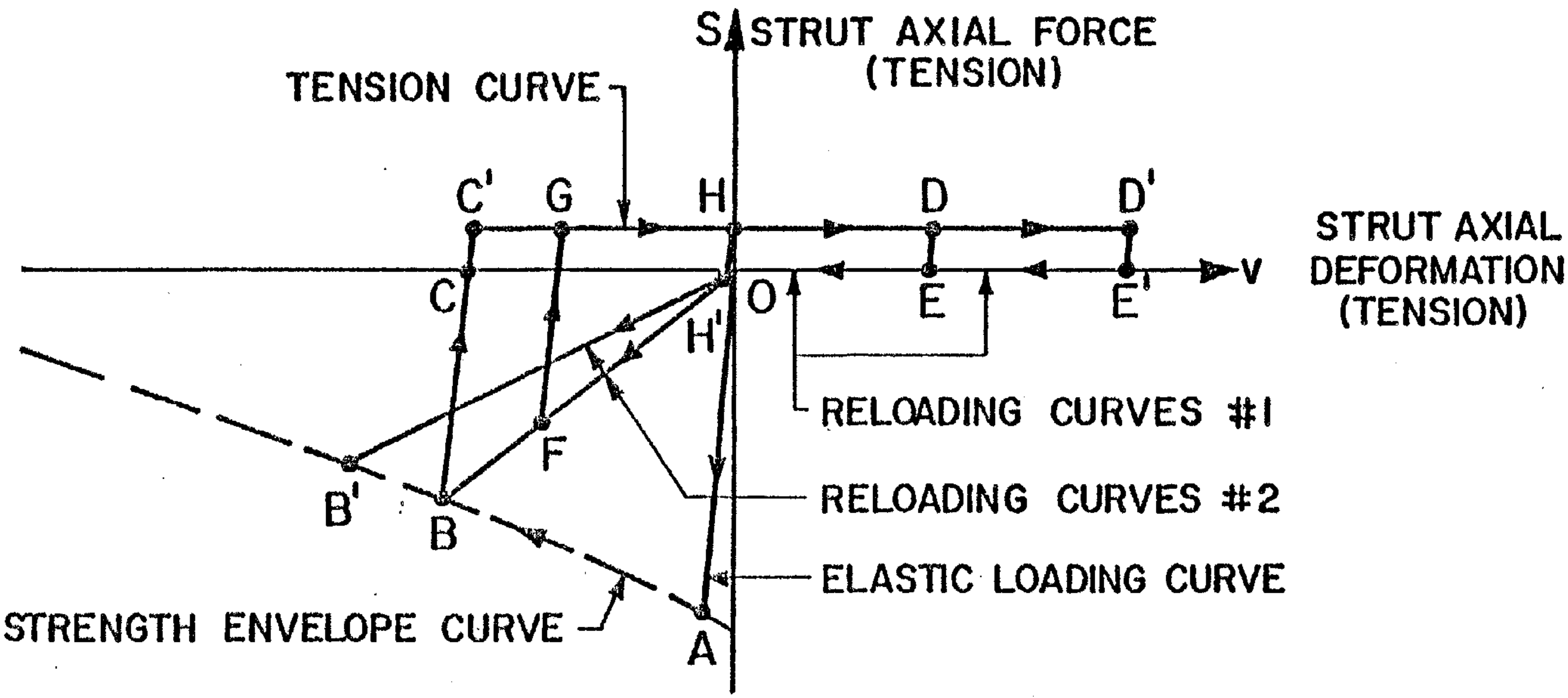

FIG. 52 MECHANICAL BEHAVIOR OF STRUT MODEL #3

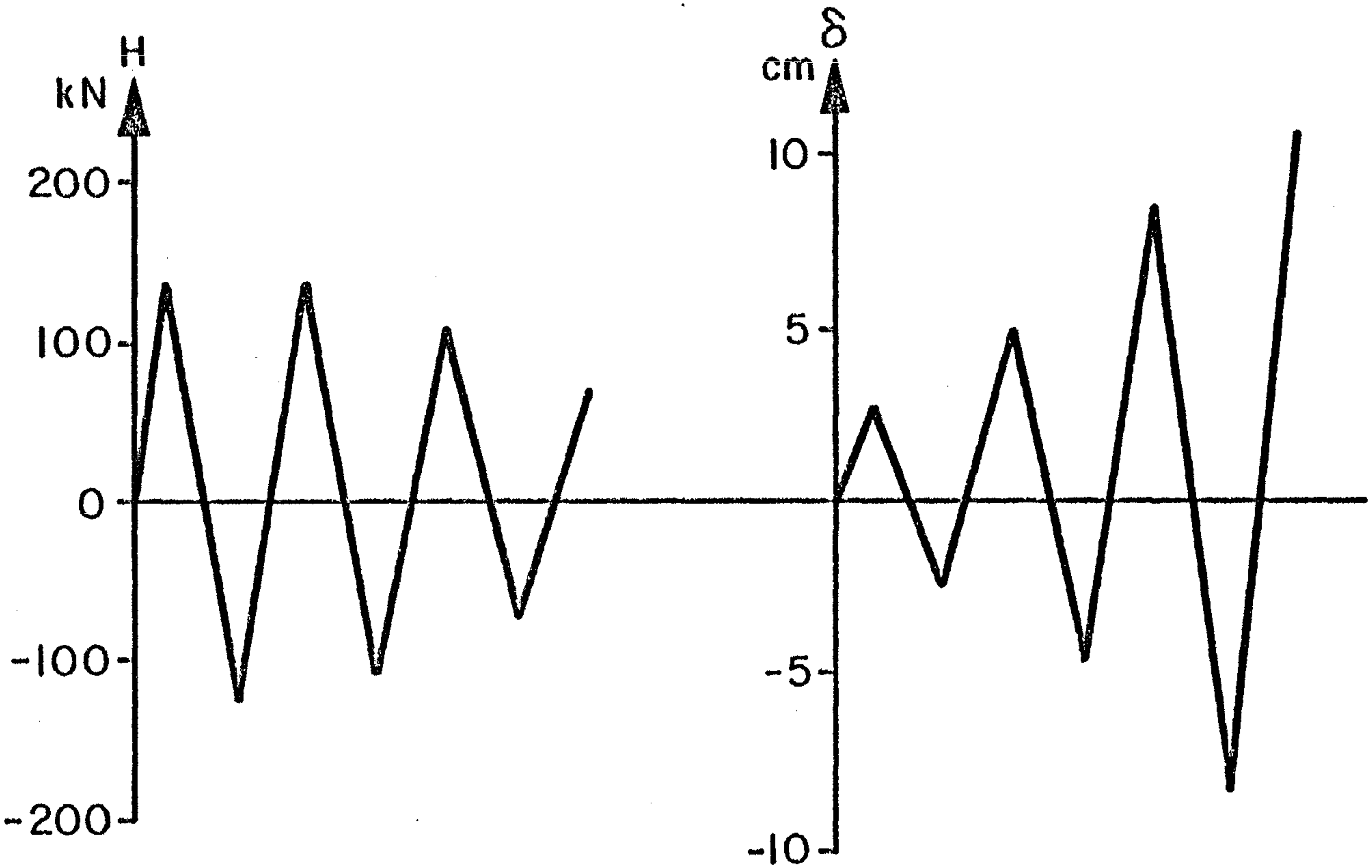

FIG. 53 EXTENDED LOADING PROGRAM USED FOR ANALYTICAL PREDICTION OF RESPONSE

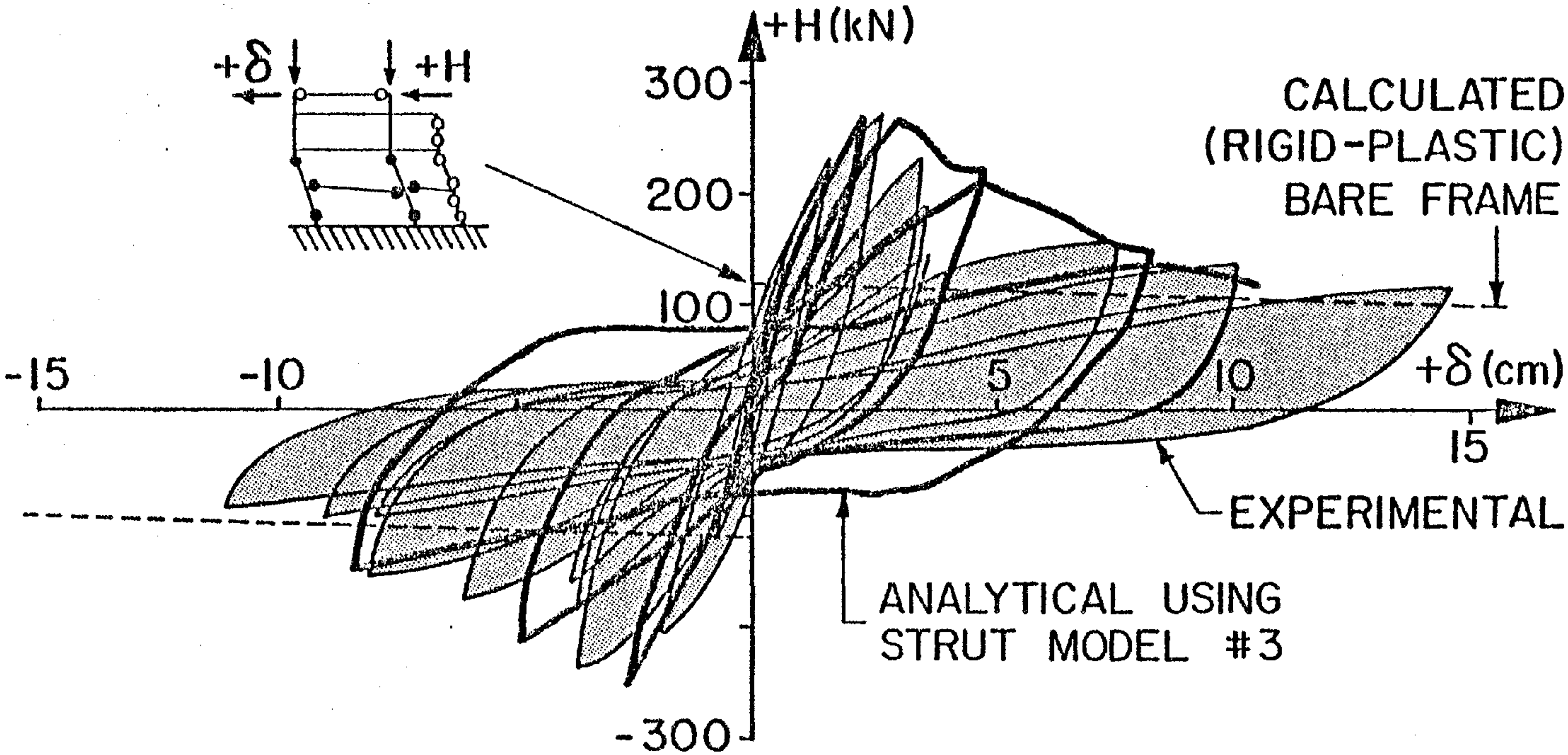

FIG. 54 COMPARISON OF EXPERIMENTAL RESPONSE (TEST #2) WITH THAT PREDICTED USING STRUT MODEL #3

APPENDIX A: LITERATURE INVESTIGATION

A.1 Experimentally Observed Behavior

From the point of view of earthquake resistant design, the most important information obtainable from experiments is the basic lateral force-deflection relationship for infilled frames. It is necessary to get load-deflection data for a variety of loadings, panel parameters, and frame parameters. While all of the important variables are obviously not known prior to carrying out experiments, several have been identified by previous researchers: the relation between panel and frame stiffness; the panel aspect ratio (height/length); the proportion of lateral to vertical load on the panel; the manner in which the load is applied; the amount and distribution of reinforcing steel in the panel; the panel material itself; the type of bond between the frame and panel; and the boundary conditions created by the testing apparatus. It is necessary to investigate the cracked and uncracked response to dynamic as well as static loads.

Some of the above areas have been studied extensively in previous experimental investigations which will be reviewed herein. Such investigations have studied the behavior of panels or infills of concrete, clay brick masonry, concrete block masonry, and clay tile. Although these materials have distinct behavior under certain conditions, it is believed that an understanding of some of the basic principles of infilled frame action can be achieved by initially studying these results without taking account of possible differences introduced by panel material characteristics. Section A.3 includes a discussion of some of the essential differences in the mechanical characteristics of commonly used infill materials.

More or less arbitrarily, the previous work has been grouped by the author into three categories: monotonic load tests, cyclic (quasi-static) load tests, and dynamic load tests.

A.1.1 Behavior under Monotonic Loading

a) Walls without Frames

During the 1950's, Benjamin and Williams carried out an extensive investigation of the lateral shear resistance of unreinforced brick masonry walls, with and without bounding frames [A5]. One- to three-eighths-scale models with aspect ratios varying from 0.8 to 3.0 were block-loaded to failure in racking. The unframed panels were invariably found to fail in flexure; that is, by the proportion of a horizontal crack across the base, starting from the windward (tension) side of the panel. No vertical loads were applied. It was concluded that the pre-cracked stiffness and failure load of an unframed panel could be fairly well predicted by simple beam theory, assuming a linear variation of flexural stress and a parabolic variation of shear stress along a horizontal line parallel to the base of the panel.

Borchelt [A9] tested clay brick and high-strength mortar panels in diagonal compression, and found that failure by diagonal tension occurred when the principal tension stress in the panel reached a critical value. Recently Blume and Proulx tested a number of 4- by 4-foot clay brick masonry panels in diagonal compression, and reached substantially the same conclusions [A8]. It was also found that increased reinforcement in the panels resulted in increased energy absorption capacity and ductility, the latter being defined as the ratio of deformation along the compression diagonal at failure, to the deformation at first cracking.

In Rumania, Negoita [A69] tested 1/4-scale plain brick masonry walls with aspect ratios ranging from 0.7 to 0.23, much lower in profile than those tested by Benjamin and Williams. Panels which were block-loaded in lateral shear were found to fail by cracking along the diagonal extending between the two load blocks. When similar panels anchored to a reinforced concrete base were subjected to a combination of vertical compression and lateral shear, they were found to fail by horizontal cracking along the base. The presence of vertical compressive loads tended to increase the average horizontal load necessary to cause such failure. Negoita concluded that the diagonal cracking indicated a failure governed by principal tension stress in the panel; the horizontal cracking caused rupture "due both to the principal stress and to the shear stress," indicating that the masonry had not been used efficiently.

Several explanations have been proposed for the variability of failure loads of masonry panels. Benjamin and Williams [A5] have suggested that variations in workmanship may be responsible. However, Fratessa and Zsutty have recently hypothesized that the manner in which the panels are loaded may significantly affect the observed first cracking loads [A25]. Although their observations were principally related to reinforced concrete shear walls, they pointed out that blocking loading tests could be misleading because they might create tensile stress concentrations which could be expected to decrease the failure load for brittle materials, and also because they are rarely representative of the actual ways in which shear elements are loaded. They recommended instead the use of flange load tests, in which the shear is distributed by a stiff member along the edges of two elements back-to-back.

To the author's knowledge, no flange load tests have been carried out on masonry panels without bounding frames. Schneider conducted a series of failure strength tests [A86] on full-scale I-shaped concrete block masonry piers, with nominal horizontal and vertical reinforcing. He found that the failure load increased with decreasing aspect ratios of the piers, and that the strength and ductility of the piers was increased by additional horizontal reinforcement. He found vertical steel comparatively ineffective in this regard. However, it is the author's opinion that the small amount of vertical steel used by Schneider was insufficient to induce significant deep beam action in the piers. Had the percentage of vertical steel been higher, it might have been found more effective in strengthening the piers in flexure.

Scrivener [A87] has studied the effect of the amount and distribution of reinforcing steel on the stiffness, strength, and ductility of masonry panels loaded (through a reinforced concrete bond beam) in lateral shear, with vertical compressive load applied to counteract flexural effects. He found no direct relation between the stiffness of the panels and the reinforcement quantity or pattern. Increased percentages of steel up to about 0.3% in either direction were effective in increasing the dutility (defined as the ratio of failure load to first cracking load). It was found that the onset of severe cracking was delayed in walls with an even distribution of reinforcement, compared to walls with peripheral reinforcement only. Vertical and horizontal reinforcement were observed to be equally effective in providing satisfactory crack behavior and increased failure loads.

b) Walls with Frames

The behavior under monotonic loading of steel and reinforced concrete frames has been studied exhuastively. But as many investigators have pointed out, the load-deflection relation for infilled frames cannot simply be obtained from a superposition of panel and frame behavior [A93]. Because the presence of the infill constrains the deflection of the frame, the stiffness of the combination will be greater than the sum of the stiffnesses of its components taken individually. After cracking occurs in the panel, the continued resistance of the combination is clearly afeected by the confining effect of the bounding frame.

Many investigators have studied this behavior. One of the first to do so was Wood [A101], who investigated the effect of cladding (infilling) on the lateral strength and stability of high-rise steel frame structures. He tested full-sized steel frames with comparatively flexible beam-column connections and infills of brick, clinker block, and hollow clay block. He found that the infill invariably strengthened and stiffened the frame, and failed itself by sudden cracking along the compressional diagonal.

Benjamin and Williams [A4, A5] studied the behavior of reinforced masonry and conrete shear panels, block loaded and enclosed in reinforced concrete bounding frames. They used full scale as well as 1/8- to 1/2-scale model walls, and observed no scale effects. Load-deflection data were gathered in the elastic range, and it was concluded that within the range of frame-to-panel stiffnesses tested, variations in concrete frame member area and steel percentage did not influence the rigidity of the wall in the uncracked range. Simple beam theory, including the effect of shear flexibility, was found to provide satisfactory agreement with measured deflections. It was found that the first cracking load was not affected by the amount of panel steel, within the range of percentages used. Two principal types of cracking were observed:

1) Walls without bounding frames, or with very weak frames, were seen to fail suddently at very low lateral loads by shear and tension across their bases, as mentioned in the previous subsection.

2) In a wall surrounded by a frame strong enough to withstand the overturning tension in the windward column and the shear in the leeward column, the first crack formed essentially along the compression diagonal of the panel. After the formation of such a crack, further resistance of the enclosed panel was found to be due to a combination of friction and wedging action.

The strength of an infilled frame following diagonal cracking was found to be related to the extent to which the panel exhibited distributed diagonal cracking, and to the ability of the leeward (compression) column to resist combined failure in shear, flexure, and compression. It was found that distributed diagonal cracking occurred in panels with aspect ratios close to 1.0, and with steel percentages of 0.25% or more in either direction. However, vertical panel steel was found to be much more effective than a corresponding amount of horizontal steel in increasing the ratio of failure load to first cracking load for the infilled frames tested. The influence of mortar bond between masonry panels and frame was studied in Reference A5, and it was concluded that

1) boundary cracking did not significantly affect the rigidity of the panel; and
2) at first cracking loads, the panels were essentially cracked free of the frames. Because of the limitations of the testing apparatus used, Benjamin and Williams were unable to record load-deflection data in the inelastic range.

Similar findings were reported by Negoita [A69]. He found that the addition of reinforced concrete beams and end columns to the plain masonry panels discussed in the above subsection, resulted in a 177% increase in rupture load for a panel with aspect ratio 0.70, only a 7% increase in rupture load for a panel with an aspect ratio of 0.23, and no increase at all for a panel with aspect ratio 0.20.

Through a series of model tests, summarized in Reference A95, Stafford Smith has found two possible failure modes for a block loaded infilled frame subject to lateral shear: local crushing in the loaded corner of the infill; and tension cracking along the compression diagonal of the panel, as discussed above. When distributed vertical compressive load was applied as well, two additional modes of failure were observed: a general compressive failure of the whole infill, roughly along a plane parallel to the base; and vertical tension cracks from the upper beam of the frame down through the panel to the foundation. Stafford Smith tested pairs of 12" wide by 8" high model steel frames with plain mortar infills, loaded "back-to-back", under different combinations of lateran and vertical load. He found that the lateral stiffness and strength (load at first cracking) were increased under vertical loads up to about one-half the vertical load necessary to cause failure acting alone [A95]. With small vertical loads, only the first two types of failure described above were noted. An optimally loaded frame would ideally fail by a combination of all four mechanisms. For higher vertical loads the lateral strength decreased, and the second two failure modes predominated.

Stafford Smith concluded that the observed increase in lateral strength accompanying the application of vertical loading was due to a decrease in diagonal tension in the center of the panel, and the creation of a favorable biaxial compressive stress state near the frame corner where the lateral shear was applied. The increase in stiffness was attributed to the increased contact length of the loaded beam on the infill and the consequent more even distribution of the lateral shear along the edge of the panel. He cautioned that the results summarized above ought not to be applied to infills lacking the rigid base support conditions present in the tests models used in his experiments.

Stafford Smith's conclusions regarding failure criteria for plain infill panels seem to be supported by the experimental investigations of Mallick and Severn [A59], who tested a series of pairs of rectangular and square model steel frames with plaster infill (aspect ratios from 0.5 to 1.0), placed back to back and loaded in lateral shear along the common frame member. They found the most common failure mode of the panels to be corner crushing, but noted that this could have been due to the fact that the plaster infill used was much stronger in tension than concrete of comparable crushing strength. They concluded that the most probable failure points would be either the point of maximum principal tension stress, or the points of frame-infill contact, the latter being the probable locations of maximum uniaxial compressive stress.

Mallick and Stafford Smith have proposed that for unreinforced panels the magnitude of the first cracking load and the nature of the crack pattern and dependent on the state of biaxial stress over the panel and the biaxial failure envelope of the infill material. Some of Benjamin and Williams' work suggests that the above may also be true for reinforced panels. However, the author feels that such a conclusion would be unwarranted on the basis of the information presented above.

Recent investigations by Mainstone [A55, A56, A57] have confirmed the usefulness of the equivalent strut concept in predicting the strength and stiffness of infilled frames. Extensive tests were carried out on plain and reinforced masonry walls, some bounded by steel frames, and others bounded by heavy steel linkages. Empirical formulas were developed for calculating the width of the equivalent strut; these generally agreed with results previously obtained by Stafford Smith [A93].

Several researchers have investigated the influence of support conditions and manner of loading on the load-deflection relationships obtained for infilled frames under monotonic loading. In addition to the work of Fratessa and Zsutty mentioned above [A26], investigations by Rosenhaupt [A82], Rosenhaupt and Mueller [A83], and Levy and Spira [A48] emphasize the significance of arch action in the creation of stress concentrations near loading or support points in vertically loaded masonry walls. In view of the brittle behavior of most infill materials, it is the author's opinion that erroneous conclusions might be drawn from panel tests unless care were taken to distribute shear loads by means of a stiff loading beam. This same point has been mentioned by Williams [99], whose work will be discussed in detail in the following section of this report.

c) Infilled Frame Assemblages

Comparatively little quantitative work has been done in this area, the earliest available reference being that of Polyakov [A78], who tested 3-bay, 3-story steel frames with masonry infills, loaded in racking along the top beam. He found that the assemblage behaved essentially as a braced system, with each of the 9 small panels carrying approximately equal portions of the total shear. He also concluded that after boundary cracking had eliminated the bond between the frame members and the infill, the entire assemblage could be idealized as a frame system with compression diagonals.

Tests to failure of actual buildings have been carried out by Ockleston [A72] and Read [A81], who conducted separate but similar investigations of the effect of infilling on the lateral stiffness and strength of multistory reinforced concrete frames. The load-deflection curves obtained showed that infilling increased both stiffness and strength, the latter by as much as a factor of seven over the strength of a nominally identical assemblage without infilling.

The most comprehensive study of such behavior is that of Fiorato et al. [A24]. A number of 1/8-scale reinforced concrete frame assemblages, most with plain clay brick masonry infill, were tested under monotonic lateral load applied to the top beam of the assemblage. The most extensively studied assemblage was a 5-story, 1-bay cantilever. The writers found this infilled assemblage to be stiffer, stronger, but less ductile than a nominally identical assemblage without infilling. The initial observed response of the infilled assemblage was similar to that of a cantilever beam, up until development of horizontal shearing cracks along a mortar joint in the infill panels. If such cracks did not form, the capacity of the assemblage developed as a beam failing in flexure. The initiation of the horizontal shearing cracks resulted in a combined resistance mechanism in which the lateral shear was resisted by the columns, which were partially braced by the intact portions of the infill. Failure of the assemblage occurred by shear, flexure, or axial tension failure of the columns. It was concluded that such an assemblage would behave either as a reinforced concrete beam or as a knee-braced frame, with the point of demarcation between the two behavior modes coinciding with the initiation of the horizontal shearing cracks. The presence of the frame was found to contribute significantly to the post-cracking strength of the assemblage.

It is believed that certain aspects of this observed behavior may have been induced by the type of infill material and method of loading used in the tests: the most striking example of this was the presence of shearing cracks, which fromed horizontally instead of diagonally in spite of the low panel aspect ratio (0.5). The formation of these cracks was probably encouraged by the highly flexural nature of the load, and by the inherent joint weakness of the low-bond masonry used. The writers themselves remark that the use of such masonry for the infills resulted in a response different from that which would have been expected from other types of panels. Had the tests been carried out using concrete or high-bond panels, and under loading conditions less flexural in character, the author believes that diagonal cracks would have formed instead, resulting in alteration of response.

A.1.2 Behavior under Cyclic (Quasi-Static) Loading

a) Walls without Frames

One of the first significant investigations in this area was that of Meli and Esteva [A65], who tested a group of reinforced panels, some of hollow concrete block and some of clay brick. Each wall was loaded cyclically either in diagonal compression or in-plane racking. While vertical load was also applied in some cases, the resultant nominal bearing stresses were only about 60 psi, compared to values of up to 500 psi used by other investigators [A99]. They found that regardless of the amount or distribution of reinforcing, the walls exhibited rapid loss of stiffness and carrying capacity after a few cycles. Similar observations were made by Alexander et al. [A1].

Another work is that of Scrivener and Williams [A88, A99]. They performed a series of tests on reinforced brick and concrete block walls subjected to cyclic quasi-static load applied in the plane of the wall through a stiff reinforced concrete bond beam. The parameters varied were the magnitude of bearing loads, wall aspect ratios, and the percentage and distribution of panel reinforcing steel. Hysteresis loops were obtained for several cycles of loading to constant deformation ; then the walls were loaded to failure. Panel reinforcing varied from 0.24 to 1.63%. Two distinct types of behavior were observed. The first, termed "flexural" by the investigators, was characterized by initial cracking in the horizontal mortar joints near the base of the wall. Following this, the wall was still capable of exhibiting stable hysteresis loops. Increasing deformations were associated with yielding of the tension steel, until failure finally occurred by crushing at the toe of the wall. It was found that "flexural" behavior was associated with walls with low bearing load, low percentages of vertical reinforcement, and high aspect ratios. High ductility (defined as the ratio of ultimate to first cracking deflection in the horizontal direction) was observed for walls which exhibited this type of behavior. Conversely, walls with high bearing loads, considerable vertical reinforcement, and low aspect ratios were found to display"shear" behavior and to possess comparatively low ductility. Although Scrivener and Williams' results corroborate the contention of Stafford Smith [A95] that the ultimate strength of shear panels is increased by the presence of bearing loads, the investigators pointed out that this increased strength was associated with an increased tendency towards shear-type behavior and consequent decreased ductility. They recommended two alternative approaches to the aseismic design of shear wall structures:

1) to design the wall elements by ultimate strength methods, adjusting the wall area, reinforcing, and aspect ratio to ensure ductile ("flexural") behavior under seismic loads; or

2) given the possibility of non-ductile ("shear") behavior, to design the walls by the working stress method for elastic behavior under the actual seismic loads likely to be experienced.

Recently, Priestley and Bridgman studied the resistance of brick masonry walls to cyclic lateral loads [A80]. Dispacement ductility factors of at least 4.0 were obtained from approximately square panels. Contrary to the conclusions of Scrivener and Williams, Priestley and Bridgman suggest that shear capacity may be significantly increased by the use of sufficient shear steel to resist the shear corresponding to the ultimate flexural load. Also, they suggest that ductility factors up to 5.0 may be achieved by placing stainless steel confining plates in the bottom few mortar courses at each end of the wall. These plates reduce the effective bed joint thickness and delay local crushing failure by decreasing the tension stresses caused by expansion of the mortar under load.

It is felt that ductility per se is a less useful criterion than energy dissipation capacity for predicting the seismic resistance of structural components, particularly those subject to brittle failure. The ductility factors observed by Scrivener and Williams as well as Priestley and Bridgman, may be difficult to achieve in real structures because of the complicated boundary conditions imposed by adjacent frames or floor diaphragms, the architectural constraints usually placed on panel aspect ratios, and the likelihood of high bearing loads. Also, while the conclusions discussed above might be applicable to simple buildings whose behavior could be idealized by that of individual shear panels, it seems probable that for complex structures, a much more complicated relationship exists between the ductile behavior of individual panel elements and ductility of the structure as a whole.

b) Walls with Frames

The behavior of steel and reinforced concrete frames under cyclic loads has been studied extensively [A2, A6, A13, A75], and will not be reviewed herein. One report on infilled frame response to cyclic loads is that of DeLisle and Heidebrecht [A21], who studied the cyclic load response of frames with slitted panels similar to those proposed by Muto [A68]. Using 0.25% panel reinforcing, they found that stable hysteresis loops were exhibited by the approximately sqaare panels, that the energy dissipated per cycle increased with increased vertical load, and that the amount of this energy dissipation was primarily influenced by the amount of cracking in the wall -- the more cracking, the more dissipation per cycle. They also found that an ordinary reinforced concrete panel dissipated more energy than a comparable slitted one. However, from some of the written discussions to DeLisle and Heidebracht's paper, it is believed that the slitted walls investigated may not have been designed and detailed in accordance with the latest available research on the subject.

Yamaguchi and Araki [A102] carried out an experimental and analytical investigation of the strength and stiffness characteristics of infilled frames made of precast reinforced concrete panels joined to steel bounding frames by flexible connectors. Cyclic load tests were performed on six single-panel models subjected to lateral shear and overturning moment. In the elastic range, the results agreed well with those obtained using a finite element analysis.

One of the most significant experimental investigations of the post-elastic response of infilled frames is the work of Esteva [A22]. Unreinforced masonry panels framed by heavy reinforced concrete members were subjected to alternating diagonal compression loads. It was found that the first 2 or 3 cycles were characterized by rapid loss of strength and stiffness, and that the process of deterioration progressed through the following distinct stages of behavior:

1) the frame and panel act together as an elastic unit;
2) the panel separates from the frame and begins to act as a compression strut;
3) the panel begins to show diagonal tension cracks along the compression diagonal; and
4) increasing deflections along the compression diagonal lead to tension cracking at the inside corner of the frame at the points of load application.

Esteva found that while application of vertical compressive load increased the first cracking load and changed the orientation of principal stresses in the wall, the infilled frame continued to exhibit stable hysteresis loops following the initial reduction in strength and stiffness. This is in contrast to the conclusions of Williams regarding unframed walls, and suggests that fundamental differences may exist between framed and unframed panels. Esteva used comparatively small vertical loads, less than 20% of the ultimate capacities of the panels in vertical compression alone. It is not known whether the same stable behavior would have been observed in the presence of larger vertical loads.

A careful investigation of the cyclic lateral load resistance of infilled frames was carried out recently by Leuchars and Scrivener [A47]. They tested three models: a reinforced concrete frame without infilling; one filled with unreinforced grouted hollow blocks; and one filled with reinforced grouted hollow blocks. The panels were connected to the frame by mortar bond only. The models were subjected to quasi-static cyclic lateral loads. No vertical loads were applied. These writers have arrived independently at observations regarding infilled frame behavior very similar to those hypothesized in Chapter 2 of the body of this report:

1) The infilled frame system acts initially as a single monolithic element.

2) After boundary cracking, the infill effectively acts as a diagonal compression strut whose equivalent properties depend on the frame and infill.

3) Failure may occur by: sliding shear along a horizontal mortar bed; local crushing of masonry in compression; or diagonal tension cracking.

A.1.3 Behavior under Dynamic Loading

Work in this area has been comparatively extensive. Unfortunately, the majority of investigators have studied only the free vibration characteristics of framed and unframed panels in the linear elastic range, with respect to such variables as typical damping values, characteristic frequencies, and mode shapes. Very little research has been concerned with the response of such structural elements after the onset of cracking, when their behavior is highly nonlinear.

a) Walls without Frames

Studies by various investigators [A10, A44, A58] have shown that in the linear elastic range, masonry walls exhibit damping ranging from 2 to 5% of critical. The only available work concerned with the post-elastic range is that of Williams [A99], who conducted a series of dynamic load tests similar to the quasi-static ones discussed in the previous subsection. Using load frequencies varying from 0.5 to 1.0 Hz, he found that types of walls which under the quasi-static tests had exhibited "shear" behavior, continued to do so, undergoing a high degree of structural deterioration after 1 or 2 cycles. However, it was found that in contrast to the ductile behavior of comparable walls tested statically, the "flexural" walls also suffered severe loss of carrying capacity with load repetition. It was noted that some of the walls which had been observed to fail in flexure under quasi-static loading, had also shown evidence of incipient failure by "sliding shear," in which the wall had cracked completely parallel to its base, but was prevented from sliding by dowel action and aggregate interlock. Williams hypothesized that in such a case dynamic loading, by dislodging pieces of masonry in the cracked zone, might increase the tendency of the wall to fail in a brittle manner.

b) Walls with Frames

A comprehensive experimental and analytical study of the dynamic inelastic response of reinforced concrete frames was recently conducted by Gulkan and Sozen [A27] and Otani [A74]. However, the dynamic response of infilled frames has not yet been explored to such an extent.

The effect of infill panels on the linear elastic response of a 4-story, 1/6th-scale model steel frame structure was investigated by Dawson and Ward [A19]. They found, not unexpectedly, that the natural frequencies of vibration of the frame were increased. A similar study was conducted by Saghera [A85], who investigated the effect of filler panels on the natural frequencies and mode shapes of a multi-story frame model made out of brass with epoxy infill.

In a subsequent study [A20], Dawson and Ward investigated the elastic dynamic response of a small-scale multistory steel frame model with cast-in-place infills of plain concrete. The results were compared with analytical predictions obtained by modeling the infills as equivalent diagonal compression struts. The elastic properties were calculated by finite element analysis of a single infilled frame sujected to lateral load. A similar study was carried out by Mallick [A62].

Ohsaki et al. subjected a full-sized model of a five-story apartment house to static and dynamic loads [A73]. They recorded displacements, cracking patterns, and shear force distributions at various stages prior to collapse of the structure. Tamura et al. tested a large model steel frame with precast concrete infill to failure under dynamic loading [A97]. While much of the data they obtained is difficult to assess quantitatively, they noted that the damping, initially about 2 to 3% of critical, increased up to 7 to 10% after the onset of cracking, owing to relative movement between the frames and infills.

One of the most informative investigations in this field is that of Mallick and Severn [A60], who obtained values of equivalent viscous damping by a variety of static and dynamic means for multistory models. Noting the increase in damping for large vibration amplitudes, they proposed that damping was produced by:

1) internal material friction;

2) friction between the frame and infill;

3) friction between pieces of the infill material itself following the onset of cracking; and

4) impact between the frame and infill due to rocking.

Although the concept of damping in composite structures is fundamental to possible analytical representations of the experimentally observed behavior discussed herein, it would be beyond the scope of this report to describe a topic to which entire books have been devoted. However, it should be mentioned that the classical work in this area is that of Jacobsen [A35,A36], and that important contributions have also been made by Jennings [A37], Mayes [A64], Hudson [A34], and Kennedy and Pancu [A40].

A.2. Analytical Investigations

Many investigators have sought analytical idealizations which would correspond to the modes of observed behavior described in the preceding section. Although behavior in the elastic range has been studied extensively, comparatively little work has been done on the complex post-cracking behavior of infilled frames, particularly those subject to dynamic loading.

A.2.1 Behavior under Monotonic Loading

a) Walls without Frames

These have traditionally been analyzed in the elastic range using simple beam theory, including the effects of shear flexibility. Among the investigators who used such an approach have been Benjamin and Williams [A4] and Krishna [A43]. The former have remarked that the variations in workmanship found in many masonry walls may tend to make theoretical predictions unreliable. Obviously, elementary beam theory cannot be applied to walls which have cracked, and becomes difficult to use even in the elastic range for a pierced wall. The latter case has been idealized using a truss analogy by Rosenhaupt [A82] and Rosenhaupt and Mueller [A83].

b) Walls with Frames

One of the first to study this field was Polyakov [A77], who used an approximate method based on elastic theory. From his experimental investigations of the strength of framed brick masonry panels loaded in compression [A78], he hypothesized a triangular distribution of stress over the infill in terms of stress functions. The panel was considered to have failed at a maximum theoretical shearing stress equal to the maximum shear stress observed for masonry in his previous experiments. He noted that in most cases the panel was cracked free of the frame (except at the compression corners) prior to failure of the infill itself, and suggested that the panel could be modeled as an equivalent compression strut. The interaction of the frame with the panel was investigated using lattice analogies by Hinkley [A31] and Benjamin and Williams [A5]. Rosenhaupt studied the same question in Reference A82 by considering the analogous problem of arching action in deep beams.

The diagonal-strut concept has been studied extensively. In a series of papers [A32,A33], Holmes proposed that the action of the infill would be similar to that of an equivalent compression strut with a thickness equal to that of the panel and a width equal to 1/3 of the length of the diagonal of the panel. An infilled frame or assemblage of such frames would then be idealized as a pin-jointed truss having rectangular panels braced by compression diagonals. Effective elastic moduli for the equivalent struts were computed on the basis of various model tests.

This approach has been refined considerably by Stafford Smith [A15, A92, A93, A94, A96], who suggested that instead of being fixed as proposed by Holmes, the width of the equivalent strut would vary with the applied loading and relative stiffnesses of the frame and infill. Assuming no bond to exist between the frame and the infill, he derived an empirical equation for the contact length, based on the theory of beams on elastic foundations. He then assumed a linearly varying stress distribution along this contact length (zero stress at the point of contact, maximum stress under the load point), and obtained expressions for the resulting stress distribution over the panel, using both a theory of elasticity approach and finite element methods. The equivalent-strut concept has not led to results which agree consistently with experimental observations, probably owing mainly to the assumption of an incorrect boundary stress distribution.

The problem has also been studied from the viewpoint of conventional elasticity. Liauw [A49,A50,A51] assumed the panel material to be isotropic and homogeneous, and used an eight-term stress function to satisfy the boundary condition of continuous compatability between frame and infill. Using the same assumptions of no separation or slip at the interface between the frame and the infill, Sachanski [A84] expressed the stress distribution over the panel in terms of the interaction forces in rigid links representing the bond between frame and panel. In a specific case in which 30 such links were used, he solved for the redundant forces using the above-mentioned compatibility conditions. Empirical "opening factors" were introduced to simplify the complex mathematical manipulations necessary to arrive at such solutions in dealing with pierced panels. The effect of openings on the lateral stiffness of infilled frames has also been investigated by Mallick and Garg [A61] and by Liauw and Lee [A52].

Smolira [A90] used a force-method analysis to obtain the lateral stiffness of an infilled frame, assuming contact between the frame and panel to take place at the compression corners only. A finite element approach was adopted by Karamanski [A39], who assumed continuity between the elastic infill and the surrounding frame, only axial deformations in the frame elements, and base fixity. In a discussion to Karamanski's paper, this approach was criticized by Mallick and Severn, who proposed the following guidelines for analyses of infilled frames [A59]:

1) the methods used must be applicable to rectangular frames loaded laterally as well as square ones loaded in diagonal compression;

2) slip between the frame and panel must be considered; and

3) the methods must not assume a contact length between the panel and frame, nor a certain stress variation along that length.

Based on these guidelines, Mallick and Severn carried out a finite element analysis which idealized the frame and panel as two separate elastic structures, connected by link elements capable of transmitting only compression and shear. Frame members were assumed to deform only in flexure, and constant strain rectangular finite elements were used to model the panel. Good agreement with experimentally determined stiffnesses was achieved, especially for square panels. Considerable attention has been devoted to the study of particular finite elements especially suited to analyses of shear walls. The reader is referred to the work of MacLeod [A54], which has been discussed in depth by Pole [A76], Felippa [A23], and Spira and Sokal [A91].

The finite element approach has also been used to model the inelastic, post-cracking behavior of infilled frames under monotonic loading. The fundamental aspects of the problem are discussed in an excellent report by Moss and Carr [A66]. The most detailed work along those lines to date is that of Franklin [A25], who analyzed the behavior of infilled reinforced concrete frames, taking into account material nonlinearity, cracking of plain concrete infill, and separation and slip between the frame and panel. It is worthwhile noting, however, that the anlysis to failure of a single infilled frame, loaded laterally by uniformly distributed horizontal shear along the top beam, required a discretization involving 98 nodes and 84 elements, and took almost 10 minutes on a CDC-6400 computer. It seems doubtful that such an approach would be applicable to large structures. Also, the fact that the resulting load-deflection relation for the above-mentioned infilled frame was very simple, practically that corresponding to rigid-plastic behavior, suggests that simpler approaches may perhaps be used to achieve comparably accurate results with much less computational effort.

c) Structural Assemblages

As implied by the above comments concerning Franklin's work, it is believed that analysis methods applicable to large structural systems pose problems quite different from those used in the analysis of single panels or groups of infilled frames. The very first analyses of infilled frame behavior, predating even those of Polyakov, were carried out by practicing engineers primarily interested in practical solutions to actual problems which they faced. One such investigation is that of Butler and Muto [A14], which discusses several semi-empirical Japanese techniques used to estimate lateral force distribution coefficients for building design. In Reference A98, Tomii presents classical procedures used in the design of reinforced concrete shear walls. Many excellent papers concerned with the behavior of shear wall and infilled frame structures may be found in Reference A18, and papers by Khan and Sbarounis [A41] and Zsutty [A104,A105] are also informative.

Computer programs are available for the linear elastic analysis of large frame structures with shear elements. Those of Clough et al. [A17] and Mamet [A63] employ the concept of story subassemblages to reduce the amount of core storage necessary; a program by Oakberg and Weaver [A71] idealizes continuous shear walls using rectangular finite elements, and uses bay rather than story subassemblages. Oakberg has remarked that finite element shear wall models seem preferable to deep column ones because the former permit a more accurate assessment of the interaction forces between shear walls and frame members.

As part of a recent experimental study of the lateral response of reinforced concrete frames with masonry infill, Fiorato et al. developed conceptual idealizations of cracked and uncracked infilled frames based primarily on two modes of behavior--beam action and knee-braced column action--which they observed. However, that reference includes only limited data to support the idealization proposed for the inelastic range. The writers noted that the "fair" agreement between calculated and observed stiffnesses in the cracked range, seemed to be very sensitive to the effective length arbitrarily chosed for the knee-braced column used in the idealization.

A.2.2 Behavior under Dynamic Loading

In the previous section a separate heading was provided for discussion of experimentally observed behavior of infilled frames under quasi-static loading. Because no comparable analytic investigations are known to the author, a review of studies of dynamic response behavior follows:

a) Walls without Frames

Several investigations have considered the wall as a deep beam (with flexural and shear stiffness) vibrating as a vertical cantilever. The work of Heidebrecht and Raina [A29], while directed principally at the problems of shear wall structures, is representative of the techniques used: assuming the walls to behave as thin-walled plates, the necessary differential equations are set up, boundary and compatibility conditions are applied, and the natural frequencies and corresponding mode shapes are evaluated.

No work comparable to that of Franklin is available for the case of cyclic or dynamic loading. The most pertinent investigation is that of Williams [A99]. In conjunction with the cyclic load tests mentioned previously, he studied the ductility requirements of short-period single degree of freedom (SDF) systems. Although these did not directly correspond to the walls which he had tested earlier, the SDF idealizations included two proposed types of stiffness degradation characteristics which were thought to be representative of the two distinct types of wall behavior observed in tests: one SDF model, corresponding to the "flexural" walls mentioned earlier, was provided with stiffness degradation characteristics as proposed by Clough [A16]; the other was provided with a type of stiffness behavior (described by Williams as "total degraded stiffness") devised to represent the most extreme case of stiffness degradation, such as that observed for one of the so-called "shear-type" walls.

According to results reported in References A88 and A99, it was found that idealized short period SDF structures (T from 0.3 to 0.6 sec) with either of the types of stiffness degradation noted above, responded to the El Centro 1940 NS ground motion accelerogram in a manner described as more "active" that that of longer period structures: a normal effect of stiffness degradation in long period structures is to reduce their reponse to accelerograms similar to that of El Centro, since decreased stiffness produces longer natural periods of vibration, which correspond to lower spectral response accelerations. On the other had, a SDF structure whose natural period of vibration is initially shorter than that corresponding to the peak spectral response, may be subjected to increased accelerations owing to decreased stiffness, and, according to Scrivener and Williams, may require greater ductility factors than longer period structures, even though both types of structures are excited by the same ground motion. It should be recognized that the results of the above study are valid only for single degree of freedom systems, and that the degrading stiffness response of a multi-degree of freedom system, particularly as regards the relationship between element ductility and overall structural ductility, must be considered in considerably more detail before such general conclusions may be warranted.

b) Walls with Frames

Analytical investigations of the dynamic characteristics of infilled frames have apparently been restricted to studies of behavior within the elastic range. Lamar and Fortoul [A46] examined the effect of brick masonry infills on the plane free vibrations of plane frames. Natural frequencies and mode shapes were compared for an idealized frame structure with and without masonry infilling, which was treated as an elastic, isotropic, homogeneous material in plane stress. No provision was made for including the effects of slip or separation of frame and panel.

In the paper by Mallick and Severn referred to earlier [A60], an infilled frame was idealized as an assemblage of linear elastic frame and panel elements, jointed together along a continuous interface. The technique was extended to dynamic analyses by the development of a consistent mass matrix for the assemblage. Natural frequencies and mode shapes calculated for different frames agreed well with experimentally determined values, as long as vibration amplitudes were kept small.

c) Structural Assemblages

The extension of the study discussed immediately above to the analysis of multistory frames was considered by Mallick and Severn in the same paper [A60], and alternative approaches were proposed:

1) a "shear structure" model which would consider the frame and panel elements to be rigid in the vertical direction; and

2) a "bending structure" idealization, which would permit the inclusion of the effects of axial column and panel deformations.

The latter method was found to give much better results for natural frequencies and mode shapes than the former when compared to the actual observed behavior of model infilled frame cantilever structures. The most recent work in this area is that of Kost [A42], who had developed a computer program for the nonlinear dynamic analysis of frames with filler panels. The only nonlinearity considered by the program is the positive bilinear elastic lateral story stiffness due to a known initial separation between the panels and frames. While many general computer programs have been written for inelastic structural analysis, none is available for the analysis of cracked infilled frames subjected to load reversals or dynamic excitation.

A.3. Material Properties

In the first section of this report it was remarked that a grasp of some basic principles involved in the structural action of infilled frames could be achieved without distinguishing among the behavior exhibited by the many different available panel materials--plain or reinforced concrete, plain or reinforced concrete block masonry, plain or reinforced clay brick masonry, and clay tile. A review of the principal observations noted in the previous sections will show that the kind of material description needed for correct analytical idealization depends on the goals of the analysis. Since studies [A4,A5] have shown that over normal ranges of steel percentages the uncracked stiffness and first cracking load of an infilled frame are practically independent of the amount and distribution of reinforcing steel, a linear elastic analysis of an infilled frame would only have to be concerned with a material model representing the biaxial stiffness and strength characteristics of the particular frame and panel materials involved.

On the other hand, References A4 and A99 indicate that the behavior of an infilled frame in the post-cracking range is very much affected by the amount and distribution of reinforcing steel. Hence for purposes of an inelastic analysis there might be a need to study such topics as the inelastic behavior of the steel, the bond-slip characteristics of the reinforced panel, the process of bond deterioration with load reversals, the nature of aggregate interlock between pieces of cracked wall material, and the possible deterioration of the panel at the interface with the frame due to friction and impact. While some of the above mentioned subjects may be investigated quantitatively, it is recognized that others are probably amenable only to empirical approximations. The following subsections will review pertinent investigations of the characteristics of common infill materials in the light of questions such as those proposed above. The reader is referred to any introductory book on structural steel design [A3,A75] for a discussion of the mechanical properties of structural steel.

A.3.1 Plain and Reinforced Concrete

A good general introduction to the uniaxial stress-strain characteristics of plain concrete may be found in textbooks such as that written by Winter and Urquhart et al. [A100]. A more complete description of the stiffness and strength characteristics of plain concrete under biaxial loading is given in Neville [A70]. Other specific references on this subject are papers by Kupfer et al. [A45] and by Bresler and Pister [A12]. The author believes that sufficient data are available to idealize the biaxial stiffness and strength characteristics of concrete until the onset of cracking. The bond-slip characteristics of deformed reinforcing bars have been studied by Lutz and Gergely [A53] among others, and a paper by Bresler and Bertero

[A11] discusses the problem of bond deterioration in reinforced concrete under repeated loads.

A.3.2 Clay Brick and Concrete Block Masonry

A good summary of early investigations of the elastic strength and stiffness characteristics of clay brick masonry may be found in Blume [A7]. More recent studies have been conducted by Hilsdorf [A30] and Williams [A99]. They reached several conclusions regarding the probable failure mechanism of low bond masonry in general, whether of clay bricks or concrete blocks: masonry is a distinctly non-homogeneous, non-isotropic material composed of two brittle components --clay or concrete block units, connected by portland cement mortar. Since the block units are generally stiffer than the mortar in uniaxial compression, they act principally to restrain the lateral (Poisson) expansion or contraction of the mortar. As a result, in masonry under vertical compression, the mortar is in a favorable state of triaxial compression (vertical load plus the biaxial restraint in the horizontal plane due to the units), while the units themselves are in a relatively unfavorable state of vertical compression and lateral biaxial tension. The nominal compressive failure stress for masonry prisms is therefore greater than the corresponding stress for mortar prisms, but less than that of the clay or concrete block units used. The masonry strength may be further reduced by size effects, inefficient bond patterns, or irregularities in workmanship.

Sinha and Hendry [A89] and Murthy and Hendry [A67] studied the shear strength of brick couplets constructed of various materials, and loaded with varying amounts of precompression during curing. Unfortunately, the lack of experimental data concerning the bi- and triaxial stiffness and strength of either masonry or block units makes it difficult to use such studies to develop quantitative relations predicting multiaxial behavior. Hilsdorf [A30] attempted this using the assumptions that mortar and concrete behave similarly under triaxial compression, and that brick under biaxial tension behaves similarly to brick under uniaxial tension. Recently, Yokel and Fattal [A103] conducted an extensive investigation of failure mechanisms of brick masonry subjected to simultaneous diagonal compression and vertical compressive edge load. They concluded that failure occurred by joint separation or by splitting. Joint separation failures were found to occur at a critical stress

$$\tilde{\tau}_c = \tilde{\tau}_o - \mu\sigma_y$$

where σ_y is the average compressive stress and μ is approximately equal to 0.4. Splitting failures were found to occur under a critical combination of principal normal stresses. This last conclusion agrees qualitatively with the results obtained for concrete by Kupfer et al. [A45].

Unfortunately, the lack of experimental data concerning the bi- and triaxial stiffness and strength of either masonry or block units makes it difficult to develop quantitative conclusions from the above behavior description. In Reference A30 Hilsdorf attempted this using the assumptions that mortar and concrete behave similarly under triaxial compression, and that brick under biaxial tension behaves similarly to brick under uniaxial tension. While these assumptions do not seem unreasonable, the author is aware of no specific experimental data to support them.

In view of the considerable influence of variations in workmanship on the strength of masonry walls [A5], it is possible that attempts to model the behavior of masonry in the detailed manner outlined above may lead to increased computational effort without any corresponding increase in accuracy. Satisfactory strength and stiffness descriptions could possibly be achieved by studying the load-deflection relation and average ultimate tensile or shear stress for entire masonry panels. In addition to the studies summarized in Blume [A7], investigations along these lines have been carried out by Polyakov [A79], Hedstrom [A28], Borchelt [A9], and Blume and Proulx [A8]. Fiorato et al. have noted [A24] that one characteristic of such tests is the tendency for cracking to take place along clearly defined failure planes, especially in the case of low-bond masonry. Hence strength characteristics of a masonry wall may be very sensitive to the bond pattern of the specimen used and its orientation in the testing apparatus. No data are available concerning the bond-slip characteristics of reinforced masonry.

A.3.3 Clay Tile Masonry

The only pertinent work available is that recently carried out by Johnson and Matthys [A38], who performed tests on clay tile-mortar assemblages made of different types of hollow-core units in order to determine typical values for ultimate strength in compression, flexure, and diagonal tension. The results showed these strengths to be very dependent on the individual core pattern of the blocks used and their orientation within an assemblage.

A 3.4 General Analytical Problems

Some of the information discussed above is summarized in an excellent paper by Moss and Carr [A66]. In addition to questions of material behavior descriptions, their study also presents some of the general concepts involved in setting up a digital computer program to handle an incremental load analysis of a nonlinear material subject to inelastic effects such as cracking. The work of Franklin [A25] includes a detailed discussion of ways in which the finite element method may be used to model the behavior of cracked, non-isotropic materials.

A.4 Summary of Previous Research

In order to focus attention on certain aspects of infilled frame behavior about which more information may be needed, the experimental and analytical studies reviewed in the previous three sections will be examined in the light of the goals proposed in the Introduction.

A.4.1 Walls without Frames

a) Monotonic Loading

Because of the possible effects of differences in loading methods and boundary conditions used in each study, it is difficult to compare the results of each investigation described previously. However, it seems that behavior in the uncracked range is well understood. Limited tests indicate that panels without bounding frames, loaded in vertical compression and lateral shear, fail suddenly when the principal stress reaches some critical value with respect to the biaxial failure envelope of the particular material used [A5, A8, A9, A69, A103]. Until cracking occurs, the load-deflection relation is practically independent of the amount and distribution of wall reinforcing (in normal amounts)[A87], and may be calculated with reasonable accuracy by elastic deep beam theory or finite element methods [A4,A60].

While little quantitative information is available on the post-cracking behavior of such panels, Scrivener's tests indicate that up to a total of about 0.3% in both directions, vertical and horizontal steel are equally effective in increasing the ductility (as defined previously) in lateral shear of panels with aspect ratios near 1.0 [A87]. In his tests, no singificant loss of vertical carrying capacity due to cracking was observed. However, this topic has not been specifically investigated in any available study.

More data are needed concerning the effect of reinforcement distribution and vertical load on post-cracking ductility of such walls. It would also be helpful to have more information about the bi- and triaxial strength and stiffness characteristics of clay brick masonry.

b) Cyclic Loading

Aside from the block loading tests of Meli and Esteva [A65], the only investigations in this area are that of Scrivener and Williams [A88,A99] and Priestley and Bridgman [A80]. While their observations regarding stiffness and strength deterioration with load repetition are informative, the author believes that much more must be learned about the influence of boundary and loading conditions before the writers' concepts of "flexural" and "shear" behavior can be meaningfully related to actual structural response. Specific information is needed on the force-deformation characteristics under cyclic load of unframed walls with boundary and loading conditions representative of those found in actual structures. For instance, Williams' experiments might be repeated using pier elements. In addition, it is believed that Priestley and Bridgman overemphasize the concept of ductility, which may be often less important than energy dissipation capacity.

While Moss and Carr [A66] have presented the basic building blocks of a model finite element program to compute the response of cracked as well as uncracked walls to cyclic loads, one may infer from Franklin's work with infilled frames [A25] that such an approach may be unnecessarily complex if only load-deflection data rather than actual cracking patterns are desired. The author believes that satisfactory analytical models may be developed to reflect the behavior of an entire panel rather than the behavior of finite elements within that panel. Therefore, more experimental information is concerned, more information must be learned about the bond-slip relation (under cyclic load) between reinforcing steel and grout before such complex methods can be expected to give results comparable to those observed in actual tests.

c) Dynamic Loading

In the elastic (uncracked) range, this problem has been studied extensively and appears amenable to the techniques of conventional finite element dynamic analyses [A60]. One little explored topic associated with such analyses is the influence of loading rate on the bi- and tri-axial stiffness characteristics of wall materials in the elastic range.

However, practically no research has been carried out in the cracked range. The author feels that while the lateral load-deflection behavior of an uncracked shear panel can be described in terms of its proportions and materials, its post-cracked behavior under cyclic or dynamic load is primarily a function of the degree to which structural integrity can be maintained. Although some investigators such as Zsutty [A105] have proposed that such integrity is predictable for walls with certain aspect ratios, it may also be considerably influenced by local variations of materials and workmanship which are outside the scope of deterministic analysis methods. There is certainly a need for extensive experimental study of the factors which contribute to maintained structural integrity in a cracked wall subjected to cyclic or dynamic lateral loads and constant vertical compression.

A.4.2 Walls with Frames

It was proposed in the previous subsection that the post-cracking behavior of an unframed wall subjected to cyclic or dynamic loading may be primarily a function of the maintenance of structural integrity, a difficult characteristic to evaluate deterministically. Although the presence of an enclosing frame may slightly affect the panel's linear elastic behavior, the most important consequences occur in the post-cracking range: besides comprising a "back-up" vertical and lateral load resistance mechanism for the entire structure, the enclosing frame tends by its confining action to increase the integrity of the cracked panel under cyclic load, in a manner conceptually similar to the way in which closely spaced spirals increase the flexural ductility of a reinforced concrete member.

a) Monotonic Loading

Several studies indicate that for typical frame member sizes and steel areas (in the case of reinforced concrete frames), the lateral stiffness and first cracking load of the infilled frame are independent of frame reinforcement [A24], panel reinforcement [A4], and boundary cracking [A5]. The author feels that this last conclusion would be correct only for the case of an infilled frame with continuous contact initially present between the frame members and the panel material. Another topic that should be investigated is the influence of frame-panel connection on ductility under monotonic loading. While the effect of shear connectors has been touched on by Mallick and Severn [A59] and Yamaguchi and Araki [A102], more data are desirable.

Mallick and Severn [A59] and Stafford Smith [A95] have proposed that for unreinforced panels, the magnitude of the cracking load and the nature of the crack pattern are dependent on the state of biaxial stress over the panel and the biaxial failure envelope of the infill material. Some of Benjamin and Williams' work [A4] suggests that this is probably true for reinforced panels as well. Since Benjamin and Williams' study [A4] indicates that the ductility of an infilled frame is highly dependent on the way in which cracks form over the infill, there is a need to perform experiments with flange loaded infilled frames to test their findings in this regard. The work of Yokel and Fattal [A103] might be extended to this type of loading.

However, this raises another question which is more open-ended: in view of the goals of this study, it is certainly desirable to derive experimental results from tests which approximate actual structural conditions as closely as possible. Since such conditions unfortunately cannot be known a priori, the researcher must try to discover the extent to which the desired results are sensitive to variations in the way that panels or frames are supported and loaded. Most investigators have loaded panels or frames through blocks in either racking or diagonal compression, a loading condition which some researchers [A26, A82, A83] have associated with the presence of significant arching action and stress concentrations. Other studies have used stiff bond beams, and in one test pier action was examined. It is believed that either flange or bond beam loading is preferable to block loading. However, little evidence is known either to support this belief or to indicate that flange load tests, for example, actually approximate the conditions prevailing in real structures, particularly with respect to the way in which cracked and uncracked panels may affect the vertical force distribution in a frame structure.

From an analytical point of view, infilled frames are tractable in the nonlinear elastic range (including the effects of separation) using the techniques of Moss and Carr [A66], Mallick and Severn [A59], or Kost [A42]. Although Franklin's work [A25] has shown that the effects of cracking may also be included, the complexity of his approach necessitates a formidable amount of data preparation and computer time for the load-deflection analysis to failure of even a single infilled frame. As mentioned previously, the author believes that it might be more desirable to develop macroscopic analytical models based on extensive experimental investigations of the behavior of entire panels.

b) Cyclic Loading

This problem is at present unsolved analytically, except in the elastic range. One obstacle seems to be our incomplete understanding of the hysteretic characteristics of commonly used frame and panel materials such as reinforced concrete and clay brick masonry. But in the author's opinion, the most significant lack of knowledge in this area is experimental - as mentioned above, more studies are needed of the behavior under cyclic load of infilled frames with realistic boundary conditions and various types of mechanical connections between the frame and the infill.

c) Dynamic Loading

A review of the experimental and analytical results discussed in the previous sections indicates that this problem may be handled as far as the elastic range is concerned using techniques such as those of Mallick and Severn [A59,A60] and Kost [A42]. However, a study of inelastic dynamic behavior of infilled frames presents all the problems found in the cyclic load case described above, plus complications introduced by changes in mechanical properties at high strain rates, and the phenomenon of material dislodgement from a cracked panel. While an extension of Franklin's procedures to the dynamic case is theoretically possible, it is doubtful that our present knowledge of material properties would justify such an approach.

A.4.3 Large Structures

The only experimental investigations of the behavior of multi-panel assemblages which present useful quantitative information are those of Mallick and Severn [A59,A60] and Fiorato *et al*. [A24]. Reference A59 considered only the elastic nonlinearity introduced by separation of the frame from the infill. This approach was also adopted in the analytical work of Kost [A42]. Limited research by Mallick and Severn [A42] seems to indicate that analysis methods for large infilled frame structures should include the effects of column shortening.

While the work of Fiorato *et al*. is the first quantitative study of infilled frame behavior in the post-cracked range, it is believed that further investigation is necessary. In particular, it is necessary to study the response of infilled frame assemblages to combinations of constant vertical load and monotonic, cyclic, or dynamic lateral loads. In the dynamic case, care should be taken to support and load the assemblage in a manner that approximates as closely as possible the action of floor-level inertia loads on a multistory, multibay infilled frame structure.

Although a brute-force extension of Franklin's procedure [A25] to the analysis of complex structures is possible, this approach seems unwise for several reasons:

1) it would undoubtedly involve the need for a prohibitive amount of computer time and storage;

2) it would involve the calculation of information (such as crack propagation data) which is unnecessary for most building analyses;

3) it may be more precise than warranted by our present knowledge of material characteristics and bond-slip relations under cyclic strains; and

4) it seems possible that the needed information could be provided by much simpler analytical idealizations.

Although information now available concerns only the monotonic behavior of large infilled framed structures, the author believes that experimental data on the response of infilled frames under dynamic lateral load will suggest that this response is predictable over certain ranges of aspect ratio, frame-to-panel stiffness, panel reinforcement, and deformation amplitude. Given such data, it should be possible to idealize an infilled frame as a structural element exhibiting certain stiffness, strength, and hysteretic characteristics in the cracked and uncracked range. Because of the comparatively small amount of computer time and storage necessary to analyze a structure composed of such elements, this approach seems adaptable to the problem of analyzing large structures.

A.5 Summary and Recommendations

Sections A.1 through A.3 of this survey have presented the results of prior research regarding the effects of infill panels on the elastic and inelastic response of frame structures. The survey covers research in several fields:

1) Experimental and analytical investigations of the elastic and inelastic behavior of:

a) walls without frames;
b) walls with frames; and
c) frame-wall assemblages.

2) Mechanical characteristics of common infill materials.

In Section A.4 those results were examined. From this examination, the following specific research topics are suggested:

1) to study the bi- and triaxial strength and stiffness characteristics of clay brick masonry;

2) to study the effect of aspect ratio and panel reinforcement on the vertical load carrying capacity and ductility of cracked, unframed walls under monotonic lateral load;

3) to investigate the effect of boundary conditions and loading methods on the monotonic load behavior of unframed walls;

4) to study the bond-slip relation between reinforcing steel and grout or mortar;

5) to study the factors (such as aspect ratio, reinforcement, boundary conditions, and vertical load) which may contribute to the preservation of structural integrity in a cracked unframed panel subject to cyclic and dynamic lateral loads;

6) to repeat Scrivener and Williams' tests [A88,A99] using pier walls instead of single wall elements;

7) to investigate the effect of boundary conditions and loading methods on the monotonic load behavior of laterally loaded infilled frames;

8) to examine the influence of various types of frame-panel connections on the strength, stiffness, and ductility of under monotonic and cyclic loading, of infilled frames with reinforced panels;

9) to study in greater detail the mechanical characteristics of concrete and masonry under bi- and triaxial cyclic loading, including

an examination of the effects of high strain rates;

10) to study the behavior under dynamic load of infilled frames with reinforced panels and realistic loading and boundary conditions.

A. 6 References

A 1. Alexander, C. M., Heidebrecht, A. C., and Tso, W. K., "Cyclic Load Tests on Shear Wall Panels," Proc. 5th WCEE, pp. 1116-1120.

A 2. Ban, S. and Muguruma, H., "Behavior of Plain Concrete under Dynamic Loading with Strain Rate Comparable to Earthquake Loading," Proc. 2nd WCEE, vol. III, pp. 1979-1994.

A 3. Beedle, Lynn S., et al., Structural Steel Design, The Ronald Press, New York, 1964.

A 4. Benjamin, Jack E. and Williams, Harry A., "The Behavior of One-Story Reinforced Concrete Shear Walls," ASCE Structural Division Journal, May 1957, pp. 1254 I-49.

A 5. Benjamin, Jack R. and Williams, Harry A., "The Behavior of One-Story Brick Shear Walls," ASCE Structural Division Journal, July 1958, pp. 1723 I-30.

A 6. Bertero, V. V. and McClure, G., "Behavior of Reinforced Concrete Frames Subjected to Repeated Reversible Loads," ACI Journal, Oct. 1964, pp. 1305-1330.

A 7. Blume, John A. and Plummer, Harry C., Reinforced Brick Masonry and Lateral Force Design, Structural Clay Products Institute, 1953.

A 8. Blume, J. A. and Proulx, J., "Shear in Grouted Brick Masonry Wall Elements," J. A. Blume and Associates Research Division, San Francisco, August 1968.

A 9. Borchelt, J. G., "Analysis of Brick Walls Subject to Axial Compression and In-Plane Shear," Proc. 2nd International Brick Masonry Conference, Stoke-on-Trent, England, April 12-15, 1970, pp. 263-265.

A 10. Borges, J. Ferry and Ravara, Artur, "Structural Behavior of Panel Structures under Earthquake Actions," Proc. International Symposium on the Effects of Repeated Loading of Materials and Structures (RILEM), Mexico City, 1966, vol. VI.

A 11. Bresler, Boris and Bertero, Vitelmo, "Behavior of Reinforced Concrete under Repeated Load," ASCE Structural Division Journal, June 1968, pp. 1567-1590.

A 12. Bresler, B. and Pister, K., "Strength of Concrete under Combined Stresses," ACI Journal, Sept. 1958, pp. 321-345.

A 13. Brown, Russell H. and Jirsa, James O., "Reinforced Concrete Beams under Load Reversals," ACI Journal, vol. 68, 1971, pp. 380-390.

A 14. Butler, Don W. and Muto, Kiyoshi, Lateral Force Distribution Coefficients and Stress Analysis for Walled Frames, together with A Method for Stress Investigation of Reinforced Concrete Buildings for Lateral Forces, Japanese Education Ministry, 1951.

A 15. Carter, C. and Stafford Smith, B., "Structural Behavior of Masonry Infilled Frames Subjected to Racking Loads," Proc. International Conference on Masonry Structural Systems, Austin, Texas, 1967.

A 16. Clough, R. W., "Effect of Stiffness Degradation on Earthquake Ductility Requirements," Report No. 66-16, Department of Civil Engineering, U. C. Berkeley, Oct. 1966.

A 17. Clough, R. W., King, I. P., and Wilson, E. L., "Structural Analysis of Multistory Buildings," ASCE Structural Division Journal, June 1964, pp. 16-34.

A 18. Coull, A. and Stafford Smith, B. (eds.), Proc. Symposium on Tall Buildings, University of Southampton, April 1966, Pergamon Press, 1967.

A 19. Dawson, R. V. and Ward, M. A., "Structural Response of Frames Before and After the Placing of Infill Walls," Proc. First Canadian Conference on Earthquake Engineering, University of British Columbia, Vancouver, B. C., May 1971.

A 20. Dawson, R. V. and Ward, M. A., "Dynamic Response of Framed Structures with Infill Walls," Proc. 5th WCEE, pp. 1507-1516.

A 21. DeLisle, Derek J. and Heidebricht, A. C., "Comparison of the Behavior of Load Bearing Shear Wall Panels Subjected to Repeated Cyclic Lateral Loading," Proc. First Canadaian Conference on Earthquake Engineering, University of British Columbia, Vancouver, B. C., May 1971.

A 22. Esteva, Luis, "Behavior under Alternating Loads of Masonry Diaphragms Framed by Reinforced Concrete Members," Proc. International Symposium on the Effects of Repeated Loading of Materials and Structures (RILEM), Mexico City, 1966, vol. V.

A 23. Felippa, Carlos A., Discussion to Reference A 54, ASCE Structural Division Journal, Jan. 1970, pp. 143-147.

A 24. Fiorato, A. E., Sozen, M. A., and Gamble, W. L., "An Investigation of the Interaction of Reinforced Concrete Frames with Masonry Filler Walls," University of Illinois, Nov. 1970.

A 25. Franklin, H. A., "Nonlinear Analysis of Reinforced Concrete Frames and Panels," SESM Report No. 70-5, U.C. Berkeley, March 1970.

A 26. Fratessa, Paul F. and Zsutty, Theodore, "A Report to the SEAONC Seismology Subcommittee of Shear Walls," Proc. 38th SEAOC Convention, Hawaii, 1969.

A 27. Gulkan, Polat and Sozen, Mete, A., "Response and Energy Dissipation of Reinforced Concrete Frames Subjected to Strong Base Motions," University of Illinois, May 1971.

A 28. Hedstrom, R. O., "Load Tests of Patterned Concrete Masonry Walls," ACI Journal, April 1961, pp. 1265-1286.

A 29. Heidebrecht, A. C. and Raina, R.K., "Frequency Analysis of Thin-Walled Shear Walls," ASCE Engineering Mechanics Division Journal, April 1971.

A 30. Hilsdorf, Hubert K., "Investigation into the Failure Mechanism of Brick Masonry Loaded in Axial Compression," Proc. International Conference on Masonry Structural Systems, Austin, Texas, 1967. (Gulf Publishing Co.)

A 31. Hinkley, Anthony T., "Analysis of a Shear Wall Supported by a Beam," ASCE Structural Division Journal, Feb. 1966, pp. 121-130.

A 32. Holmes, Malcolm, "Steel Frames with Brickwork and Concrete Infilling," Institution of Civil Engineers (ICE), vol. 19, pp. 473-478, 1961.

A 33. Holmes, Malcolm, "Combined Loading on Infilled Frames," ICE, vol. 25, pp. 31-38, 1963.

A 34. Hudson, D. E., "Equivalent Viscous Friction for Hysteretic Systems with Earthquake-like Excitations," Proc. 3rd WCEE.

A 35. Jacobsen, Lydik S., "Damping in Composite Structures," Proc. 2nd WCEE, 1960, vol. II, pp. 1029-1044.

A 36. Jacobsen, Lydik S., "Frictional Effects in Composite Structures Subjected to Earthquake Vibrations," Technical Report to California State Department of Public Works, Department of Mechanical Engineering, Stanford University, March 1959.

A 37. Jennings, Paul C., "Equivalent Viscous Damping for Yielding Structures," ASCE Engineering Mechanics Division Journal, Feb. 1968, pp. 103-116.

A 38. Johnson, Frank B. and Matthys, John H., "Structural Strength of Hollow Clay Tile Assemblages," ASCE Structural Division Journal, Feb. 1973, pp. 259-275.

A 39. Karamanski, Todor, "Calculating Infilled Frames by the Method of Finite Elements," Proc. Symp. Tall Buildings, see Reference A 18.

A 40. Kennedy, C. C. and Pancu, C. D. P., "Use of Vectors in Vibration Measurements and Analysis," Journal of Aeronautical Science, Nov. 1947, pp. 603-624.

A 41. Khan, F. R. and Sbarounis, J. A., "Interaction of Shear Walls and Frames," ASCE Structural Division Journal, June 1964, pp. 307-312.

A 42. Kost, Edward Garrison, "Nonlinear Dynamic Analysis of Frames with Filler Panels," John A. Blume and Associates Report No. JAB-99-100, San Francisco, Nov. 1972.

A 43. Krishna, Jai, et al., "Behavior of Load Bearing Brick Walls during Earthquake," Proc. 3rd Symposium on Earthquake Engineering, School of Earthquake Engineering, Roorkee, India, 1966.

A 44. Krishna, Jai and Chandra, Brijesh, "Strengthening of Brick Buildings in Seismic Zones," Proc. 4th WCEE, 1969, vol. III, pp. B-6, 11-20.

A 45. Kupfer, Helmut, Hilsdorf, Hubert K., and Rusch, Hubert, "Behavior of Concrete under Biaxial Stress," ACI Journal, August 1969, pp. 656-666.

A 46. Lamar, Simon and Fortoul, Celso, "Brick Masonry Effect in Vibrations of Frames," Proc. 4th WCEE, vol. II, pp. A-3, 91-98.

A 47. Leuchars, J. M. and Scrivener, J. C., "Masonry Infill Panels Subjected to Cyclic In-Plane Loading," Proc. South Pacific Regional Conference of the NZNSEE, Wellington, N. Z., May 1975.

A 48. Levy, M. and Spira, E., "Experimental Study of Masonry Walls Strengthened by Reinforced Concrete Elements," Paper No. 35-II, International Association for Bridge and Structural Engineering, 1975.

A 49. Liauw, T. C., "Elastic Behavior of Infilled Frames," ICE, May/August 1970, vol. 46, pp. 343-349.

A 50. Liauw, T. C., "Stress Analysis for Panel of Infilled Frames," Building Science Series, 8, 2, June 1973, pp. 105-112.

A 51. Liauw, T. C., "On Infilled Frames," Proc. 4th Australasian Conference on the Mechanics of Structures and Materials, Dept. of Civil Engineering, University of Queensland, Brisbane, August 1973, pp. 137-144.

A 52. Liauw, T. C. and Lee, S. W., "Multi-story Infilled Frames," Proc. Regional Conference on Tall Buildings, Bangkok, 1974, pp. 315-334.

A 53. Lutz, L. A. and Gergely, P., "Mechanics of Bond and Slip of Deformed Bars in Concrete," ACI Journal, Nov. 1967, pp. 711-721.

A 54. MacLeod, Iain A., "New Rectangular Finite Element for Shear Wall Analysis," ASCE Structural Division Journal, March 1969, pp. 399-409.

A 55. Mainstone, R. J., "On the Stiffnesses and Strengths of Infilled Frames", Current Paper CP 2/72, Building Research Station, Feb. 1972, Reprinted from Proc. Institution of Civil Engineers, 1971 Supplement (iv), Paper 7360 S, pp. 57-90.

A 56. Mainstone, R. J. and Weeks, G. A., "The Influence of a Bounding Frame on the Racking Stiffness and Strengths of Brick Walls", Current Paper CP 3/72, Building Research Station, Feb. 1972, also published in Proc. Second International Brick Masonry Conference (SIBMAC), 1971, pp. 165-171.

A 57. Mainstone, J. J., "Supplementary Note on the Stiffnesses and Strengths of Infilled Frames", Current Paper CP 13/74, Building Research Station, Feb. 1974.

A 58. Mallick, D. V., "Structural Damping of Brick Masonry in Different Mortars", Proc. 2nd Symposium on Earthquake Engineering, University of Roorkee, India, 1962.

A 59. Mallick, D. V. and Severn, R. T., "The Behavior of Infilled Frames under Static Loading," ICE, Sept./Dec. 1967, vol. 38, pp. 639-656.

A 60. Mallick, D. V., and Severn, R. T., "Dynamic Characteristics of Infilled Frames," ICE, Jan./April 1968, vol. 39, pp. 261-287.

A 61. Mallick, D. V. and Garg, R. P., "Effects of Openings on the Lateral Stiffness of Infilled Frames," Proc. Institution of Civil Engineers, 49, Paper No. 7371, June 1971, pp. 193-210.

A 62. Mallick, D. V., "Dynamic Characteristics of Single Story Infilled Frames with Brick Panels," Bulletin of the Indian Society of Earthquake Technology, 9,3, Paper No. 126, Sept. 1972, pp. 109-117.

A 63. Mamet, J. C., Mufti, A. A., and Jaeger, L. G., "New Developments in the Analysis of Shear Wall Buildings," Proc. First Canadian Conference on Earthquake Engineering, see Reference A 19.

A 64. Mayes, Ronald L., "The Effect of Coulomb Damping on Single and Multi-Degree of Freedom Structures," Ph.D. thesis, School of Engineering, University of Auckland, New Zealand, Sept. 1972.

A 65. Meli, R. and Esteva, L., "Behavior of Hollow Masonry Walls When Subjected to Alternating Lateral Load," 2nd National Congress of Seismic Engineering, Veracruz (Mexico), May 1968. (In Spanish, translation University of Canterbury, New Zealand.)

A 66. Moss, P. J. and Carr, A. J., "Aspects of the Analysis of Frame-Panel Interaction," Bulletin of the New Zealand Society for Earthquake Engineering, Vol. 4, No. 1, March 1971, pp. 126-144.

A 67. Murthy, C. K. and Hendry, A. W., "Preliminary Investigation of the Shear Strength of One-Sixth-Scale Model Brickwork," Technical Note 65, University of Edinburgh, Department of Civil Engineering, 1965.

A 68. Muto, K., "Earthquake Resistant Design of 36-Storied Kasumigaseki Building," Special Report for 4th WCEE, Muto Institute of Structural Mechanics, Tokyo, August 1968.

A 69. Negoita, Alexander, "Bearing Walls in Earthquake Areas," Build International, January/February 1972, pp. 43-53.

A 70. Neville, A. M., "Hardened Concrete: Physical and Mechanical Aspects," ACI Monograph, Detroit, 1971.

A 71. Oakberg, R. G., and Weaver, W. Jr., "Analysis of Frames with Shear Walls by Finite Elements," Proc. Symposium on Applications of Finite Element Methods in Civil Engineering, Vanderbilt University, Nov. 1969.

A 72. Ockleston, A. J., "Load Tests on a Three Story Reinforced Concrete Building in Johannesburg," The Structural Engineer, Vol. 33, No. 10, October 1955, pp. 304-322.

A 73. Ohsaki, Yorihiko et al., "Experimental Study on Five-Story Full-Size Apartment House of Reinforced Concrete Walled Frames," Japan Building Research Institute. (No date given, received EERC Library 1972.)

A 74. Otani, Shunsuke, "SAKE: A Computer Program for Inelastic Analysis of R/C Frames to Earthquake," University of Illinois, November 1974.

A 75. Plastic Design in Steel: A Guide and Commentary, ASCE Manual No. 41, Second Edition, 1971.

A 76. Pole, Gordon M., Discussion of Reference A 54, ASCE Structural Division Journal, Jan. 1970, pp. 140-143.

A 77. Polyakov, S. V., "Masonry in Framed Buildings: An Investigation into the Strength and Stiffness of Masonry Infilling," (English translation), Moscow, 1957.

A 78. Polyakov, S. V., "On the Interaction Between Masonry Filler Walls and Enclosing Frame When Loaded in the Plane of the Wall," Translations in Earthquake Engineering, Earthquake Engineering Research Institute, 1960, pp. 36-42. (San Francisco).

A 79. Polyakov, S. V., "Some Investigations of the Problem of the Strength of Elements of Buildings Subjected to Horizontal Loads," Proc. Symp. on Tall Buildings, see Reference A 18.

A 80. Priestley, M. J. N., and Bridgman, D. O., "Seismic Resistance of Brick Masonry Walls," Bulletin of the New Zealand National Society for Earthquake Engineering, Vol. 7, No. 4, December 1974.

A 81. Read, J. B., "Testing to Destruction of Full-Size Portal Frames," Technical Report TRA/390, Cement and Concrete Association, London, August 1965.

A 82. Rosenhaupt, Saky, "Experimental Study of Masonry Walls on Beams," ASCE Structural Division Journal, June 1962, pp. 137-166.

A 83. Rosenhaupt, Saky and Mueller, G., "Openings in Masonry Walls on Settling Supports," ASCE Structural Division Journal, June 1963, pp. 107-131.

A 84. Sachanski, S., "Analysis of the Earthquake Resistance of Frame Buildings Taking into Consideration the Carrying Capacity of the Filling Masonry," Proc. 2nd WCEE, Vol. III, pp. 2127-2135.

A 85. Saghera, Santokh S., "Effects of Shear Walls on Dynamic Response of Frames," Proc. Symp. Applications of FEM, see Reference A71.

A 86. Schneider, Robert R., "Shear in Concrete Masonry Piers," Proc. 38th SEAOC Convention, Hawaii, 1969.

A 87. Scrivener, J. C., "Static Racking Tests on Concrete Masonry Walls," Proc. International Conference on Masonry Structural Systems, Austin, Texas, 1967, see Reference A30.

A 88. Scrivener, J. C. and Williams, D., "Behavior of Reinforced Masonry Shear Walls under Cyclic Loading," Bull. New Zealand Soc. E.Q. Engineering, Vol. 4, No. 2, April 1971, pp. 316-330.

A 89. Sinha, B. P. and Hendry, A. W., "Further Investigations of Bond Tension, Bond Shear and the Effect of Precompression on the Shear Strength of Model Brick Masonry Couplets," Technical Note 80, University of Edinburgh, Department of Civil Engineering.

A 90. Smolira, M., "Analysis of Infilled Shear Walls," Proc. Institution of Civil Engineers, Paper No. 7672, Dec. 1973, pp. 895-912.

A 91. Spira, Ephraim and Sokal, Yehuda, Discussion to Reference A54, ASCE Structural Division Journal, August 1970, pp. 1799-1802.

A 92. Stafford Smith, Bryan, "Lateral Stiffness of Infilled Frames," ASCE Structural Division Journal, Dec. 1962, pp. 183-199.

A 93. Stafford Smith, Bryan, "Behavior of Square Infilled Frames," ASCE Structural Division Journal, Feb. 1966, pp. 381-403.

A 94. Stafford Smith, Bryan, "The Composite Behavior of Infilled Frames," Proc. Symp. Tall Buildings, see Reference A 18.

A 95. Stafford Smith, Bryan, "Model Test Results of Vertical and Horizontal Loading of Infilled Frames," ACI Journal, August 1968, pp. 618-624.

A 96. Stafford Smith, Bryan and Carter, C., "A Method of Analysis for Infilled Frames," ICE, Vol. 44, Sept/Dec. 1969, pp. 31-48.

A 97. Tamura, R. et al., "A Vibration Test of a Large Model Steel Frame with Precast Concrete Panel Until Failure," Proc. 4th WCEE, Vol. I, pp. B-2, 16-30.

A 98. Tomii, Masahide, "Design Procedures of Concrete Shear Walls," Kyushu University, Japan, April 1966.

A 99. Williams, D., "Seismic Behavior of Reinforced Masonry Shear Walls," Ph.D. thesis, University of Canterbury, New Zealand, 1971.

A100. Winter, George et al., Design of Concrete Structures, 7th Ed. McGraw-Hill, 1964.

A101. Wood, R. H., "Stability of Tall buildings," Proc. ICE, Sept. 1958, pp. 69-102.

A102. Yamaguchi, Ikuo and Araki, Toshisada, "Study on the Flexible Shear Walls," Takenaka Technical Research Laboratory, September 1973.

A103. Yokel, Felix and Fattal, S. George, "A Failure Hypothesis for Masonry Shear Walls," NBSIR 75-703, Center for Building Technology, National Bureau of Standards, May 1975.

A104. Zsutty, Theodore, "A Review and Analysis of the Shear Wall Design Problem," draft obtained from Prof. A. C. Scordelis, U. C. Berkeley, Nov. 1970.

A105. Zsutty, Theodore, "Design of Shear Wall Systems for Non-Elastic Behavior during a Major Earthquake," Report to Shear Wall Subcommittee of SEAONC, August 1971.

APPENDIX B: MECHANICAL CHARACTERISTICS OF MATERIALS

B.1 Reinforcing Steel

Tensile tests were carried out to determine the mechanical characteristics of each type of reinforcing bar used to construct the models tested in the experimental phase of this study. All bars of each size were selected from the same heat, ensuring uniform characteristics within each size. Four sizes of deformed reinforcement were tested:

1) #7 bars, used in the base;

2) #4 bars, used as longitudinal reinforcement for the columns;

3) #3 bars, used as longitudinal reinforcement for the beams;

4) #2 bars, used as longitudinal reinforcement for the beams, and as panel reinforcement.

Two sizes of undeformed wire were also tested:

1) USS #5 Gage Wire, used for spiral reinforcement in the columns; and

2) USS #11 Gage Wire, used for transverse reinforcement in the beams.

Each test is described below:

B 1.1 #7 Bar

A single specimen was machined over a length of 305 mm (12 in) to an average diameter of 17.75 mm (0.699 in), tapering to a minimum diameter of 17.70 mm (0.697 in) at the center. The specimen was mounted in a three-range Baldwin hydraulic testing machine with a maximum capacity of 534 kN (120 k), and was loaded in tension at a rate of 222 kN/min (50 k/min) until yield and 45.5 μ/sec (micro-mm/mm sec) thereafter. Strains were measured over a gage length of 127 mm (5 in) using two linear variable differential transformers (LVDT's) in an extensometer mount. The results are shown in Fig. B 1 and are summarized below:

$f_{y\ upper}$ = 528 MPa (76.6 ksi)

$f_{y\ lower}$ = 501 MPa (72.6 ksi)

$\varepsilon_{\text{strain hardening}}$ = 0.00921

$E_{\text{strain hardening}}$ = 5164 MPa (749 ksi)

f_{max} = 692 MPa (100.3 ksi)

ε_{ult} = 0.116

A modulus of 200000 MPa (29000 ksi) was found adequate for all reinforcing steel.

B.1.2 #4 Bar

A single specimen was machined over a length of 305 mm (12 in) to an average diameter of 10.87 mm (0.428 in), tapering to a minimum diameter of 10.85 mm (0.427 in) at the center. The specimen was tested similarly to the #7 bar. The results are shown in Fig B 2 and are summarized below:

$f_{y\ upper}$ = 550 MPa (79.8 ksi)

$f_{y\ lower}$ = 512 MPa (74.2 ksi)

$\varepsilon_{\text{strain hardening}}$ = 0.0133

$E_{\text{strain hardening}}$ = 6550 MPa (950 ksi)

ε_{ult} = 0.156

f_{max} = 741 MPa (107.5 ksi)

B.1.3 #3 Bar

A single specimen was machined over a length of 305 mm (12 in) to an average diameter of 7.67 mm (0.302 in), tapering to a minimum diameter of 7.62 mm (0.300 in) at the center. The specimen was tested similarly to the #7 bar. The results are shown in Fig B 3 and are summarized below:

$f_{y\ upper}$ = 485 MPa (70.3 ksi)

$f_{y\ lower}$ = 470 MPa (68.2 ksi)

$\varepsilon_{strain\ hardening}$ = 0.0211

$E_{strain\ hardening}$ = 5000 MPa (725 ksi)

ε_{ult} = 0.156

f_{max} = 652 MPa (94.5 ksi)

B.1.4 #2 Deformed Bar

Tests were carried out as described in Ref. 42. The results are shown in Fig B 4 and are summarized below:

f_y = 506 MPa (73.4 ksi)

f_{max} = 729 MPa (105.8 ksi)

B.1.5 USS #5 Gage Wire

A tensile test was carried out on an unmachined specimen with a diameter of 5.25 mm (0.2065 in), mounted in a Baldwin hydraulic testing machine with a maximum capacity of 267 kN (60 k). The specimen was loaded at the rate of 50 μ/sec, and strains were measured over a gage length of 152 mm (6 in) using two dial gages in an extensometer mount. The results are shown in Fig. B 5 and are summarized below:

$f_{0.2\%\ offset}$ = 670 MPa (97 ksi)

ε_{ult} = 0.025

f_{max} = 678 MPa (98.4 ksi)

B.1.6 USS #11 Gage Wire

A tensile test was conducted on an unmachined specimen with a diameter of 3.00 mm (0.1183 in). The procedure was similar to that used for the #5 gage wire. The results are shown in Fig B 6 and are summarized below:

$$f_{0.2\%\ \text{offset}} = 703\ \text{MPa}\ (102\ \text{ksi})$$

$$\varepsilon_{ult} = 0.1\ \text{(approximate)}$$

$$f_{max} = 759\ \text{MPa}\ (110.1\ \text{ksi})$$

B.2. Concrete

Compression tests were carried out on numerous cylinders measuring 6 in by 12 in (152 mm by 305 mm), which were cast at the same time as each model. All cylinders were tested at a loading rate of approximately 500 μ/min.

Modulus of rupture tests were conducted on beams measuring 5 in by 6 in by 20 in (127 mm by 152 mm by 508 mm), loaded at a rate of 13.3 kN/min (3 k/min) on a Baldwin hydraulic testing machine with a maximum capacity of 267 kN (60 k).

B.2.1 Model #1

This model was used for the bare frame test (Test #1) and later infilled with clay units for Test #2. The mix proportions are shown in Fig B 7. Sixteen cylinders were cast, and all were compacted by rodding, stripped at 7 days, and air-cured next to the model. The compressive strengths obtained are shown in Figs. B 8 and B 9. Four beams were cast for modulus of rupture tests. These specimens were also stripped at seven days and air-cured next to the model. The values obtained for modulus of rupture, are shown in Fig. B 10.

B.2.2 Model #2

This model was infilled with clay units and used for Test #3. The mix proportions are shown in Fig. B 11. Twenty cylinders were cast, and all were connected by rodding, stripped at seven days, and cured next to the model. The compressive strengths obtained are shown in

Figs. B 12 and B 13. Four beams were cast for modulus of rupture tests, stripped at seven days, and cured next to the model. The values obtained for modulus of rupture are shown in Fig. B 14.

B.2.3 Model #3

This model was infilled with concrete block units and used for Test #4. The mix proportions were as shown in Fig. B 15. Twenty-four cylinders were cast. To examine the correlation between previous compressive tests of rodded cylinders and the probable strength of the vibrated concrete in the models themselves, fifteen of these were compacted by vibration and the rest by rodding. No significant differences were found between clinders compacted by the two methods. The compressive strengths obtained are shown in Figs. B 16 and B 17. Four beams were cast for modulus of rupture tests, stripped at seven days, and cured next to the model. The values obtained for modulus of rupture are shown in Fig. B 18.

Note that specimens from all three models reached maximum compressive strength at about 60 days, after which the strength decreased by about 5 %. This was due to the shrinkage cracking resulting from air curing.

B.3 Masonry Elements

In order to predict the experimental behavior of the infilled frame models, extensive tests were carried out to determine the mechanical characteristics of the infill materials.

B.3.1 Clay and Concrete Block Units

Fig. B 19 and B 20 show the dimensions of the clay and concrete units. Six clay units were capped with sulfur and tested in compression in a four-range Baldwin hydraulic testing machine with a maximum capacity of 534 kN (120 k), using a loading rate of 44.5 kn/min (10 k/min) as specified by Section 24-25 of the 1973 UBC Standards [43]. Six concrete units were similarly capped and tested. The results for each type of block are presented in Fig. B 21 and B 22.

B.3.2 Mortar

As stated in the text, all infilled models were constructed using mortar conforming to the standards for Type "S" mortar by Table 24-21-B of the 1973 UBC Standards [43]. Typical mix proportions were 1 part portland cement, 1/2 part hydrated lime, and 3 parts sand by volume. Field compressive tests were carried out by Section 24-23 of the 1973 UBC Standards [43]. A total of six 2-in-diameter cylinders were taken from each panel of each infilled frame during construction. Some specimens were cast using mortar which had previously been spread briefly on masonry units to simulate placement conditions, while others were cast using mortar which had not been spread on the units. These two types of specimen are referred to in the figures as "buttered" and "unbuttered", respectively. Specimens were stripped at two to three days and fog cured. After various intervals, the cured specimens were removed from the fog room, capped with sulfur, and tested in compression at a load rate of 17.8 kN/min (4 k/min). The results for each set of cylinders for each of the three models are shown in Figs. B 23 through B 28.

B.3.3 Grout

Grout for each infilled model was mixed according to the specifications of Section 24-21 of the 1973 UBC Standards [43]. Typical proportions were one part portland cement to three parts Olympia top sand by volume. As each panel was grouted, two field test grout prisms were cast as recommended in Section 24-23 of the 1973 UBC Standards. The prisms measured approximately 51 mm by 51 mm by 102 mm) (2 in by 2 in by 4 in). All prisms were fog cured and stripped at two to three days. At twenty-eight days they were removed from the fog room, capped with sulfur, and tested in compression at a loading rate of 17.8 kN/min (4 k/min). The mix proportions and results for each set of grout prisms for each model are shown in Figs. B 23 through B 28.

B.3.4 Masonry

At an early stage of the investigation, it was decided to carry out preliminary tests of the mechanical characteristics of each kind of grouted masonry used in the infill panels. Because many references [44] noted the difficulty of determining the shear modulus experimentally, it was decided to determine compressive strength and modulus, only, by means of compressive tests on grouted masonry prisms. As explained in the test, these values were used to interpret the failure process for each infilled model, and to develop analytical idealizations of panel behavior.

Because the mix proportions of mortar and grout were not identical for all infilled frame models, it was necessary to construct four different types of test prisms, representing: 1) the masonry used to infill the infilled bare frame (Test #2); 2) the masonry used for the lowest panel (panel #1) of the virgin frame with clay infill; 3) the masonry used in panels #2 and #3 of this same model; and 4) the masonry used in all three panels of the virgin frame with concrete block infill. A few clay prisms were constructed four units high, corresponding to h/D ratios of about 2. However, most were constructed eight units high, corresponding to h/D ratios of about 4. To approximate as closely as possible the actual model conditions, all test prisms were air-cured near the models. After capping them with sulfur, the prism specimens were tested in compression in a four-range Baldwin hydraulic testing machine with a maximum capacity of 267 kN (60 k), using a loading rate of 44.5 kN/min (10 k/min). Stresses were computed based on the gross area of the prisms; strains were computed using the readings from two dial gages placed between the platens of the testing machine. Stress values for strength determination were corrected for h/D ratio by Section 2404 of the 1970 UBC [25]. However, stress values used to determine the modulus were not so corrected. The results for each type of test prism and each model are shown in Figs. B 29 through B 32. Tests at 14, 27, and 107 days showed that curing was essentially complete after four weeks. For each type of prism, variations in strength and modulus with time after construction are shown in Fig. B 33 and B 34. Average values of strength and stiffness for clay prisms were found to be 24.1 MPa and 8274 MPa, respectively (3.5 ksi and 1200 ksi), while for concrete block prisms, the values were 19.0 MPa and 9653 MPa. The possible effects of local variations in panel strength on the failure processes of each infilled frame model are discussed in Section 5.7.

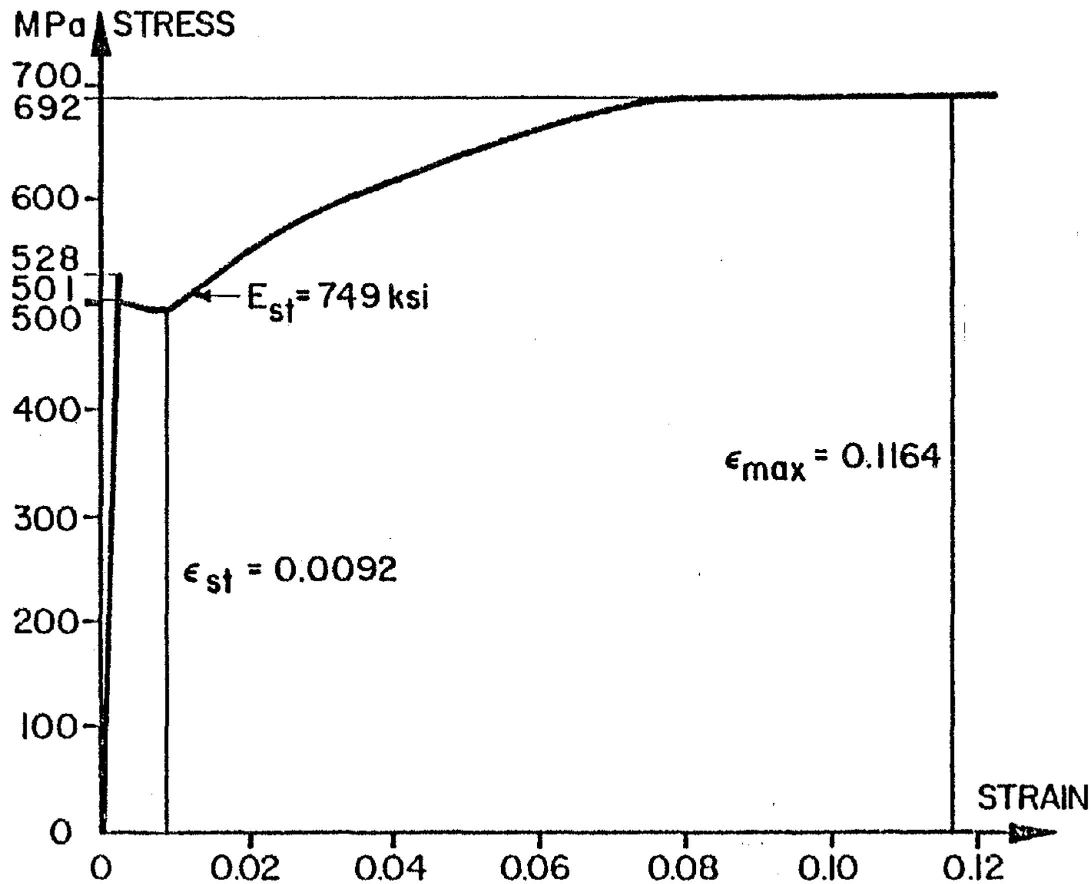

FIG. B.1 STRESS-STRAIN DIAGRAM FOR #7 BAR

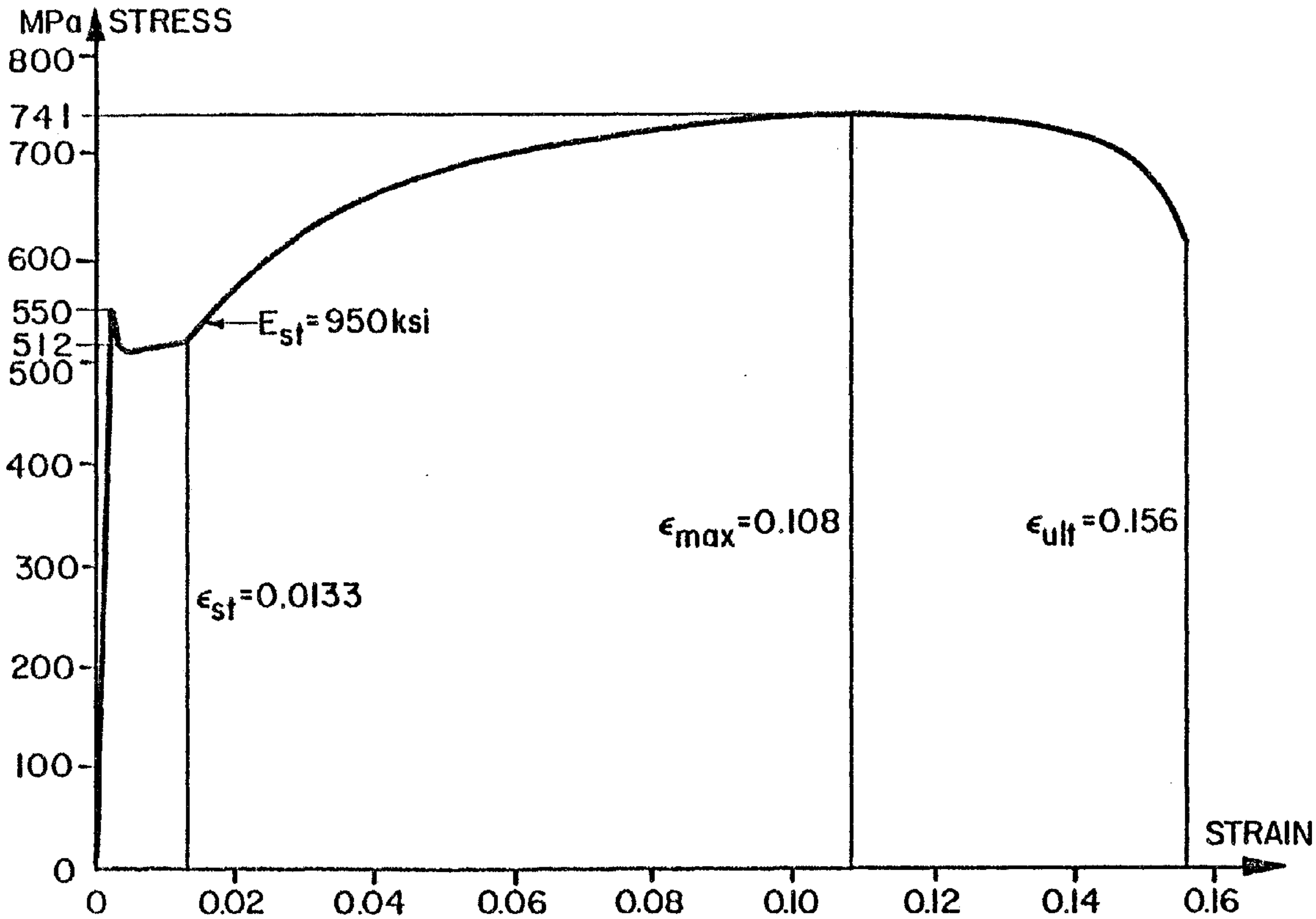

FIG. B.2 STRESS-STRAIN DIAGRAM FOR #4 BAR

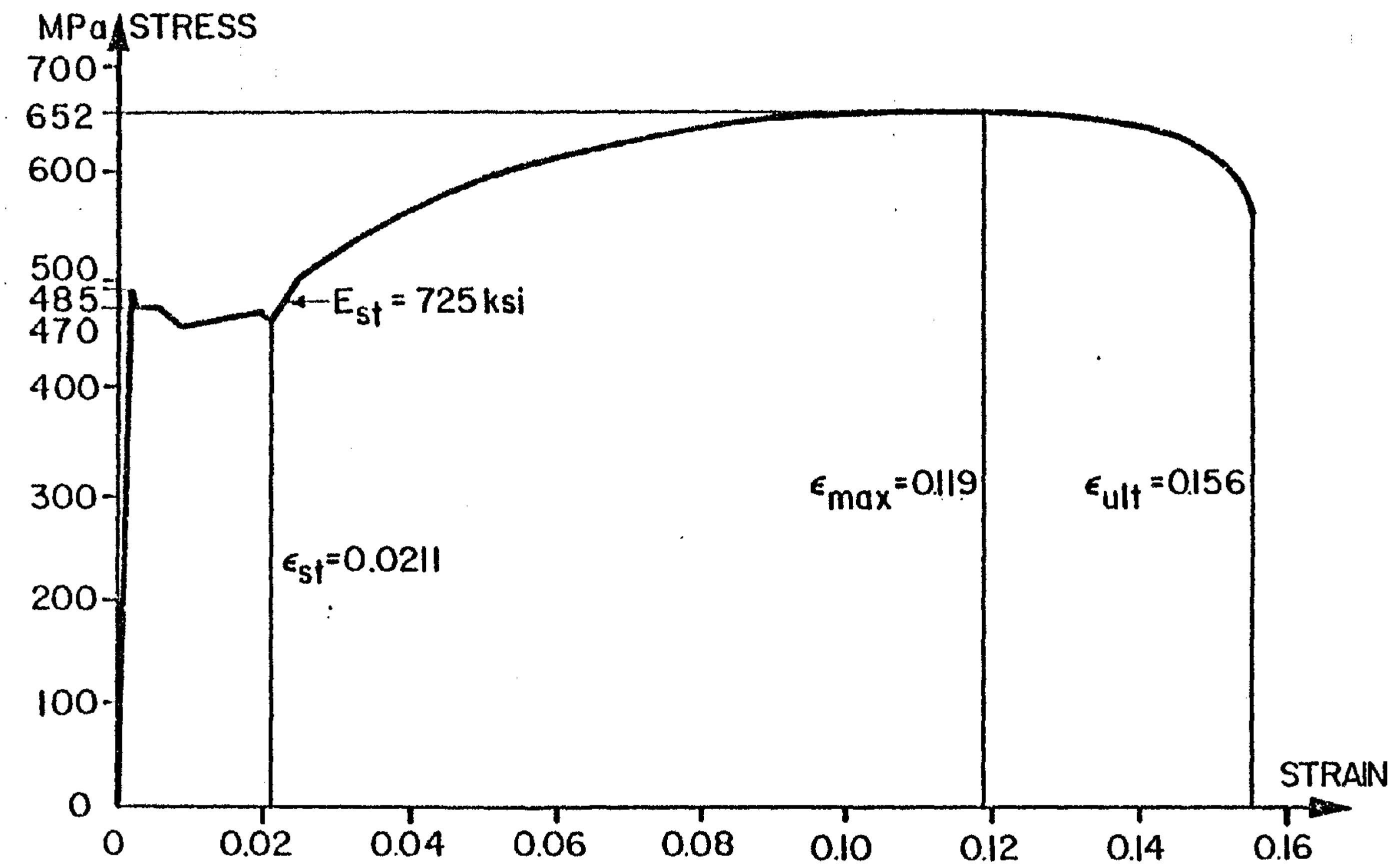

FIG. B.3 STRESS-STRAIN DIAGRAM FOR #3 BAR

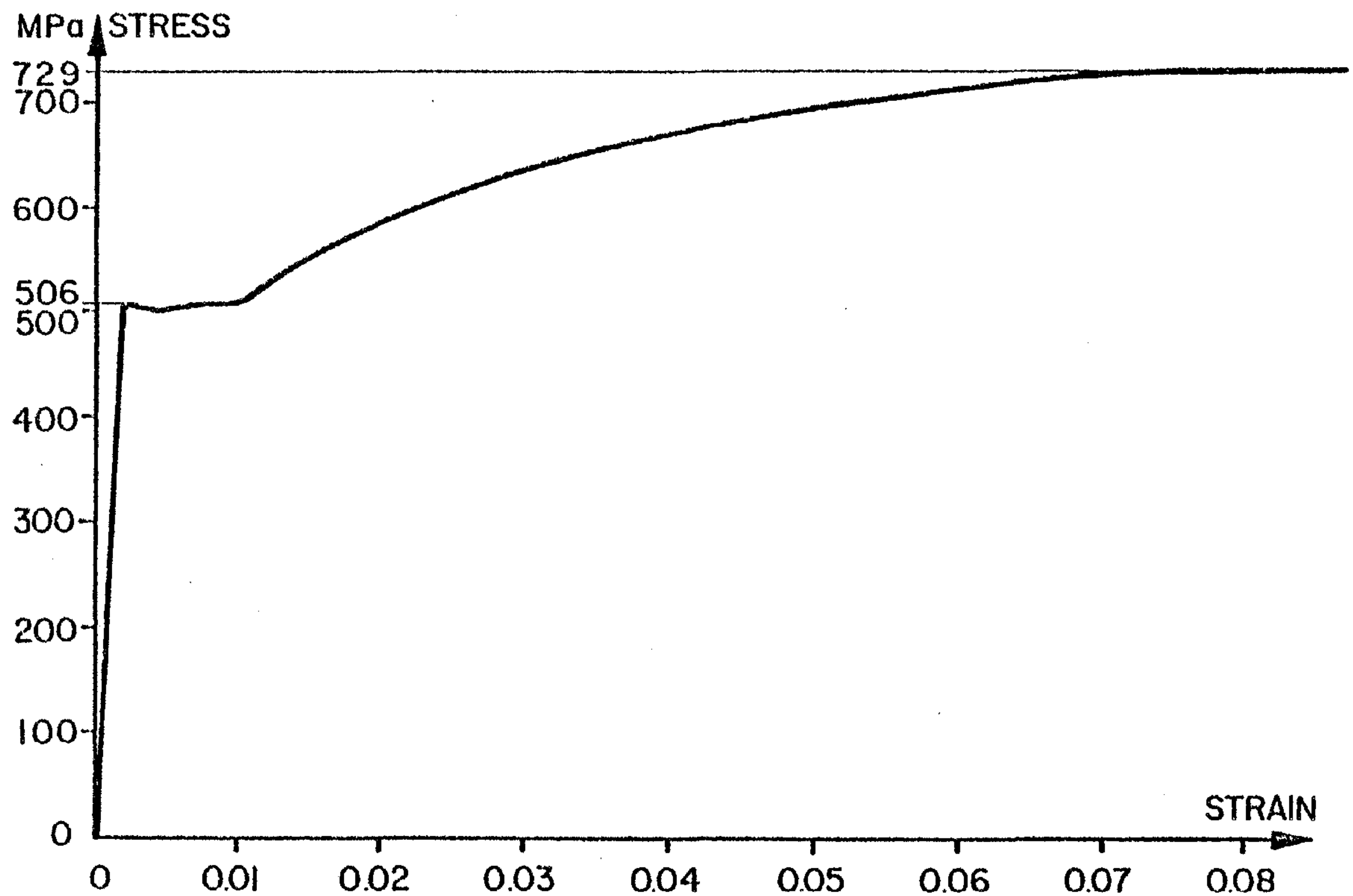

FIG. B.4 STRESS-STRAIN DIAGRAM FOR #2 DEFORMED BAR

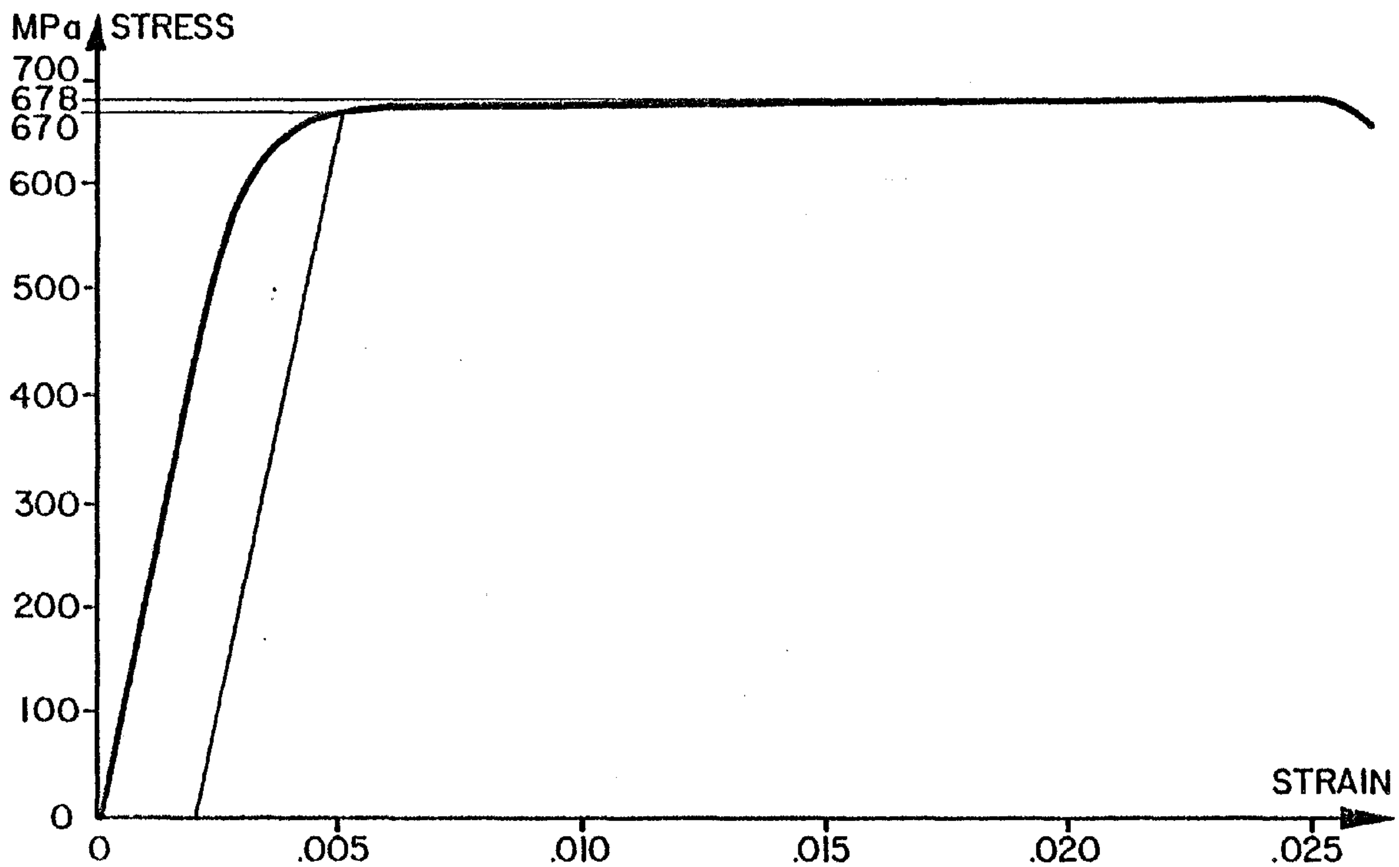

FIG. B.5 STRESS-STRAIN DIAGRAM FOR USS #5 GAGE WIRE

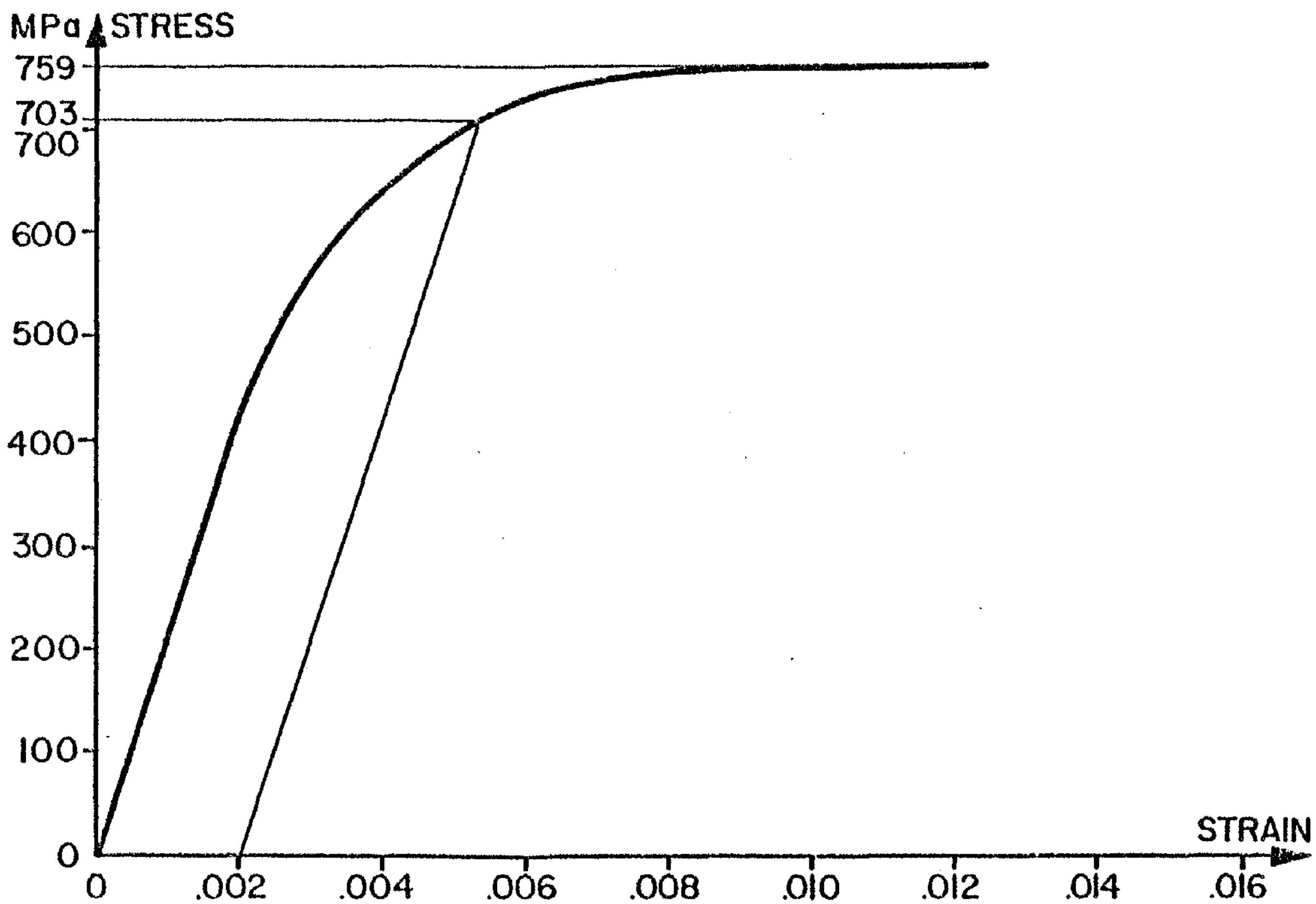

FIG. B.6 STRESS-STRAIN DIAGRAM FOR USS #11 GAGE WIRE

University of California
Department of Civil Engineering

Division of Structural Engineering
and Structural Mechanics

CONCRETE LABORATORY CASTING DATA SHEET

Date Cast 5/27/75 Project 0-21997 Name Klingner
Mix No. Infill Wall #1 Specimen
Desired Slump 5 in.± in. Desired Air Cont 1 ± %
Unit wt. (v)= 144 lb/cu.ft. Admixture Amount

MATERIAL	SSD Aggregates: Parts by wt. (a)	SSD Aggregates: Wt. for 1 cu. yd. batch (lb.) 27av ÷ T	Aggregates, as stocked: Moisture Adjustment (%)	Moisture Adjustment (lb)	Adj. wt. for 1 cu. yd. batch (lb.) (b)	Wt. for v= 0.2 cu.yd. batch, lb. (v)·(b)
Cement II Type, Santa Cruz Brand, C976 No.	1.00	608			608	121.6
Other ___ Pozzolan, Expansive Components, etc.						
Water	0.66	401		-24.2	376.8	75.4
Fine Sand Antioch	0.57	346	+2.8	+9.7	355.7	71.1
Coarse Sand Eliot State	2.02	1227	+1.1	+13.5	1240.7	24.8
Fine Gravel 1/8 x 1/4" Pleasanton	2.15	1306	+0.08	+1.0	1307	261.4
Coarse Gravel				+24.2		
Total T =	6.40	3888			3888	778
Admixture, concentration						

PROPERTY	Batch Number 1	2	3	4	5	6	7	8	9
Wt. mixer water, lb.									
Slump, in.									
Kelly Ball pen't, in.									
Amt. of Admixture									
Air content, %									
Temperature °F									
Wt. conc. + cont., lb.									
Wt. container, lb.									
Wt. concrete=A, lb.									
Vol. cont.=B, cu. ft.									
Unit wt.= A÷B, pcf									

16 Cylinders cast in ___ molds; compacted by rodding
Cylinders numbered ___ to ___ 7/72 GH

FIG. B.7 CONCRETE MIX PROPORTIONS FOR MODEL #1

Cylinder	Age, Days	f_c MPa	f_c Ksi	$\bar{f}_c$ MPa	$\bar{f}_c$ Ksi
1/16	7	13.5	1.96		
2/16	7	13.4	1.95	13.5	1.96
3/16	7	13.6	1.97		
4/16	14	21.5	3.12	21.4	3.11
5/16	14	21.4	3.10		
6/16	20	23.1	3.35	22.8	3.31
7/16	20	22.5	3.27		
8/16	29	24.1	3.50	24.5	3.55
9/16	29	24.8	3.60		
10/16	42	26.2	3.80	26.6	3.86
11/16	42	27.0	3.91		
	(Test #1)				
12/16	98	26.8	3.88	25.9	3.75
13/16	98	25.0	3.62		
	(Test #2)				
14/16	248	26.3	3.82		
15/16	248	25.9	3.75	26.1	3.78
16/16	248	26.1	3.78		

Fig. B.8. CONCRETE COMPRESSIVE TEST RESULTS, MODEL #1

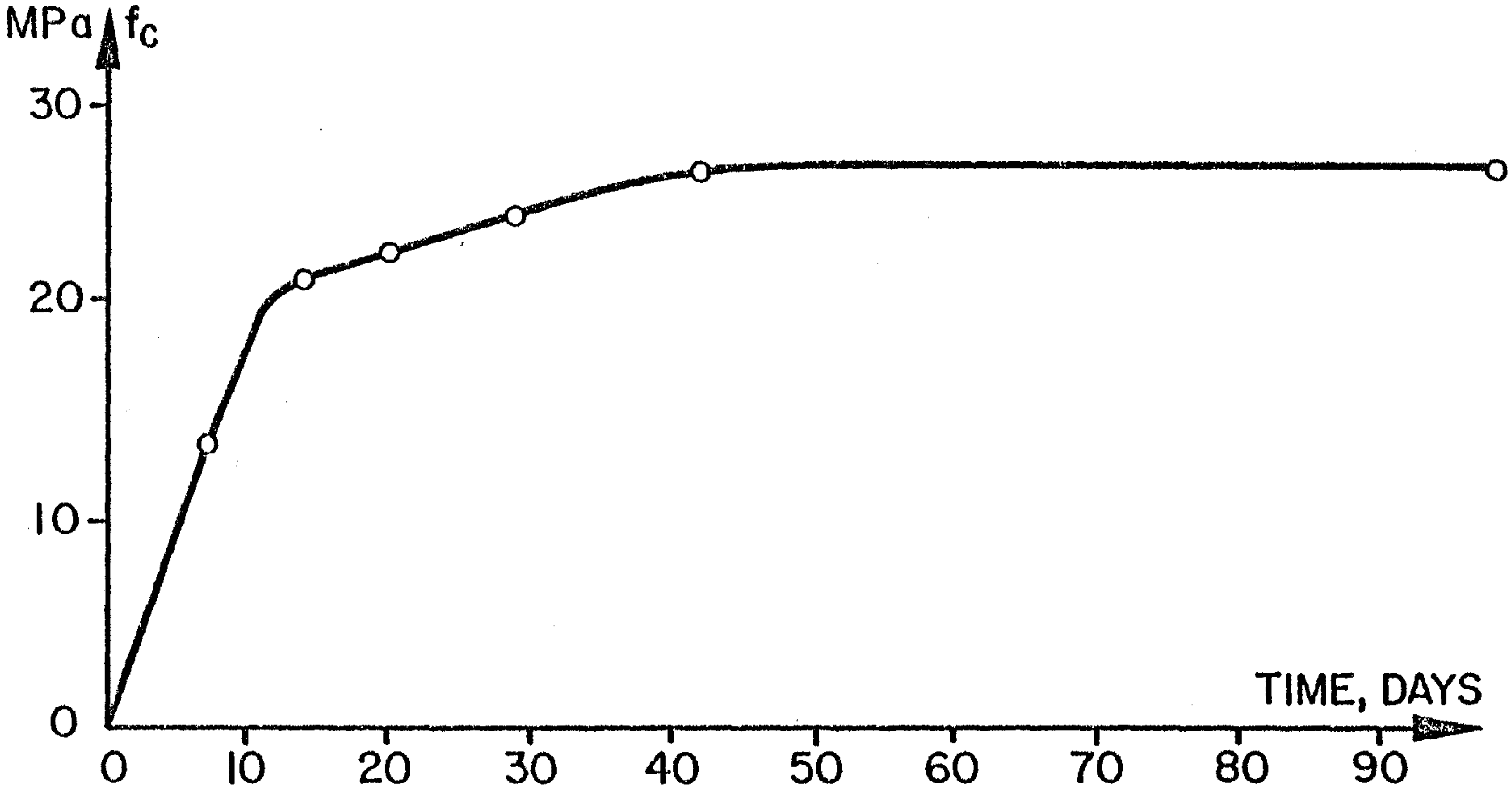

FIG. B.9 CONCRETE COMPRESSIVE STRENGTH, BARE FRAME (MODEL #1)

Specimen	Age, Days	f_t MPa	f_t psi	$f_t/\sqrt{f_c}$ MPa	$f_t/\sqrt{f_c}$ psi
	(Test #1)				
1/4	98	4.32	626	0.83	9.9
2/4	98	4.07	591		
	(Test #2)				
3/4	248	4.52	655	0.86	10.3
4/4	248	4.25	617		

Fig. B.10 MODULUS OF RUPTURE, MODEL #1

University of California
Department of Civil Engineering

Division of Structural Engineering
and Structural Mechanics

CONCRETE LABORATORY CASTING DATA SHEET

Date Cast 9/15/75 Project 0-21997 Name Klingner
Mix No. Infill Wall #2 Specimen
Desired Slump 5 in.± in. Desired Air Cont 1 ± %
Unit wt. (v)= 144 lb/cu.ft. Admixture Amount

MATERIAL	SSD Aggregates		Aggregates, as stocked			
	Parts by wt.	Wt. for 1 cu. yd. batch (lb.)	Moisture Adjustment (%)	Moisture Adjustment (lb)	Adj. wt. for 1 cu. yd. batch (lb.)	Wt. for v= 0.2 cu.yd. batch, lb.
	(a)	27aw ÷ T			(b)	(v)·(b)
Cement II Type, Santa Cruz Brand, C976 No.	1.026	623.8			623.8	124.76
Other Pozzolan, Expansive Components, etc.						
Water	0.68	426		-50.27	375.7	75.14
Fine Sand Antioch		346	+3.83	+13.25	359.3	71.85
Coarse Sand Pleasanton		1227	+2.67	+36.76	1263.8	252.75
Fine Gravel 1/8 × 1/4 Pleasanton		1306	+0.02	+0.26	1305.8	261.15
Coarse Gravel						
Total T =		3929			3929	786.
Admixture, concentration						

PROPERTY	Batch Number 1	2	3	4	5	6	7	8	9
Wt. mixer water, lb.									
Slump, in.									
Kelly Ball pen't, in.									
Amt. of Admixture									
Air content, %									
Temperature °F									
Wt. conc. + cont., lb.									
Wt. container, lb.									
Wt. concrete=A, lb.									
Vol. cont.=B, cu. ft.									
Unit wt.= A÷ B, pcf									

Cylinders cast in. molds; compacted by

Cylinders numbered to

7/72 GH

FIG. B.11 CONCRETE MIX PROPORTIONS FOR MODEL #2

Cylinder	Age, Days	f_c MPa	f_c ksi	$\bar{f}_c$ MPa	$\bar{f}_c$ ksi
5/20	7	12.3	1.78	12.4	1.80
6/20	7	12.5	1.82		
7/20	14	19.6	2.84	19.2	2.79
8/20	14	18.9	2.74		
9/20	21	21.2	3.07	21.6	3.13
10/20	21	22.1	3.20		
11/20	28	23.0	3.34	23.2	3.36
12/20	28	23.3	3.38		
13/20	56	23.8	3.45	23.6	3.42
14/20	56	23.4	3.39		
	(Test #3)				
15/20	189	21.0	3.05		
16/20	189	21.0	3.04		
17/20	189	21.9	3.18	22.0	3.19
18/20	189	22.5	3.27		
19/20	189	22.9	3.32		
20/20	189	22.6	3.28		

Fig. B.12. CONCRETE COMPRESSIVE STRENGTH, MODEL #2

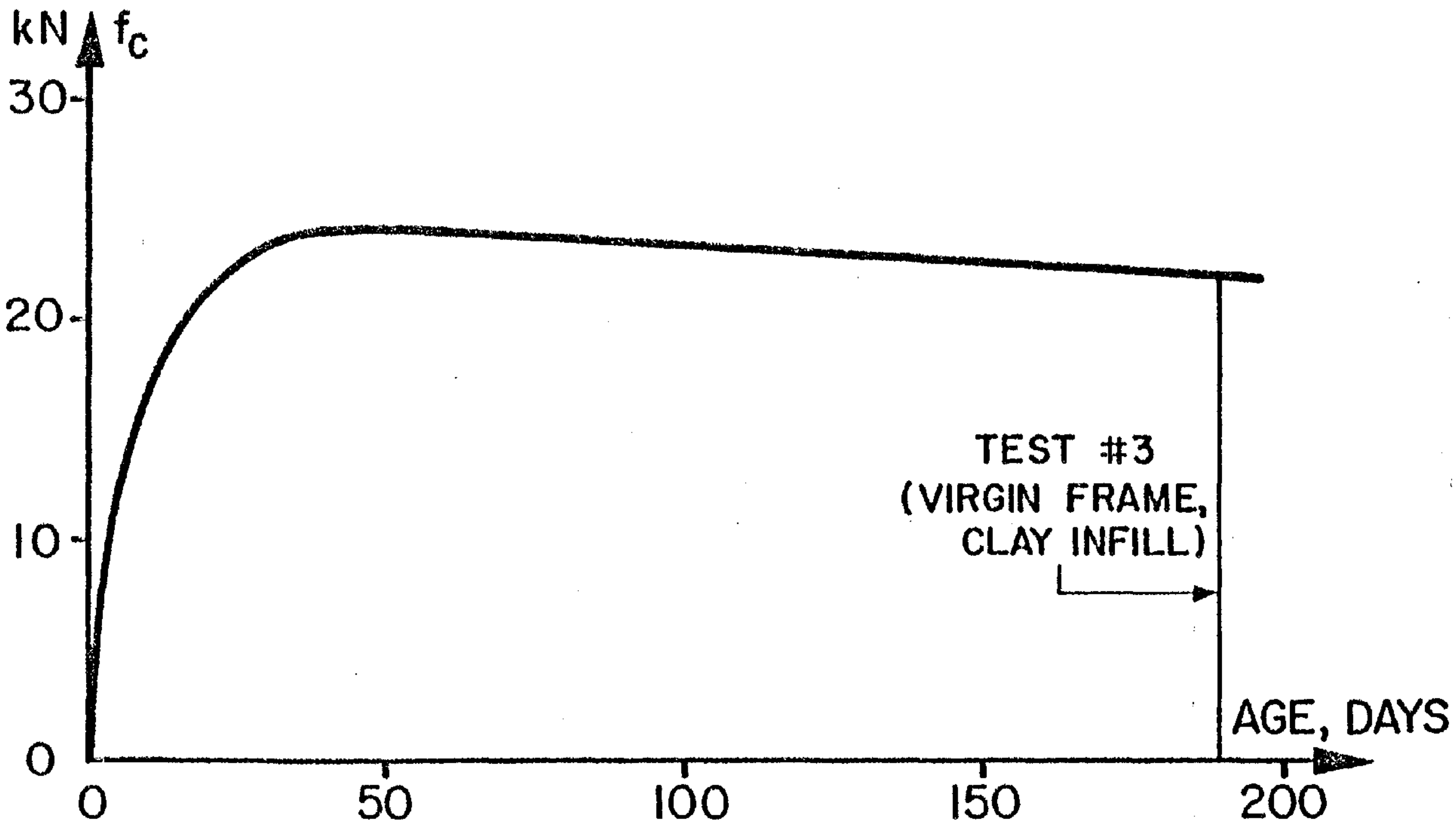

FIG. B.13 CONCRETE COMPRESSIVE STRENGTH, VIRGIN FRAME WITH CLAY INFILL (MODEL #2)

Cylinder	Age, Days	f_t		$f_t/\sqrt{f_c}$	
		MPa	psi	MPa	psi
	(Test #3)				
1/4	197	4.33	628	0.98	11.8
2/4	197	4.21	610		
3/4	197	4.94	717		
4/4	197	4.94	717		

Fig. B.14 MODULUS OF RUPTURE, MODEL #2

University of California
Department of Civil Engineering

Division of Structural Engineering
and Structural Mechanics

CONCRETE LABORATORY CASTING DATA SHEET

Date Cast 11/6/75 Project O-21997 Name Klingner
Mix No. Infill Wall #3 Specimen
Desired Slump 5 in. ± in. Desired Air Cont 1 ± %
Unit wt. (w) = 145 lb/cu.ft. Admixture Amount

MATERIAL	SSD Aggregates: Parts by wt. (a)	SSD Aggregates: Wt. for 1 cu.yd. batch (lb.) 27aw ÷ T	Aggregates, as stocked: Moisture Adjustment (%)	Moisture Adjustment (lb)	Adj. wt. for 1 cu. yd. batch (lb.) (b)	Wt. for v= 0.2 cu.yd. batch, lb. (v)·(b)
Cement II (Type) Santa Cruz (Brand) C976 (No.)	1.00	626			626	125.2
Other Pozzolan, Expansive Components, etc.						
Water	0.63	395		-51	344	68.2
Fine Sand Antioch FM=1.54	0.55	345	+3.6	+12	357	71
Coarse Sand Eliot State F.M.=2.94	1.97	1234	+2.8	+35	1269	254
Fine Gravel Pleasanton 1/4×1/8	2.10	1315	0.3	+4	1319	264
Coarse Gravel						
Total T =	6.25				3915	783
Admixture, concentration:						

PROPERTY	Batch Number 1	2	3	4	5	6	7	8	9
Wt. mixer water, lb.									
Slump, in.									
Kelly Ball pen't, in.									
Amt. of Admixture									
Air content, %									
Temperature °F									
Wt. conc.+ cont., lb.									
Wt. container, lb.									
Wt. concrete=A, lb.									
Vol. cont.=B, cu. ft.									
Unit wt.= A÷ B, pcf									

Cylinders cast in molds; compacted by
Cylinders numbered to

7/72 GH

FIG. B.15 CONCRETE MIX PROPORTIONS FOR MODEL #3

Fig. B.16. CONCRETE COMPRESSIVE STRENGTH, MODEL #3

Cylinder	Method of Compaction	Age, Days	f_c MPa	f_c ksi	$\bar{f}_c$ MPa	$\bar{f}_c$ ksi
1/24	vibrated	7	15.7	2.27	15.6	2.26
2/24	vibrated	7	15.5	2.25		
3/24	vibrated	8	16.6	2.41	16.6	2.41
4/24	vibrated	8	16.6	2.41		
5/24	rodded	8	16.4	2.38	16.1	2.34
6/24	rodded	8	15.9	2.30		
7/24	vibrated	14	21.3	3.09	21.6	3.13
8/24	vibrated	14	21.9	3.18		
11/24	rodded	14	21.5	3.12	21.6	3.13
12/24	rodded	14	21.7	3.14		
9/24	vibrated	20	24.5	3.56	24.4	3.54
10/24	vibrated	20	24.3	3.52		
13/24	vibrated	28	27.9	4.04	27.4	3.97
14/24	vibrated	28	26.9	3.90		
16/24	rodded	28	27.5	3.99	26.9	3.90
17/24	rodded	28	26.3	3.82		
15/24	vibrated	63	29.4	4.26	29.3	4.25
19/24	vibrated	63	29.2	4.23		
18/24	rodded	63	30.8	4.47	30.3	4.40
21/24	rodded	63	29.9	4.33		
		(Test #4)				
20/24	vibrated	182	27.2	3.94	27.9	4.05
23/24	vibrated	182	28.7	4.16		
24/24	rodded	182	27.8	4.03	27.3	3.96
22/24	rodded	182	26.8	3.88		

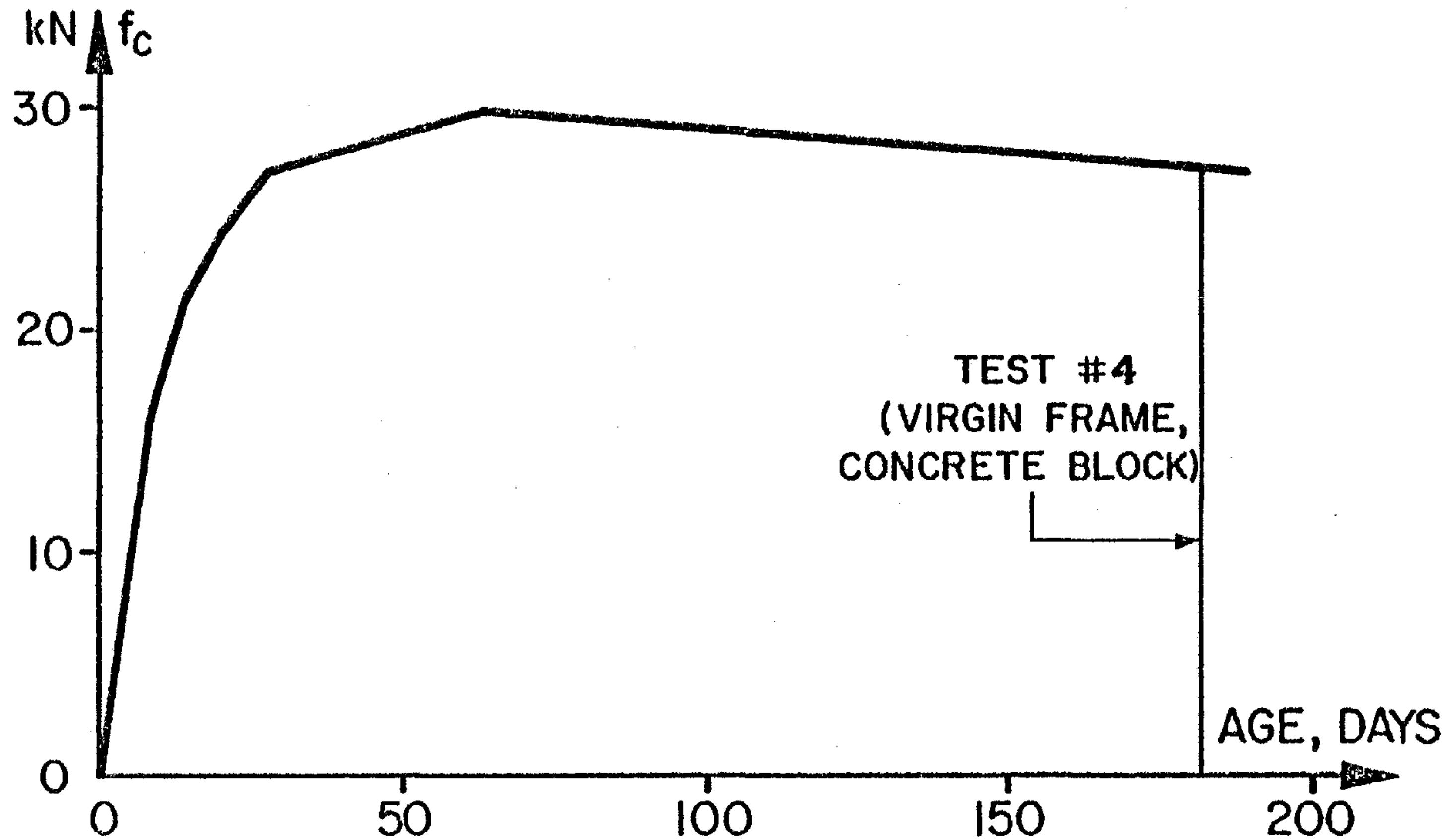

FIG. B.17 CONCRETE COMPRESSIVE STRENGTH, VIRGIN FRAME WITH CONCRETE BLOCK INFILL (MODEL #3)

Specimen	Age, Days	f_t MPa	f_t psi	$f_t/\sqrt{f_c}$ MPa	$f_t/\sqrt{f_c}$ psi
	(Test #4)				
1/4	182	5.24	760		
2/4	182	4.81	697	0.94	11.3
3/4	182	4.52	655		
4/4	182	5.21	755		

Fig. B.18 MODULUS OF RUPTURE, MODEL #3

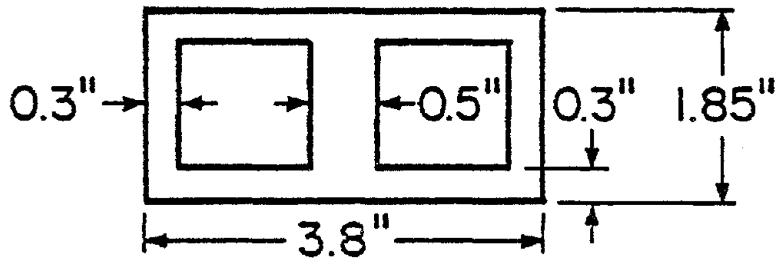

CLAY UNIT 1 in. HIGH (NOMINAL)

FIG. B.19 CLAY UNITS

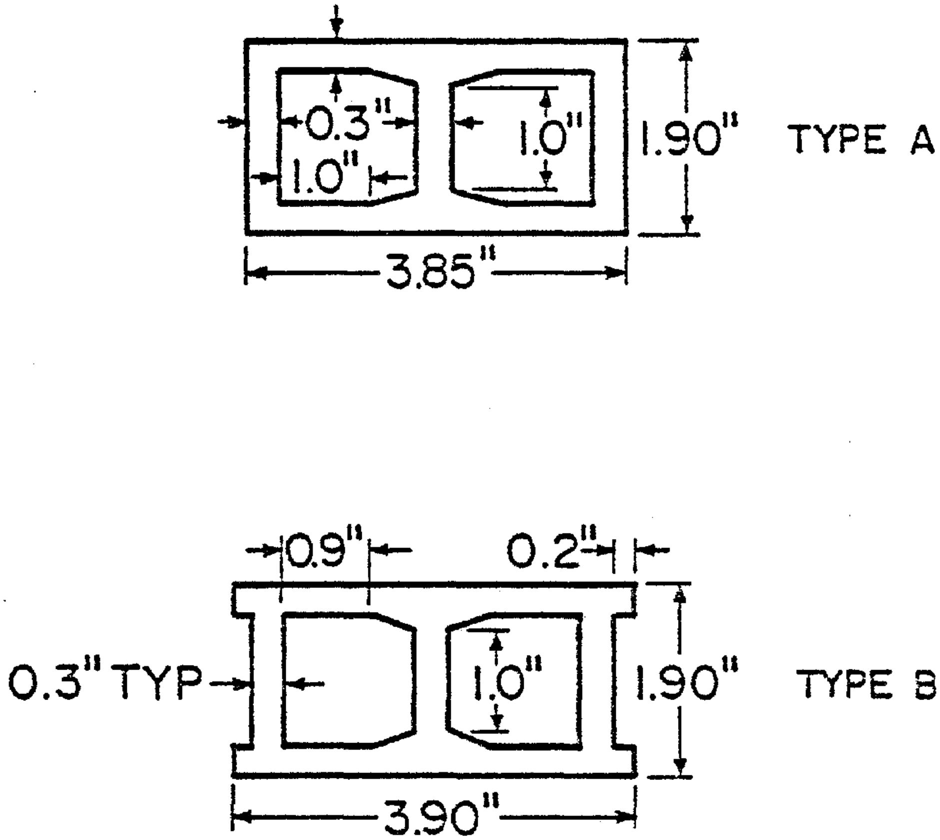

CONCRETE UNITS 2 in. HIGH (NOMINAL)

FIG. B.20 CONCRETE BLOCK UNITS

Specimen	Failure Stress MPa	Failure Stress Ksi	Average Stress MPa	Average Stress Ksi
1	37.8	5.48		
2	37.3	5.41		
3	43.3	6.28	42.1	6.11
4	51.5	7.47		
5	40.7	5.90		

Fig. B.21. COMPRESSIVE STRENGTH OF CLAY UNITS

Specimen	Type	Stress on Net Area MPa	Stress on Net Area Ksi
1	A	15.8	2.29
2	A	28.1	4.07
3	A	28.0	4.06
4	B	23.5	3.41
5	B	28.0	4.06
6	B	13.3	1.93

Failure stresses varied widely due to variations in porosity of brick walls.

sandy blocks: $\bar{f}_{block} \simeq$ 14 MPa (2.1 Ksi)

good blocks: $\bar{f}_{block} \simeq$ 27 MPa (3.9 Ksi)

Fig. B.22 COMPRESSIVE STRENGTH OF CONCRETE UNITS

Fig. B.23 COMPRESSIVE STRENGTH OF MORTAR AND GROUT, INFILLED BARE FRAME (TEST #2)

Panel 1

Mortar					Grout			
Specimen	Age, Days	Compaction	f_m		Specimen	Age, Days	f_g	
			MPa	Ksi			MPa	Ksi
1/6	18	unbuttered	25.6	3.72	1/2	28	13.7	1.98
2/6	18	unbuttered	28.5	4.13	2/2	28	12.7	1.84
3/6	28	unbuttered	28.9	4.19				
4/6	28	unbuttered	29.2	4.24				
5/6	28	buttered	34.8	5.04				
6/6	28	buttered	30.4	4.41				

Panel 2

Mortar					Grout			
Specimen	Age, Days	Compaction	f_m		Specimen	Age, Days	f_g	
			MPa	Ksi			MPa	Ksi
1/4	14	buttered	26.8	3.89	1/2	28	26.6	3.86
2/4	14	buttered	26.5	3.84	2/2	28	30.7	4.45
3/4	28	buttered	29.6	4.30				
4/4	28	buttered	28.1	4.07				

Fig B.23 (CONTINUED)

Panel 3

Mortar					Grout			
Specimen	Age, Days	Compaction	f_m		Specimen	Age, Days	f_g	
			MPa	Ksi			MPa	Ksi
1/4	14	buttered	27.0	3.91	1/2	28	22.6	3.28
2/4	14	buttered	26.3	3.81	2/2	28	21.3	3.09
3/4	28	buttered	30.4	4.41				
4/4	28	buttered	28.0	4.35				

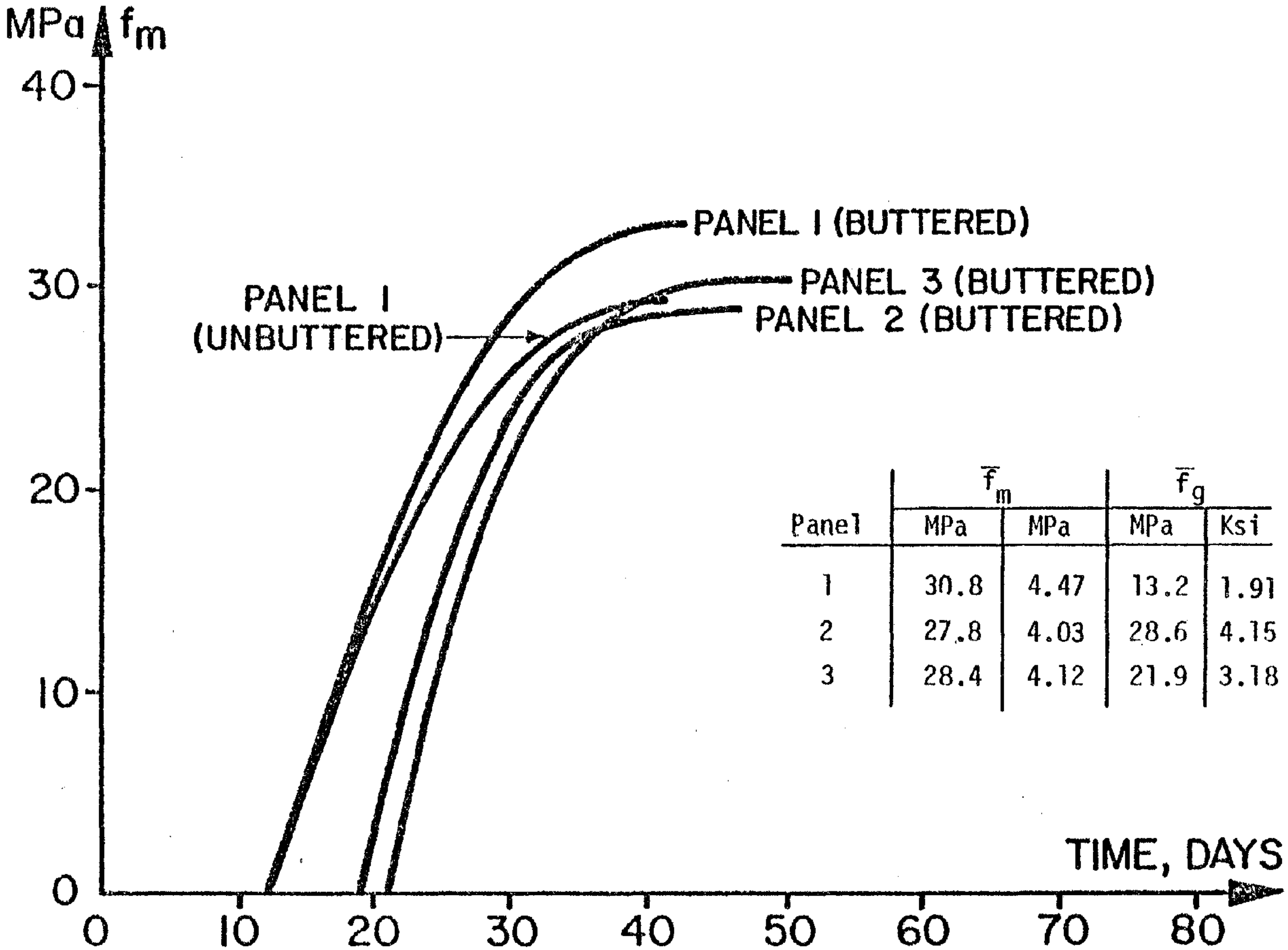

Panel	$\bar{f}_m$ MPa	MPa	$\bar{f}_g$ MPa	Ksi
1	30.8	4.47	13.2	1.91
2	27.8	4.03	28.6	4.15
3	28.4	4.12	21.9	3.18

FIG. B.24 COMPRESSIVE STRENGTHS OF MORTAR AND GROUT, INFILLED BARE FRAME (TEST #2)

Fig. B.25 COMPRESSIVE STRENGTHS OF MORTAR AND GROUT, VIRGIN FRAME WITH CLAY INFILL (TEST #3)

Panel 1

Mortar					Grout			
No.	Age, Days	Compaction	f_m		No.	Age, Days	f_g	
			MPa	Ksi			MPa	Ksi
4/6	14	unbuttered newer	10.2	1.48	1/2	28	24.1	3.49
5/6	14	buttered newer	12.8	1.86	2/2	28	25.6	3.72
1/6	29	unbuttered older	23.9	3.47				
2/6	29	unbuttered older	25.6	3.72				
3/6	29	unbuttered newer	11.9	1.72				
6/6	29	buttered newer	14.7	2.13				

Panel 2

Mortar					Grout			
No.	Age, Days	Compaction	f_m		No.	Age, Days	f_g	
			MPa	Ksi			MPa	Ksi
4/6	14	unbuttered	21.7	3.15	1/2	28	24.0	3.48
5/6	14	buttered	25.4	3.69	2/2	28	24.7	3.58
1/6	28	unbuttered	25.2	3.66				
2/6	28	unbuttered	25.3	3.67				
3/6	28	buttered	31.1	4.51				
6/6	28	buttered	28.3	4.11				

Fig. B.25. (CONTINUED)

Panel 3

Mortar					Grout			
No.	Age, Days	Compaction	f_m		No.	Age, Days	f_g	
			MPa	Ksi			MPa	Ksi
3/6	14	buttered	30.2	4.38	1/2	28	24.6	3.57
4/6	14	unbuttered	27.6	4.01	2/2	28	24.3	3.54
1/6	28	buttered	34.1	4.95				
2/6	28	buttered	37.2	5.39				
5/6	28	unbuttered	30.6	4.44				
6/6	28	unbuttered	30.2	4.38				

Panel	$\bar{f}_m$ MPa	$\bar{f}_m$ Ksi	$\bar{f}_g$ MPa	$\bar{f}_g$ Ksi
1	19.0	2.76	24.9	3.61
2	27.5	3.99	24.3	3.53
3	33.0	4.79	24.5	3.55

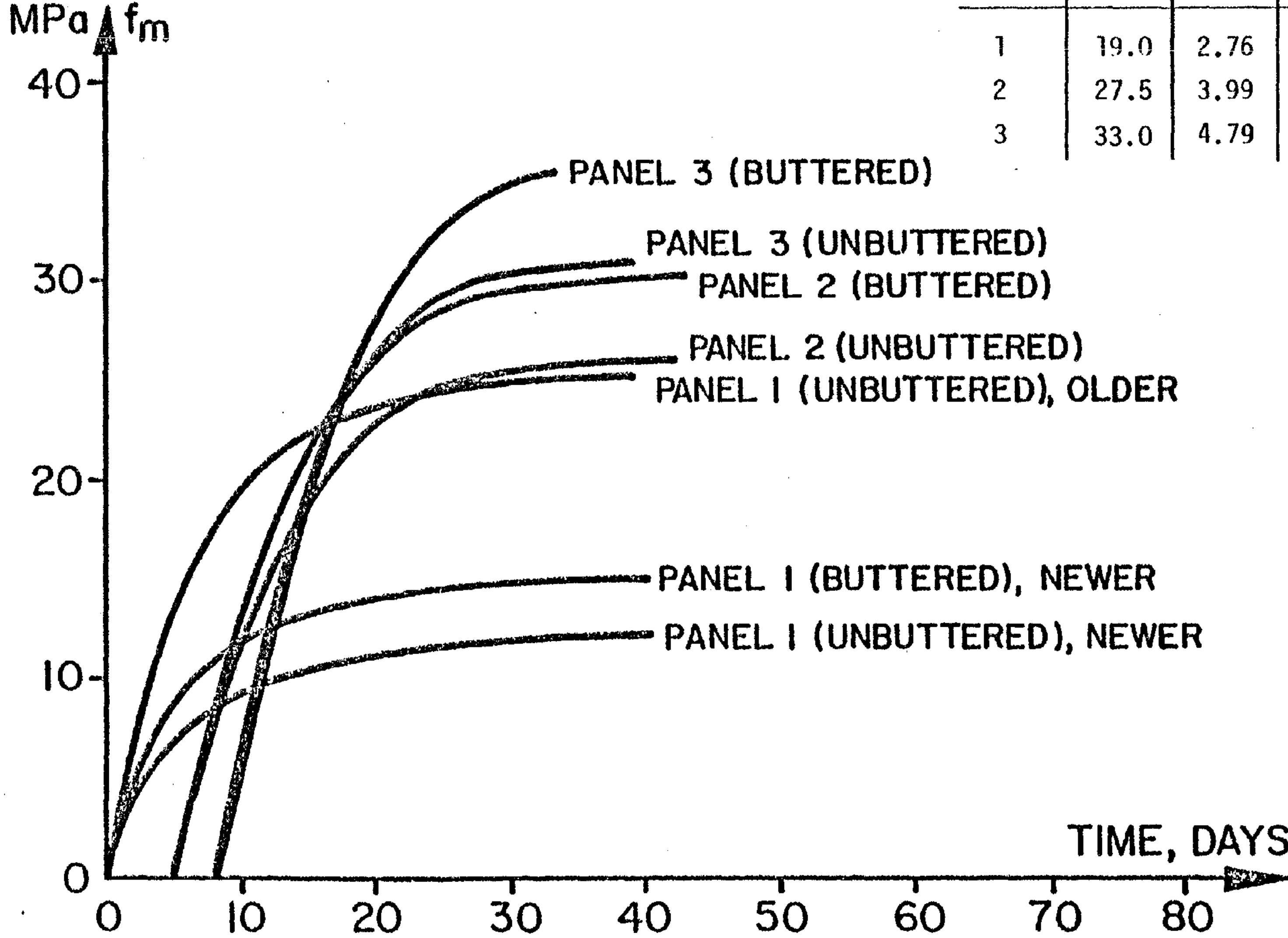

FIG. B.26 COMPRESSIVE STRENGTHS OF MORTAR AND GROUT, VIRGIN FRAME WITH CLAY INFILL (TEST #3)

Fig. B.27 COMPRESSIVE STRENGTHS OF MORTAR AND GROUT, VIRGIN FRAME WITH CONCRETE BLOCK INFILL (TEST #4)

Panel 1

Mortar				Grout			
Specimen	Age, Days	f_m		Specimen	Age, Days	f_g	
		MPa	Ksi			MPa	Ksi
1/4	14	32.7	4.74	1/2	28	21.8	3.16
2/4	14	33.8	4.90	2/2	28	22.5	3.27
3/4	28	37.3	5.41				
4/4	28	37.9	5.49				

Panel 2

Mortar				Grout			
Specimen	Age, Days	f_m		Specimen	Age, Days	f_g	
		MPa	Ksi			MPa	Ksi
1/4	14	27.4	3.97	1/2	28	13.2	1.91
2/4	14	28.1	4.08	2/2	28	14.4	2.09
3/4	28	31.9	4.63				
4/4	28	31.9	4.62	(these specimens were unpuddled)			

Panel 3

Mortar				Grout			
Specimen	Age, Days	f_m		Specimen	Age, Days	f_g	
		MPa	Ksi			MPa	Ksi
1/4	14	32.3	4.68	1/2	28	25.1	3.64
2/4	14	31.0	4.49	2/2	28	24.3	3.53
3/4	28	35.2	5.11				
4/4	28	34.8	5.04				

(All specimens buttered)

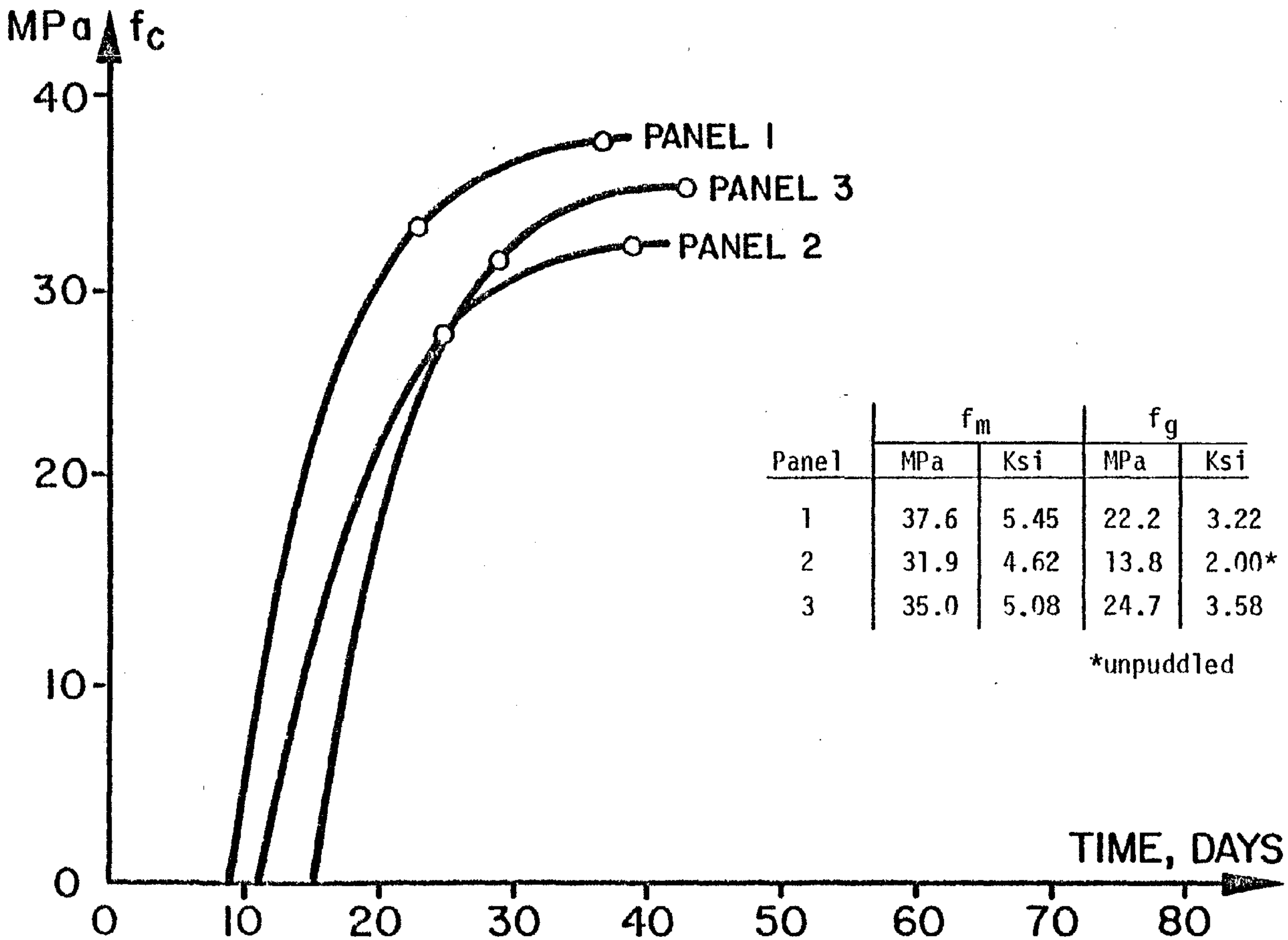

	f_m		f_g	
Panel	MPa	Ksi	MPa	Ksi
1	37.6	5.45	22.2	3.22
2	31.9	4.62	13.8	2.00*
3	35.0	5.08	24.7	3.58

*unpuddled

FIG. B.28 COMPRESSIVE STRENGTHS OF MORTAR AND GROUT, VIRGIN FRAME WITH CONCRETE BLOCK INFILL (TEST #4)

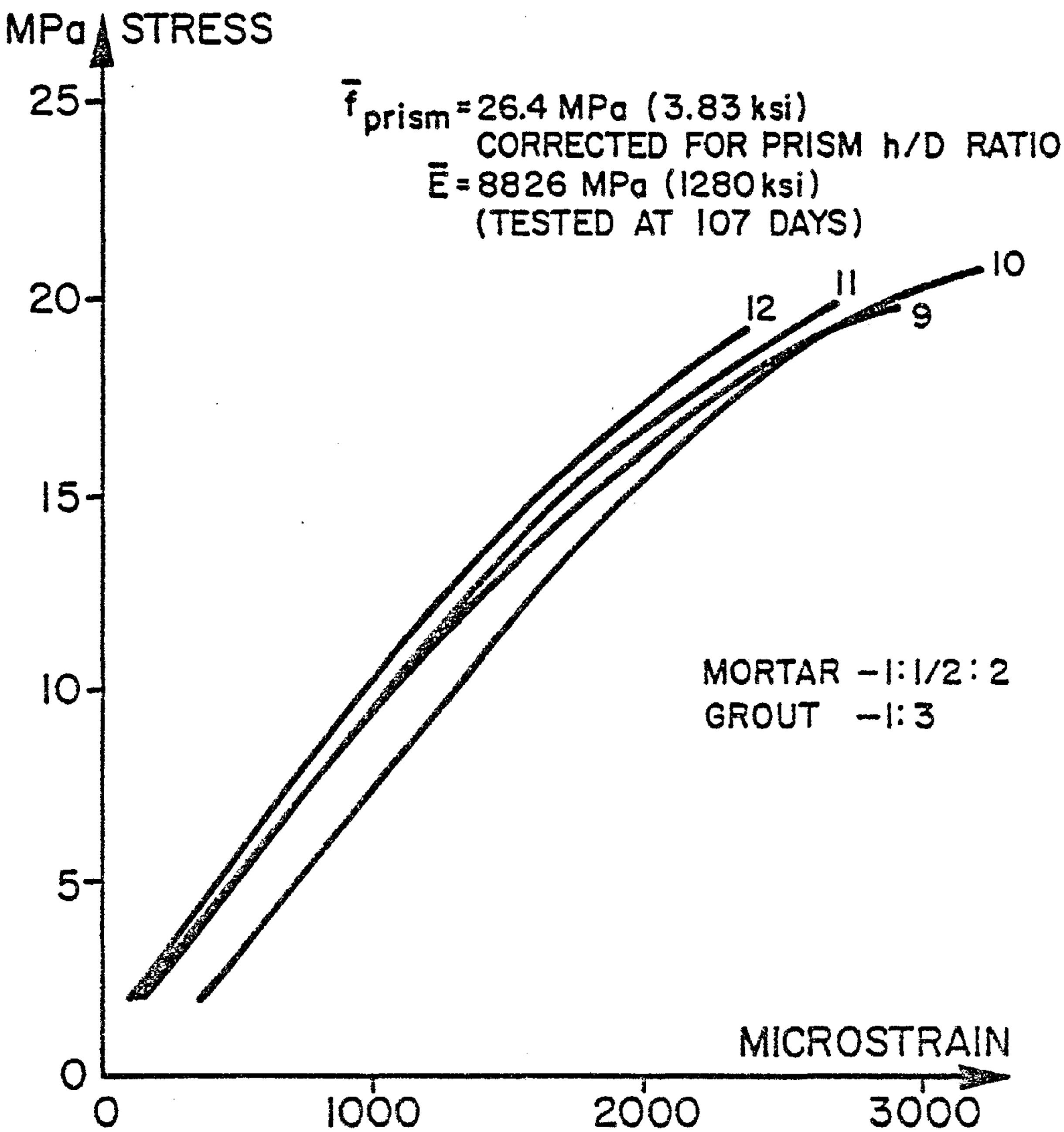

FIG. B.29 STRESS-STRAIN RELATIONSHIP FOR GROUTED MASONRY PRISMS CORRESPONDING TO INFILLED BARE FRAME (TEST #2)

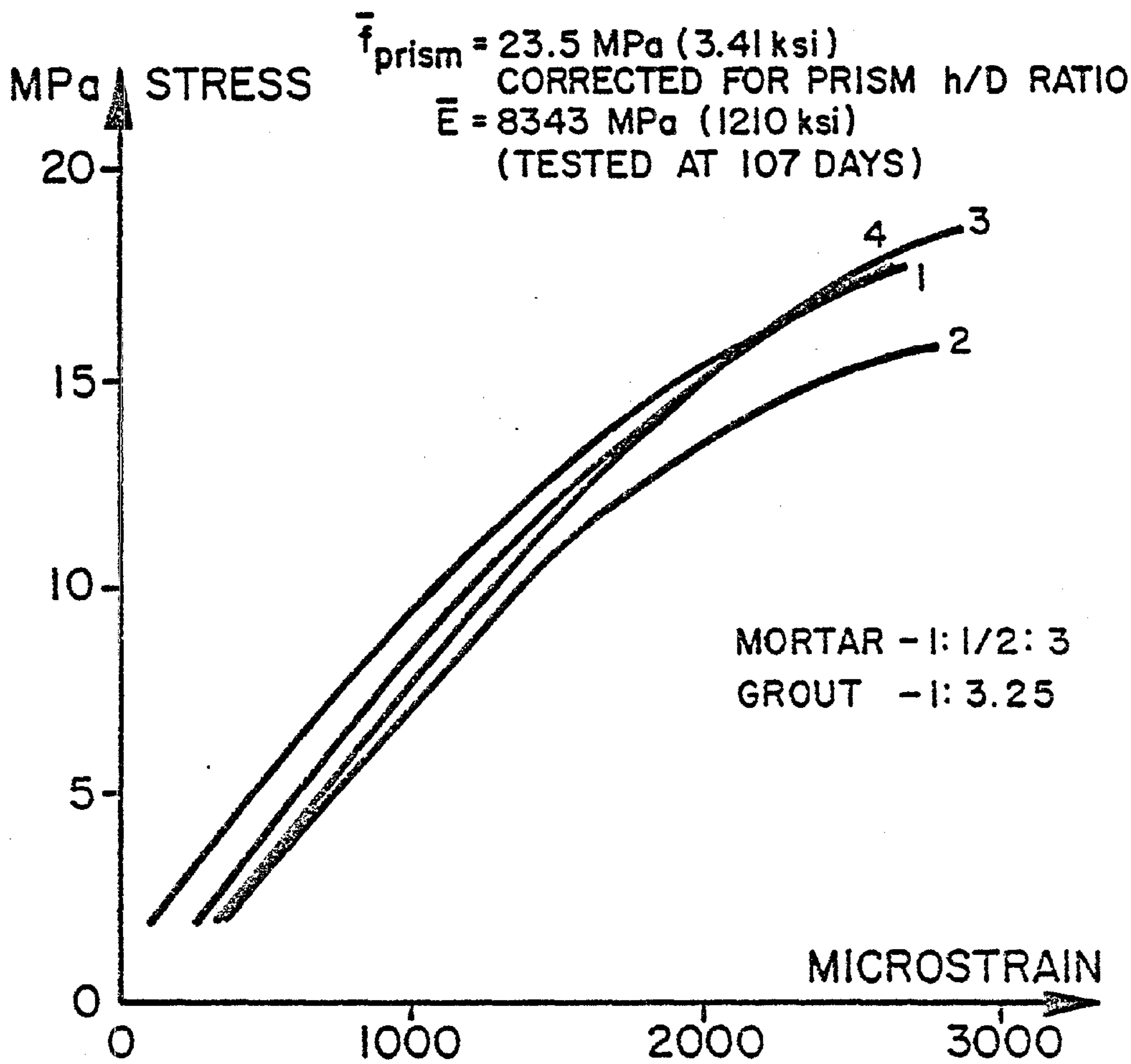

FIG. B.30 STRESS-STRAIN RELATIONSHIP FOR GROUTED MASONRY PRISMS CORRESPONDING TO PANEL #1 OF VIRGIN FRAME WITH CLAY PANELS (TEST #3)

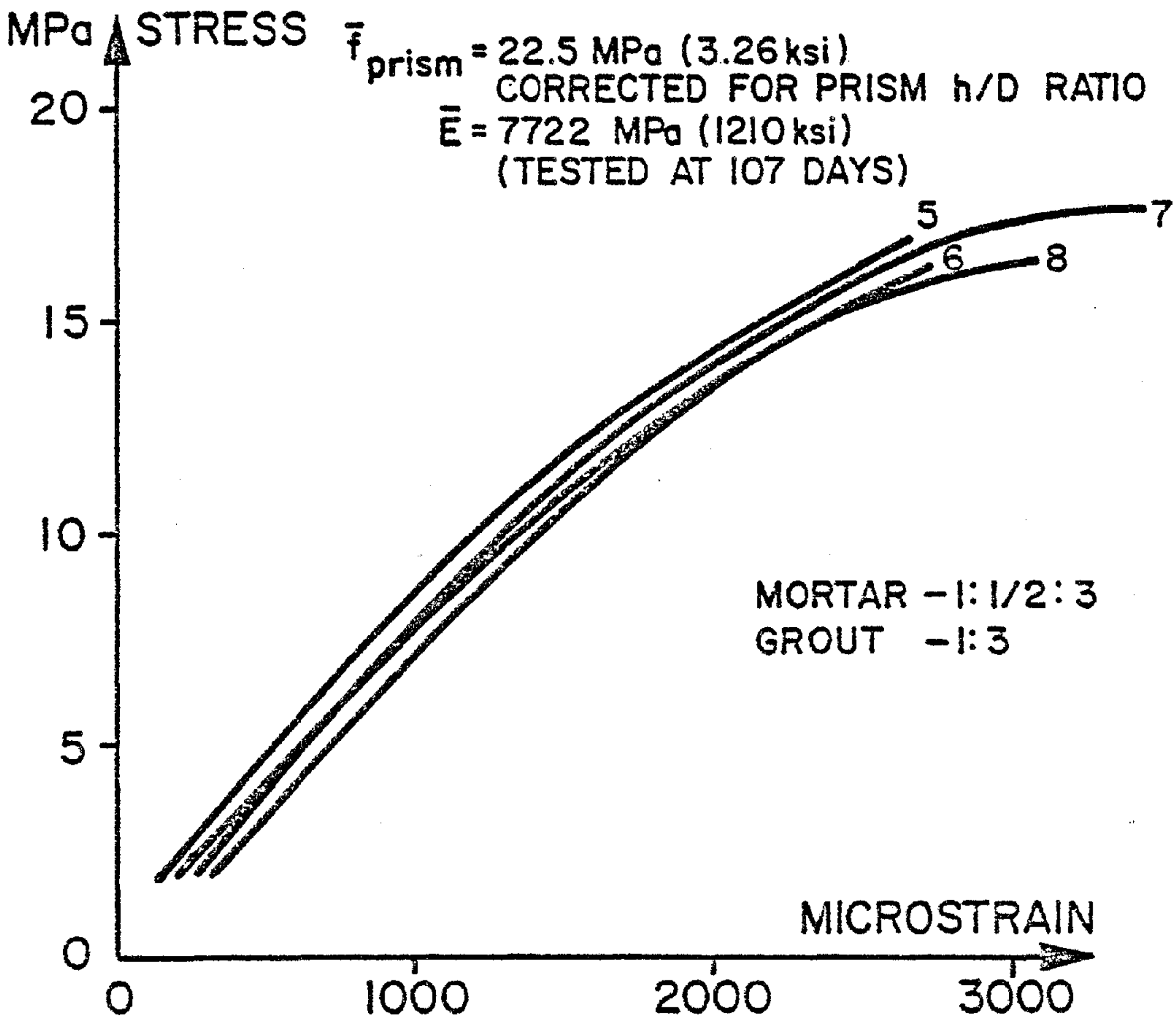

FIG. B.31 STRESS-STRAIN RELATIONSHIP FOR GROUTED MASONRY PRISMS CORRESPONDING TO PANELS #2 AND #3 OF VIRGIN FRAME WITH CLAY PANELS (TEST #3)

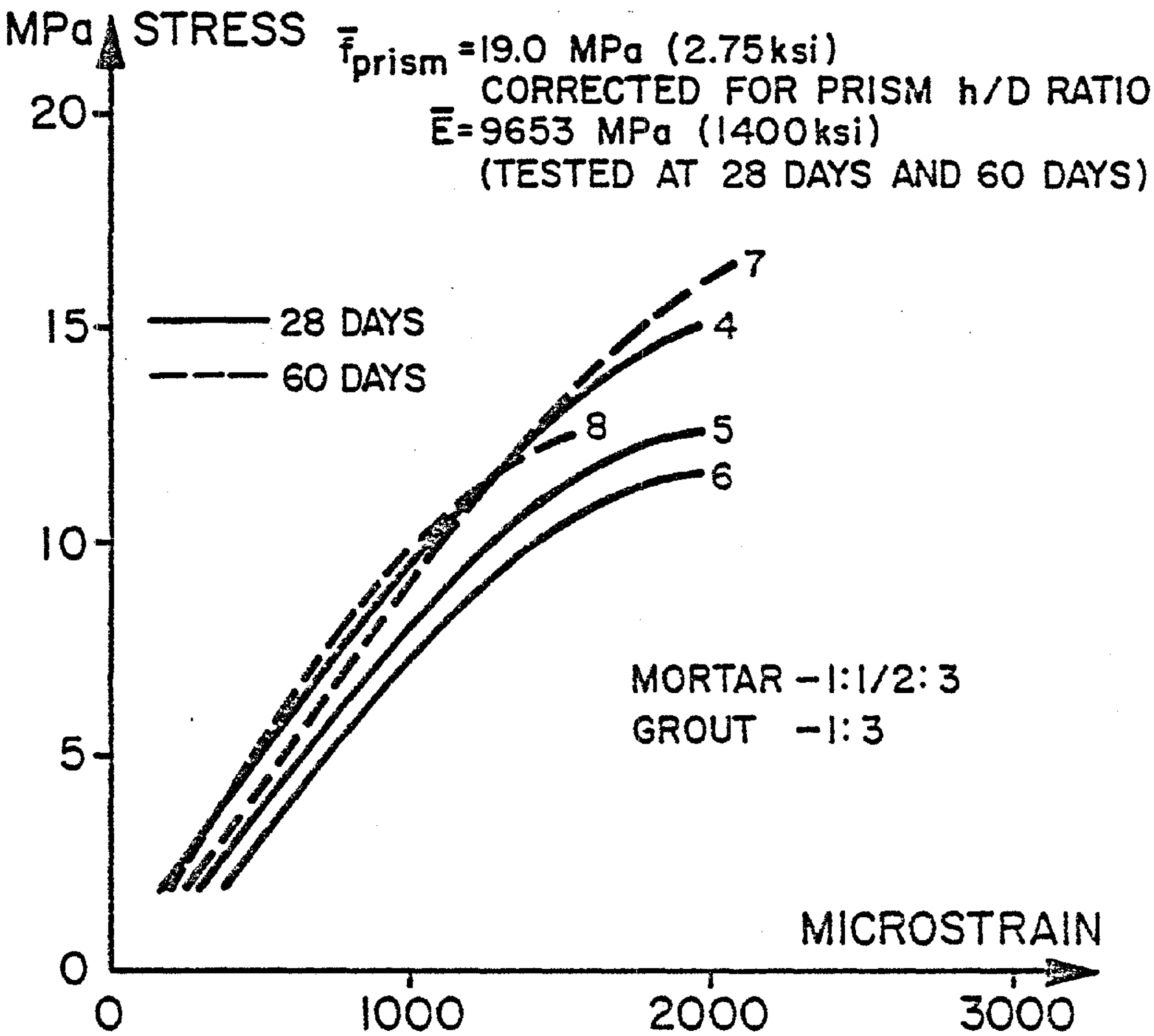

FIG. B.32 STRESS-STRAIN RELATIONSHIP FOR GROUTED MASONRY PRISMS CORRESPONDING TO VIRGIN FRAME WITH CONCRETE BLOCK PANELS (TEST #4)

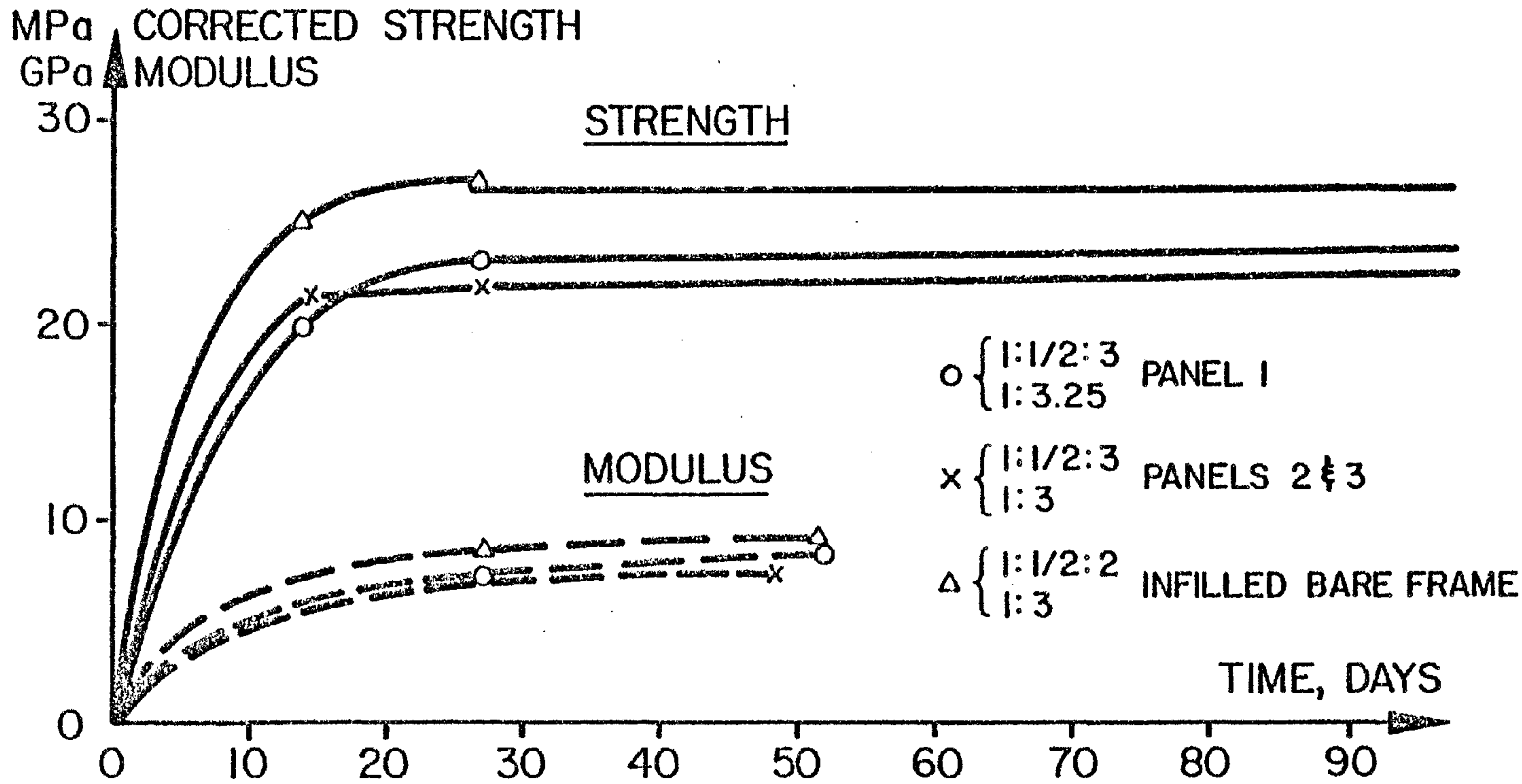

FIG. B.33 VARIATION WITH TIME OF STRENGTH AND MODULUS OF CLAY MASONRY PRISMS

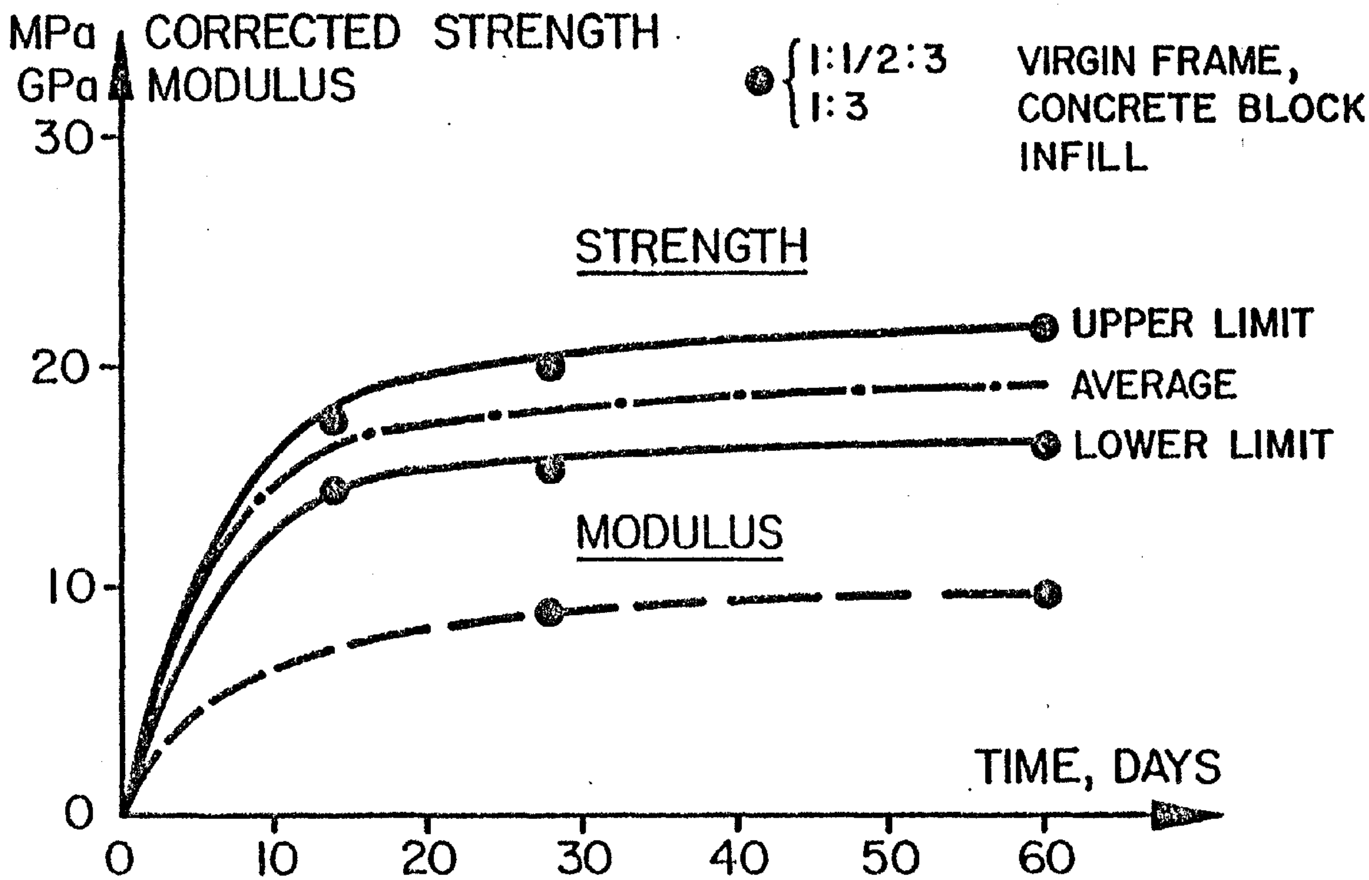

FIG. B.34 VARIATION WITH TIME OF STRENGTH AND MODULUS OF CONCRETE BLOCK PRISMS

APPENDIX C: EQUIPMENT AND INSTRUMENTATION

As explained in Section 5.3 of the text, many different types of equipment and instrumentation were used throughout the tests, to control the loading for each model as well as measure its response. These are discussed in detail below and in Reference 35.

C.1 Loading Equipment

Loading equipment comprised the following components, shown schematically in Fig. C.1:

1) Lateral Actuator: a 1557 kN (350 k) capacity, double-action hydraulic actuator with a bore of 356 mm (14 in) and a stroke of 305 mm (12 in).

2) Axial Actuators: two double-acting hydraulic actuators with 1557 kN capacity, 356 mm bore, and 254 mm (10 in) stroke.

3) Hydraulic System: the testing facility's built-in hydraulic system supplied oil at 20.7 MPa (3000 psi), delivered to the actuators through servovalves with a capacity of 3.4 kg/min (5 gpm) with a pressure drop of 6.9 MPa (1000 psi).

C.2 Loading Control

Actuator loads were controlled using three MTS Model 406 controllers, connected as shown schematically in Fig. C.1. The loading program was applied using manual program input. Because the bare frame was comparatively flexible, Test #1 was conducted entirely under displacement control. The infilled frame tests were begun using load control (the force in the lateral actuator load cell), and were switched to displacement control (the lateral displacement of the exterior column at the level of the lateral load) after the specimens began to yield.

C.3 Instrumentation

Many different response parameters were measured throughout each test, e.g., lateral deflections, column shortening, shear distortion of the panels, rotations at beam-column joints, and average strains in reinforcing steel. Specific types of instrumentation were best suited to the measurement of each parameter:

1) Linear Potentiometers (LP): these were used to measure relatively large displacements, such as the lateral displacement at various levels, the diagonal (shearing) deformations of the panels, and the shortening of the columns. Two types of linear potentiometers were used:

a) Helipot 1000-Ω LP's with a stroke of 152 mm (6 in) and a sensitivity of 0.10 % of full travel; and

b) Waters "Longfellow" Linear Motion Position Transducers, with a resistance of 5000 Ω, a stroke of 152 mm (6 in), and a sensitivity of 0.10 % of full travel.

2) Load Cells: Two types were used. The first type, used to monitor actuator forces, was constructed by bonding strain gages to specially-machined load cells attached to the actuator shafts. Strains in the load cells were used to compute the loads applied by each actuator. Details of the construction and calibration of these load cells can be found in Ref. 35. The second type, used to monitor force levels in the struts, is labelled "S.G." in Figs. 15 and 16 of the text. These were specially constructed for this test program. Each load cell of this type was constructed using four 120-Ω precision strain gages (Micro-Measurements CEA-06-250UW-120), two in the longitudinal direction and two in the transverse direction, bonded to the strut with highly stable oven-cured epoxy cement. The gages were wired in a full bridge, and the load cell was calibrated in tension and compression using an hydraulic universal testing machine.

3) Clip gages: These gages, shown in detail in Fig. C.2, were used to measure relative axial displacement of concrete sections along the first story height in the columns of the infilled frame models. They were mounted on tapped steel pins embedded in the concrete. Relative displacements of the pins resulted in curvature changes in the brass strip and consequent voltage changes across the passive side of a four-arm bridge which was composed of strain gages bonded to the strip.

4) Weldable Strain Gages: "Microdot" weldable strain gages were used to measure average strains in the column longitudinal steel near the base of the columns, and specifically to indicate the onset of yielding in that steel. The gages were welded to prepared sections of reinforcement, and used as the single active arm of a four-arm bridge.

5) Linear Variable Differential Transformers (LVDT): These were used to measure small deflections, on the order of 1 mm. As shown in Fig. C.3, rigid yokes were attached perpendicular to the axis of a member, at a distance of about 152 mm (6 in) apart. It was possible to measure relative rotations from section to section by subtracting the voltage changes recorded by the two LVDT's.

C.4 Amplifiers and Recorders

Three types of recorders were used:

1) Esterline Angus Model 530 (XY);

2) Esterline Angus Model 540 (XYY); and

3) Electro Instruments Model 500 (XY).

When necessary, the low-level signals from transducers were amplified by Daytronic amplifiers. These amplifiers were equipped with modular input stages to accept either strain gage input or LVDT input as required.

C.5 Low-Speed Scanner

Output from all transducers was fed to a multi-channel relay box connected to a Data Technology Model 370 integrating digital voltmeter. Scanning of the relay box channels was controlled by a Data General "Nova" computer which was programmed to permit the conversion of transducer voltages to appropriate units. Readings for each channel were recorded using a magnetic tape unit and teletype which were also connected to the Nova. Further data reduction was carried out using the facilities of the Computer Center at the University of California at Berkeley. The magnetic tape output from the scanner was directly compatible with the input requirements of the Center's CDC-6400 computer and Calidoscope operating system.

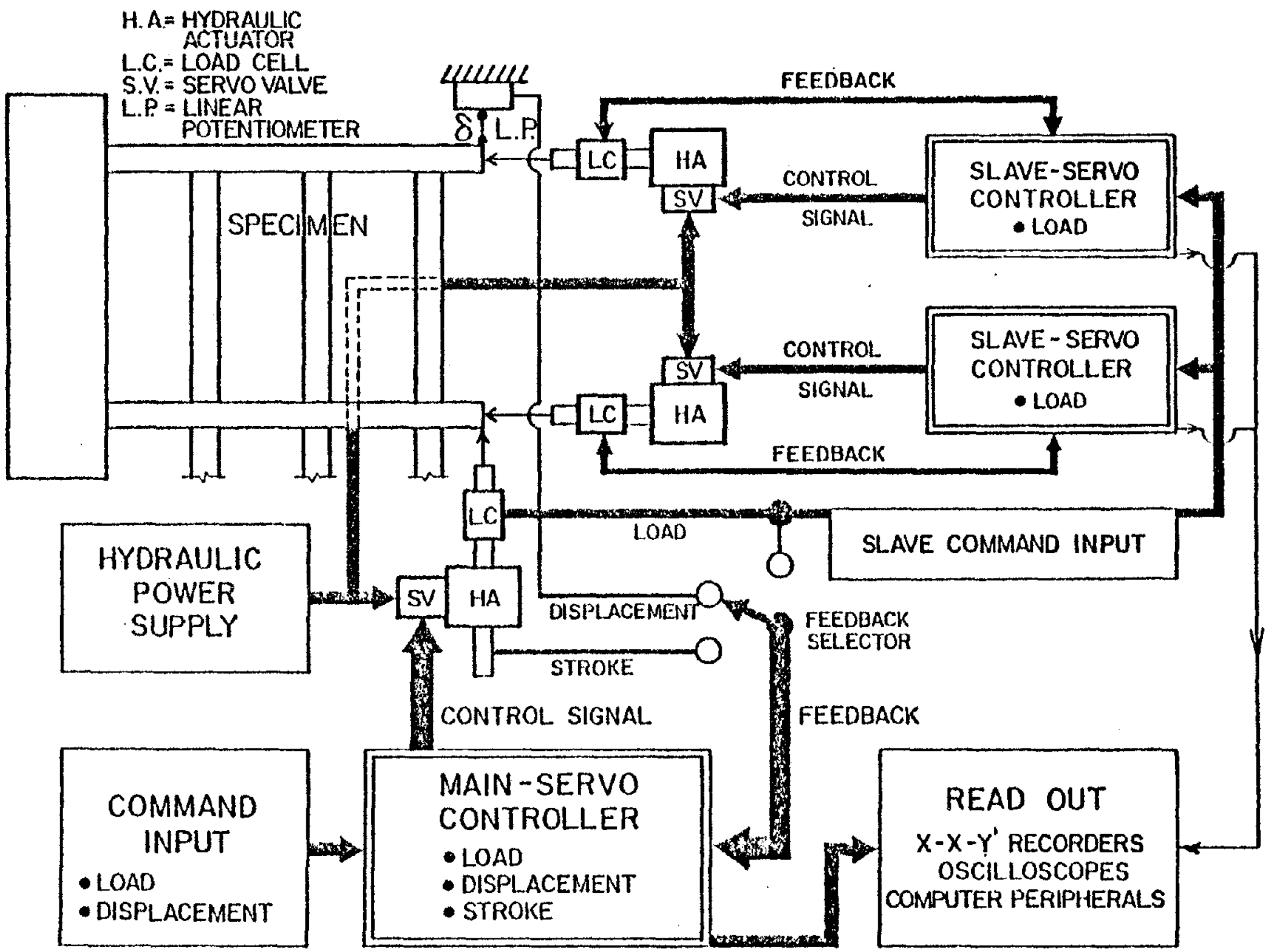

FIG. C.1 SERVO-HYDRAULIC SYSTEM

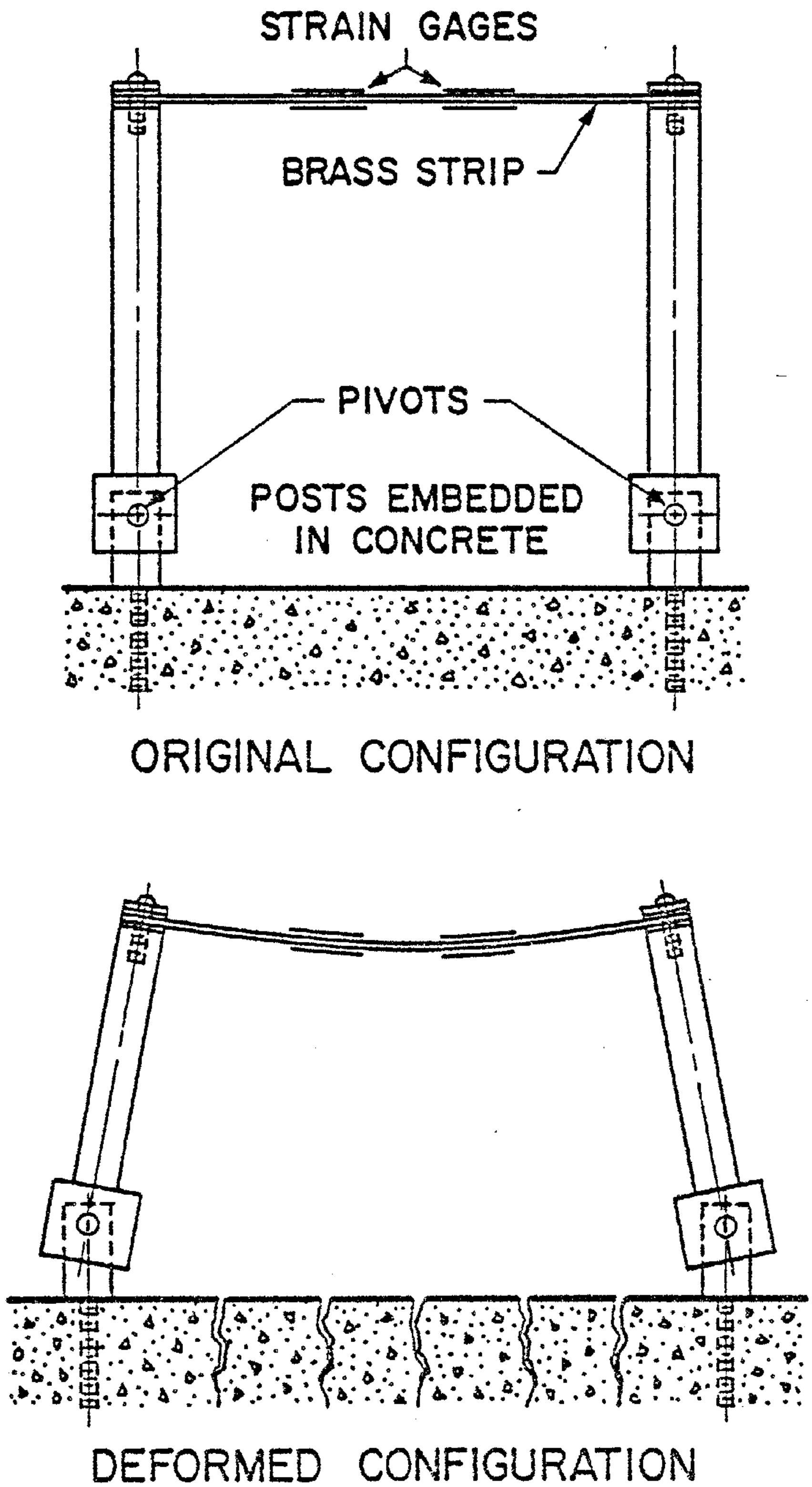

FIG. C.2 USE OF CLIP GAGES TO MEASURE CONCRETE DEFORMATIONS

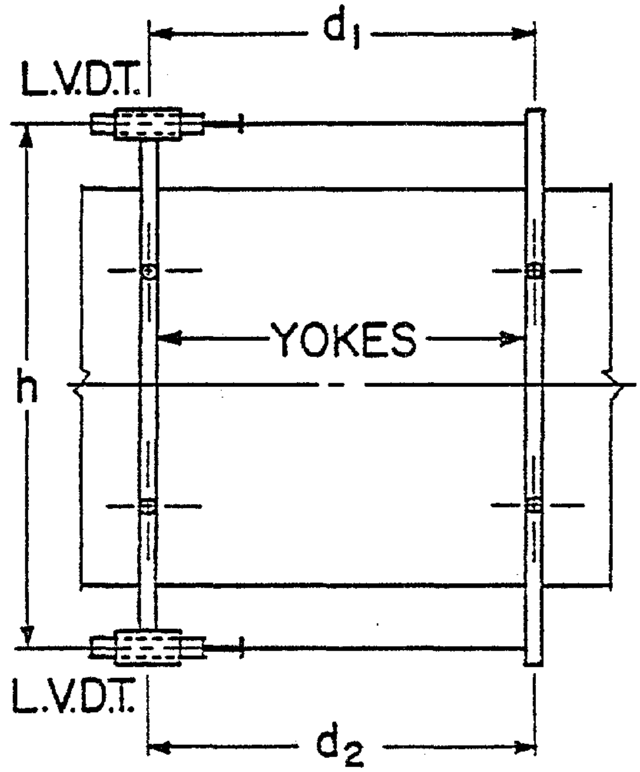

AVERAGE ANGLE CHANGE BETWEEN YOKES

$$\theta = \frac{(\Delta d_1 - \Delta d_2)}{h}$$

FIG. C.3 USE OF LVDT's AND YOKES TO MEASURE ROTATIONS

APPENDIX D: DETAILS OF EACH TEST

D.1 Test #1: Bare Frame Test

Dimensions of the bare frame specimen are shown in Fig. D1, and the test setup is shown in Fig. D2. The instrumentation was as shown in Fig. D3.

The model was subjected to the cyclic loading program shown in Fig. D4. As explained in the text, the objective of this load program was to examine the mechanical behavior of the bare frame without damaging it severely. Elastic analyses of the entire end frame had shown that the proper relationship between shear and overturning moment could be maintained using the loading pattern shown in Fig. D5. The entire test was carried out under displacement control. The following descriptions refer to the load points noted in Fig. D6.

LP 0.- The axial loads were applied incrementally to the columns, and the struts connecting tips of the cantilever beams were tightened.

LP 1-12.- The specimen was cycled with full load reversal at service condition lateral load levels. Hairline cracks were observed in the beams near the column faces at all three levels, beginning at the built-in ends of the cantilever beams.

LP 13-19.- Lateral loads were increased monotonically. Beam cracking increased, and diagonal cracks began to form at the interior beam-column joints at all three levels, indicating the development of increased stress in the beam longitudinal steel and consequent high shear within the joints. Continued loading resulted in the deterioration of bond between the beam longitudinal steel and the concrete in the confined cores of the interior beam-column joints. Beam longitudinal steel began to pull through the joints, causing significant increases in crack widths in the beams at column faces near the beam-column connections. A maximum deflection of about 51 mm (2 in) was reached at the level of lateral load application.

LP 20-24.- The specimen was returned to approximately zero lateral load and loaded monotonically in the opposite direction.

LP 25-28.- The load was reduced to zero and then increased again to restore the displacement to approximately zero. Hairline cracking was observed in all the beams, in a sense opposite to that observed during the monotonic loading to LP 19. The lateral load was again returned to zero, the struts connecting the cantilever beams were disconnected, and the axial loads were removed incrementally.

LP 29-38.- The axial loads were reapplied and the struts connected as before. The specimen was loaded in the opposite direction to the previous maximum displacement excursion, to a maximum tip displacement of slightly more than 51 mm (2 in). Shear cracks formed at the interior beam-column joints, in the opposite direction from those noted previously at load point 19. In addition, diagonal cracks formed at the exterior beam-column joints on all three levels, indicating the presence of high shear due to the onset of strain-hardening in the beam longitudinal steel near the column faces. Cracks opened at the column bases, and the clip gages there began to indicate the start of pullout of the column longitudinal steel from the base of the specimen.

LP 39-49.- The model was reloaded to a final displacement of about 51 mm (2 in), in the same direction as the original inelastic excursion of LP 19. Except for shear cracks at the exterior beam-column joints (in the opposite direction from those noted at LP 38), few new cracks were noted. However, the cracks at the column faces (exterior as well as interior columns) widened on all three levels, increasing in width to about 3/64" at the upper two floors and 1/32" at the first floor. This widening, caused by the onset of strain hardening in the beam longitudinal steel and consequent loss of bond and anchorage in the interior and exterior beam-column joints, resulted in a loss of stiffness and strength in the second cycle compared to the first, as may be seen in Fig. D6.

LP 49-58.- The model was again returned to the zero displacement position. As noted above, the formation of cracks across the entire beam depth at the column faces, resulted in significant pinching in the load-displacement hysteretic curves. The struts were disconnected, and the axial loads were removed incrementally.

The final plastic hinge pattern is shown in Fig. D6. Using moment-curvature diagrams calculated by the RCCOL5 computer program, the moments at hinge regions were calculated based on the amount of damage observed at each region. The lateral collapse load of the resulting mechanism was calculated, taking into account the external virtual work done by the axial loads (second-order theory). The resulting collapse load - a function of tip displacement - is plotted in Fig. D6. It may be seen that the lateral resistance of the model closely approaches the collapse load of the corresponding bare frame mechanism, calculated according to second-order theory.

As for all tests, the lateral forces plotted in Fig. D6 include the lateral force component produced by the axial load actuators. Unless specifically indicated, however, they do not include the equivalent lateral force produced by axial loads acting parallel to the original column axes (P-Δ effect).

The response of the bare frame to cycles of lateral load reversal was characterized principally by a gradual transition from elastic behavior to that of a sidesway mechanism. This transition was caused primarily by loss of stiffness in the interior beam-column joints, and not by the development (in the classical sense) of hinge regions near member ends there. This loss of joint stiffness was caused by bond deterioration of the beam longitudinal steel in the confined cores of the interior beam-column joints. As a consequence, the model experienced significant deterioration of lateral stiffness and strength, and its cyclic load resistance was limited by P-Δ effects.

D.2 Test #2: Bare Frame, Infilled with Clay Units

As explained in the text, the objectives of the first infilled frame test were:

1) to examine the mechanical behavior under cyclic load of the infilled frame; and

2) to investigate the effect on this behavior, of the previous response history of the bare frame alone.

To obtain the greatest amount of information, it was decided to subject the model to a loading program of full load reversals at increasing maximum amplitude. The upper limit of this program was set by the calculations of Section 3.4, which had indicated that the model could not resist a lateral load in excess of about 400 kN (90 k). It was determined that service level excitations such as those consistent with the lateral force requirements of the 1973 UBC, would correspond to cyclic lateral loads of at most 45 kN (10 k). Therefore this was the lowest load level at which the model was cycled.

Elastic analyses of the entire prototype end frame were carried out to determine the relationship between lateral shear and overturning moment at the third floor level, and this relationship was used to calculate the equivalent axial load couple necessary to reproduce the proper relation between lateral load and overturning moment in the model. This relation is shown in Fig. D7. The instrumentation used is shown in Fig. D8. The following description of the test refers to the load points noted in Figs. D9-D10.

LP 0-14.- Axial loads were applied, the beam struts were connected, and the model was cycled under displacement control for 5 cycles at approximately 10 k maximum load. No cracks were noted (all models had been whitewashed to facilitate crack detection).

LP 14-30.- The model was loaded for 5 cycles to approximately ± 89 kN (20 k). After one cycle at this load level (LP 16), hairline cracks were observed at the vertical interfaces between the second-story panels and the columns. After one more cycle (LP 19), edge cracks also formed around the third story panel, and horizontal cracks began to form in the mortar joints of panel #1 (the lowest panel). After the last cycle at this load level (LP 29), short diagonal cracks were noted through the clay units in the second panel, and slight crushing was noted in the upper left-hand corner of that panel. The overall crack orientation was similar to that expected in a monolithic deep beam: horizontal cracks near the base, becoming increasingly inclined in the upper stories as the ratio of moment to shear decreased.

LP 31-43.- When the load level was increased to 133 kN (30 k), diagonal cracking through the clay units was observed in all three panels. At this load, the nominal panel shear was 1.40 MPa (0.202 ksi). Continued cycling at this load level produced increased cracking in both directions in all panels. As shown in Fig. D 11, the crack orientation at LP 41 was approximately diagonal in all panels, indicating that the overall response mechanism of the model had changed from that of a deep beam to that of a braced frame.

LP 44-55.- Cycling at increasing load levels produced increased diagonal cracking in all panels.

LP 57.- When lateral load was increased to approximately 50 k, a rapid increase in diagonal crack width was noted in the lower interior corner of panel #2, as well as some local crushing at the upper exterior corner of panel #1. This load corresponded to a nominal panel shear of 2.33 MPa (0.338 ksi). At the same time, crushing was noted in the upper interior corner of panel #1, and spalling was observed at the base of the compression (exterior) column. The instrumentation confirmed rapid increases in shear deformation of panel #2 (implying degradation of the equivalent struts there), and also in the shear deformation of the first floor interior beam-column joint. This joint degradation was probably triggered by pullthrough of longitudinal beam steel there, owing to deterioration sustained during the test previously conducted on the bare frame.

LP 60.- Deterioration of panel #2 increased under load reversal. The cracked region at the lower interior corner failed in compression. Face shells separated from the block webs and grout cores, in a manner similar to that observed during prism tests. Diagonal shear cracks formed in the first floor beams near the exterior beam-column joint, indicating the development of high compressive forces in the equivalent strut in panel #1. Large increases were noted in the shear deformation (and accompanying degradation) of panels #1 and 2. The decreased lateral resistance of the model resulted in a reduction in the maximum lateral load, and hence a corresponding reduction in the force level in panel #3, which at that time was not seriously damaged. Because of this force reduction, damage did not spread to panel #3, but rather was confined to the lower two panels. The continued higher relative stiffness and strength of panel #3 led to the concentration of inelastic deformations in the columns at their bases, and near the top of panel #2.

LP 61-93.- Continued cycling at increasing maximum deflections caused gradual deterioration of panels #1 and #2. The deflection pattern of the model became closer and closer to that of the sidesway mechanism illustrated in Fig. D 10. The ultimate lateral resistance of this model approached that of the bare frame mechanism with this hinge pattern, and assigning to each hinge a plastic moment capacity in accordance with the given degree of damage at each critical region.

Using a procedure similar to that corresponding to the bare frame, the lateral resistance was computed for the infilled bare frame's plastic hinge pattern (Fig. D 10), taking into account the second-order effects of axial loads. This collapse load, plotted in Fig. D 10. is closely approached by the experimental load-deflection curve. A similar kinematic approach was used to check the maximum resistance of the infilled model. Assuming the same hinge pattern as before, the hinge moments consistent with light damage were used to calculate the internal virtual work corresponding to a virtual sidesway displacement. To this was added the virtual work contributed by the equivalent diagonal struts in the two lower panels, assuming average stresses of 24.1 MPa (3.5 ksi) (the average crushing value obtained in prism tests) and effective widths of 254 mm (10 in), obtained as shown in Appendix E. Maximum upper bound lateral resistance was calculated to be about 378 kN (85 k), compared with the 267 kN (60 k) actually obtained. It is probable that this error was principally due to overestimation of the frame contribution at the relatively small level of rotations reached at the time of maximum strut resistance. However, the equivalent strut concept was found to predict maximum upper bound strengths in reasonable agreement with experimental data, even using very simple analytical techniques. As discussed in Chapter 6, this concept was used in conjunction with more sophisticated techniques to give very accurate analytical predictions of experimental behavior for the class of infilled frames considered herein.

The response of the infilled bare frame to combined vertical loads, cycles of reversed lateral loads, and associated overturning moment, was characterized by the following response mechanisms:

1) initial elastic response as a monolithic deep beam

2) gradual transition to braced frame behavior, indicated successively by:

   a) separation of the panels from the frame

   b) formation of diagonal cracks in all panels

   c) formation of shear cracks in the beams near panel corners, indicating the development of high compressive forces in the equivalent diagonal struts.

3) a decrease in lateral stiffness and strength due to increasing degradation of the struts in one or more panels

4) concentration of inelastic deformations in frame members bounding the panels subjected to the greatest degradation, and the formation of a sidesway mechanism which corresponded to the given pattern of critical regions and which was imposed by the relative severity of damage in each panel

5) strength asymptotically approaching that of the corresponding bare frame mechanism, and load-deflection characteristics with increased pinching due to the large amount of panel degradation.

D.3 Test #3: Virgin Frame, Infilled with Clay Units

As explained in the text, one of the principal objectives of this test was to investigate the response of a model infilled frame to a loading program characterized by the application of large pulses near the start of the load sequence. Because it has been proposed that this type of loading history may be critical for structures with a tendency toward brittle failure, the loading program used was intended specifically to test the resistance of engineered infills to brittle failure and incremental collapse. The applied load program is shown in Fig. D 12, and the corresponding displacement program in Fig. D 13. Instrumentation is shown in Fig. D8, and the following descriptions refer to load points noted on the load-deflection history of Fig. D 14.

LP 0-13A.- Following the application of axial loads and connection of the beam struts as before, the specimen was cycled to service level loads (± 44.5 kN) under load control, using a ratio of overturning moment to lateral force corresponding to the infilled frame (Fig. D7). No cracking was observed.

LP 13A-15.- The servocontroller was switched from load to displacement control, and one more service load cycle was completed to check the response. Then the specimen was loaded monotonically to its maximum load, passing through the load points noted below.

LP 16-18.- As the load was increased to approximately 133 kN (30 k), cracks were noted at the vertical and horizontal edges of all three panels. Horizontal cracks were observed at the base of panel #1, and in panel #2.

LP 19.- At a load of approximately 178 kN (40 k), horizontal cracks were noted throughout panel #1. In addition, diagonal cracks began to form in all three panels, indicating the transition to diagonal compression strut behavior.

LP 21.- At about 244 kN (55 k), diagonal cracks were observed through the block units in all three panels. Cracks 1/32" in width were noted at the base of the interior (tension) column.

LP 22-24.- The specimen reached its maximum load of about 311 kN (70 k) at LP 23, and the resistance decreased rapidly to 267 kN (60 k) at LP 24. The decrease in resistance was caused by crushing of the equivalent strut in the lower exterior corner of panel #1, and the subsequent opening of wide (about 4 mm) diagonal tension cracks near the center of this panel. The panel was extensively cracked.

LP 25-46.- The model was unloaded gradually and reloaded in the original direction. A maximum load of about 222 kN (50 k) was reached. Panel #1 showed increasing damage along the compression diagonal, and buckling of horizontal panel reinforcement was noted at the lower exterior corner where the original crushing failure began.

LP 48-56.- The two pulses to which the model was subjected, resulted in a significant residual deflection of about 25 mm (1 in), corresponding to an average story drift of slightly less than 1 %. The model was then subjected to one cycle at a maximum load of about 67 kN (15 k) to observe its resistance to incremental collapse, which might be produced in an actual structure by a pulse-type strong ground motion followed by comparatively weak aftershocks. While the lateral stiffness of the structure had decreased by at least a factor of three from the original value, no tendency towards incremental collapse was noted.

LP 57-80.- The structure was subjected to four cycles of complete load reversal to a maximum load of about 178 kN (40 k). As may be seen in Fig. D 13, deflection reversal was not complete, owing to the residual deflection produced by the initial pulses. Load reversal produced increasing concentrations of rotations in the columns at all four corners of panel #1, beginning at the upper interior corner. Then tension cracks at the base of the interior column increased to 3 mm (1/8 in) in width, and spalling was observed in the exterior (compression) column along the entire height of panel #1. At LP 73, the transfer ratio between lateral and axial loads was changed to a value between that of the infilled frame and that of the bare frame.

LP 81-91.- The specimen was subjected to complete displacement reversals of about ± 13 mm (0.5 in). Stiffness was reduced from the virgin condition, but the model remained stable.

LP 92-122.- The model was subjected to cycles of displacement reversal to the limits of travel of the lateral actuator and displacement feedback control - about 127 mm (5 in) in one direction, and 109 mm (4.3 in) in the other. This series of cycles produced complete spalling of the exterior column in the first story, general disintegration of the central zone of panel #1, and wide (5 mm) cracks in the interior column at the top and bottom corners of panel #1. Crushing was noted at the lower exterior corner of panel #2, indicating the formation of an equivalent strut there. Diagonal cracks formed in the first floor beam near the exterior column. These cracks formed because much of the force in the diagonal compression strut in panel #2 was taken by this beam after the disintegration of panel #1. Following this, panel #2 began to crush, and the instrumentation indicated increasing shear deformation in that panel. Deterioration of the first-floor exterior and interior beam-column joints was observed; degradation of the interior joints was characterized by complete pull-through of the beam longitudinal steel. The final condition was marked by increasing disintegration near the lower edge of panel #2, and increased shear deformation and damage in the first-floor beam at the face of the exterior column. However, little deterioration was observed within the confined core of the joint itself. At LP 110, the transfer ratio between the axial and lateral loads was changed to that corresponding to the bare frame.

In spite of the difference in loading programs, the failure sequence observed for this specimen was qualitatively very similar to that of the previous infilled frame test.

D.4 Test #4: Virgin Frame, Infilled with Concrete Units

The loading program used for this test is shown in Fig. D 15, and is of the type previously used in Tests #1 and #2. The instrumentation used, and the resulting load-deflection curves, are shown in Fig. D8 , and D 16, respectively. Two objectives of this final test of the initial series were: 1) to investigate the differences in mechanical behavior between models infilled with concrete units as opposed to clay units; and 2) to observe the response of the degraded model to extreme cyclic displacements. Significant stages in the response of the model are described below, with reference to the load points shown in Fig. D 16.

LP 0-26.- After incremental application of the axial loads, the beam struts were tightened and the model was subjected to cycles of complete load reversal at service levels of 27 kN (6 k) and then 44.5 kN (10 k). No cracking was observed.

LP 27-37.- The model was subjected to two cycles of reversal to a maximum load of ± 89 kN (20 k). Horizontal cracks were observed in panel #1, particularly along the base of this panel. The servocontroller was changed from load to displacement feedback control.

LP 38-58.- The specimen was subjected to two cycles with a maximum load of ± 133 kN (30 k). Cracks were noted in all panels, with orientations similar to those predicted for a deep beam.

LP 59-67.- When the maximum load was increased to ± 178 kN (40 k), extensive hairline cracks were observed along the diagonals of all panels, indicating the transition to braced frame behavior. Edge separation was not as prevalent as in the two previous infilled frame tests.

LP 67-76.- When the maximum load was increased to ± 222 kN (50 k) for two cycles of reversal, diagonal cracks were noted at all beam-column joints, indicating the development of yield-level moments in the beams.

LP 76-89.- At maximum loads of about 267 kN (60 k), local crushing was observed in the lower exterior corner of panel #2 (LP 81). The maximum load (294 kN, or 66 k) was reached at LP 87. Unlike the other two infilled frame tests, panel deterioration was triggered by the rapid formation of a horizontal crack completely across the midheight of panel #2. This crack passed along the bed joint where the vertical dowels from panel #1 had been cut off, and is discussed in Section 5.7. Following the propagation of this horizontal crack, sharp increases in shear deformation were observed in panel #2, and local crushing started in panels #1 and #3.

LP 89-109.- The specimen was subjected to cycles of reversal with maximum displacements of first ± 25 mm (1 in) and then ± 38 mm (1.5 in). Because shear deformations were concentrated in panel #2, hinges began to form in both columns near the corners of this panel. Longitudinal cracks were observed along the lengths of both columns at the second story. It is believed that these were caused by the combination of high compressive axial forces and the high shear due to complete moment reversal over less than a story height. At LP 105, local crushing was observed in the upper interior corner of panel #1, adjacent to the zone of high damage in panel #2.

LP 110-122.- The specimen was cycled with reversal, first to ± 51 mm (2 in), then to ± 76 mm (3 in). At LP 114, shear cracks were noted at the exterior end of the beam separating panels #2 and #3, and at LP 116, a sudden crushing failure occured across the bottom edge of panel #3. The load was returned to zero and the transfer ratio between lateral and axial loads was changed to a value between the original infilled frame value and that corresponding to the bare frame (LP 117).

LP 122-130.- The specimen was cycles with reversals to maximum displacements of ± 102 mm (4 in). More crushing was observed in the lower part of panel #3.

LP 130-146.- The specimen was subjected to several cycles of displacement to the stroke limits of the lateral actuator. Maximum displacements were 197 mm (7.75 in) in one direction and 105 mm (4.13 in) in the other. The difference between these was close to the nominal actuator travel of 305 mm (12 in). The larger value corresponds to an average story drift in excess of 6 %. Since deformations at this time were concentrated in panels #2 and #3, the local story drift was actually almost 9 %. At LP 132, a hinge region formed below the third floor interior beam-column connection, making a total of three hinges in that column and reducing its stability significantly. Even under such extreme conditions, the model continued to dissipate significant amounts of energy and to support the simulated gravity loads (column axial loads) in a stable manner.

D.5 Remarks Concerning Energy Dissipation

Fig. 37 of the text shows the energy dissipated per cycle by each specimen, normalized by one-half the maximum displacement variation for that cycle. While it can be seen immediately that all three infilled frames dissipated far more energy than the bare frame, it is also apparent that the curves for each infilled frame differ from one another. Some of these differences can be explained in terms of the loading programs used for each test and others are due to the individual characteristic of the failure sequences of each infilled model. It is worthwhile to relate the shape of each curve to both of these factors:

D.5.1 Infilled Bare Frame (Test #2)

Initially, normalized energy dissipation per cycle increased rapidly with increasing deflections, owing to increased panel cracking and the dissipation caused by friction across these cracks. Dissipation was greatest just prior to crushing of the critical equivalent compression strut, after which it dropped sharply because of the decrease in overall shear resistance of the subassemblage, and also because of the pinching effect produced by crack openings. Subsequent increased panel deterioration led to increased friction but also to decreased strength, and as a result, the normalized dissipation continued to decrease gradually with increasing deflections.

D.5.2 Virgin Frame, Clay Infill (Test #3)

The most interesting features of this curve are that, unlike the others, it does not show the sharp decrease associated with crushing of the critical equivalent strut, and that it indicates increasing dissipation for displacements of more than 5 cm. It is believed that the first feature is due primarily to the different loading program used for Test #3. Because the first portion of this program (Fig. 19) was dominated by a single large pulse in one direction, the model did not experience complete deflection reversal during this stage. As a result, the model, when reloaded, did not exhibit the loss of stiffness (pinching effect) associated with crack closure. As can be seen in Fig. 21, pinching and loss of strength began to occur rapidly as soon as the model was subjected to deflection reversals in the second phase of the loading program. The cycles to ± 8 cm and ± 12 cm show significant deterioration in strength and stiffness under constant-amplitude cycling. The second feature is due to the fact that Fig. 37 was prepared using energy dissipation data for the first cycle only at any given displacement variation, and therefore does not reflect the subsequent decrease in normalized dissipation during subsequent cycles at that same displacement. A comparison of Figs. 20-22 shows that, because of its relatively light initial damage, this specimen subsequently exhibited the greatest comparative loss of strength under constant amplitude cycling. If the dissipation from these cycles had been included in Fig. 37, the curve for this specimen would have been similar to the other two for displacements greater than 5 cm.

D.5.3 Virgin Frame, Concrete Block Infill (Test #4)

The most significant feature of this curve is the comparatively low energy dissipation at and immediately following the failure of the critical strut. The failure sequence for this specimen was unique in that it included the sudden propagation of a horizontal shear crack completely across the second panel. As explained in Section 5.7 of the text, the loss of strength resulting from this horizontal crack was much greater than that resulting from the diagonal cracks observed in the other two tests. This comparatively low post-cracking strength is reflected in Fig. 37. Note that subsequent diagonal cracking in this panel caused increased friction and a resulting increase in energy dissipation for this specimen at deflections greater than 5 cm.

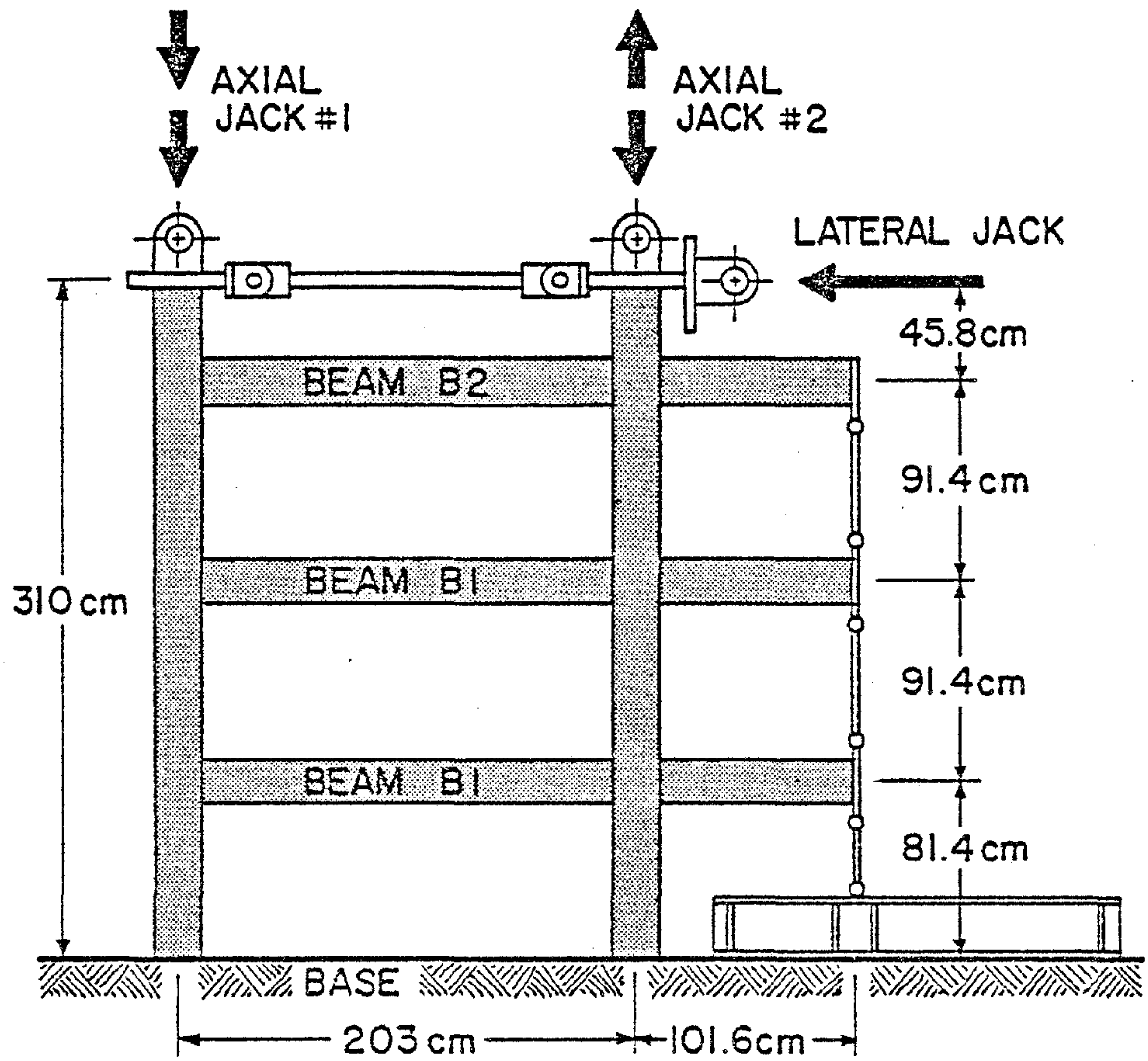

FIG. D.1 BARE FRAME SPECIMEN

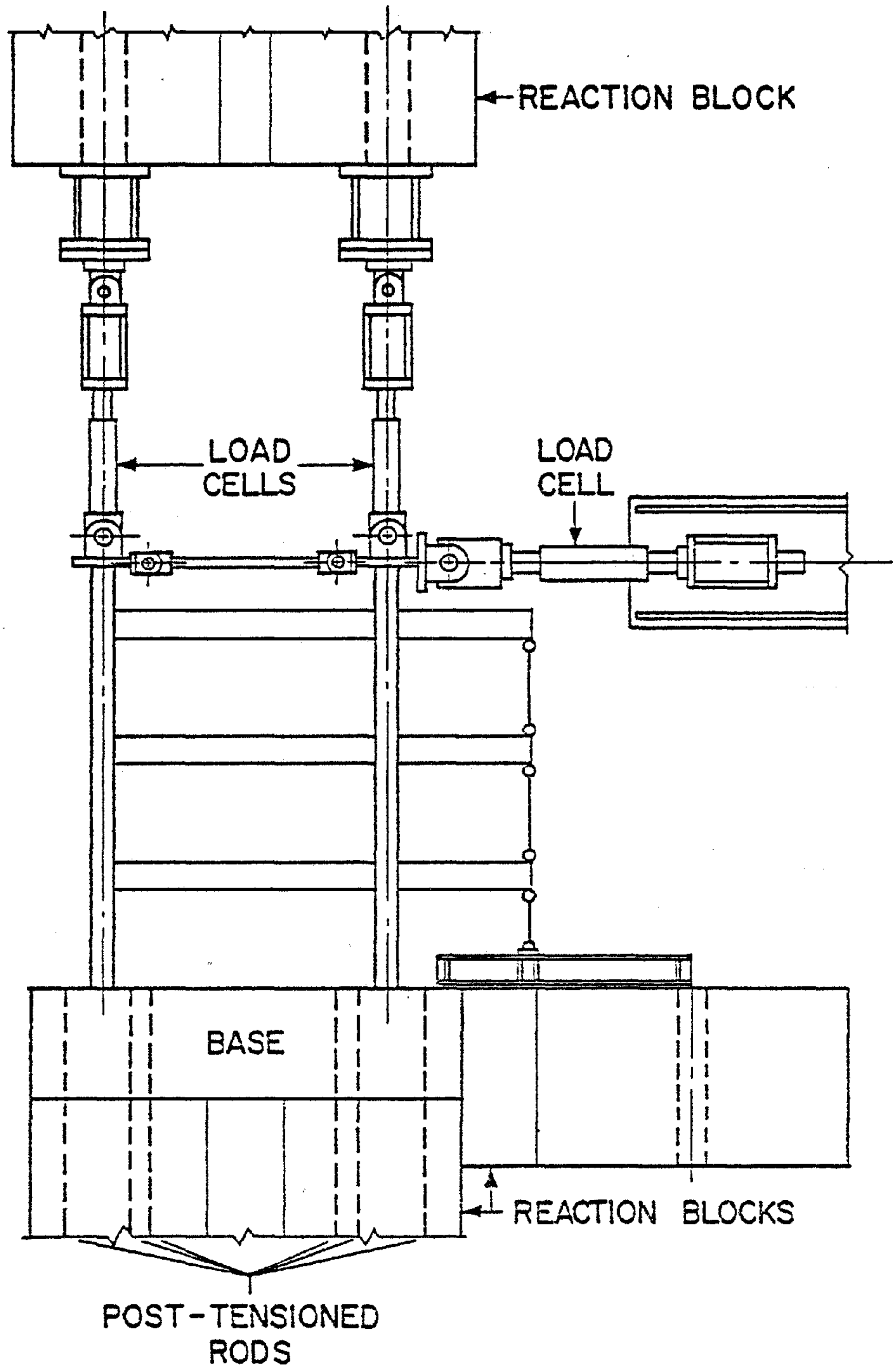

FIG. D.2 TEST SETUP

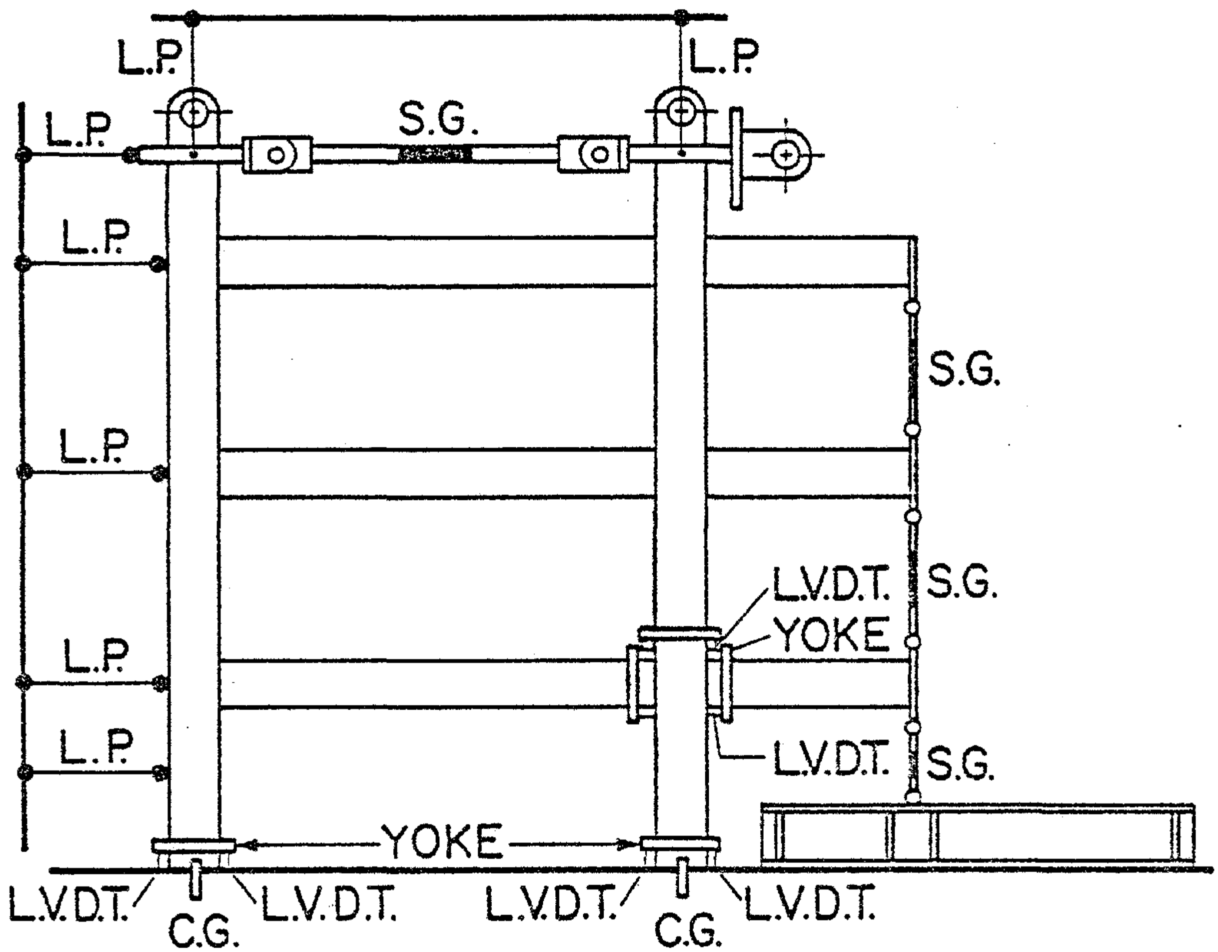

L.P. = LINEAR POTENTIOMETER
C.G. = CLIP GAGE
S.G. = STRAIN GAGE
L. V. D. T. = LINEAR VARIABLE DIFFERENTIAL TRANSFORMER

FIG. D.3 BARE FRAME INSTRUMENTATION

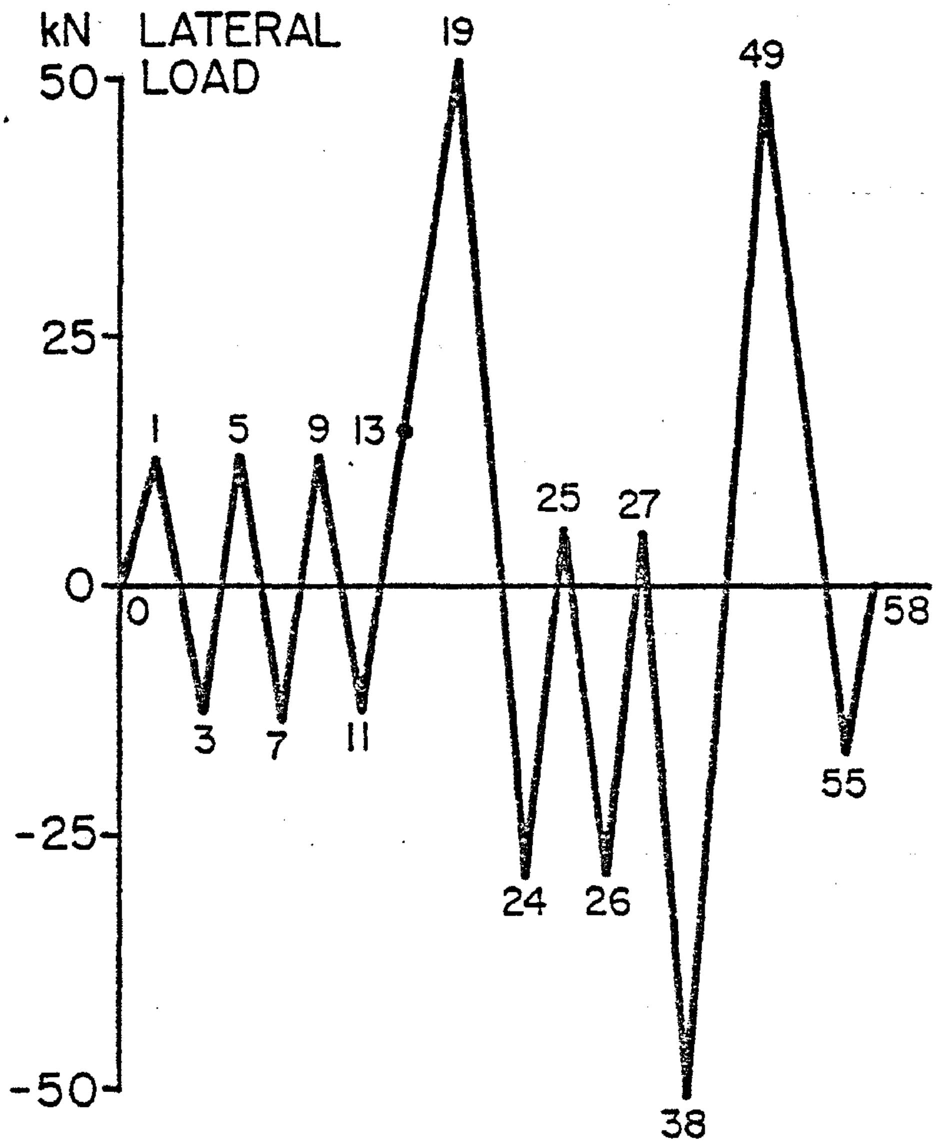

FIG. D.4 LOADING PROGRAM - TEST #1

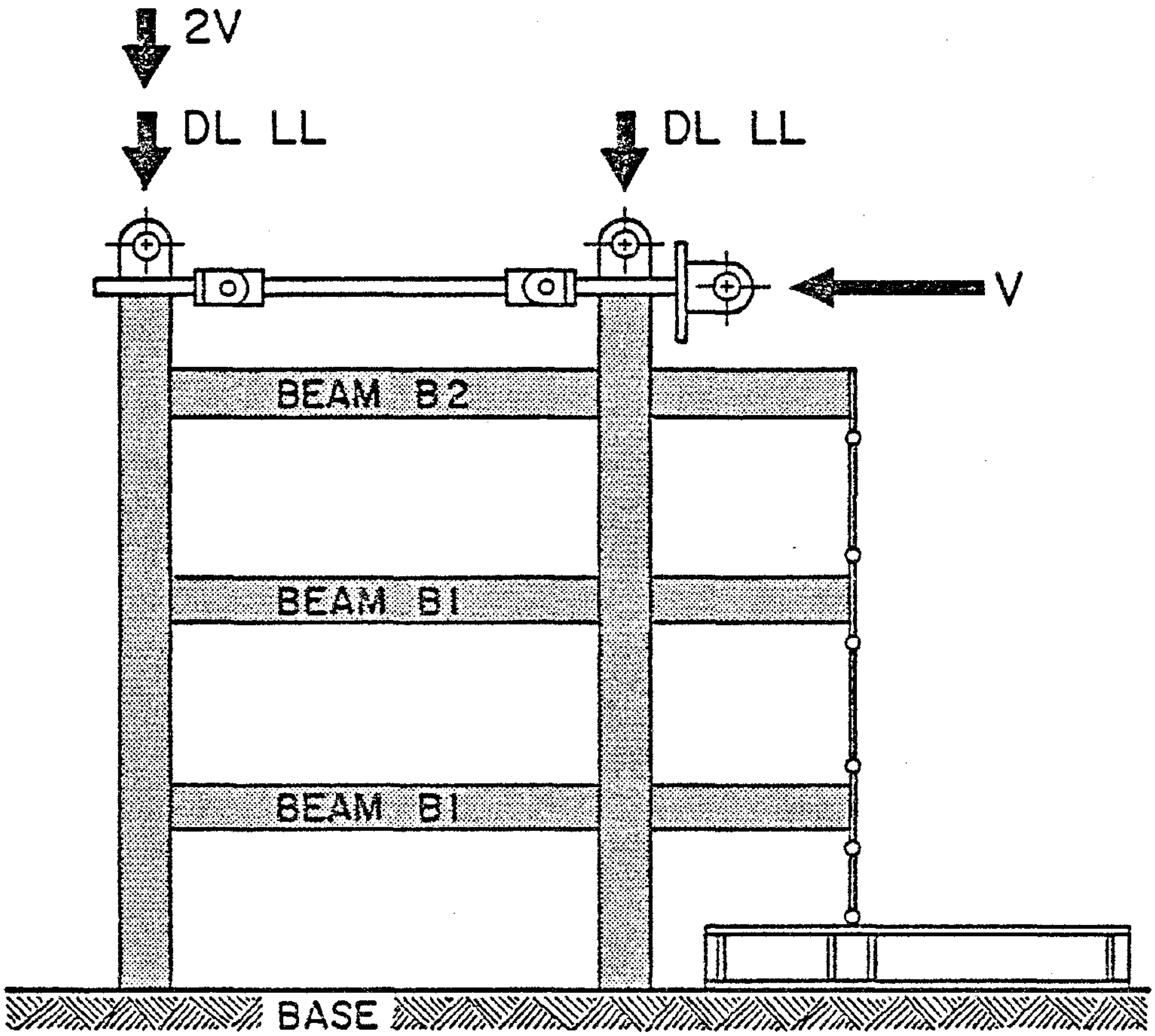

FIG. D.5 LOADING PATTERN USED FOR BARE FRAME

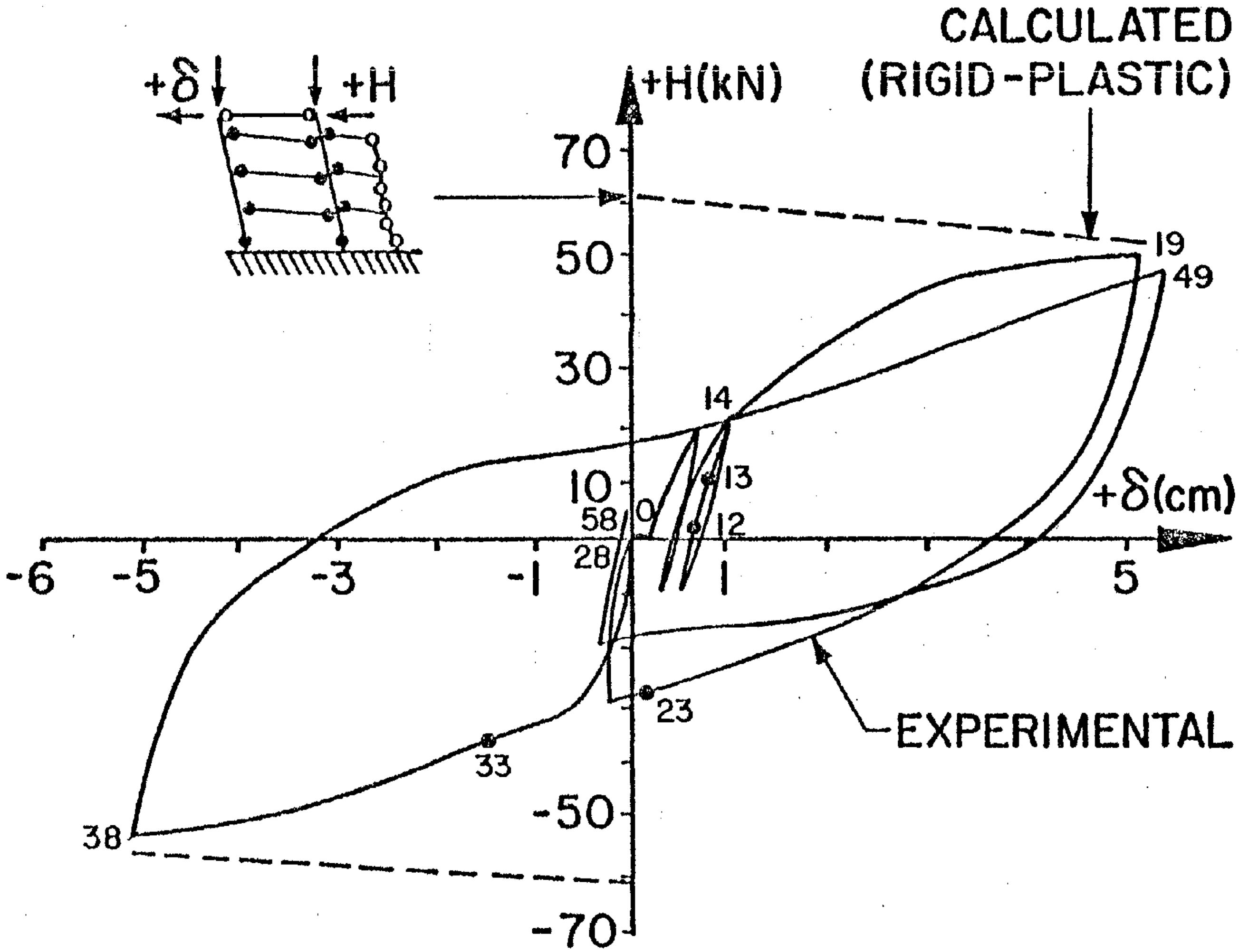

FIG. D.6 LATERAL LOAD - DEFLECTION RELATIONSHIP - BARE FRAME (TEST #1)

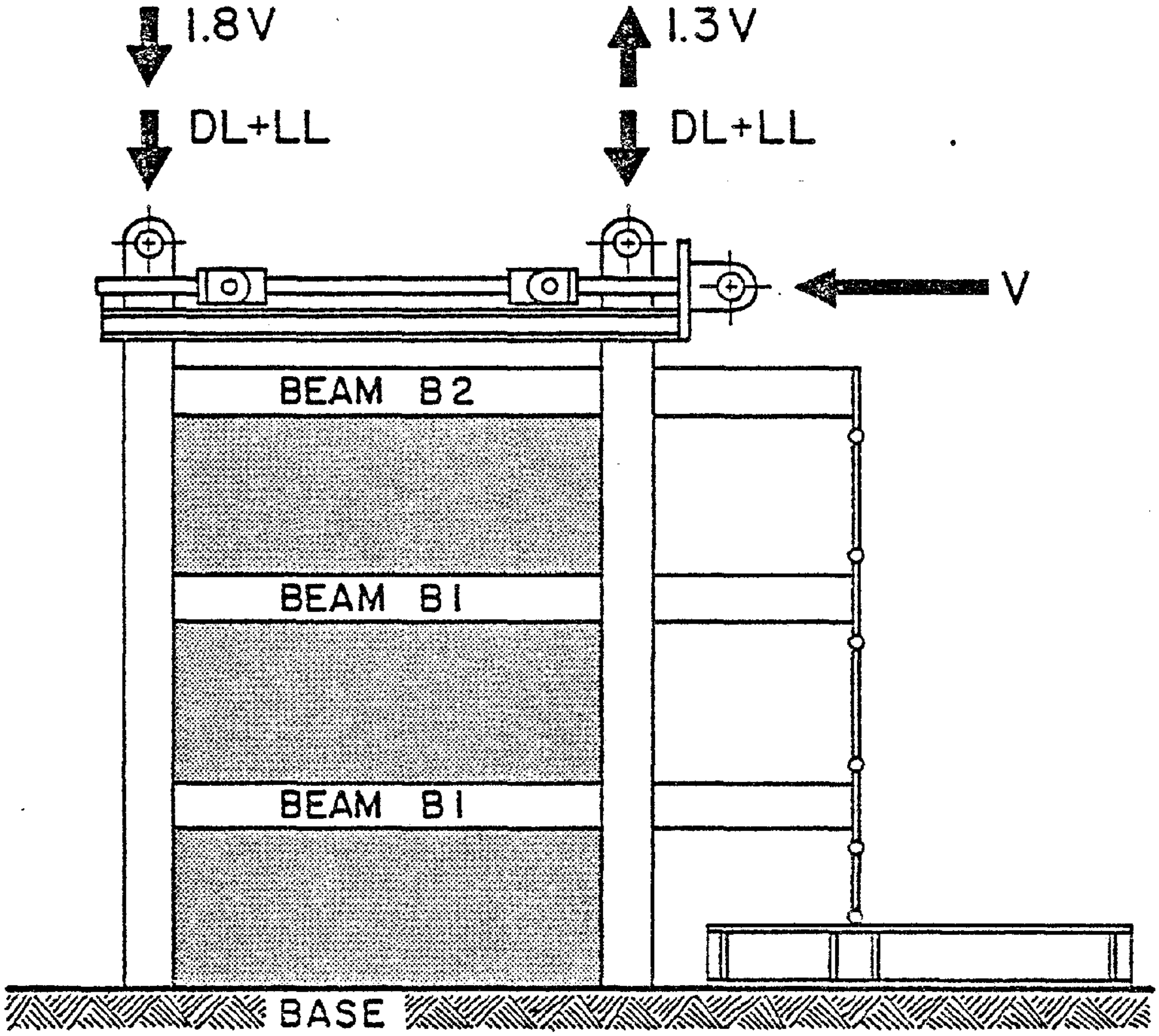

FIG. D.7 LOADING PATTERN USED FOR INFILLED FRAMES

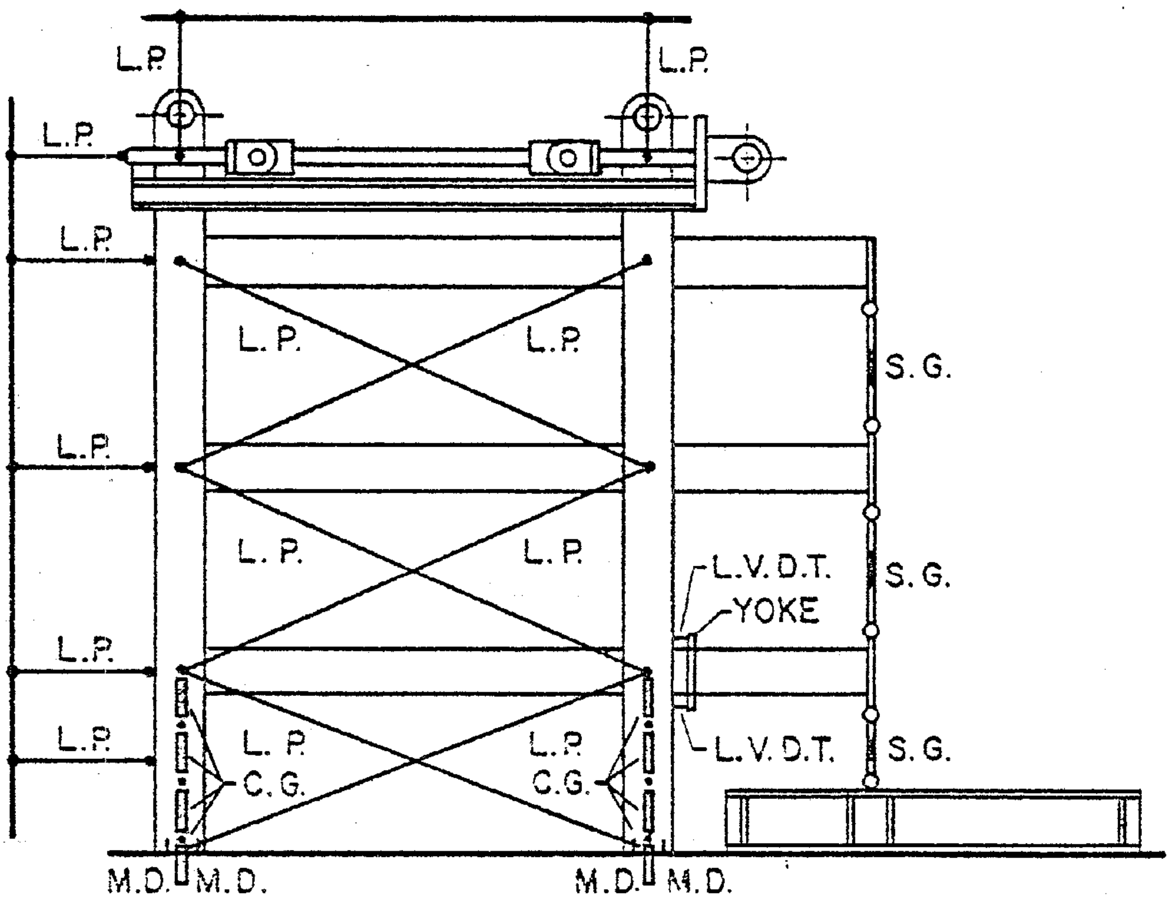

L. V. D. T. = LINEAR VARIABLE DIFFERENTIAL TRANSFORMER
M. D. = MICRODOT GAGE
C. G. = CLIP GAGE
L. P. = LINEAR POTENTIOMETER
S. G. = STRAIN GAGE

FIG. D.8 INFILLED FRAME INSTRUMENTATION

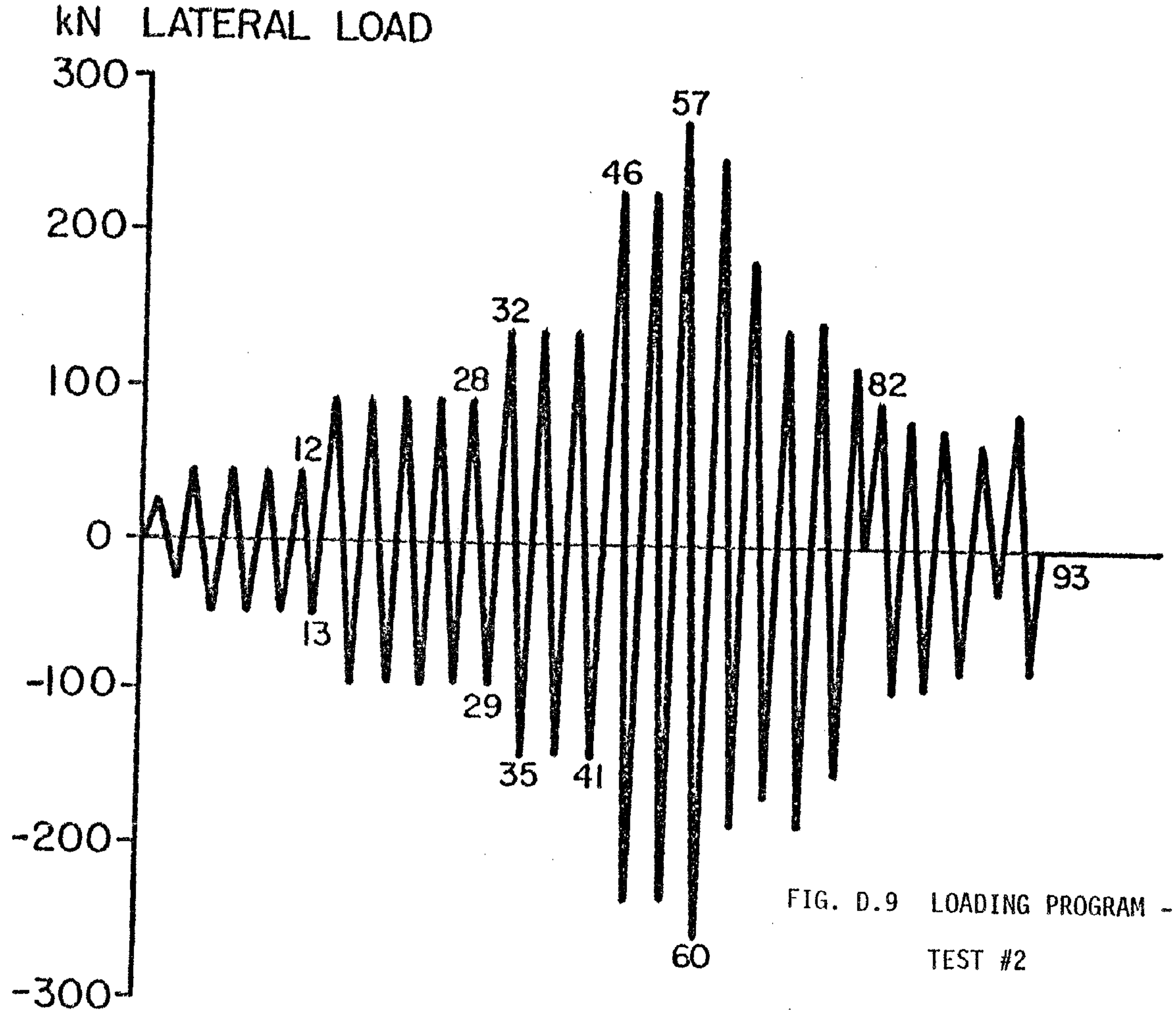

FIG. D.9 LOADING PROGRAM - TEST #2

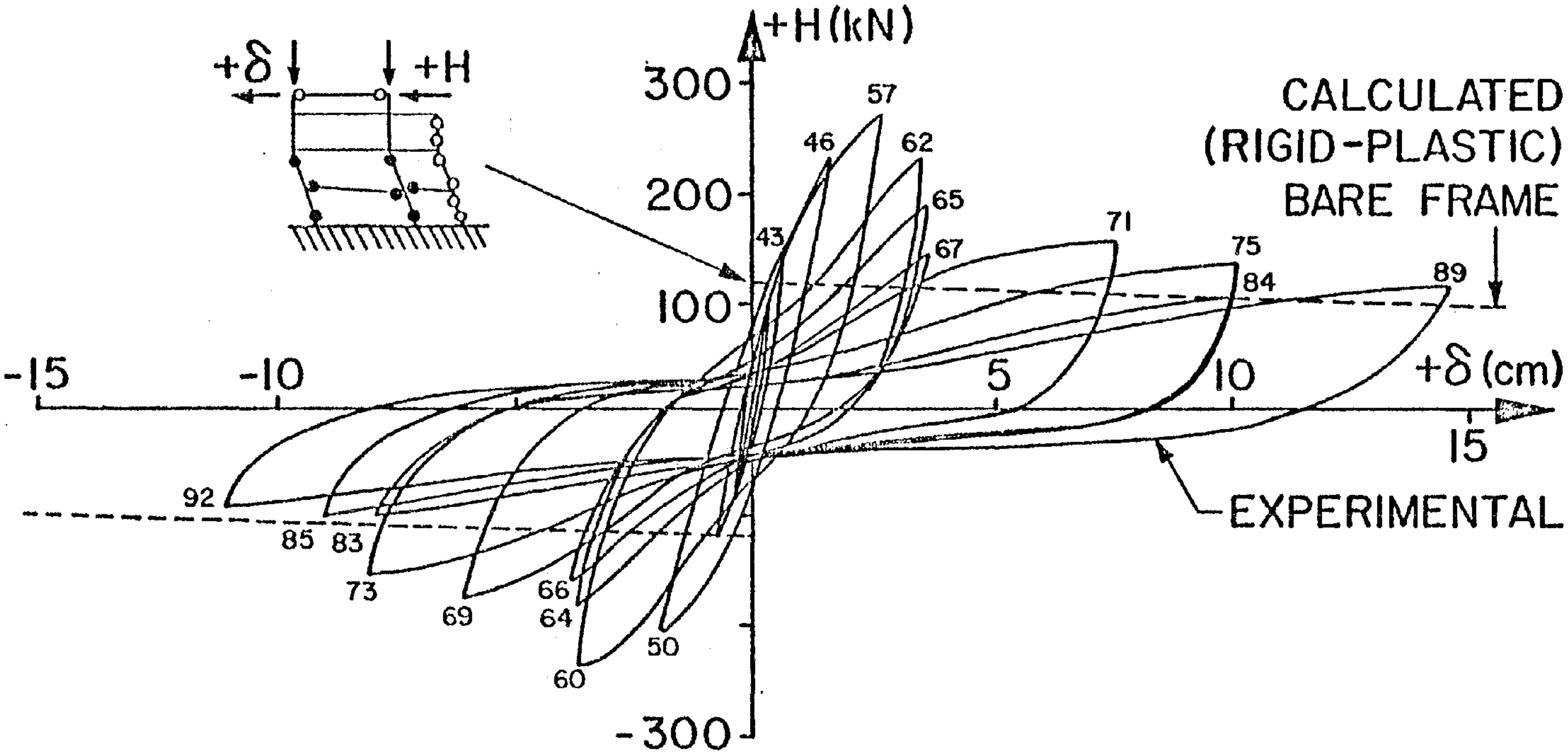

FIG. D.10 LATERAL LOAD - DEFLECTION RELATIONSHIP - INFILLED BARE FRAME (TEST #2)

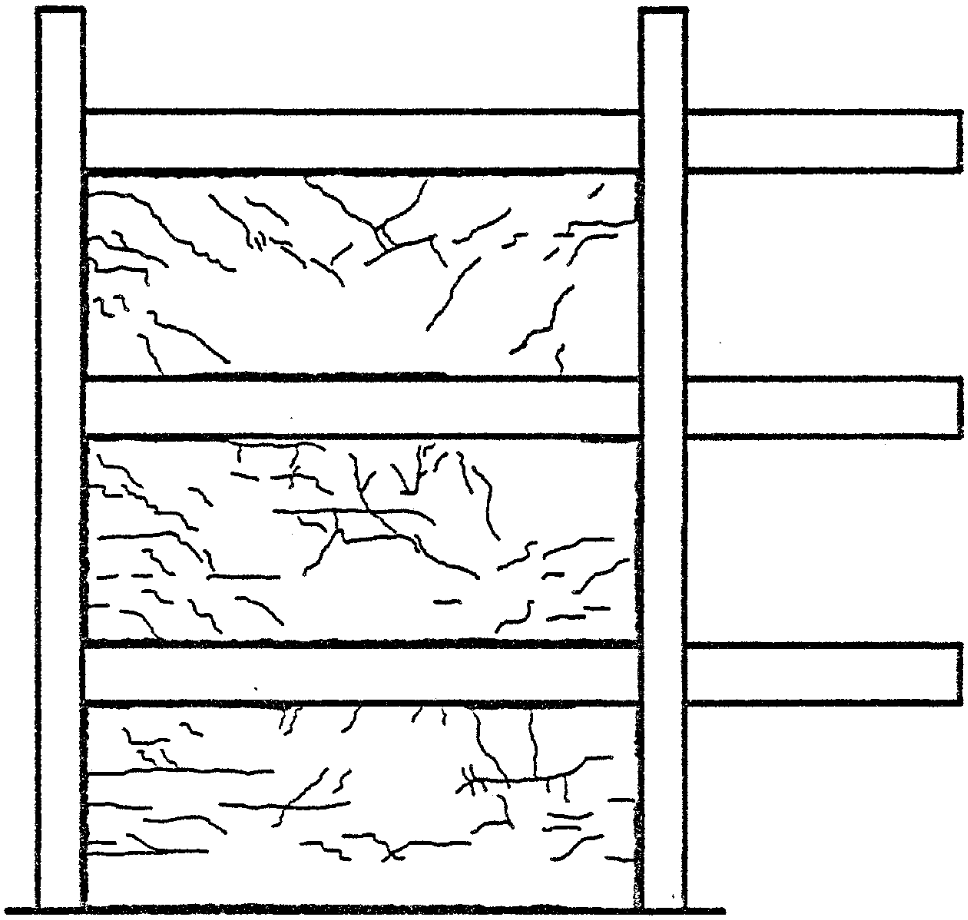

FIG. D.11 ORIENTATION OF PANEL CRACKS AT LOAD POINT 41, TEST #2

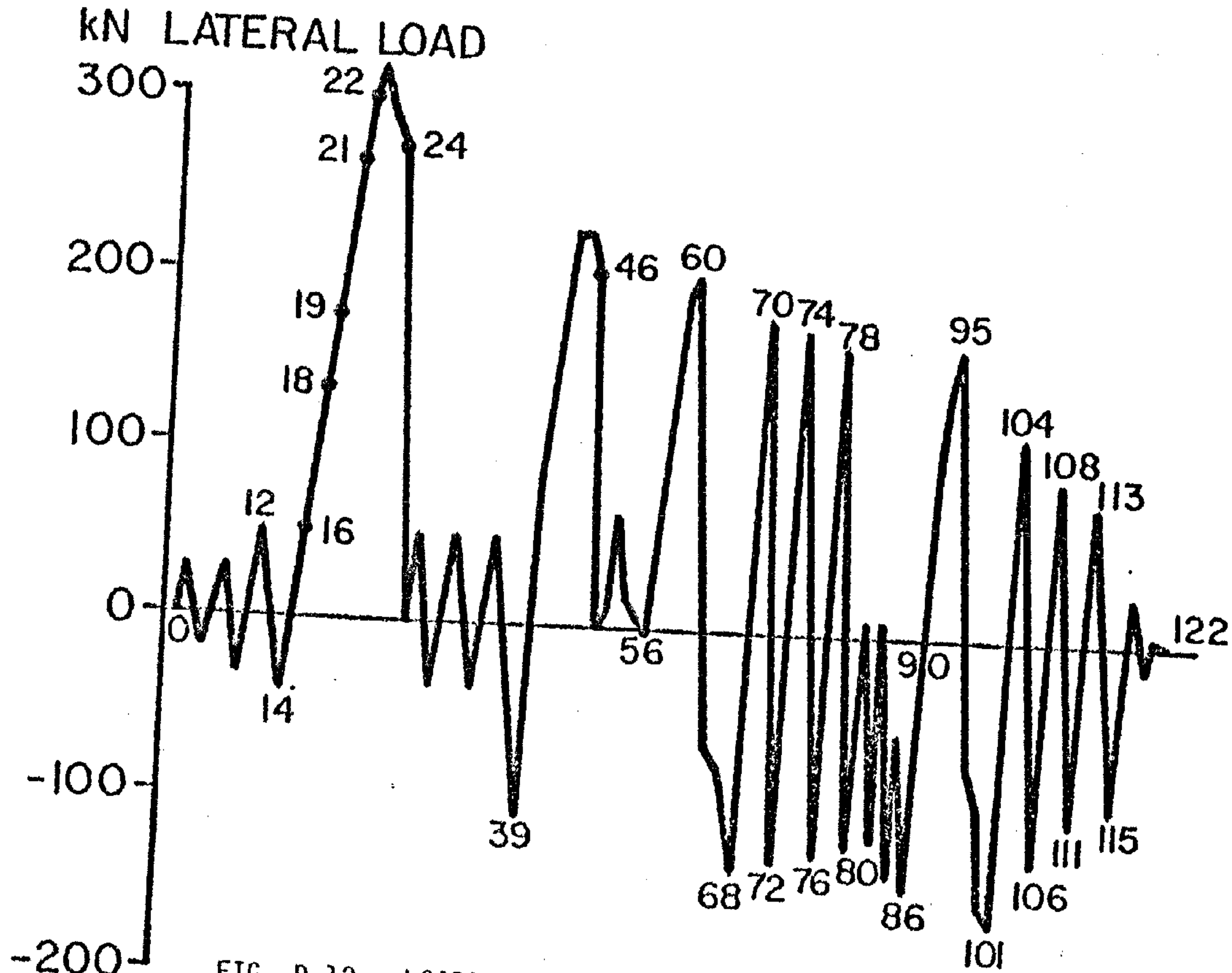

FIG. D.12 LOADING PROGRAM - TEST #3

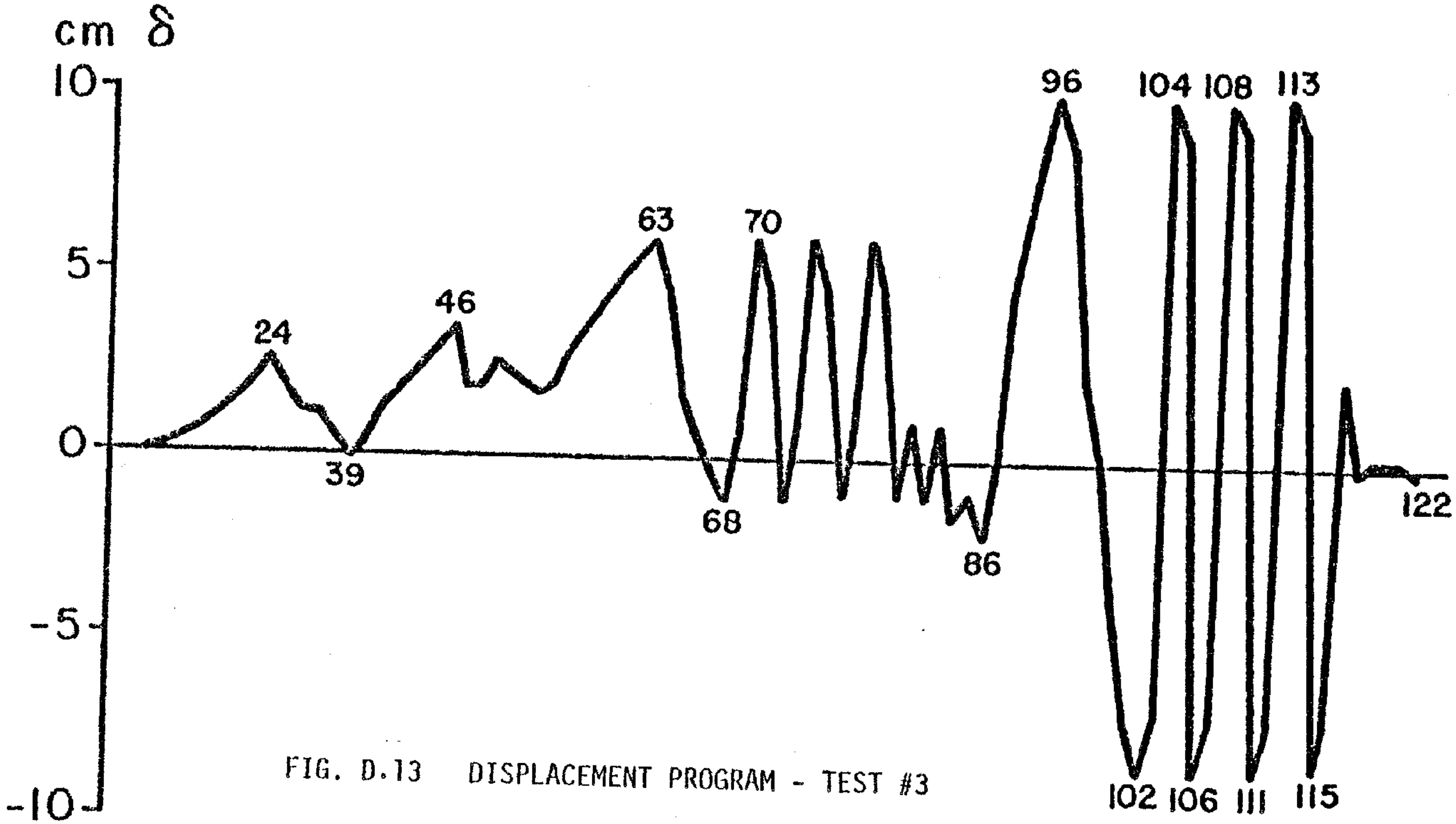

FIG. D.13 DISPLACEMENT PROGRAM - TEST #3

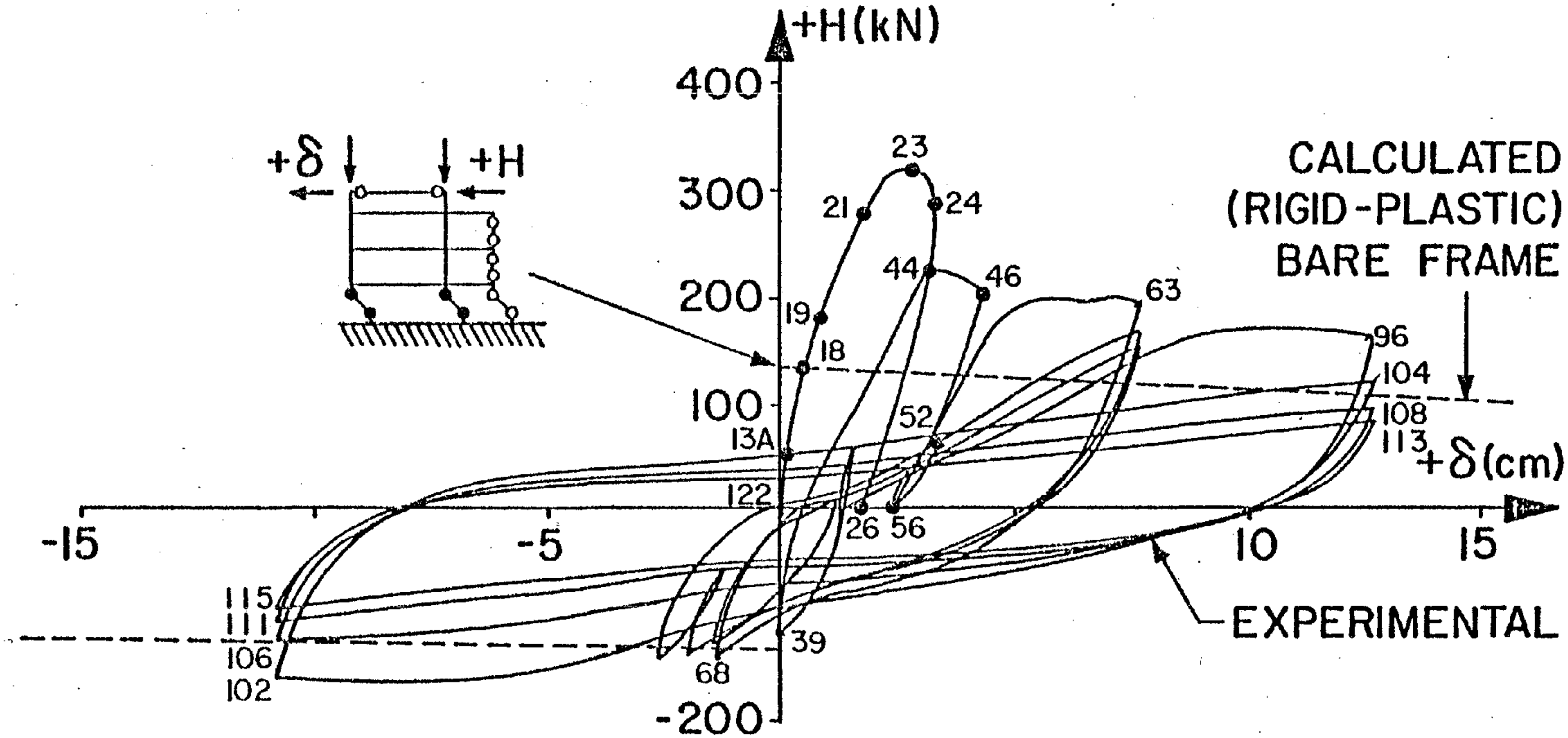

FIG. D.14 LATERAL LOAD - DEFLECTION RELATIONSHIP - VIRGIN FRAME, CLAY INFILL (TEST #3)

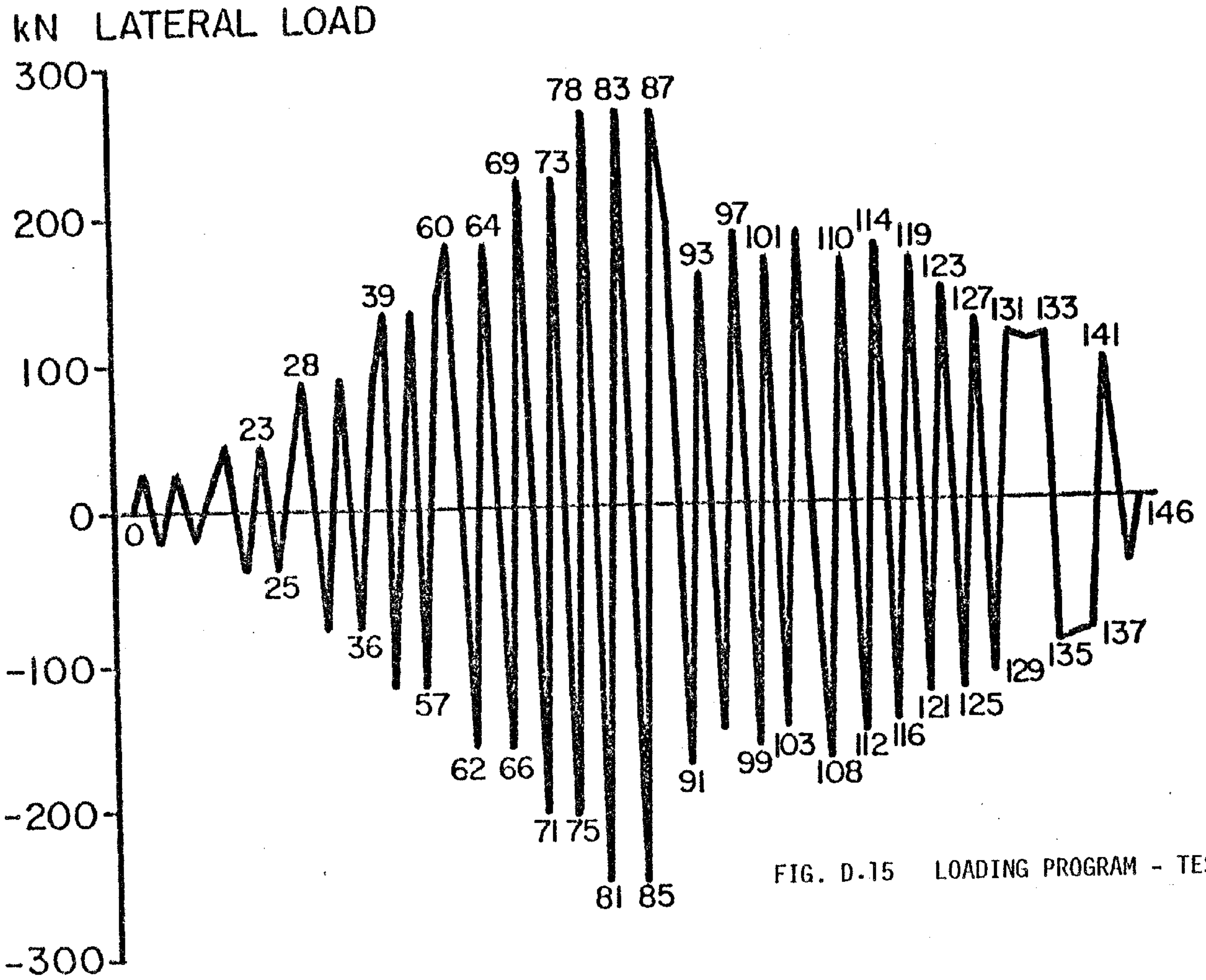

FIG. D-15 LOADING PROGRAM - TEST #4

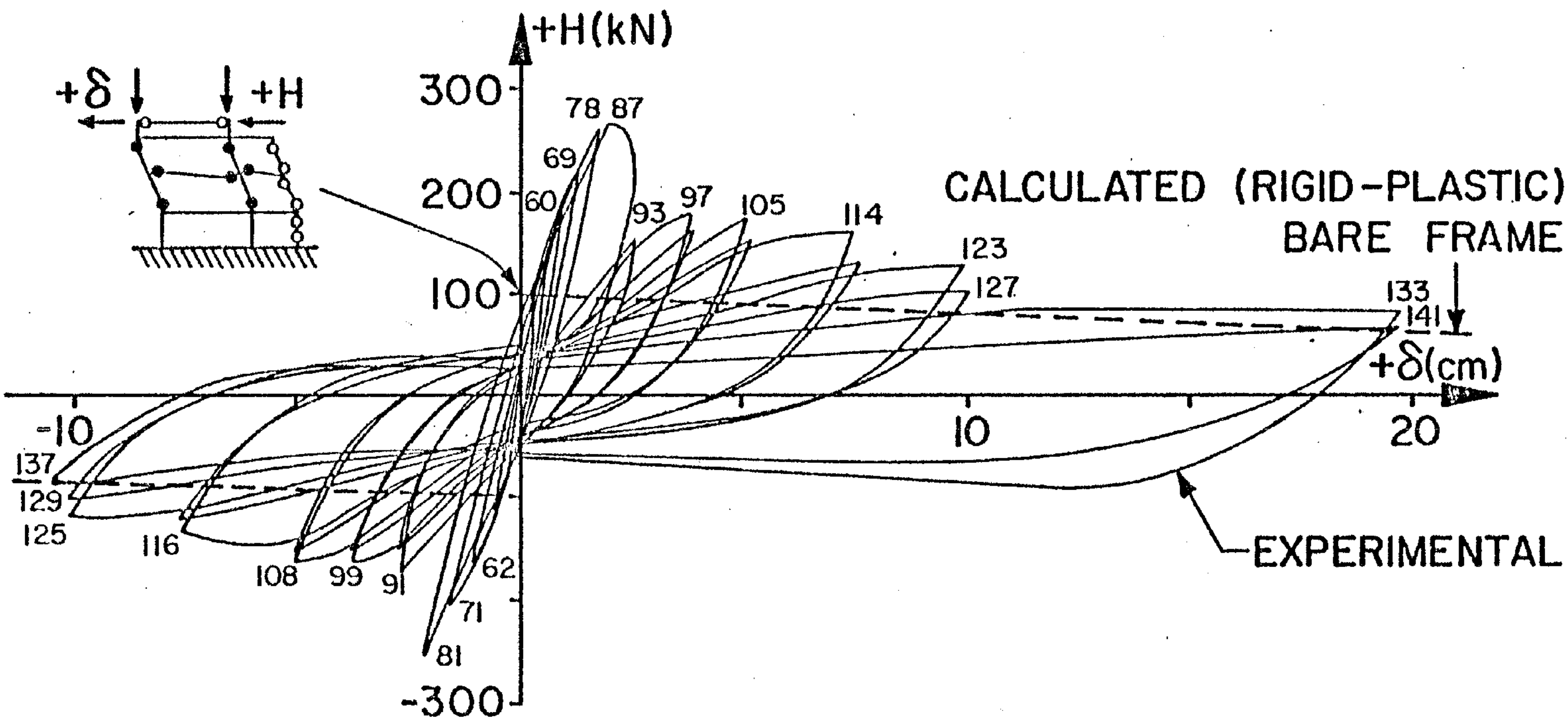

FIG. D.16 LATERAL LOAD-DEFLECTION RELATIONSHIP - VIRGIN FRAME, CONCRETE BLOCK INFILL (TEST #4)

APPENDIX E: ANALYSIS DETAILS

Chapter 6 herein discusses the general procedures followed in developing analysis methods for the bare and infilled frame specimens. The purpose of this Appendix is to describe in detail the calculations necessary to carry out the principal steps of these analyses, and to present a listing and user's guide for the ANSR-I subroutines developed as discussed in Chapter 6.

E.1 Equivalent Multi-Member Beam Properties

The computer program RCCOL5 [32] was used to calculate theoretical moment-curvature diagrams for each beam based on the actual geometry and mechanical characteristics as obtained from the material tests described in Chapter 4 and Appendix B. One such diagram, for Beam B1 of the model, is shown in Fig. E.1. It was decided to idealize this diagram using five line segments, shown in Fig. E.1 by the heavy lines connecting the origin to point "A", that point to point "B", and so on. The beam-column element used with the ANSR-I program idealizes the member as having a bilinear moment-rotation relationship as shown in Fig. E.2. This type of element may be used to approximate the flexural characteristics of a member with a bilinear moment-curvature relationship. Therefore the five-segment curve of Fig. E.1 was matched by modeling Beam B1 using four parallel members, each having linear elastic-perfectly plastic moment-rotation characteristics. Given the curvature and moment values (x_i, y_i) corresponding to the four intersection points (A,B,C,D), the elastic stiffnesses, m_i, of each equivalent member were found as the solutions of a set of four simultaneous linear algebraic equations:

$$y_i = \sum_{j=0}^{i-1} m_i x_i + x_i \sum_{j=i}^{4} m_j$$

Fig. E.1 shows how the resulting four equivalent moment-curvature relationships combine to give the desired multilinear diagram. This procedure was also used for Beam B2, which required three parallel members instead of four (Fig. E.3).

E.2 Equivalent Bilinear Column Properties

The computer program RCCOL5 was used to calculate theoretical moment-curvature diagrams as a function of axial load, for the model column section. As shown in Fig. E.4, these curves are only approxi-bilinear, and this might suggest a modeling procedure similar to that used for the beams. However, unlike the beams, it was necessary to model the columns using beam-column elements whose yield criteria included axial forces as well as moments. The use of a multiple-element idealization might in this case have led to inconsistent deformations of the individual elements. Therefore it was decided to model the columns using a single element with a bilinear moment-rotation relationship. As shown in Fig. E.4, three moment-curvature curves were plotted, corresponding to the range of axial loads expected for the columns.

Equivalent elastic and yielded stiffnesses were computed to fit the curves for the model column over this range of axial loads. The points labelled "A", "B", and "C" in Fig. E.4 may be considered to indicate yielding of the idealized bilinear column under different values of axial force. Together with an assumed balance point axial force of 222 kN (50k), these points were used to construct a moment-axial force interaction diagram for the idealized bilinear column (Fig. E.5). Within the range of axial forces of interest in this study, the idealized diagram closely approximates the moment-axial force interaction diagram previously calculated for the actual column using RCCOL5.

E.3 Equivalent Strut Widths

As noted in Subsection 2.1.1 of the text, equivalent strut widths have been determined by many investigators to depend principally on the panel aspect ratio and the ratio of panel stiffness to frame stiffness. Widths typically vary from about one-third to one-eighth of the length of the panel diagonal. The former value was originally recommended by Holmes [7]. Later investigators [13,14] have recommended other empirical formulas. The ones used herein are taken from Ref. 14:

$$\lambda_h h = \sqrt[4]{\frac{E' t \sin 2\Theta}{4 E I_h h'}}$$

and

$$\left(\frac{w'_{ek}}{w'}\right) = 0.175\ (\lambda_h h)^{-0.4}$$

where

h, h', Θ, and w' refer to Fig. E.6

w'_{ek} is the effective strut width for stiffness

E' is the panel modulus

E is the frame modulus

I_h is the column moment of inertia

t is the panel thickness

In our case,

h = 32 in (0.813 m) for the bottom panel, and 36 in (0.914 m) for the others

E = 3600 ksi (24822 MPa)

t = 2 in (51 mm) nominal

$E' = 1200$ ksi (8274 MPa)

$I_h = 135.16$ in^4 (5.62×10^{-5} m^4) gross transformed section

$h' = 28$ in (0.711 m)

so that

$\lambda_h h = 2.35$ in (60 mm) for the bottom panel, and 2.65 in (67 mm) for the others

since

$w' = (28)^2 + (74)^2 = 79.12$ in (2.00 m),

$w'_{ek} = 9.83$ in (250 mm) for the bottom panel, and 9.38 in (238 mm) for the others

Because the equivalent strut width of the lower panel is close to the widths of the other two panels, it was decided to use the average value of 9.61 in (244 mm) for all struts. In the author's opinion, the considerable scatter in the data points used to determine the empirical formulas of Ref. 14 does not justify the use of a strut width more precise than 10 in, and it was decided to use this nominal figure. The error between 9.61 in (244 mm) and 10 in (254 mm) is less than 5%, and the use of the former figure was believed to imply an unwarranted precision. The strut area was then calculated to be

$$2 \text{ in} \times 10 \text{ in} = 20 \text{ in}^2 \ (0.26 \text{ m}^2)$$

E.4 User's Guide to Infill Strut Element

The following guide should be used with Ref. 39.

Data Format for Element Type 10

a) Control Information (10I5, 6F10.0)

Columns 1- 5: Element group indicator (=10)

6-10: No. of elements in this group

11-15: Element no. of first element in group (default = 1)

16-20: No. of material types (default = 1)

21-50: not used

51-55: Initial stiffness damping factor, β_o

56-60: Current tangent stiffness damping factor, β_T

b) <u>Material Property Information</u> (I5, 4F10.0)

Columns 1- 5: Material no., in sequence starting with 1

6-15: Young's modulus of elasticity, E

16-25: Yield stress in compression

26-35: Yield stress in tension

36-45: Degrading strength parameter, γ (≥ 0)

c) <u>Element Generation Commands</u> (4I5, I10, 3I5)

Columns 1- 5: Element no., or number of first element in a sequentially numbered series of elements to be generated by this card.

6-10: Node number at element end i

11-15: Node number at element end j

16-20: Material number (default = 1)

21-30: Cross sectional area

31-35: Node number increment for element generation (default = 1)

40: Code for large displacement effects

$= \begin{cases} 1 & \text{large displacement effects} \\ 0 & \text{small displacement effects} \end{cases}$

45: Time history output code $= \begin{cases} 1 & \text{required} \\ 0 & \text{not required} \end{cases}$

E.5 Computer Listing

The use of the infill strut element requires four subroutines to the ANSR-I program: INEL10, STIF10, RESP10, and OUT10. These are listed on the following pages.

```
      SUBROUTINE INEL10(LPAR,FLPAR,NDOF,NINFC,NDKOD,X,Y,Z,NJT)
C
C     ****************************************************************
C     INFILL STRUT ELEMENTS    (ELEMENT GROUP INDICATOR = 10)
C     ****************************************************************
C
      DIMENSION LPAR(1),FLPAR(1),NDKOD(NJT,6),X(1),Y(1),Z(1),COM(1)
      COMMON /TAPES / NIU,NOU,NT1,NT2,NT3,NT4,NT5,NTEMP
      COMMON /INFEL / IMEM,KST,LM(6),NODE(2),EPROP(4),AREA,KGEOM,KTHO,
     *                XYZ(3,2),SL,T(3,3),DU1X,DU1Y,DU1Z,Q1(6),SKP(6,6),
     *                KOD,KODP,VTOT,VENP,VENN,SENP,SENN,TVENP,TVENN,
     *                TSENP,TSENN,SDAMP,CT,STOT
      COMMON /WORK  / PROP(4,100),NODC(2),WORK(1598)
      EQUIVALENCE (IMEM,COM(1))
C
      DIMENSION AST(2)
      DATA AST /2H  ,2H */
C
      NGR   = LPAR(1)
      NMEM  = LPAR(2)
      NFST  = LPAR(3)
      NMAT  = LPAR(4)
      DKO   = FLPAR(1)
      DKT   = FLPAR(2)
      IF (NFST.LE.0) NFST = 1
      IF (NMAT.LE.0) NMAT = 1
C
      NDOF  = 6
      NINFC = 92
      KST   = 1
C
      DO 100 I=3,NINFC
100   COM(I) = 0.0
C
C     READ AND PRINT MATERIAL PROPERTIES
C
      WRITE(NOU,2000) NGR,NMEM,NFST,NMAT,NDOF,NINFC,DKO,DKT
C
      DO 110 I=1,NMAT
110   READ (NIU,1000) M,(PROP(J,M),J=1,4)
C
      WRITE(NOU,2010) (M,(PROP(J,M),J=1,4),M=1,NMAT)
C
C     READ, GENERATE AND PRINT ELEMENT INFORMATION
C
      IMEM = NFST
      NLAST= NFST + NMEM - 1
      WRITE(NOU,2020)
C
140   READ (NIU,1010) N,NODC,MT,AO,   ND,KG,KTH
C
      IF (MT.LE.0) MT = 1
      IF (ND.EQ.0) ND = 1
```

```
C
150   IF (N - IMEM) 290,160,210
C
160   DO 170 I=1,2
      NOD = NODC(I)
      NODE(I) = NOD
      II = 3*I
      LM(II-2) = NDKOD(NOD,1)
      LM(II-1) = NDKOD(NOD,2)
      LM(II)   = NDKOD(NOD,3)
      XYZ(1,I) = X(NOD)
      XYZ(2,I) = Y(NOD)
170   XYZ(3,I) = Z(NOD)
C
      DX1   = XYZ(1,2) - XYZ(1,1)
      DX2   = XYZ(2,2) - XYZ(2,1)
      DX3   = XYZ(3,2) - XYZ(3,1)
      SL    = SQRT(DX1**2 + DX2**2 + DX3**2)
      AL    = SQRT(DX1**2 + DX3**2)
      IF (AL.LE.0.) GO TO 175
      T(2,2) =  AL/SL
      EXP = -DX2/(AL*SL)
      T(2,3) =  DX3*EXP
      T(2,1) =  DX1*EXP
      GO TO 180
175   T(2,1) = 1.0
      T(2,2) = 0.0
      T(2,3) = 0.0
180   T(1,1) = DX1/SL
      T(1,2) = DX2/SL
      T(1,3) = DX3/SL
      T(3,1) = T(1,2)*T(2,3) - T(1,3)*T(2,2)
      T(3,2) = T(1,3)*T(2,1) - T(1,1)*T(2,3)
      T(3,3) = T(1,1)*T(2,2) - T(1,2)*T(2,1)
C
      NDIF  = ND
      MTYP  = MT
      KGEOM = KG
      KTHO  = KTH
      AREA  = A0
      EPROP(1) = PROP(1,MT)*A0/SL
      EPROP(2) = PROP(4,MT)
      EPROP(3) = -ABS(PROP(2,MT)*A0)
      EPROP(4) = PROP(3,MT)*A0
C
      ASTT  = AST(1)
      IF (N.NE.NLAST) 140,210
C
190   DO 195 I=1,2
      NOD = NODE(I) + NDIF
      NODE(I) = NOD
      II = 3*I
      LM(II-2) = NDKOD(NOD,1)
```

```
      LM(II-1) = NDKOD(NOD,2)
      LM(II)   = NDKOD(NOD,3)
      XYZ(1,I) = X(NOD)
      XYZ(2,I) = Y(NOD)
195   XYZ(3,I) = Z(NOD)
C
      DX1  = XYZ(1,2) - XYZ(1,1)
      DX2  = XYZ(2,2) - XYZ(2,1)
      DX3  = XYZ(3,2) - XYZ(3,1)
      TL=SL
      SL   = SQRT(DX1**2 + DX2**2 + DX3**2)
      AL    = SQRT(DX1**2 + DX3**2)
      IF (AL.LE.0.) GO TO 200
      T(2,2) =  AL/SL
      EXP = -DX2/(AL*SL)
      T(2,3) =  DX3*EXP
      T(2,1) =  DX1*EXP
      GO TO 205
200   T(2,1) = 1.0
      T(2,2) = 0.0
      T(2,3) = 0.0
205   T(1,1) = DX1/SL
      T(1,2) = DX2/SL,
      T(1,3) = DX3/SL
      T(3,1) = T(1,2)*T(2,3) - T(1,3)*T(2,2)
      T(3,2) = T(1,3)*T(2,1) - T(1,1)*T(2,3)
      T(3,3) = T(1,1)*T(2,2) - T(1,2)*T(2,1)
      EPROP(1)=EPROP(1)*TL/SL
      ASTT = AST(2)
C
210   WRITE(NOU,2025) ASTT,IMEM,NODE,MTYP,AREA,      KGEOM,KTHO
C
C     COMPUTE CONNECTIVITY AND TRANSFER INFORMATION
C
      CALL BAND (LM,NDOF)
      CALL COMPACT
C
C     CHECK LAST ELEMENT
C
      IF (IMEM.EQ.NLAST) GO TO 300
      IMEM = IMEM + 1
      IF (IMEM.EQ.N) GO TO 160
      GO TO 190
C
290   WRITE(NOU,2030) N
C
1000  FORMAT (I5,4F10.0)
1010  FORMAT (4I5,1F10.0,3I5)
2000  FORMAT (26H ELEMENT GROUP INDICATOR = I3,
     *        24H (INFILL STRUT ELEMENTS)///
     *        5X,39HNUMBER OF ELEMENTS IN THIS GROUP       = I5/
     *        5X,39HNUMBER OF FIRST ELEMENT IN THIS GROUP = I5/
     *        5X,39HNUMBER OF DIFFERENT MATERIAL TYPES     = I5//
```

```
     *         5X,39HNUMBER OF DEGREES OF FREEDOM           = I5/
     *         5X,39HLENGTH OF ELEMENT INFORMATION          = I5//
     *         5X,39HDAMPING COEFFICIENT, BETA-O            = F11.5/
     *         5X,39HDAMPING COEFFICIENT, BETA-T            = F11.5///
     *         20H MATERIAL PROPERTIES//5X,4HMAT.,8X,4HEMOD,15X,
     *         12HYIELD STRESS,14X,5HGAMMA/5X,4H NO.,19X,12H COMPRESSION,
     *         5X,12H   TENSION  /)
2010  FORMAT (I9,E12.4,2F17.3,F12.3)
2020  FORMAT (///20H ELEMENT INFORMATION//
     *         5X,4HELEM,5X,4HNODE,5X,4HNODE,5X,4HMAT.,8X,4HAREA,
     *                        5X,4HGEOM,5X,4HHIST/
     *         5X,4H NO.,5X,4H   I,5X,4H   J,5X,4H NO.,12X,
     *         5X,4HCODE,5X,4HCODE/)
2025  FORMAT (A2,I7,3I9,1F12.3,2I9)
2030  FORMAT (//34H **** ELEMENT CARD NOT IN SEQUENCE,I5//)
C
300   RETURN
      END
      SUBROUTINE STIF10(ISTEP,NDOF,NINFC,CDKO,CDKT,COMS,FK,INDFK)
C
C     *******************************************************************
C     TANGENT STIFFNESS FOR INFILL STRUT ELEMENT
C     *******************************************************************
C
      DIMENSION COMS(1),FK(NDOF,NDOF),COM(1)
      COMMON /INFEL / IMEM,KST,LM(6),NODE(2),EPROP(4),AREA,KGEOM,KTHG,
     *                XYZ(3,2),SL,T(3,3),DU1X,DU1Y,DU1Z,QI(6),SKP(6,6),
     *                KOD,KODP,VTOT,VENP,VENN,SENP,SENN,TVENP,TVENN,
     *                TSENP,TSENN,SDAMP,CT,STOT
      COMMON /WORK  / UD(3),B(6),SK(6,6),WORK(1955)
      EQUIVALENCE (IMEM,COM(1))
C
      JMEM = IMEM
      DO 100 J=1,NINFC
100   COM(J) = COMS(J)
C
C     LINEAR PART OF EFFECTIVE STIFFNESS
C
      CE = EPROP(1)
      IF (KOD.EQ.0) CT = CE
      IF (ISTEP.LE.0) GO TO 105
      CT = CT*(1. + CDKT) + CE*CDKO
C
105   UD(1) = 1.0 + DU1X
      UD(2) = DU1Y
      UD(3) = DU1Z
C
      DO 120 I=1,3
      SUM = 0.0
      DO 110 J=1,3
110   SUM = SUM + UD(J)*T(J,I)
      B(I+3) = SUM
120   B(I) = - SUM
```

```
C                                                                         STIF1037
      DO 130 I=1,NDOF                                                     STIF1038
      CC = CT*B(I)                                                        STIF1039
      DO 130 J=1,NDOF                                                     STIF1040
130   SK(I,J) = CC*B(J)                                                   STIF1041
C                                                                         STIF1042
C     ADD NONLINEAR PART OF STIFFNESS                                     STIF1043
C                                                                         STIF1044
      IF (KGEOM.EQ.0) GO TO 140                                           STIF1045
      PL = (STOT + SDAMP)/SL                                              STIF1046
      SK(1,1) = SK(1,1) + PL                                              STIF1047
      SK(1,4) = SK(1,4) - PL                                              STIF1048
      SK(2,2) = SK(2,2) + PL                                              STIF1049
      SK(2,5) = SK(2,5) - PL                                              STIF1050
      SK(3,3) = SK(3,3) + PL                                              STIF1051
      SK(3,6) = SK(3,6) - PL                                              STIF1052
      SK(4,4) = SK(4,4) + PL                                              STIF1053
      SK(5,5) = SK(5,5) + PL                                              STIF1054
      SK(6,6) = SK(6,6) + PL                                              STIF1055
C                                                                         STIF1056
C     COMPUTE CHANGE OF STIFFNESS AND STORE CURRENT STIFFNESS             STIF1057
C                                                                         STIF1058
140   DO 150 I=1,NDOF                                                     STIF1059
      DO 150 J=1,NDOR                                                     STIF1060
      FK(I,J) = SK(I,J) - SKP(I,J)                                        STIF1061
      FK(J,I) = FK(I,J)                                                   STIF1062
      SKP(J,I) = SK(I,J)                                                  STIF1063
150   SKP(I,J) = SK(I,J)                                                  STIF1064
C                                                                         STIF1065
C     UPDATE INFORMATION                                                  STIF1066
C                                                                         STIF1067
      KST  = 0                                                            STIF1068
      KODP = KOD                                                          STIF1069
      DO 160 J=1,NINFC                                                    STIF1070
160   COMS(J) = COM(J)                                                    STIF1071
C                                                                         STIF1072
      RETURN                                                              STIF1073
      END                                                                 STIF1074
      SUBROUTINE RESP10(NDOF,NINFC,MFST,KPR,COMS,Q,VEL,ACC,FE,FD,TIME,    RESP10 2
     *                   DKO,DKT,C7,C8,KUPD,KITRN)                        RESP10 3
C                                                                         RESP10 4
C     ********************************************************************RESP10 5
C     STATE DETERMINATION FOR THREE DIMENSIONAL TRUSS ELEMENT             RESP10 6
C     ********************************************************************RESP10 7
C                                                                         RESP10 8
      DIMENSION COMS(1),Q(1),VEL(1),ACC(1),FE(1),FD(1),COM(1)             RESP10 9
      COMMON /TAPES / NIU,NOU,NT1,NT2,NT3,NT4,NT5,NTEMP                   RESP1010
      COMMON /INFEL / IMEM,KST,LM(6),NODE(2),EPROP(4),AREA,KGEOM,KTHO,    RESP1011
     *                XYZ(3,2),SL,T(3,3),DU1X,DU1Y,DU1Z,Q1(6),SKP(6,6),   RESP1012
     *                KOD,KODP,VTOT,VENP,VENN,SENP,SENN,TVENP,TVENN,      RESP1013
     *                TSENP,TSENN,SDAMP,CT,STOT                           RESP1014
      COMMON /WORK  / UD(3),B(6),WORK(1991)                               RESP1015
      EQUIVALENCE (IMEM,COM(1))                                           RESP1016
```

```
C
      DO 100 J=1,NINFC
100   COM(J) = COMS(J)
      IF (IMEM.EQ.MFST) KHED = 0
C
C     INITIALIZE
C
      IF (KUPD.EQ.3) GO TO 390
      KODE = KOD
C
      UD(1) = 1.0 + DU1X
      UD(2) = DU1Y
      UD(3) = DU1Z
      DO 120 I=1,3
      SUM = 0.0
      DO 110 J=1,3
110   SUM = SUM + UD(J)*T(J,I)
      B(I+3) = SUM
120   B(I) = - SUM
C
      GO TO (125,125,390,345), KUPD
C
C     INCREMENT DISPLACEMENTS
C
125   DO 130 I=1,NDOF
130   Q1(I) = Q1(I) + Q(I)
C
C     COMPUTE LINEAR STRAIN INCREMENT
C
      DV = 0.0
      DO 135 I=1,NDOF
135   DV = DV + B(I)*Q(I)
C
C     ADD NONLINEAR STRAIN INCREMENT
C
      IF (KGEOM.EQ.0) GO TO 138
      Q41 = Q(4) - Q(1)
      Q52 = Q(5) - Q(2)
      Q63 = Q(6) - Q(3)
      DUX = (T(1,1)*Q41 + T(1,2)*Q52 + T(1,3)*Q63)/SL
      DUY = (T(2,1)*Q41 + T(2,2)*Q52 + T(2,3)*Q63)/SL
      DUZ = (T(3,1)*Q41 + T(3,2)*Q52 + T(3,3)*Q63)/SL
      DV  = DV + 0.5*SL*(DUX**2 + DUY**2 + DUZ**2)
C
C     COMPUTE STRESS INCREMENT
C     ASSIGN STIFFNESS BASED ON CURRENT VALUE OF KOD
C
  138 FACAC = 0.0
  139 FACTOR = 1.0 - FACAC
      KKODE = KODE + 2
      GO TO (140,150,180,190,210),KKODE
C
C     KODE = -1---ON TENSION CURVE, CHECK DV
```

```
C
  140 IF (DV) 150,141,141
C
C     ON TENSION CURVE, LOADING
C
  141 CT = 0.0
      VTOT = VTOT + FACTOR*DV
      GO TO 220
C
C     INSIDE REGION DEFINED BY CURVES
C
  150 CT = EPROP(1)
      KODE = 0
      IF (DV) 151,151,172
C
C     ELASTIC, HEADED TOWARDS ENVELOPE OR LOADING CURVES.
C
C     CHECK TO SEE WHICH LOADING CURVE GOVERNS.
C
  151 IF (VTOT) 152,152,176
C
C     ELASTIC, HEADING TOWARDS ENVELOPE CURVE OR LOADING CURVE NO.2
C     COMPUTE INCREMENT OF DV NECESSARY TO HIT LOADING CURVE NO.2
C
  152 VPRIME = VENN
      IF (VENP.GT.ABS(VENN)) VPRIME = -VENP
      SLOAD = EPROP(3)*EXP(EPROP(2)*VPRIME)
      IF (VENP-VPRIME) 154,153,154
  153 SLOPE = CT
      GO TO 156
  154 SLOPE = SLOAD/VPRIME
      IF (SLOPE-CT) 155,156,156
  155 V2 = (STOT - CT*VTOT)/(SLOPE - CT)
      F1 = (V2 - VTOT)/DV
C
C     USING NEWTON-RAPHSON ITERATION, COMPUTE INCREMENT OF DV
C     NECESSARY TO HIT ENVELOPE CURVE.
C
  156 V1 = VTOT
      DO 157 I=1,20
      V2 = V1 - (STOT+CT*(V1-VTOT) - EPROP(3)*EXP(EPROP(2)*V1))/(CT -
     1EPROP(3)*EPROP(2)*EXP(EPROP(2)*V1))
      IF (ABS(V2-V1).LT.1.E-8) GO TO 158
      V1 = V2
  157 CONTINUE
  158 F2 = (V2-VTOT)/DV
      IF (SLOPE.GE.CT) GO TO 160
      IF (F1 - F2) 159,160,160
  159 IF (F1 - FACTOR) 161,170,170
  160 IF (F2 - FACTOR) 195,170,170
C
C     ENTIRE DV CANNOT BE APPLIED.  LOADING CURVE NO.2 GOVERNS.
C
```

```
  161 FACAC = FACAC + F1
      KODE = 2
      VTOT = VTOT + F1*DV
      STOT = STOT + F1*CT*DV
      IF (FACAC - 0.9999999) 139.220.220
C
C     ENTIRE REMAINING DV CAN BE APPLIED.
C
  170 VTOT = VTOT + FACTOR*DV
      STOT = STOT + FACTOR*CT*DV
      GO TO 220
C
C     INSIDE REGION DEFINED BY CURVES. HEADED TOWARDS TENSION CURVE.
C
C
C     COMPUTE INCREMENT OF DV NECESSARY TO HIT TENSION CURVE.
C
  172 F3 = (EPROP(4) - STOT)/(CT*DV)
      IF (F3 - FACTOR) 175.170.170
C
C
C     ENTIRE REMAINING DV CANNOT BE APPLIED. TENSION CURVE GOVERNS.
C
  175 FACAC = FACAC + F3
      VTOT = VTOT + F3*DV
      STOT = STOT + F3*DV*CT
      KODE = -1
      IF (FACAC - 0.9999999) 139.220.220
C
C     COMPUTE INCREMENT OF DV NECESSARY TO HIT LOADING CURVE NO.1. AS
C     LONG AS DEFORMATION IS GREATER THAN ZERO
C
  176 V1 = VTOT - STOT/CT
      IF (V1) 152,178.178
C
C
C     LOADING CURVE NO.1 GOVERNS.
C
  178 F1 = (V1 - VTOT)/DV
      IF (F1 - FACTOR) 179.170.170
C
C     ENTIRE DV CANNOT BE APPLIED.  LOADING CURVE NO.1 GOVERNS.
C
  179 FACAC = FACAC + F1
      KODE = 1
      VTOT = VTOT + F1*DV
      STOT = STOT + F1*CT*DV
      IF (FACAC - 0.9999999) 139.139.220
C
C     ON LOADING CURVE NO.1.  CHECK DV.
C
  180 IF (DV) 101.181.150
C
```

```
C     ON LOADING CURVE NO.1.  COMPUTE INCREMENT OF DV NECESSARY TO HIT
C     LOADING CURVE NO.2.
C
  181 FAC = -VTOT/DV
      CT = 0.0
      IF (FAC - FACTOR) 185,170,170
C
C     ON LOADING CURVE NO.1.  ENTIRE REMAINING DV CANNOT BE APPLIED.
C     LOADING CURVE NO.2 GOVERNS.
C
  185 FACAC = FACAC + FAC
      KODE = 2
      VTOT = VTOT + FAC*DV
      IF (FACAC - 0.9999999) 139,220,220
C
C     ON LOADING CURVE NO.2.  CHECK DV.
C
  190 IF (DV) 191,191,150
C
C     ON LOADING CURVE NO.2.  COMPUTE INCREMENT OF DV NECESSARY TO HIT
C     ENVELOPE CURVE.
C
  191 VPRIME = VENN
      IF (VENP.GT.ABS(VENN)) VPRIME = -VENP
      SLOAD = EPROP(3)*EXP(EPROP(2)*VPRIME)
      CT = SLOAD/VPRIME
      F2 = (VPRIME - VTOT)/DV
      IF (F2 - FACTOR) 195,170,170
C
C     ENTIRE REMAINING DV CANNOT BE APPLIED. ENVELOPE CURVE GOVERNS.
C
  195 FACAC = FACAC + F2
      KODE = 3
      VTOT = VTOT + F2*DV
      STOT = STOT + F2*DV*CT
      IF (FACAC - 0.9999999) 139,220,220
C
C     ON ENVELOPE CURVE, CHECK DV
C
  210 IF (DV) 211,211,150
C
C     ON ENVELOPE CURVE, APPLY REMAINING DV.
C
  211 VTOT = VTOT + DV*FACTOR
      STOT = EPROP(3)*EXP(EPROP(2)*VTOT)
      CT = STOT*EPROP(2)
  220 KOD = KODE
      IF (KGEOM.EQ.0) GO TO 275
      DU1X = DU1X + DUX
      DU1Y = DU1Y + DUY
      DU1Z = DU1Z + DUZ
      UD(1) = 1.0 + DU1X
      UD(2) = DU1Y
```

```
      UD(3) = DU1Z
      DO 270 I=1,3
      SUM = 0.0
      DO 260 J=1,3
260   SUM = SUM + UD(J)*T(J,I)
      B(I+3) = SUM
270   B(I) = - SUM
C
C     COMPUTE DAMPING STRESS
C
275   IF (TIME.EQ.0.) GO TO 290
      DVD = 0.0
      DO 280 I=1,NDOF
280   DVD = DVD + B(I)*VEL(I)
      CE = EPROP(1)
      IF (KODE.EQ.0) CT = CE
      SDAMP = (DKO*CE + DKT*CT)*DVD
C
C     ACCUMULATE ENVELOPES AND UPDATE ELEMENT INFORMATION
C
290   IF (KUPD.NE.1) GO TO 345
C
      IF (SENP.GE.STOT) GO TO 300
      SENP  = STOT
      TSENP = TIME
      GO TO 310
300   IF (SENN.LE.STOT) GO TO 310
      SENN  = STOT
      TSENN = TIME
310   IF (VENP.GE.VTOT) GO TO 320
      VENP  = VTOT
      TVENP = TIME
      GO TO 330
320   IF (VENN.LE.VTOT) GO TO 330
      VENN  = VTOT
      TVENN = TIME
330   CONTINUE
C
      KST = 0
      IF (KOD.NE.KODP.OR.KGEOM.NE.0) KST = 1
      DO 340 J=1,NINFC
340   COMS(J) = COM(J)
C
C     COMPUTE EQUIVALENT ELASTIC NODAL LOADS
C
345   DO 350 I=1,NDOF
350   FE(I) = STOT*B(I)
C
C     DAMPING LOADS
C
      IF (TIME.EQ.0.) GO TO 390
      SD = - SDAMP
      IF (KITRN.EQ.1) GO TO 370
```

```
      DVD = 0.0
      CC7 = 1.0 + C7
      DO 360 I=1,NDOF
360   DVD = DVD + B(I)*(CC7*VEL(I) + C8*ACC(I))
      SD = SD + (DKO*CE + DKT*CT)*DVD
C
370   DO 380 I=1,NDOF
380   FD(I) = SD*B(I)
C
C     PRINT TIME HISTORY
C
390   IF (KPR.EQ.0.OR.KTHO.EQ.0) GO TO 400
C
      IF (KHED.NE.0) GO TO 395
      KHED = 1
      KKPR = IABS(KPR)
      WRITE(NOU,2000) KKPR,TIME
C
395   WRITE(NOU,2010) IMEM,NODE,KOD,STOT,VTOT
C
2000  FORMAT (///18H RESULTS FOR GROUP,I3,
     *        33H (INFILL STRUT ELEMENTS). TIME = E11.4///
     *        5X,4HELEM,5X,4HNODE,5X,4HNODE,4X,5HYIELD,8X,5HAXIAL,
     *        4X,9H   TOTAL  /
     *        5X,4H NO.,5X,4H   I,5X,4H   J,4X,5H CODE,8X,5HFORCE,
     *        4X,9HEXTENSION/)
2010  FORMAT (4I9,F13.2,1F13.5)
C
400   RETURN
      END
      SUBROUTINE OUT10(COMS,NINFC,MFST)
C
C     ****************************************************************
C     OUTPUT OF ENVELOPE VALUES FOR INFILL STRUT ELEMENT
C     ****************************************************************
C
      DIMENSION COMS(1),COM(1)
      COMMON /TAPES / NIU,NOU,NT1,NT2,NT3,NT4,NT5,NTEMP
      COMMON /INFEL / IMEM,KST,LM(6),NODE(2),EPROP(4),AREA,KGEOM,KTHO,
     *               XYZ(3,2),SL,T(3,3),DU1X,DU1Y,DU1Z,Q1(6),SKP(6,6),
     *               KOD,KODP,VTOT,VENP,VENN,SENP,SENN,TVENP,TVENN,
     *               TSENP,TSENN,SDAMP,CT,STOT
      EQUIVALENCE (IMEM,COM(1))
C
      DO 100 J=1,NINFC
100   COM(J) = COMS(J)
C
      IF (IMEM.EQ.MFST) WRITE(NOU,2000)
C
      WRITE(NOU,2010) IMEM,NODE,SENP,TSENP,SENN,TSENN,VENP,TVENP,
     *               VENN,TVENN
C
2000  FORMAT (22H INFILL STRUT ELEMENTS///
```

```
     *        5X,4HELEM,3X,4HNODE,3X,4HNODE,11X,20HMAXIMUM AXIAL FORCES,OUT10 25
     *        19X,18HMAXIMUM EXTENSIONS.                                  OUT10 26
     *        /5X,4H NO.,3X,4H  I ,3X,4H  J ,5X,7HTENSION,3X,4HTIME,      OUT10 27
     *        6X,5HCOMPN,3X,4HTIME,5X,8HPOSITIVE,3X,4HTIME,3X,            OUT10 28
     *        8HNEGATIVE,3X,4HTIME/)                                      OUT10 29
2010  FORMAT (I8,2I7,2X,2(F11.2,F7.2),2X,2(F11.5,F7.2))                   OUT10 30
C                                                                         OUT10 31
      RETURN                                                              OUT10 32
      END                                                                 OUT10 33
```

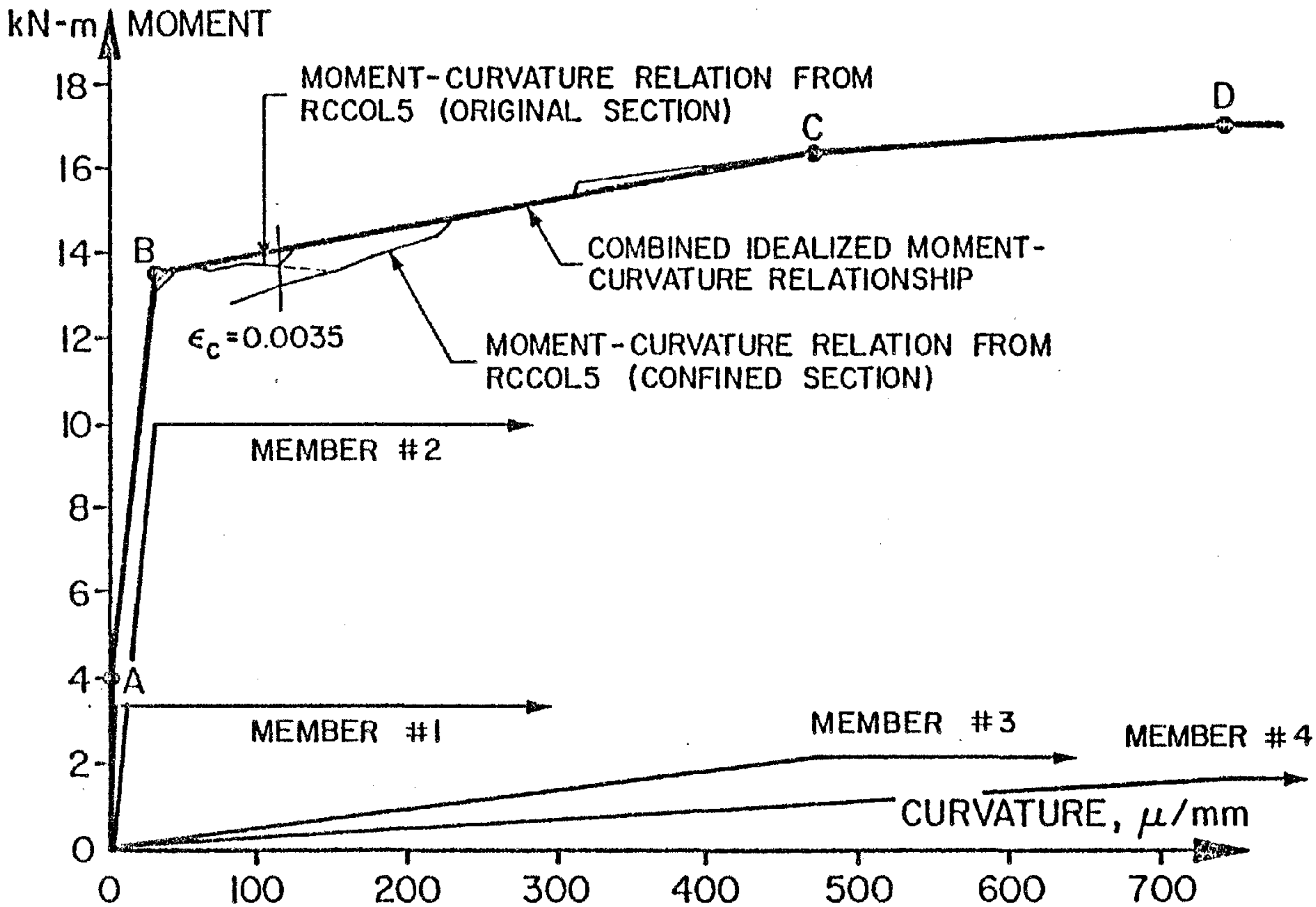

FIG. E.1 IDEALIZED MOMENT-CURVATURE RELATIONSHIP FOR BEAM B1
(SHOWING MOMENT-CURVATURE DIAGRAMS OF CONSTITUENT MEMBERS)

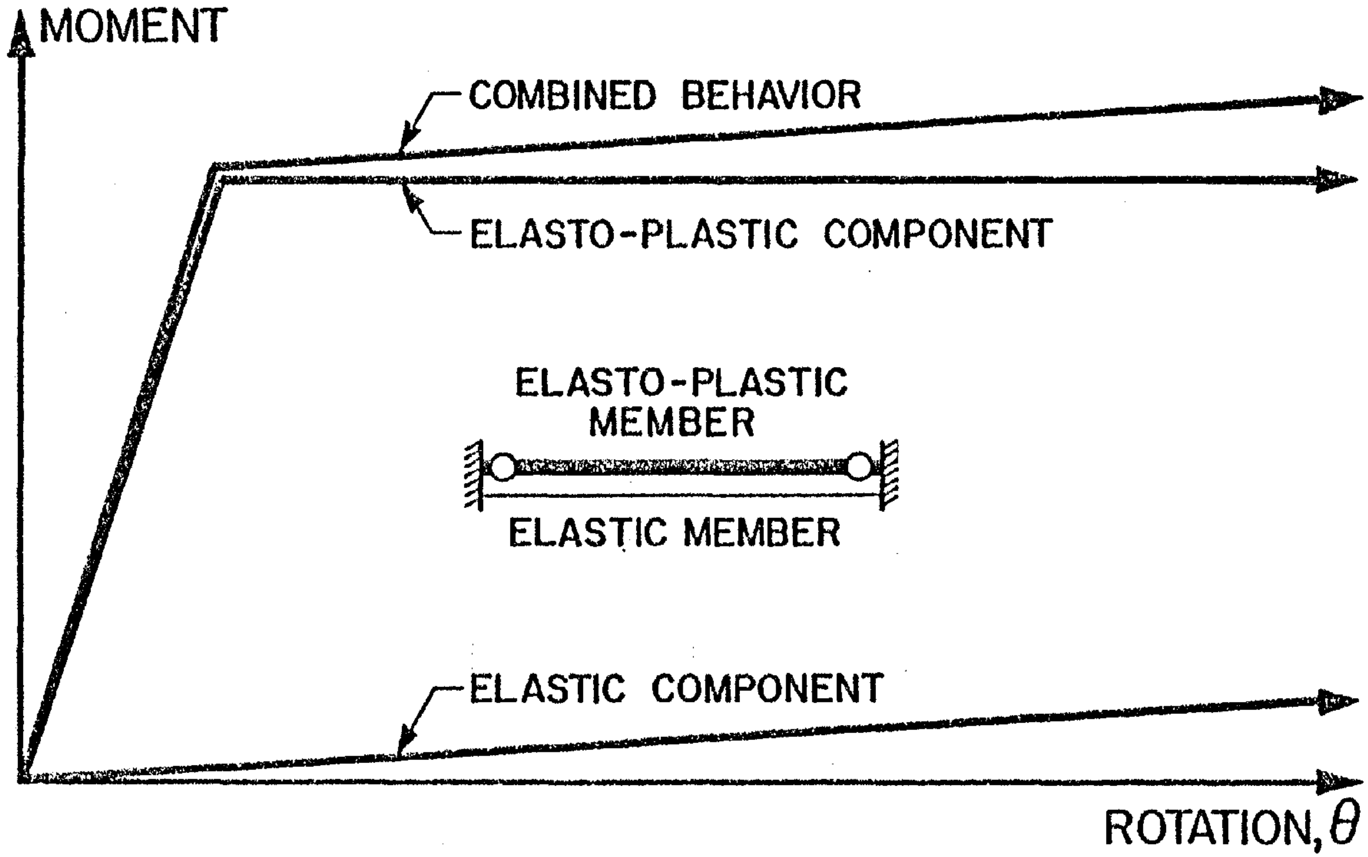

FIG. E.2 MOMENT-ROTATION BEHAVIOR OF TWO-COMPONENT MODEL

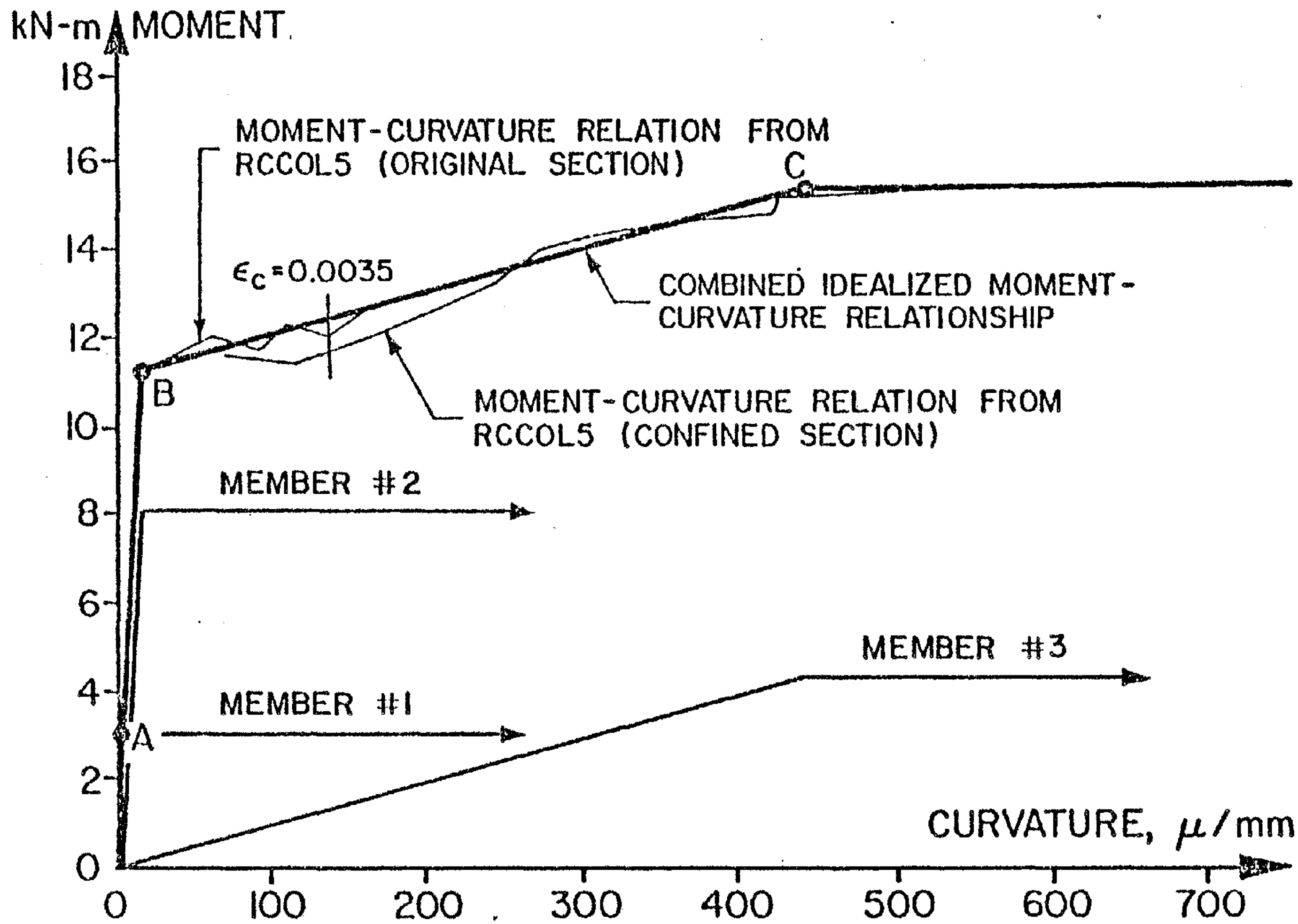

FIG. E.3 IDEALIZED MOMENT-CURVATURE RELATIONSHIP FOR BEAM B2
(SHOWING MOMENT-CURVATURE DIAGRAMS OF CONSTITUENT MEMBERS)

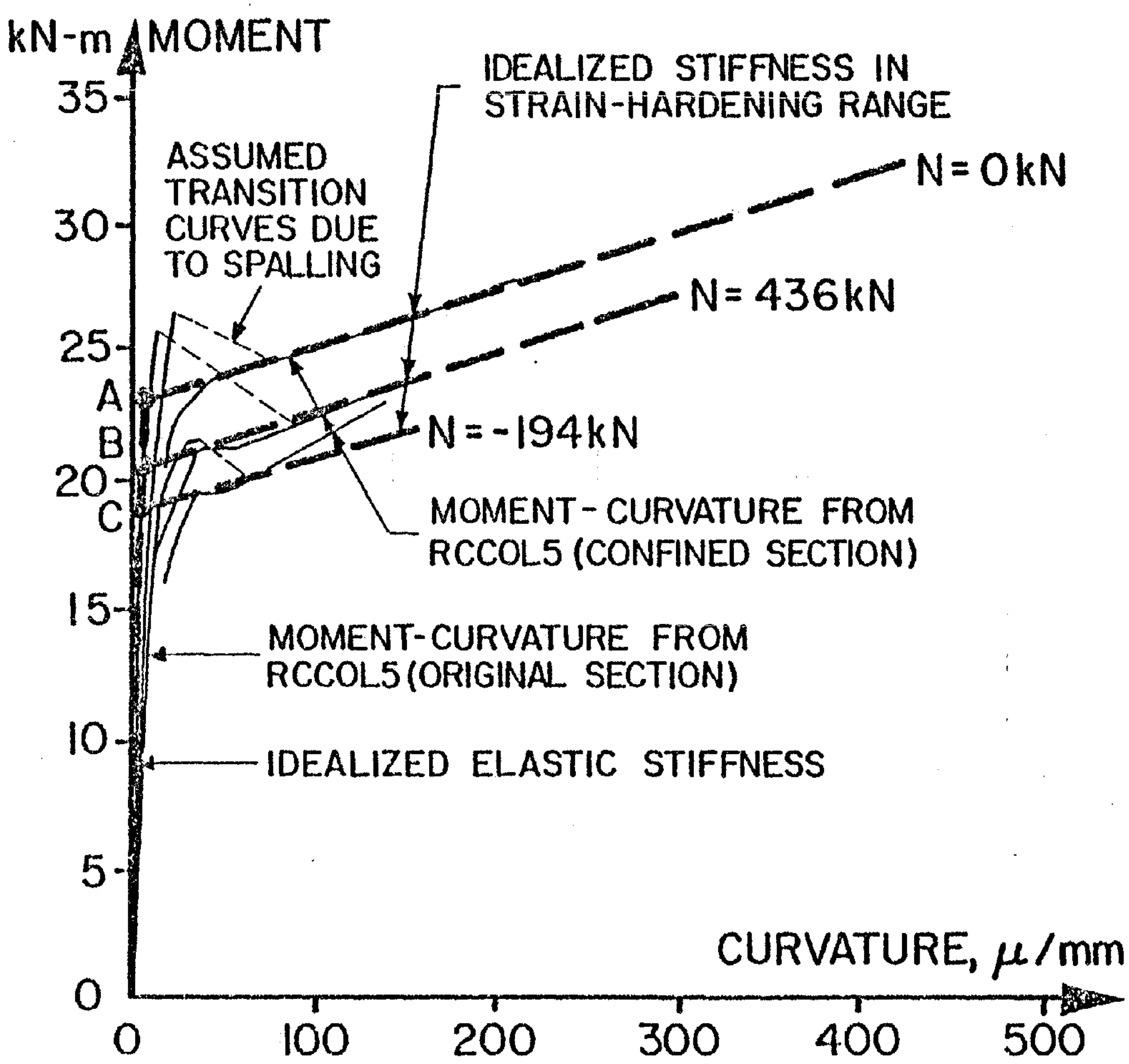

FIG. E.4 IDEALIZED BILINEAR MOMENT-CURVATURE RELATIONSHIP FOR COLUMNS

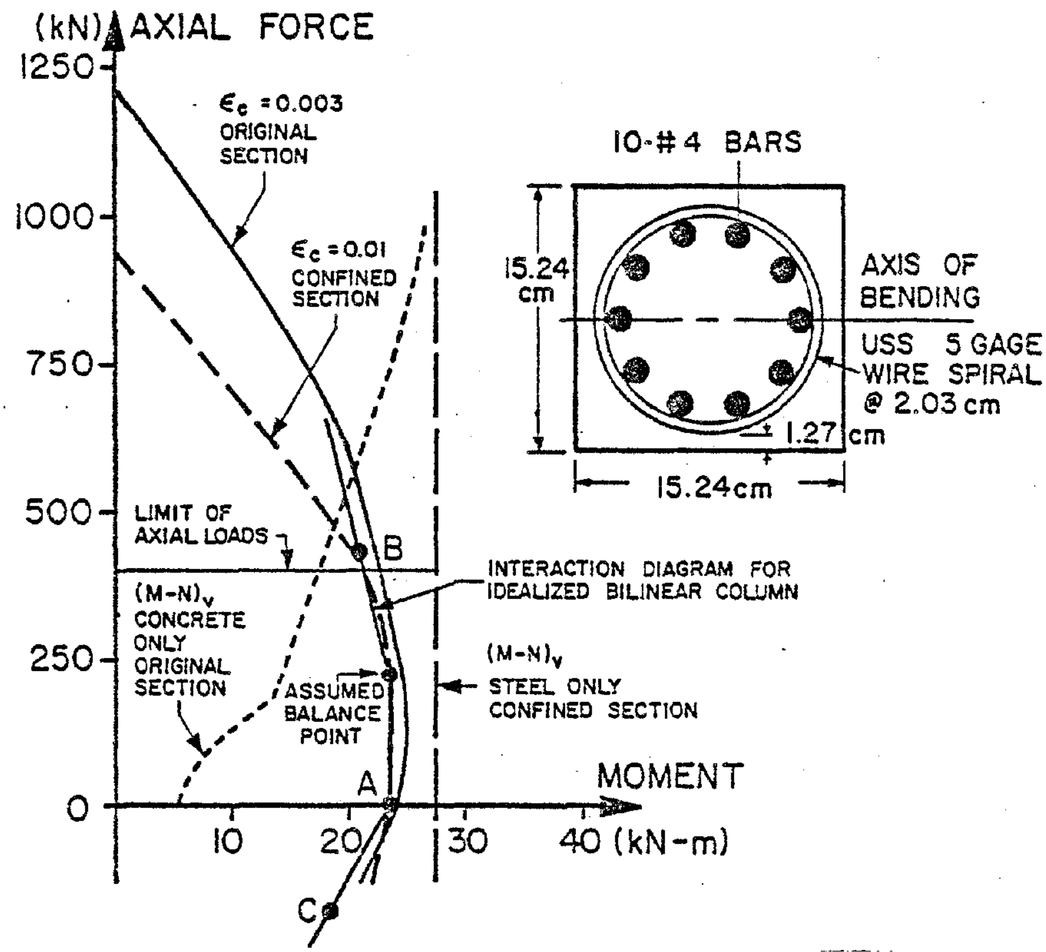

FIG. E.5 COMPARISON OF MOMENT-AXIAL FORCE INTERACTION DIAGRAMS
FOR IDEALIZED AND ACTUAL MODEL COLUMNS

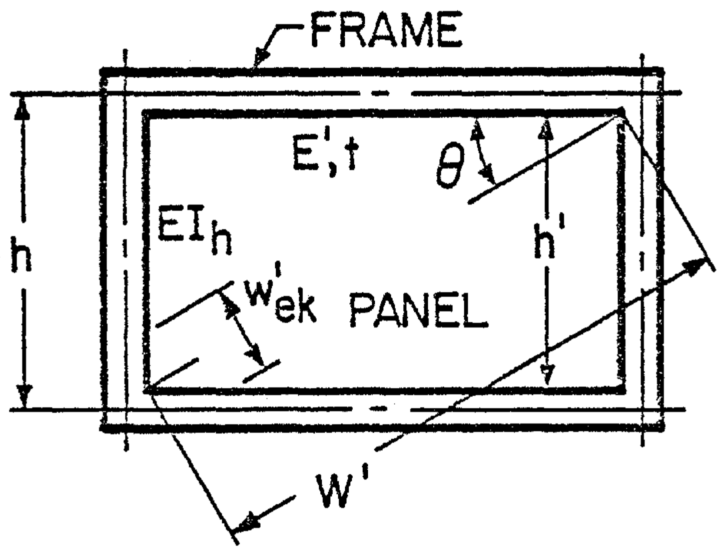

FIG. E.6 NOMENCLATURE USED IN SECTION E.3

EARTHQUAKE ENGINEERING RESEARCH CENTER REPORTS

EERC 67-1 "Feasibility Study Large-Scale Earthquake Simulator Facility," by J. Penzien, J. G. Bouwkamp, R. W. Clough and D. Rea - 1967 (PB 187 905)

EERC 68-1 Unassigned

EERC 68-2 "Inelastic Behavior of Beam-to-Column Subassemblages Under Repeated Loading," by V. V. Bertero - 1968 (PB 184 888)

EERC 68-3 "A Graphical Method for Solving the Wave Reflection-Refraction Problem," by H. D. McNiven and Y. Mengi 1968 (PB 187 943)

EERC 68-4 "Dynamic Properties of McKinley School Buildings," by D. Rea, J. G. Bouwkamp and R. W. Clough - 1968 (PB 187 902)

EERC 68-5 "Characteristics of Rock Motions During Earthquakes," by H. B. Seed, I. M. Idriss and F. W. Kiefer - 1968 (PB 188 338)

EERC 69-1 "Earthquake Engineering Research at Berkeley," - 1969 (PB 187 906)

EERC 69-2 "Nonlinear Seismic Response of Earth Structures," by M. Dibaj and J. Penzien - 1969 (PB 187 904)

EERC 69-3 "Probabilistic Study of the Behavior of Structures During Earthquakes," by P. Ruiz and J. Penzien - 1969 (PB 187 886)

EERC 69-4 "Numerical Solution of Boundary Value Problems in Structural Mechanics by Reduction to an Initial Value Formulation," by N. Distefano and J. Schujman - 1969 (PB 187 942)

EERC 69-5 "Dynamic Programming and the Solution of the Biharmonic Equation," by N. Distefano - 1969 (PB 187 941)

Note: Numbers in parenthesis are Accession Numbers assigned by the National Technical Information Service. Copies of these reports may be ordered from the National Technical Information Service, 5285 Port Royal Road, Springfield, Virginia, 22161. Accession Numbers should be quoted on orders for the reports (PB --- ---) and remittance must accompany each order. (Foreign orders, add $2.50 extra for mailing charges.) Those reports without this information listed are not yet available from NTIS. Upon request, EERC will mail inquirers this information when it becomes available to us.

EERC 69-6 "Stochastic Analysis of Offshore Tower Structures," by A. K. Malhotra and J. Penzien - 1969 (PB 187 903)

EERC 69-7 "Rock Motion Accelerograms for High Magnitude Earthquakes," by H. B. Seed and I. M. Idriss - 1969 (PB 187 940)

EERC 69-8 "Structural Dynamics Testing Facilities at the University of California, Berkeley," by R. M. Stephen, J. G. Bouwkamp, R. W. Clough and J. Penzien - 1969 (PB 189 111)

EERC 69-9 "Seismic Response of Soil Deposits Underlain by Sloping Rock Boundaries," by H. Dezfulian and H. B. Seed - 1969 (PB 189 114)

EERC 69-10 "Dynamic Stress Analysis of Axisymmetric Structures under Arbitrary Loading," by S. Ghosh and E. L. Wilson - 1969 (PB 189 026)

EERC 69-11 "Seismic Behavior of Multistory Frames Designed by Different Philosophies," by J. C. Anderson and V. V. Bertero - 1969 (PB 190 662)

EERC 69-12 "Stiffness Degradation of Reinforcing Concrete Structures Subjected to Reversed Actions," by V. V. Bertero, B. Bresler and H. Ming Liao - 1969 (PB 202 942)

EERC 69-13 "Response of Non-Uniform Soil Deposits to Travel Seismic Waves," by H. Dezfulian and H. B. Seed - 1969 (PB 191 023)

EERC 69-14 "Damping Capacity of a Model Steel Structure," by D. Rea, R. W. Clough and J. G. Bouwkamp - 1969 (PB 190 663)

EERC 69-15 "Influence of Local Soil Conditions on Building Damage Potential during Earthquakes," by H. B. Seed and I. M. Idriss - 1969 (PB 191 036)

EERC 69-16 "The Behavior of Sands under Seismic Loading Conditions," by M. L. Silver and H. B. Seed - 1969 (AD 714 982)

EERC 70-1 "Earthquake Response of Concrete Gravity Dams," by A. K. Chopra - 1970 (AD 709 640)

EERC 70-2 "Relationships between Soil Conditions and Building Damage in the Caracas Earthquake of July 29, 1967," by H. B. Seed, I. M. Idriss and H. Dezfulian - 1970 (PB 195 762)

EERC 70-3 "Cyclic Loading of Full Size Steel Connections," by E. P. Popov and R. M. Stephen - 1970 (PB 213 545)

EERC 70-4 "Seismic Analysis of the Charaima Building, Caraballeda, Venezuela," by Subcommittee of the SEAONC Research Committee: V. V. Bertero, P. F. Fratessa, S. A. Mahin, J. H. Sexton, A. C. Scordelis, E. L. Wilson, L. A. Wyllie, H. B. Seed and J. Penzien, Chairman - 1970 (PB 201 455)

EERC 70-5 "A Computer Program for Earthquake Analysis of Dams," by A. K. Chopra and P. Chakrabarti - 1970 (AD 723 994)

EERC 70-6 "The Propagation of Love Waves across Non-Horizontally Layered Structures," by J. Lysmer and L. A. Drake - 1970 (PB 197 896)

EERC 70-7 "Influence of Base Rock Characteristics on Ground Response," by J. Lysmer, H. B. Seed and P. B. Schnabel - 1970 (PB 197 897)

EERC 70-8 "Applicability of Laboratory Test Procedures for Measuring Soil Liquefaction Characteristics under Cyclic Loading," by H. B. Seed and W. H. Peacock - 1970 (PB 198 016)

EERC 70-9 "A Simplified Procedure for Evaluating Soil Liquefaction Potential," by H. B. Seed and I. M. Idriss - 1970 (PB 198 009)

EERC 70-10 "Soil Moduli and Damping Factors for Dynamic Response Analysis," by H. B. Seed and I. M. Idriss - 1970 (PB 197 869)

EERC 71-1 "Koyna Earthquake and the Performance of Koyna Dam," by A. K. Chopra and P. Chakrabarti - 1971 (AD 731 496)

EERC 71-2 "Preliminary In-Situ Measurements of Anelastic Absorption in Soils Using a Prototype Earthquake Simulator," by R. D. Borcherdt and P. W. Rodgers - 1971 (PB 201 454)

EERC 71-3 "Static and Dynamic Analysis of Inelastic Frame Structures," by F. L. Porter and G. H. Powell - 1971 (PB 210 135)

EERC 71-4 "Research Needs in Limit Design of Reinforced Concrete Structures," by V. V. Bertero - 1971 (PB 202 943)

EERC 71-5 "Dynamic Behavior of a High-Rise Diagonally Braced Steel Building," by D. Rea, A. A. Shah and J. G. Bouwkamp - 1971 (PB 203 584)

EERC 71-6 "Dynamic Stress Analysis of Porous Elastic Solids Saturated with Compressible Fluids," by J. Ghaboussi and E. L. Wilson - 1971 (PB 211 396)

EERC 71-7 "Inelastic Behavior of Steel Beam-to-Column Subassemblages," by H. Krawinkler, V. V. Bertero and E. P. Popov - 1971 (PB 211 335)

EERC 71-8 "Modification of Seismograph Records for Effects of Local Soil Conditions," by P. Schnabel, H. B. Seed and J. Lysmer - 1971 (PB 214 450)

EERC 72-1 "Static and Earthquake Analysis of Three Dimensional Frame and Shear Wall Buildings," by E. L. Wilson and H. H. Dovey - 1972 (PB 212 904)

EERC 72-2 "Accelerations in Rock for Earthquakes in the Western United States," by P. B. Schnabel and H. B. Seed - 1972 (PB 213 100)

EERC 72-3 "Elastic-Plastic Earthquake Response of Soil-Building Systems," by T. Minami - 1972 (PB 214 868)

EERC 72-4 "Stochastic Inelastic Response of Offshore Towers to Strong Motion Earthquakes," by M. K. Kaul - 1972 (PB 215 713)

EERC 72-5 "Cyclic Behavior of Three Reinforced Concrete Flexural Members with High Shear," by E. P. Popov, V. V. Bertero and H. Krawinkler - 1972 (PB 214 555)

EERC 72-6 "Earthquake Response of Gravity Dams Including Reservoir Interaction Effects," by P. Chakrabarti and A. K. Chopra - 1972 (AD 762 330)

EERC 72-7 "Dynamic Properties on Pine Flat Dam," by D. Rea, C. Y. Liaw and A. K. Chopra - 1972 (AD 763 928)

EERC 72-8 "Three Dimensional Analysis of Building Systems," by E. L. Wilson and H. H. Dovey - 1972 (PB 222 438)

EERC 72-9 "Rate of Loading Effects on Uncracked and Repaired Reinforced Concrete Members," by S. Mahin, V. V. Bertero, D. Rea and M. Atalay - 1972 (PB 224 520)

EERC 72-10 "Computer Program for Static and Dynamic Analysis of Linear Structural Systems," by E. L. Wilson, K.-J. Bathe, J. E. Peterson and H. H. Dovey - 1972 (PB 220 437)

EERC 72-11 "Literature Survey - Seismic Effects on Highway Bridges," by T. Iwasaki, J. Penzien and R. W. Clough - 1972 (PB 215 613)

EERC 72-12 "SHAKE-A Computer Program for Earthquake Response Analysis of Horizontally Layered Sites," by P. B. Schnabel and J. Lysmer - 1972 (PB 220 207)

EERC 73-1 "Optimal Seismic Design of Multistory Frames," by V. V. Bertero and H. Kamil - 1973

EERC 73-2 "Analysis of the Slides in the San Fernando Dams during the Earthquake of February 9, 1971," by H. B. Seed, K. L. Lee, I. M. Idriss and F. Makdisi - 1973 (PB 223 402)

EERC 73-3 "Computer Aided Ultimate Load Design of Unbraced Multistory Steel Frames," by M. B. El-Hafez and G. H. Powell - 1973

EERC 73-4 "Experimental Investigation into the Seismic Behavior of Critical Regions of Reinforced Concrete Components as Influenced by Moment and Shear," by M. Celebi and J. Penzien - 1973 (PB 215 884)

EERC 73-5 "Hysteretic Behavior of Epoxy-Repaired Reinforced Concrete Beams," by M. Celebi and J. Penzien - 1973

EERC 73-6 "General Purpose Computer Program for Inelastic Dynamic Response of Plane Structures," by A. Kanaan and G. H. Powell - 1973 (PB 221 260)

EERC 73-7 "A Computer Program for Earthquake Analysis of Gravity Dams Including Reservoir Interaction," by P. Chakrabarti and A. K. Chopra - 1973 (AD 766 271)

EERC 73-8 "Behavior of Reinforced Concrete Deep Beam-Column Subassemblages under Cyclic Loads," by O. Kustu and J. G. Bouwkamp - 1973

EERC 73-9 "Earthquake Analysis of Structure-Foundation Systems," by A. K. Vaish and A. K. Chopra - 1973 (AD 766 272)

EERC 73-10 "Deconvolution of Seismic Response for Linear Systems," by R. B. Reimer - 1973 (PB 227 179)

EERC 73-11 "SAP IV: A Structural Analysis Program for Static and Dynamic Response of Linear Systems," by K.-J. Bathe, E. L. Wilson and F. E. Peterson - 1973 (PB 221 967)

EERC 73-12 "Analytical Investigations of the Seismic Response of Long, Multiple Span Highway Bridges," by W. S. Tseng and J. Penzien - 1973 (PB 227 816)

EERC 73-13 "Earthquake Analysis of Multi-Story Buildings Including Foundation Interaction," by A. K. Chopra and J. A. Gutierrez - 1973 (PB 222 970)

EERC 73-14 "ADAP: A Computer Program for Static and Dynamic Analysis of Arch Dams," by R. W. Clough, J. M. Raphael and S. Majtahedi - 1973 (PB 223 763)

EERC 73-15 "Cyclic Plastic Analysis of Structural Steel Joints," by R. B. Pinkney and R. W. Clough - 1973 (PB 226 843)

EERC 73-16 "QUAD-4: A Computer Program for Evaluating the Seismic Response of Soil Structures by Variable Damping Finite Element Procedures," by I. M. Idriss, J. Lysmer, R. Hwang and H. B. Seed - 1973 (PB 229 424)

EERC 73-17 "Dynamic Behavior of a Multi-Story Pyramid Shaped Building," by R. M. Stephen and J. G. Bouwkamp - 1973

EERC 73-18 "Effect of Different Types of Reinforcing on Seismic Behavior of Short Concrete Columns," by V. V. Bertero, J. Hollings, O. Kustu, R. M. Stephen and J. G. Bouwkamp - 1973

EERC 73-19 "Olive View Medical Center Material Studies, Phase I," by B. Bresler and V. V. Bertero - 1973 (PB 235 986)

EERC 73-20 "Linear and Nonlinear Seismic Analysis Computer Programs for Long Multiple-Span Highway Bridges," by W. S. Tseng and J. Penzien - 1973

EERC 73-21 "Constitutive Models for Cyclic Plastic Deformation of Engineering Materials," by J. M. Kelly and P. P. Gillis - 1973 (PB 226 024)

EERC 73-22 "DRAIN - 2D User's Guide," by G. H. Powell - 1973 (PB 227 016)

EERC 73-23 "Earthquake Engineering at Berkeley - 1973" - 1973 (PB 226 033)

EERC 73-24 Unassigned

EERC 73-25 "Earthquake Response of Axisymmetric Tower Structures Surrounded by Water," by C. Y. Liaw and A. K. Chopra - 1973 (AD 773 052)

EERC 73-26 "Investigation of the Failures of the Olive View Stairtowers during the San Fernando Earthquake and Their Implications in Seismic Design," by V. V. Bertero and R. G. Collins - 1973 (PB 235 106)

EERC 73-27 "Further Studies on Seismic Behavior of Steel Beam-Column Subassemblages," by V. V. Bertero, H. Krawinkler and E. P. Popov - 1973 (PB 234 172)

EERC 74-1 "Seismic Risk Analysis," by C. S. Oliveira - 1974 (PB 235 920)

EERC 74-2 "Settlement and Liquefaction of Sands under Multi-Directional Shaking," by R. Pyke, C. K. Chan and H. B. Seed - 1974

EERC 74-3 "Optimum Design of Earthquake Resistant Shear Buildings," by D. Ray, K. S. Pister and A. K. Chopra - 1974 (PB 231 172)

EERC 74-4 "LUSH - A Computer Program for Complex Response Analysis of Soil-Structure Systems," by J. Lysmer, T. Udaka, H. B. Seed and R. Hwang - 1974 (PB 236 796)

EERC 74-5 "Sensitivity Analysis for Hysteretic Dynamic Systems: Applications to Earthquake Engineering," by D. Ray - 1974 (PB 233 213)

EERC 74-6 "Soil-Structure Interaction Analyses for Evaluating Seismic Response," by H. B. Seed, J. Lysmer and R. Hwang - 1974 (PB 236 519)

EERC 74-7 Unassigned

EERC 74-8 "Shaking Table Tests of a Steel Frame - A Progress Report," by R. W. Clough and D. Tang - 1974

EERC 74-9 "Hysteretic Behavior of Reinforced Concrete Flexural Members with Special Web Reinforcement," by V. V. Bertero, E. P. Popov and T. Y. Wang - 1974 (PB 236 797)

EERC 74-10 "Applications of Reliability-Based, Global Cost Optimization to Design of Earthquake Resistant Structures," by E. Vitiello and K. S. Pister - 1974 (PB 237 231)

EERC 74-11 "Liquefaction of Gravelly Soils under Cyclic Loading Conditions," by R. T. Wong, H. B. Seed and C. K. Chan - 1974

EERC 74-12 "Site-Dependent Spectra for Earthquake-Resistant Design," by H. B. Seed, C. Ugas and J. Lysmer - 1974

EERC 74-13 "Earthquake Simulator Study of a Reinforced Concrete Frame," by P. Hidalgo and R. W. Clough - 1974 (PB 241 944)

EERC 74-14 "Nonlinear Earthquake Response of Concrete Gravity Dams," by N. Pal - 1974 (AD/A006583)

EERC 74-15 "Modeling and Identification in Nonlinear Structural Dynamics, I - One Degree of Freedom Models," by N. Distefano and A. Rath - 1974 (PB 241 548)

EERC 75-1 "Determination of Seismic Design Criteria for the Dumbarton Bridge Replacement Structure, Vol. I: Description, Theory and Analytical Modeling of Bridge and Parameters," by F. Baron and S.-H. Pang - 1975

EERC 75-2 "Determination of Seismic Design Criteria for the Dumbarton Bridge Replacement Structure, Vol. 2: Numerical Studies and Establishment of Seismic Design Criteria," by F. Baron and S.-H. Pang - 1975

EERC 75-3 "Seismic Risk Analysis for a Site and a Metropolitan Area," by C. S. Oliveira - 1975

EERC 75-4 "Analytical Investigations of Seismic Response of Short, Single or Multiple-Span Highway Bridges," by Ma-chi Chen and J. Penzien - 1975 (PB 241 454)

EERC 75-5 "An Evaluation of Some Methods for Predicting Seismic Behavior of Reinforced Concrete Buildings," by Stephen A. Mahin and V. V. Bertero - 1975

EERC 75-6 "Earthquake Simulator Study of a Steel Frame Structure, Vol. I: Experimental Results," by R. W. Clough and David T. Tang - 1975 (PB 243 981)

EERC 75-7 "Dynamic Properties of San Bernardino Intake Tower," by Dixon Rea, C.-Y. Liaw, and Anil K. Chopra - 1975 (AD/A008406)

EERC 75-8 "Seismic Studies of the Articulation for the Dumbarton Bridge Replacement Structure, Vol. I: Description, Theory and Analytical Modeling of Bridge Components," by F. Baron and R. E. Hamati - 1975

EERC 75-9 "Seismic Studies of the Articulation for the Dumbarton Bridge Replacement Structure, Vol. 2: Numerical Studies of Steel and Concrete Girder Alternates," by F. Baron and R. E. Hamati - 1975

EERC 75-10 "Static and Dynamic Analysis of Nonlinear Structures," by Digambar P. Mondkar and Graham H. Powell - 1975 (PB 242 434)

EERC 75-11 "Hysteretic Behavior of Steel Columns," by E. P. Popov, V. V. Bertero and S. Chandramouli - 1975

EERC 75-12 "Earthquake Engineering Research Center Library Printed Catalog" - 1975 (PB 243 711)

EERC 75-13 "Three Dimensional Analysis of Building Systems," Extended Version, by E. L. Wilson, J. P. Hollings and H. H. Dovey - 1975 (PB 243 989)

EERC 75-14 "Determination of Soil Liquefaction Characteristics by Large-Scale Laboratory Tests," by Pedro De Alba, Clarence K. Chan and H. Bolton Seed - 1975

EERC 75-15 "A Literature Survey - Compressive, Tensile, Bond and Shear Strength of Masonry," by Ronald L. Mayes and Ray W. Clough - 1975

EERC 75-16 "Hysteretic Behavior of Ductile Moment Resisting Reinforced Concrete Frame Components," by V. V. Bertero and E. P. Popov - 1975

EERC 75-17 "Relationships Between Maximum Acceleration, Maximum Velocity, Distance from Source, Local Site Conditions for Moderately Strong Earthquakes," by H. Bolton Seed, Ramesh Murarka, John Lysmer and I. M. Idriss - 1975

EERC 75-18 "The Effects of Method of Sample Preparation on the Cyclic Stress-Strain Behavior of Sands," by J. Paul Mulilis, Clarence K. Chan and H. Bolton Seed - 1975

EERC 75-19 "The Seismic Behavior of Critical Regions of Reinforced Concrete Components as Influenced by Moment, Shear and Axial Force," by B. Atalay and J. Penzien - 1975

EERC 75-20 "Dynamic Properties of an Eleven Story Masonry Building," by R. M. Stephen, J. P. Hollings, J. G. Bouwkamp and D. Jurukovski - 1975

EERC 75-21 "State-of-the-Art in Seismic Shear Strength of Masonry - An Evaluation and Review," by Ronald L. Mayes and Ray W. Clough - 1975

EERC 75-22 "Frequency Dependencies Stiffness Matrices for Viscoelastic Half-Plane Foundations," by Anil K. Chopra, P. Chakrabarti and Gautam Dasgupta - 1975

EERC 75-23 "Hysteretic Behavior of Reinforced Concrete Framed Walls," by T. Y. Wong, V. V. Bertero and E. P. Popov - 1975

EERC 75-24 "Testing Facility for Subassemblages of Frame-Wall Structural Systems," by V. V. Bertero, E. P. Popov and T. Endo - 1975

EERC 75-25 "Influence of Seismic History of the Liquefaction Characteristics of Sands," by H. Bolton Seed, Kenji Mori and Clarence K. Chan - 1975

EERC 75-26 "The Generation and Dissipation of Pore Water Pressures during Soil Liquefaction," by H. Bolton Seed, Phillippe P. Martin and John Lysmer - 1975

EERC 75-27 "Identification of Research Needs for Improving a Seismic Design of Building Structures," by V. V. Bertero - 1975

EERC 75-28 "Evaluation of Soil Liquefaction Potential during Earthquakes," by H. Bolton Seed, I. Arango and Clarence K. Chan 1975

EERC 75-29 "Representation of Irregular Stress Time Histories by Equivalent Uniform Stress Series in Liquefaction Analyses," by H. Bolton Seed, I. M. Idriss, F. Makdisi and N. Banerjee 1975

EERC 75-30 "FLUSH - A Computer Program for Approximate 3-D Analysis of Soil-Structure Interaction Problems," by J. Lysmer, T. Udaka, C.-F. Tsai and H. B. Seed - 1975

EERC 75-31 "ALUSH - A Computer Program for Seismic Response Analysis of Axisymmetric Soil-Structure Systems," by E. Berger, J. Lysmer and H. B. Seed - 1975

EERC 75-32 "TRIP and TRAVEL - Computer Programs for Soil-Structure Interaction Analysis with Horizontally Travelling Waves," by T. Udaka, J. Lysmer and H. B. Seed - 1975

EERC 75-33 "Predicting the Performance of Structures in Regions of High Seismicity," by Joseph Penzien - 1975

EERC 75-34 "Efficient Finite Element Analysis of Seismic Structure - Soil - Direction," by J. Lysmer, H. Bolton Seed, T. Udaka, R. N. Hwang and C.-F. Tsai - 1975

EERC 75-35 "The Dynamic Behavior of a First Story Girder of a Three-Story Steel Frame Subjected to Earthquake Loading," by Ray W. Clough and Lap-Yan Li - 1975

EERC 75-36 "Earthquake Simulator Study of a Steel Frame Structure, Volume II - Analytical Results," by David T. Tang - 1975

EERC 75-37 "ANSR-I General Purpose Computer Program for Analysis of Non-Linear Structure Response," by Digambar P. Mondkar and Graham H. Powell - 1975

EERC 75-38 "Nonlinear Response Spectra for Probabilistic Seismic Design and Damage Assessment of Reinforced Concrete Structures," by Masaya Murakami and Joseph Penzien - 1975

EERC 75-39 "Study of a Method of Feasible Directions for Optimal Elastic Design of Framed Structures Subjected to Earthquake Loading," by N. D. Walker and K. S. Pister - 1975

EERC 75-40 "An Alternative Representation of the Elastic-Viscoelastic Analogy," by Gautam Dasgupta and Jerome L. Sackman - 1975

EERC 75-41 "Effect of Multi-Directional Shaking on Liquefaction of Sands," by H. Bolton Seed, Robert Pyke and Geoffrey R. Martin - 1975

EERC 76-1 "Strength and Ductility Evaluation of Existing Low-Rise Reinforced Concrete Buildings - Screening Method," by Tsuneo Okada and Boris Bresler - 1976

EERC 76-2 "Experimental and Analytical Studies on the Hysteretic Behavior of Reinforced Concrete Rectangular and T-Beams," by Shao-Yeh Marshall Ma, Egor P. Popov and Vitelmo V. Bertero - 1976

EERC 76-3 "Dynamic Behavior of a Multistory Triangular-Shaped Building," by J. Petrovski, R. M. Stephen, E. Gartenbaum and J. G. Bouwkamp - 1976

EERC 76-4 "Earthquake Induced Deformations of Earth Dams," by Norman Serff and H. Bolton Seed - 1976

EERC 76-5 "Analysis and Design of Tube-Type Tall Building Structures," by H. de Clercq and G. H. Powell - 1976

EERC 76-6 "Time and Frequency Domain Analysis of Three-Dimensional Ground Motions, San Fernando Earthquake," by Tetsuo Kubo and Joseph Penzien - 1976

EERC 76-7 "Expected Performance of Uniform Building Code Design Masonry Structures," by R. L. Mayes, Y. Omote, S. W. Chen and R. W. Clough - 1976

EERC 76-8 "Cyclic Shear Tests on Concrete Masonry Piers, Part I - Test Results," by R. L. Mayes, Y. Omote and R. W. Clough 1976

EERC 76-9 "A Substructure Method for Earthquake Analysis of Structure - Soil Interaction," by Jorge Alberto Gutierrez and Anil K. Chopra - 1976

EERC 76-10 "Stabilization of Potentially Liquefiable Sand Deposits using Gravel Drain Systems," by H. Bolton Seed and John R. Booker - 1976

EERC 76-11 "Influence of Design and Analysis Assumptions on Computed Inelastic Response of Moderately Tall Frames," by G. H. Powell and D. G. Row - 1976

EERC 76-12 "Sensitivity Analysis for Hysteretic Dynamic Systems: Theory and Applications," by D. Ray, K. S. Pister and E. Polak - 1976

EERC 76-13 "Coupled Lateral Torsional Response of Buildings to Ground Shaking," by Christopher L. Kan and Anil K. Chopra - 1976

EERC 76-14 "Seismic Analyses of the Banco de America," by V. V. Bertero, S. A. Mahin, and J. A. Hollings - 1976

EERC 76-15 "Reinforced Concrete Frame 2: Seismic Testing and Analytical Correlation," by Ray W. Clough and Jawahar Gidwani - 1976

EERC 76-16 "Cyclic Shear Tests on Masonry Piers, Part II - Analysis of Test Results," by R. L. Mayes, Y. Omote and R. W. Clough 1976

EERC 76-17 "Structural Steel Bracing Systems: Behavior Under Cyclic Loading," by E. P. Popov, K. Takanashi and C. W. Roeder 1976

EERC 76-18 "Experimental Model Studies on Seismic Response of High Curved Overcrossings," by David Williams and William G. Godden - 1976

EERC 76-19 "Effects of Non-Uniform Seismic Disturbances on the Dumbarton Bridge Replacement Structure," by Frank Baron and Raymond E. Hamati - 1976

EERC 76-20 "Investigation of the Inelastic Characteristics of a Single Story Steel Structure using System Identification and Shaking Table Experiments," by Vernon C. Matzen and Hugh D. McNiven 1976

EERC 76-21 "Capacity of Columns with Splice Imperfections," by E. P. Popov, R. M. Stephen and R. Philbrick - 1976

EERC 76-22 "Response of the Olive View Hospital Main Building during the San Fernando Earthquake," by Stephen A. Mahin, Robert Collins, Anil K. Chopra and Vitelmo V. Bertero - 1976

EERC 76-23 "A Study on the Major Factors Influencing the Strength of Masonry Prisms," by N. M. Mostaghel, R. L. Mayes, R. W. Clough and S. W. Chen - 1976

EERC 76-24 "GADFLEA - A Computer Program for the Analysis of Pore Pressure Generation and Dissipation during Cyclic or Earthquake Loading," by J. R. Booker, M. S. Rahman and H. Bolton Seed - 1976

EERC 76-25 "Rehabilitation of an Existing Building: A Case Study," by B. Bresler and J. Axley - 1976

EERC 76-26 "Correlative Investigations on Theoretical and Experimental Dynamic Behavior of a Model Bridge Structure," by Kazuhiko Kawashima and Joseph Penzien - 1976

EERC 76-27 "Earthquake Response of Coupled Shear Wall Buildings," by Thirawat Srichatrapimuk - 1976

EERC 76-28 "Tensile Capacity of Partial Penetration Welds," by Egor P. Popov and Roy M. Stephen - 1976

EERC 76-29 "Analysis and Design of Numerical Integration Methods in Structural Dynamics," by Hans M. Hilber - 1976

EERC 76-30 "Contribution of a Floor System to the Dynamic Characteristics of Reinforced Concrete Buildings," by L. J. Edgar and V. V. Bertero

EERC 76-31 "The Effects of Seismic Disturbances on the Golden Gate Bridge," by Frank Baron, Metin Arikan and Raymond E. Hamati - 1976

EERC 76-32 "Infilled Frames in Earthquake-Resistant Construction," by R. E. Klingner and V. V. Bertero - 1976

EERC 77-1 "PLUSH - A Computer Program for Probabilistic Finite Element Analysis of Seismic Soil-Structure Interaction," by Miguel P. Romo-Organista, John Lysmer and H. Bolton Seed - 1977